2.10 Appendices

2.10.1 Computer Program Descriptions

2.10.1.1 GACAP. The GACAP code, developed at GA, was used to evaluate the impact limiter crush force and crush depth that would occur during a drop event. GACAP has the option to compute the stresses in the cask using beam analysis techniques. This option was not used. Instead, ANSYS quasi-static finite-element analysis was used to evaluate the cask stresses, as shown in Sections 2.10.2 and 2.10.6.

GACAP uses finite element numerical integration analysis to determine the dynamic response of the cask. The cask is modeled using a lumped mass elastic beam representation as shown in Fig. 2.10.1-1. There is no damping assumed in the model. The only dissipation of energy occurs in the inelastic crushing of the impact limiters. Crushing of the impact limiters is modeled using force-deflection data.

GACAP prints impact limiter forces and deflections; the cask node positions, velocities, and accelerations; and beam forces, moments, and stresses at user-specified time intervals. A summary of maximum values is provided at the end of the run. Also, the code outputs the full energy state information. The energy state informs the user of the makeup of the remaining kinetic, potential and elastic energy.

GACAP will also compute the cask loads, stresses and accelerations based on the cask acting as a rigid body. This option is discussed in Section 2.10.1.1.1(d). GA used this option to compute the cask accelerations.

The code was verified by comparisons with the DYNA3D (Ref. 2.10.1-1) and SCANS (Ref. 2.10.1-2) codes and was run on the CRAY XMP-48 and YMP8/864 computers at the San Diego Supercomputer Center.

2.10.1.1.1 Theory of Modeling.

a. Formulation. The code models the cask with a series of aligned beam elements and mass nodes numbered from left to right. The basic mass and stiffness formulations of the code are standard. Equation 2.10.1-1 characterizes the equations of motion in the local coordinate system for a straight line of massless beam elements and n lumped node masses (each with three degrees of freedom X, Y, θ).

$$[M] \quad \{\ddot{X}\} = \{F_{lim}\} + \{F_g\} - [K] \quad \{X\}, \qquad (2.10.1\text{-}1)$$

where

[M] = the mass/mass moment of inertia matrix, which is diagonalized,

$\{\ddot{X}\}$ = the displacement and rotation acceleration vector,

{X} = the displacement and rotation vector,

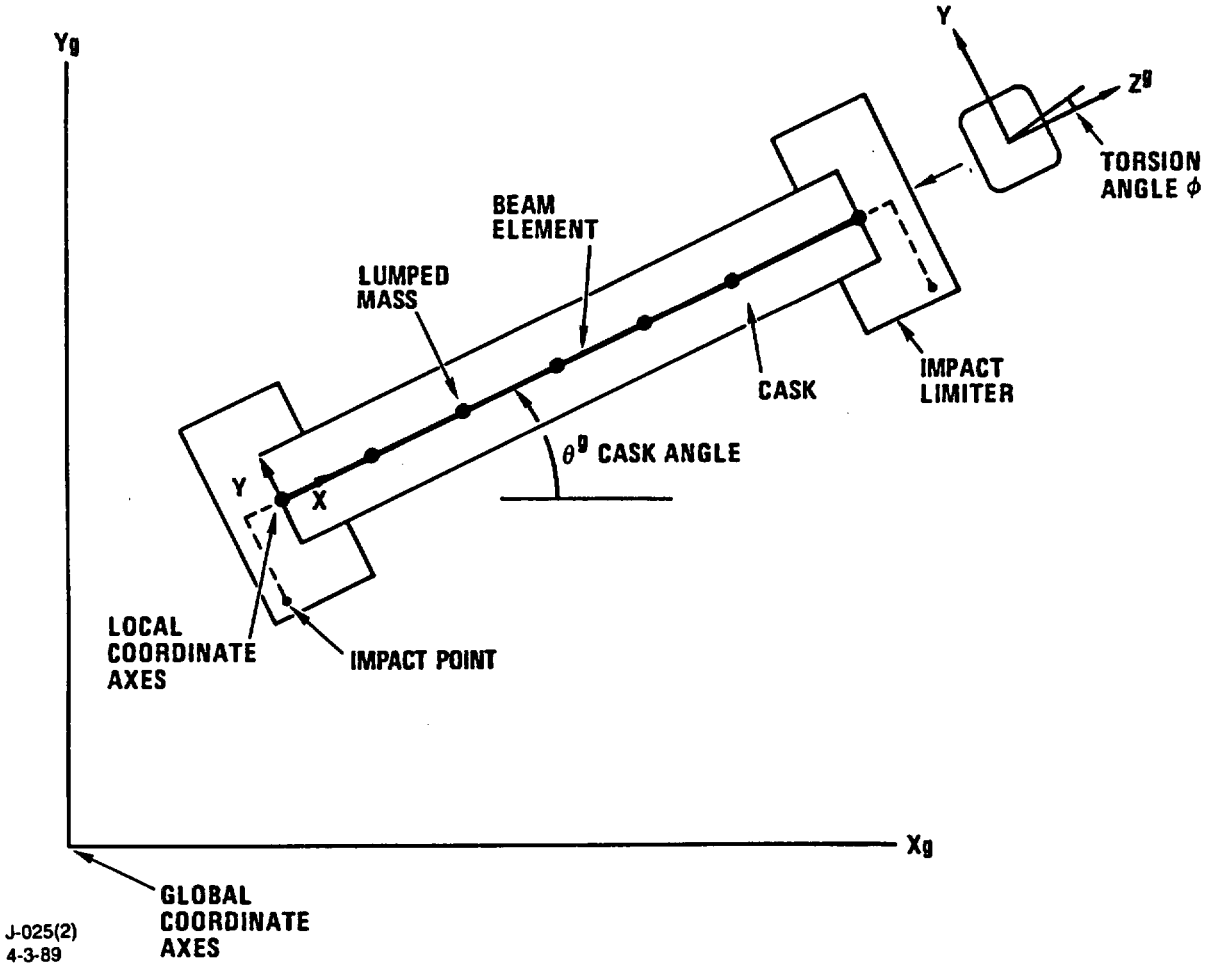

Fig. 2.10.1-1. Model of a cask using lumped mass and beam representation

$\{F_{lim}\}$ = the force vector imposed by the limiters,
$\{F_g\}$ = the body force vector from the acceleration of gravity,
$[K]$ = the stiffness matrix of the beam structure.

This equation is in the local beam coordinate system, which has the coordinates and directions of node 1 of the cask model. There are 3*n degrees of freedom in Eq. 2.10.1-1. The sequence is X_1, Y_1, θ_1, X_2, Y_2, θ_2 ... X_n, Y_n, θ_n.

The stiffness matrix [K] is assembled from the 6 x 6 stiffness matrices of the individual beam elements. This 6 x 6 symmetric element matrix can be characterized for element i as

$$\begin{bmatrix} A_i & B_i \\ & \\ B_i^T & C_i \end{bmatrix}$$

where A, B, and C are 3 x 3 submatrices and B^T is the transpose of B.

The element stiffness matrices are assembled into the total stiffness matrix [K]

$$\{F\} = [K]\{X\}. \qquad (2.10.1\text{-}2)$$

Here {X} vector, X_i, Y_i, θ_i, are the coordinates of the nodes in the local coordinate system, and the {F} vector F_{Xi}, F_{Yi}, $M_{\theta i}$ are the resultant loads on the nodal points, also in the local system.

Equation 2.10.1-1 is used to compute the accelerations in the directions of the local coordinate system. The local accelerations are then rotated into the directions of the global coordinate system and integrated to obtain incremental displacements:

$$\underset{\{3*n,1\}}{\{\ddot{X}_j^g\}} = \underset{[3*n,3*n]}{[R_{ji}]} \quad \underset{\{3*n,1\}}{\{\ddot{X}_i\}}, \qquad (2.10.1\text{-}3)$$

where
n = the number of nodes,
$\{\ddot{X}_j^g\}$ = the acceleration vector in the global coordinate system,
$\{\ddot{X}_i\}$ = the acceleration vector in the local coordinate system,
$[R_{ji}]$ = the rotation matrix.

GACAP solves these equations explicitly, using central difference integration of the accelerations. The local deformed state of the beam is updated by using the resulting deflection and rotation.

The local displacement/rotation vector {X} is then multiplied by the stiffness matrix [K] to produce the forces and moments imposed by the beams on the nodes.

b. Impact Limiter Forces. GACAP provides the user with flexibility in the treatment of the impact limiters. The impact limiter is "slaved" to a node by a rigid connection between the impact limiter contact point and the node. The impact limiters are massless in the model.

Their masses are lumped into the respective nodal mass. The limiters impose forces and moments on specified model nodes. The model for the impact limiter can be seen in Fig. 2.10.1-1. The left side limiter is shown connected to the first node; however, limiters can be connected to any node in the model. The model can also include several impact limiters connected to different nodes, each with its own load-deflection tables. The code positions the cask vertically so that the initial impacting limiter just contacts the impact plane at the start of the run. The GA-4 cask analysis "slaved" the impact limiters to the end nodes.

The impact limiter normal force will always act at the contact point, producing moments on the connected cask node. The code calculates the impact limiter force by interpolating from the user-defined force-deflection tables, using the vertical displacement overlap of the contact point with the impact plane.

The code accommodates impact limiter designs in which the behavior can change depending on the direction (torsion angle, see Fig. 2.10.1-1) relative to the cross section of the cask. Each force deflection table for an impact limiter is associated with a cask angle θ^g and a torsion angle ϕ (see Fig. 2.10.1-1). Since the model is two-dimensional, the initial torsion angle is used throughout the calculation. A linear interpolation of the tables is made for both the cask angle and the torsion angle. Cask angle specification for the tables must be between 0 and 90°. Since the cask impact limiters are round and symmetric, the same values were used for all torsion angles. Different load-deflection curves were input for cask angles θ at every 15°.

The user may include a horizontal friction force in the GACAP analysis. This force is dependent on the magnitude of the impact limiter normal force. The code treats the friction force at each limiter as a viscous damper that opposes the horizontal velocity of the limiter on the impact plane. No friction was used on the GA-4 cask analyses in order to conservatively have the kinetic energy be absorbed only by crushing of the impact limiters and not by other means.

c. Section Properties. GACAP provides the user with flexibility to input the desired section properties. The program computes stiffness properties for two of the four cross-section inputs provided. These two cross sections are the circular cylinder and the rounded-corner square box. The moments of inertia for either of these cross sections are independent of the torsion angle. The user may also input the properties of the beam sections, as shown in Fig. 2.10.1-2.

CROSS SECTION	TYPE OF INPUT	
CYLINDERS	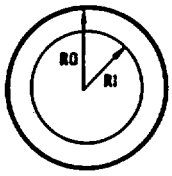	E, G
ROUNDED-CORNER BOX SECTIONS	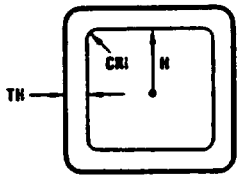	E, G
ARBITRARY SHAPE		$EA/_L$, $EI/_L3$ $EI/_L2$, $EI/_L$, f
		E, G, A, I, f

WHERE

E = ELASTIC MODULUS
A = AREA OF THE CROSS SECTION
I = MOMENT OF INERTIA
L = LENGTH OF BEAM
G = SHEAR MODULUS
f = SHEAR FORM FACTOR

J-025(16)
4-3-89

Fig. 2.10.1-2. Different types of section properties input accepted by GACAP

The code allows for mixed multiple-beam input between adjacent nodes. The parallel beam stiffnesses are simply added together to create the model. The user may define the properties of the beams between adjacent nodes independently. Therefore, the code can be used to analyze cask designs with variable cross sections. For the GA-4 analyses, the code calculates the rounded-corner box properties.

The code allows the user either to input directly the mass moment of inertia of each node or to have the code calculate this parameter. The second option was used during the GA-4 analyses.

d. Rigid-Body Beam Loads. The code has an option to compute the loads and stresses assuming the cask acts as a rigid body. With this option, the code separates the components of the loads and stresses due to rigid-body motion from loads and stresses due to elastic deformation. The rigid-body loads and stresses are extracted from the combined rigid-body/elastic loads by first computing the rigid-body accelerations. The rigid-body components of acceleration (two translational and one rotational) are computed as follows:

$$\ddot{X}_c^g = \frac{\sum_{i=1}^{n} m_i \ddot{X}_i^g}{m_c},$$

$$\ddot{Y}_c^g = \frac{\sum_{i=1}^{n} m_i \ddot{Y}_i^g}{m_c},$$

$$\ddot{\theta}_c^g = \frac{\sum_{i=1}^{n} I_{mi} \ddot{\theta}_i^g + \sum_{i=1}^{n} m_i \left(\ddot{Y}_i^g dx_i - \ddot{X}_i^g dy_i \right)}{I_{mc}},$$

where

m_i = mass of node i,

$m_c = \sum_{i-1}^{n} m_i$ = mass of cask,

I_{mi} = mass moment of inertia of node i,

I_{mc} = mass moment of inertia of cask,

dx_i and dy_i are distances from the beam center to node i.

To calculate the beam loads with these rigid-body accelerations, each node is given accelerations in the local coordinate system dependent on its position from the center of gravity:

$$\ddot{X}_{ci} = \ddot{X}^g_c \cos\theta^g + \ddot{Y}^g_c \sin\theta^g,$$

$$\ddot{Y}_{ci} = \ddot{Y}^g_c \cos\theta^g - \ddot{Y}^g_c \sin\theta^g + \ddot{\theta}^g_c(d_i),$$

$$\ddot{\theta}_{ci} = \ddot{\theta}^g_c,$$

where

d_i = distance (along cask axis) from cask centroid to node i.

These rigid-body nodal accelerations are used to compute body forces and moments on the nodes. The body forces along with the forces imposed by the impact limiters and gravity comprise the rigid-body force-moment loading on the cask.

The rigid-body nodal loads in the local coordinate directions are:

$$N_{xj} = F_{x(lim)j} \cos\theta^g + F_{y(lim)j} \sin\theta^g - m_{jg} \sin\theta^g - m_j\ddot{X}_{cj},$$

$$N_{yj} = F_{y(lim)j} \cos\theta^g + F_{x(lim)j} \sin\theta^g - m_{jg} \cos\theta^g - m_j\ddot{Y}_{cj},$$

$$M_j = M_{(lim)j} - I_{mj}\ddot{\theta}_{cj},$$

where

$F_{x(lim)j}$ is the force in the global x direction imposed on node j by the limiters,

$F_{y(lim)j}$ is the force in the global y direction imposed on node j by the limiters,

M_j is the moment imposed on node j by the limiters.

The beam loads on beam i are then:

Axial force

$$F_{Ai} = \sum_{j=1}^{i} (N_{xj}) \quad \text{(left side)},$$

$$-F_{Ai} \quad \text{(right side)};$$

Shear force

$$F_{Si} = \sum_{j=1}^{i} (N_{yj}) \quad \text{(left side)},$$

$$-F_{Si} \quad \text{(right side)};$$

Moment

$$F_{left,Mi} = \sum_{j=1}^{i} M_j - \sum_{k=1}^{i-1} F_{Sk}\ell_k \text{(left side)},$$

$$F_{right,Mi} = -(F_{left,Mi} - F_{Si}\ell_i) \quad \text{(right side)};$$

where ℓ = length of the beam element.

Positive moment on the left side is tension on top.
Positive moment on the right side is compression on top.

$i \leq n-1$.

Given the rigid-body loads at the nodes, the rigid-body stresses are computed as described below (Section 2.10.1.1.1.e).

To calculate the beam loads from the rigid-body accelerations, each node is given accelerations in the local coordinate system dependent on its position in relation to the CG. The rigid-body nodal accelerations are used to compute body forces and moments on the nodes. The body forces along with the forces imposed by the impact limiters and gravity, comprise the rigid-body force-moment loading on the cask.

e. Computation of Stresses.

GACAP converts the beam moments and the axial and shear forces into stresses in order to help evaluate the performance of the cask. The stresses are calculated as follows:

$\sigma_b = M\,c/I$,
$\sigma_a = F_a / A$,
$\tau = V / A$,

where

σ_b = average bending stress through the section thickness,
M = maximum bending moment from GACAP,
I = moment of inertia of cask (with the GA-4 analysis including both the cask body and the fuel cavity liner cross sections);
c = in the GA-4 analysis we used the distance from centroid of cask to center of cask body wall on the corner since this location produces the highest primary membrane stresses on the cask;
σ_a = axial stresses due to axial force,
F_a = axial force from GACAP;
A = cask body cross-sectional area; in the GA-4 analysis we used only the containment boundary area, conservatively ignoring the cavity liner area;
τ = shear stress,
V = shear force from GACAP.

Once these stresses are calculated, the primary membrane stress intensity is calculated by obtaining the principal stresses due to the following stress components:

$\sigma_{xx} = \sigma_b + \sigma_a$ and τ.

2.10.1.1.2 Verification.

Comparison with the SCANS Code. GACAP has been compared with the Lawrence Livermore Laboratory SCANS code. SCANS is based on the same formulation as GACAP. Table 2.10.1-1 shows that both codes give equivalent results during primary impact or when the cask does not rebound.

The primary difference between GACAP and SCANS results arises from the fact that SCANS eliminates the beam dynamics during the free flight of the cask (rebound). When this assumption is simulated in GACAP, the secondary impacts also compare identically.

TABLE 2.10.1-1
COMPARISON OF RESULTS BETWEEN SCANS AND GACAP

IDENTICAL 30-FT SIDE DROP ANALYSES	SCANS	GACAP
Max. crush (in.) top/bottom	10.5	10.5
Max. deceleration, g's	41.9	41.9
Max. rigid-body moment (kip-in.)(center node)	47,000	47,140
Max. rigid-body shear (kips)	808	808

2.10.1.2 ANSYS Computer Program. The ANSYS (Ref. 2.10.1-3, 2.10.1-4, and 2.10.1-5) computer program is a large-scale, finite-element general purpose computer program used for the solution of several classes of engineering problems. The analytical capabilities used in this design phase were (1) static, elastic, and plastic stress analysis and (2) steady-state and transient heat-transfer analysis.

The program employs the matrix displacement method of analysis based upon finite-element idealization. The library of finite elements available included more than 40 for static analyses and 20 for heat-transfer analyses. The primary elements used in this analysis were the two-dimensional bar/gap, two-dimensional plane, and three-dimensional solid elements.

Loadings used in the structural analyses were forces, displacement, pressure, and temperature. Loading for the heat-transfer analyses were internal heat generation, convection and radiation boundaries, and specified temperatures or heat flows.

The ANSYS program uses the wave-front (or frontal) direct solution method for the system of simultaneous linear equations developed by matrix displacement method. The program is able to solve large problems.

Postprocessing routines are available for algebraic modification, differentiation, and integration of calculated results. Post routines also plot distorted geometries, stress contours, and temperature contours.

2.10.1.3 PATRAN Plus. PATRAN Plus (PATRAN), Ref. 2.10.1-6, is an engineering software package which provides solid geometry construction, finite-element modeling, and enhanced graphics. In conjunction with separate interface codes, PATRAN provides pre- and postprocessing capability for a number of recognized engineering analysis codes, such as NASTRAN, ANSYS, ABAQUS, and SINDA. PATRAN may also be used independently to construct, manipulate, and display three-dimensional geometric entities without regard to a finite-element mesh.

Widely used throughout industry, both PATRAN and the translator code PAT/ANSYS are well-suited to perform the finite-element and solids modeling required in this project.

2.10.1.4 ILMOD. GA developed the computer code ILMOD to compute the load-versus-deflection curves for impact limiters with standard unidirectional honeycomb. ILMOD calculates the footprint of the crushed impact limiter for any orientation and depth. It calculates the area of each section of crushed honeycomb involved in the footprint through basic trigonometric and geometrical formulas. It then calculates the total load based on the crushed area and the user-supplied crush strength of each section of crushed honeycomb. The code calculates the complete impact limiter load-versus-deflection tables for crush orientations ranging from side (0°) to end (90°).

The equations in ILMOD were verified by hand calculations and by using the solid modeling program PATRAN described earlier. Two impact limiter configurations were modeled with PATRAN. The footprint area for several drop angles and crush depths was compared to ILMOD area calculations. For all cases, the ILMOD and PATRAN results compared very well.

The results were validated by comparison to 1/4-scale test results (Section 2.10.3.5).

2.10.1.5 References for Appendix 2.10.1.

2.10.1-1 Hallquist, J. O., and D. J. Benson, "DYNA3D User's Manual," UCID-19592, Rev. 3, Lawrence Livermore Laboratory, July 1987.

2.10.1-2 "SCANS: A Microcomputer-Based Analysis System for Shipping Cask Design Review," Theory Manuals, Vols. 2 and 3, January 1989.

2.10.1-3 "ANSYS, Engineering Analysis System, User's Manual," Version 4.2b, Swanson Analysis Systems, June 1985.

2.10.1-4 "ANSYS Verification Manual for Revision 5.1," Swanson Analysis Systems, December 1994.

2.10.1-5 "ANSYS Verification Manual for Revision 5.2," Swanson Analysis Systems, September 1995.

2.10.1-6 "PATRAN Plus, User's Manual," Release 2.2, PDA Engineering, July 1987.

THIS PAGE LEFT BLANK INTENTIONALLY

2.10.2 Cask Finite Element Analysis

Two ANSYS finite element models were used to evaluate the stresses in the cask wall for normal, hypothetical accident, and special requirement conditions. These models are referred to as either the "corner" or "flat" model. The label identifies the location of the cask cross section relative to the horizontal impact surface for the drops. For the corner model, a corner of the cask impacts the horizontal surface. For the flat model, a flat side of the cask impacts the horizontal surface. The corner model uses a plane of symmetry which passes through the cask wall corners and the flat model is symmetric about the center of the flat wall of the cask, as shown in Fig. 2.10.2-1. The ANSYS models were used to evaluate static loads only. Internal and external pressure cases were considered, as well as statically equivalent, dynamic load cases. The dynamic load cases simulated a 30-ft end drop and side drops with either both or a single impact limiter (oblique drop case) reacting the drop load. These "base cases" are used in this section and Section 2.10.6 to evaluate all drop orientations.

To adequately and efficiently evaluate the normal and hypothetical accident conditions, a summary of worst case accelerations for a range of impact angles and drop heights was developed for the dynamic load cases, using the GACAP computer program, and is described in Section 2.10.4. These results are summarized in Table 2.10.4-6. As shown in the table, the results are given in terms of the acceleration in the lateral and axial cask directions for different angle drops from either 1 ft (normal conditions) or 30 ft (hypothetical accident conditions). To find the stresses in the cask wall resulting from these different dynamic load cases, the stresses for the base case end drop and the base case oblique drop were scaled by the appropriate axial and transverse g-levels given in Table 2.10.4-6. After superposing the lateral and axial dynamic stress distributions, the results were combined with the appropriate pressure case results to obtain the complete stress distribution for the load case. The resulting stresses are combined to find the stress intensity, SI, and to determine the design margin for different sections along the cask wall.

In the following subsections the two ANSYS models are described, the loading conditions defined and the analysis procedure is explained. Section 2.10.6 presents the results of the analyses for the normal and hypothetical operating conditions and the 10CFR71.61 external water pressure requirement for irradiated fuel shipments.

2.10.2.1 ANSYS Model Descriptions. The GA-4 shipping cask has a non-axisymmetric cross section, which must be simulated using three-dimensional models. Since there is cross-sectional symmetry about the lines shown in Fig. 2.10.2-1, it was not necessary to model the entire cask. Using the two lines of cross-sectional symmetry, two ANSYS models were developed, a flat model and a corner model. The flat model used symmetry about the cross-sectional line which passes through the center of the flat section of the cask wall. The corner model used cross-sectional symmetry about the line which passes through the corners of the cask. The resulting models represent half sections of the total geometry and include the closure, FSS, cavity liner and the cask body with the bottom head. The impact limiter support structure (ILSS), the DU structure, and neutron shield shell are not explicitly included in the models. The ILSS adds stiffness in the closure/flange and bottom head regions; therefore, the model stress results are conservative (i.e., higher stresses) in those regions. The effects of the

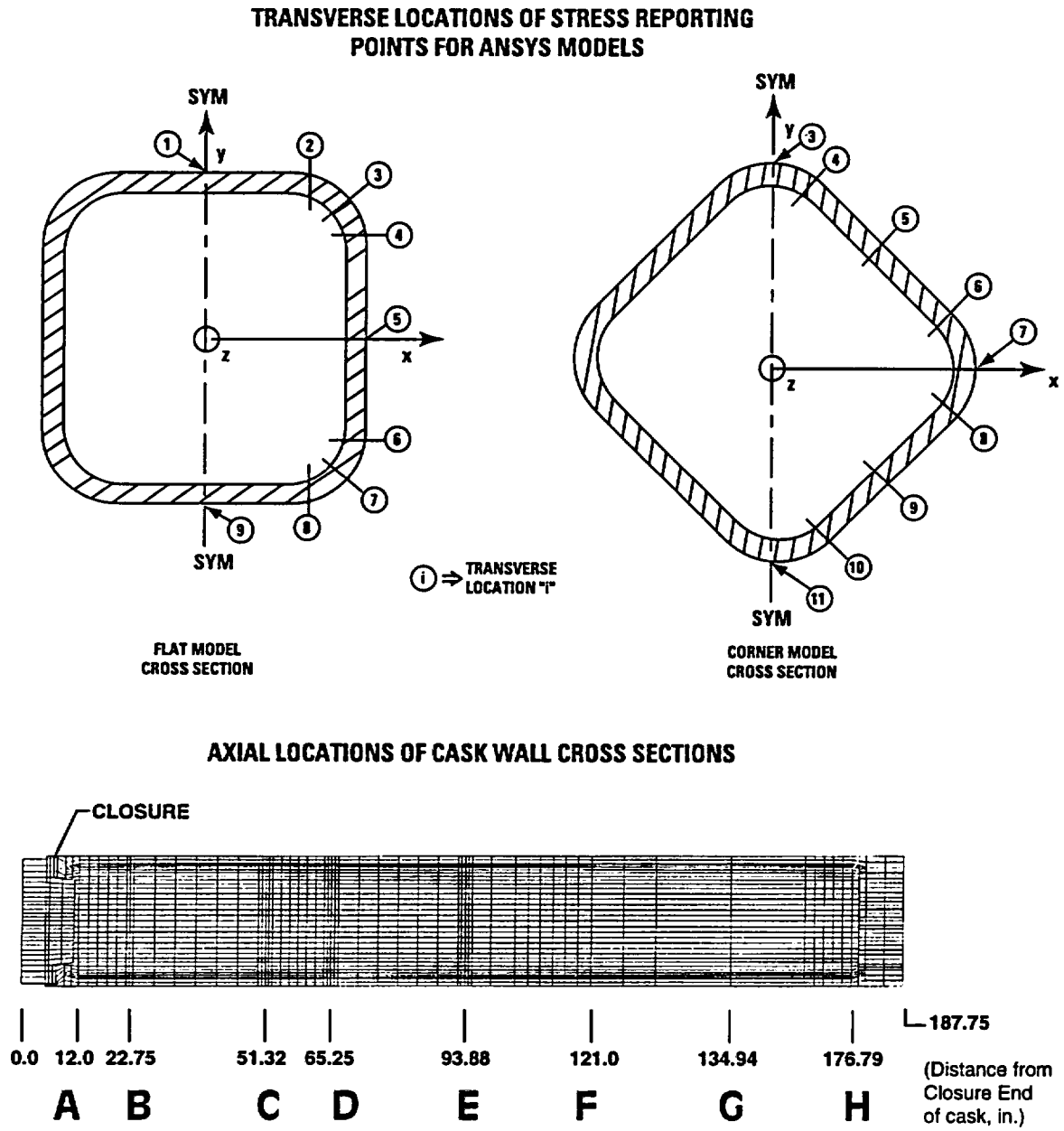

Fig. 2.10.2-1. Schematic of GA-4 cask wall showing symmetry planes

DU and the neutron shield are simulated as mass added to the cask wall, to give the proper weight distribution. Ignoring the stiffness of the DU and neutron shield shell makes the model's stress results conservative for the cask wall.

Although the models have different impact orientations, the finite element discretization was essentially the same. The ANSYS input for the geometric model, material properties, boundary conditions, and loadings was generated using a FORTRAN program. The following subsections provide the details about the element types, model geometries, material and section properties and boundary conditions. The loadings for the base case analyses are described in Section 2.10.2.2.

2.10.2.1.1 ANSYS Element Types and Model Mesh Size Study. The ANSYS models used for the base case analyses have five types of elements. The element types used include SOLID45, SHELL63, LINK8, CONTAC52 and MASS21. The SOLID45 elements were used to simulate the cask containment boundary which includes the cask wall, closure, flange and bottom. A few SOLID45 elements were used for the attachment of the cavity liner to the flange portion of the cask. The remainder of the cavity liner and the FSS were simulated using the SHELL63 elements. LINK8 elements were used to simulate the bolts securing the closure to the cask body and the tie-to-ground for the model. The closure/flange mating surface and radial interface were simulated as gaps with CONTAC52 elements. Additionally, CONTAC52 elements were used to simulate the radial load transfer capability of the DU between the cavity liner and the cask wall. The purpose of these gaps was to assure that the closure was supported by the flange in the side drop events and that the FSS/cavity liner followed the displacement of the cask wall. MASS21 elements were used to simulate the inertial effects of the fuel, FSS, cavity liner and DU during the side drop cases.

Element type SOLID45 is an isoparametric, three-dimensional solid, which can be represented by four, six or eight nodes. Each node has three degrees of freedom: X, Y or Z translations. Although this element has plasticity, creep, swelling, stress stiffening, large deflection and large strain capabilities, they were not used in the cask analysis. Either six or eight node SOLID45's were used with isotropic, linearly elastic material properties.

The SHELL63 element is a three or four-node, elastic shell with both bending and membrane capabilities. There are six degrees of freedom at each node which include X, Y, and Z translations and rotations about the X, Y and Z axes. For the cask analysis, the SHELL63's were assumed to be a uniform thickness with isotropic, linearly elastic material properties and that the cavity liner and FSS experienced small deflections. In particular, the stress stiffening and large deflection capabilities of the SHELL63 were not used.

The LINK8 element is a three-dimensional spar. It is a uniaxial tension-compression element with three displacement degrees of freedom (X, Y and Z directions) at each node. As with the SOLID45 element, plasticity, creep, swelling, and stress stiffening capabilities are available. There is no bending capability for the element. The element is defined by two nodes, its cross-sectional area, the initial strain and selected material properties. For the cask analysis, the LINK8 elements representing the bolts included the bolt cross-sectional area, an initial strain representative of the bolts' preload and a constant, elastic modulus. The LINK8's, which were used to check the model's load balance, used a cross-sectional area, a constant, elastic modulus and an initial strain of zero.

CONTAC52 elements are used to represent node-to-node interaction of two surfaces which may slide relative to each other or come in contact with each other without penetration. "The element is capable of supporting only compression in the direction normal to the surfaces and shear (Coulomb friction) in the tangential direction." (ANSYS Manual) There are three displacement degrees of freedom and the element can be initially preloaded in the normal direction or given a gap specification. As used in the cask models, this element type was used to prevent penetration of the closure by the flange and to assure that the cavity liner behaved as it would if the DU were explicitly included in the finite element model. The effects of sliding friction were neglected and initial contact between the various surfaces was assumed.

MASS21 is a mass, point element having up to six degrees of freedom: translations in the nodal x, y and z directions and rotations about the nodal x, y and z axes. It is possible to assign different mass and rotational inertia terms to each coordinate direction. In the cask model, these elements were assigned mass values in the three coordinate directions.

To minimize the number of nodes and elements used in the ANSYS models a study was performed to determine the model mesh size required to provide accurate stress results. A 20-in.-long quarter-section of the cask wall cross section, representing the geometry along the length of the cask, was simulated for an internal pressure load case. Three different element divisions were used with either six, three or two elements through the wall thickness. The base case used a fine mesh grid with six elements through the thickness, meshed with a 1:1:1 (in the x-direction: y-direction: z-direction) aspect ratio in the corner portion of the model. The different mesh configurations modeled are shown in Fig. 2.10.2-2. Symmetry boundary conditions were applied to the lines of symmetry shown in the figure. The axial ends of the model were also assumed to have symmetrical boundary conditions. This assured that the ends remained in a plane, but the axial fixity is conservative for a direct comparison with the cask simulation. A uniform internal pressure of 100 psi was applied to the walls and a static ANSYS analysis was run.

The study indicated that two elements through the thickness meshed at approximately 1:1:1 (X:Y:Z, using the 3-D element) produced bending stresses through the thickness within six percent of the fine-grid model. The element aspect ratio of the ANSYS base case models was, therefore, kept close to 1:1:1 in the stress reporting locations with two elements through the thickness. It should be mentioned that the inside corner region is a high stress gradient location under the loading condition studied (internal pressure) and that the pressure induced stresses are relatively small compared to the induced axial stress from the drops. The axial induced stresses are more or less uniform through the thickness; therefore, the overall accuracy is expected to be significantly higher than six percent.

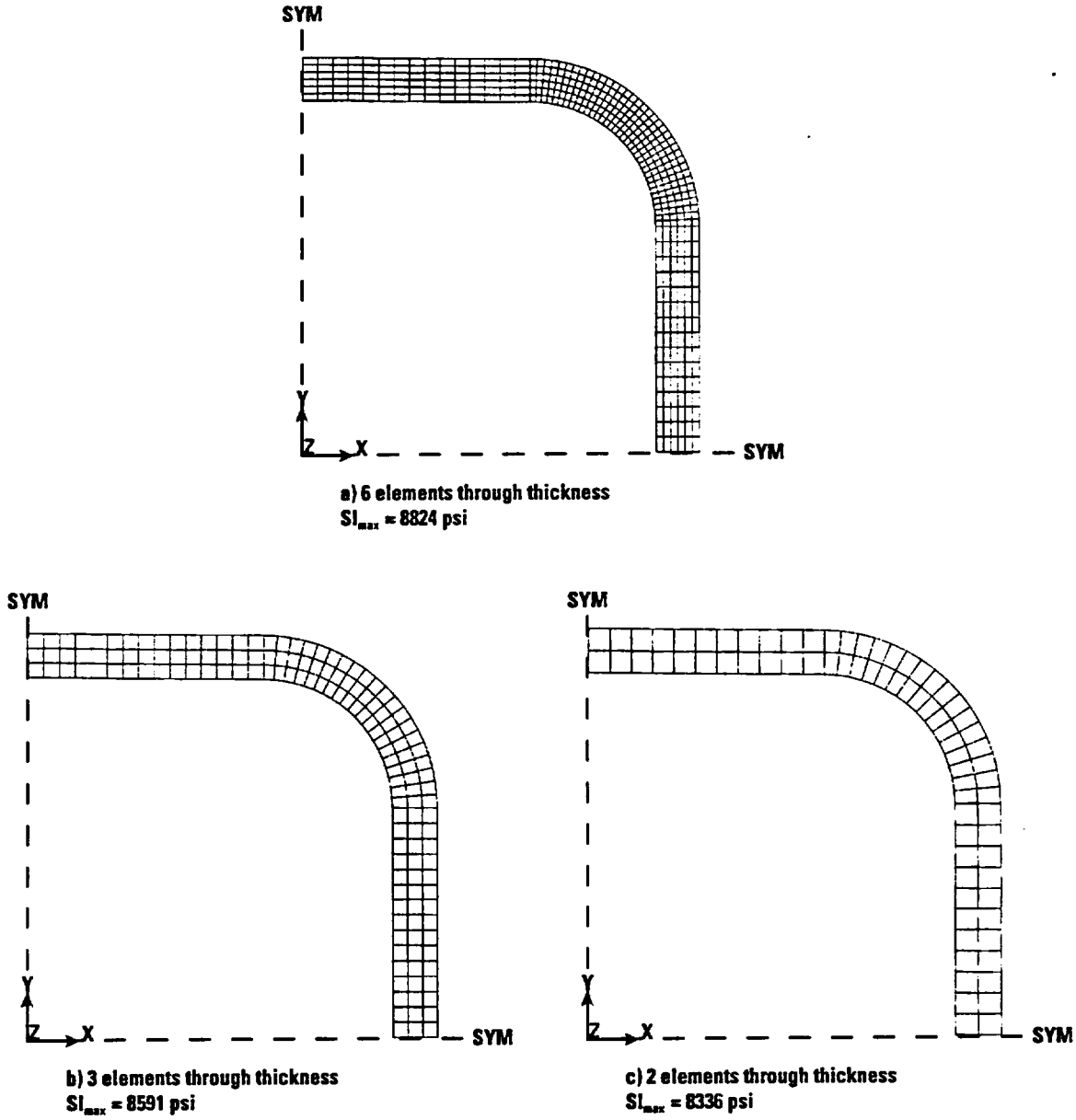

Fig. 2.10.2-2. Finite element mesh size models and results

2.10.2.1.2 Flat Model Geometry. The flat model has one flat wall parallel to the ground. The model uses 16,044 nodes and 23,314 elements to describe the geometry. To facilitate post-processing of ANSYS results, the finite element model was broken into various components representative of the actual geometry. The major components selected for definition were the FSS, the cavity liner, the constant thickness portion of the cask wall, the bottom plate, the flange, and closure. Additional portions of the model included the contact elements, the mass elements, the bolt and tie-to-ground elements. The flat model has bolts simulated at seven locations. Two of the bolts are located on the plane of symmetry, so the total bolt cross-sectional area was equivalent to six bolts. The components, element and material types, number of nodes and elements for each and the volumes associated with each of the components are summarized in Table 2.10.2-1. ANSYS model plots were used to show each of the major components in Figs. 2.10.2-3 through 2.10.2-8. Symmetry boundary conditions were assumed in the Y-Z plane (fixed in the X direction) at the model's symmetry boundary for the entire length of the cask. The ANSYS flat model is presented in Fig. 2.10.2-9 and an isometric view of the closure end showing the FSS and cavity liner in Fig. 2.10.2-10 (the gap elements between the cavity liner and containment wall were removed in this view). The model's weight is compared with the actual cask in Table 2.10.2-3. The total weight is representative of both the flat and corner models. The model densities and lumped masses for the side drop conditions were chosen to match the per length weight distribution of the cask.

TABLE 2.10.2-1
DETAILS OF ANSYS FLAT MODEL OF THE GA-4 CASK

Component Label	Element No.-Type	Material Type	Number of Nodes	Number of Elements	Volume (in.^{3})
FSS	2-SHELL63	8	1045	1296	3665.36
LINER (Cavity Liner)	2-SHELL63 9-SOLID45	4	3105	2640	2,417.92
CASKWALL	9-SOLID45	3	7425	4752	11,658.4
BOTTOM	9-SOLID45 10-SOLID45	5	2031	1664	3434.88
FLANGE	9-SOLID45	2	1620	1056	1011.91
CLOSURE	9-SOLID45 10-SOLID45	1	1515	1412	2619.08
Bolts and Ties-to-ground	6-LINK8	6-Ties 9-Bolts	18	10	26.5218
Miscellaneous	3-MASS21 5-CONTAC52	1 7 and 10	1542 5320	6724 3760	N/A N/A
SUM	N/A	N/A	N/A	23,314	24,834.1
Whole Model	N/A	N/A	16,044	23,314	24,834.1

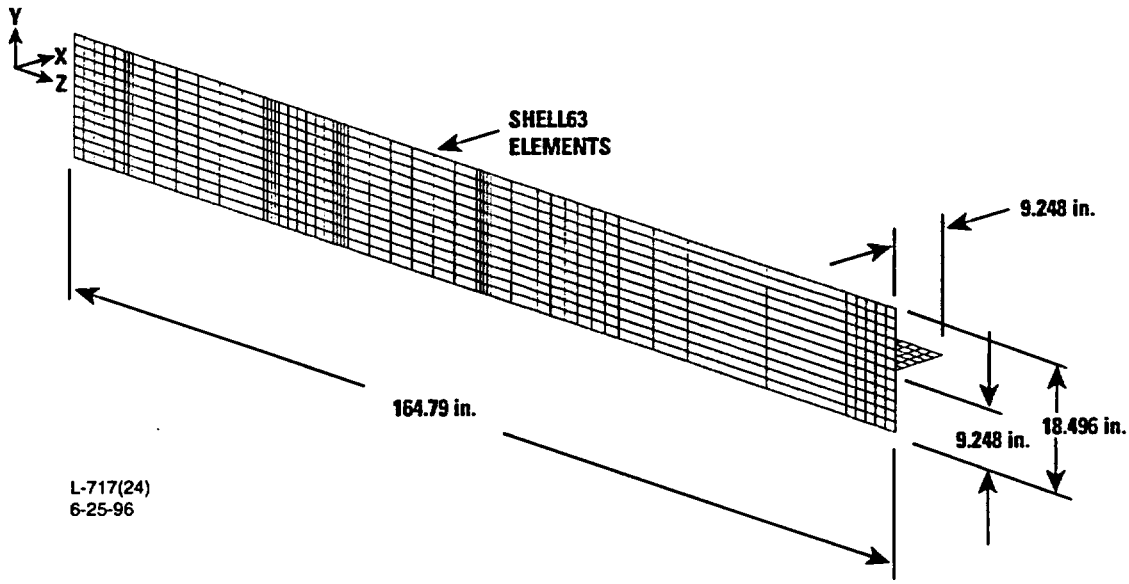

Fig. 2.10.2-3. FSS component of the ANSYS flat model of the GA-4 cask

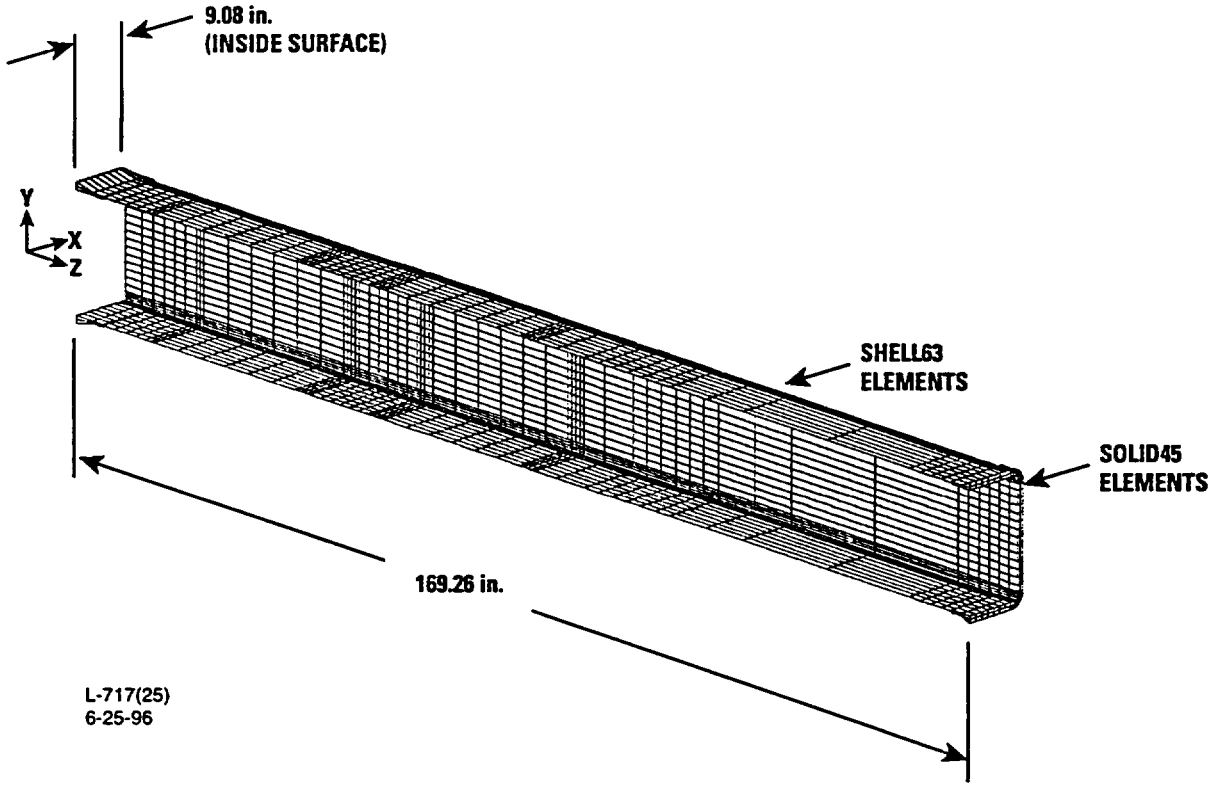

Fig. 2.10.2-4. LINER component of the ANSYS flat model of the GA-4 cask

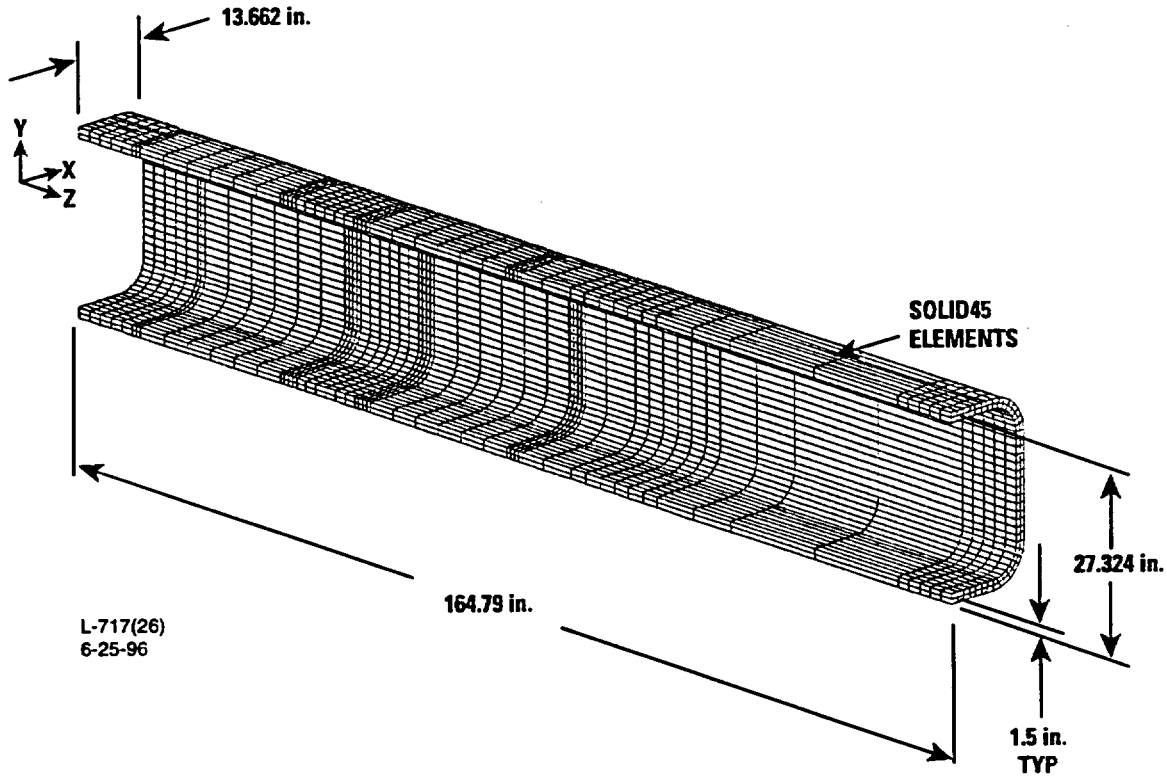

Fig. 2.10.2-5. CASKWALL component of the ANSYS flat model of the GA-4 cask

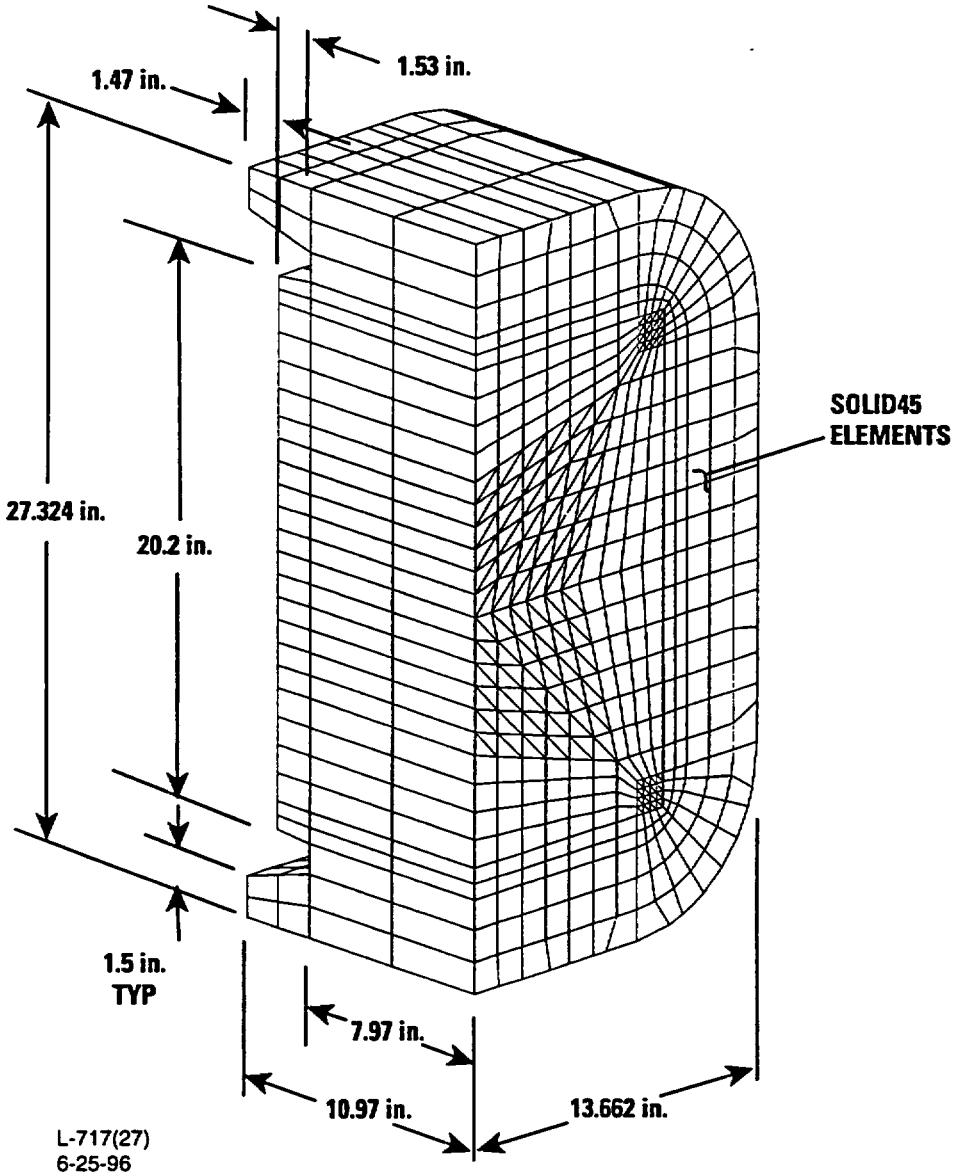

Fig. 2.10.2-6. BOTTOM component of the ANSYS flat model of the GA-4 cask

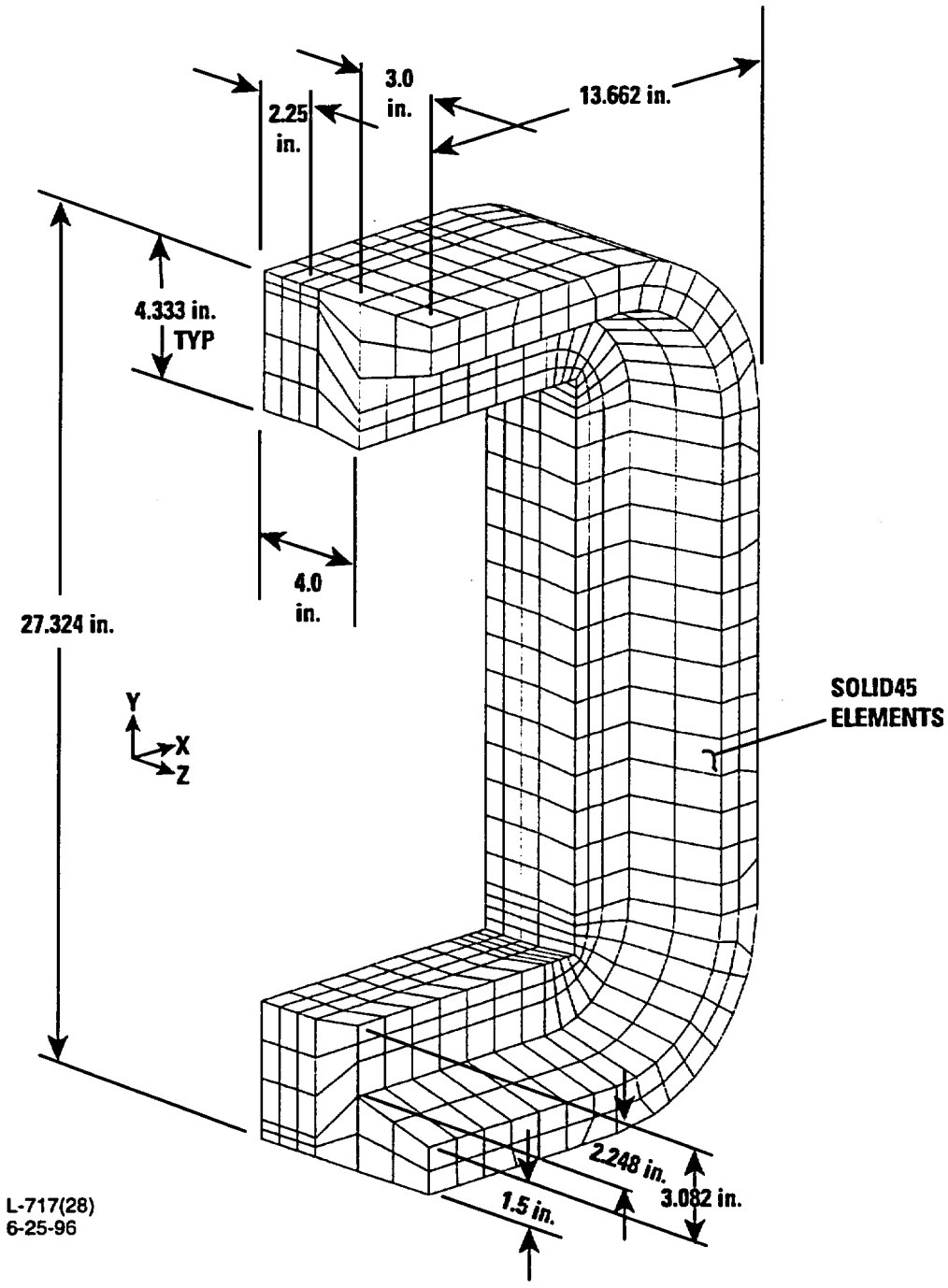

Fig. 2.10.2-7. FLANGE component of the ANSYS flat model of the GA-4 cask

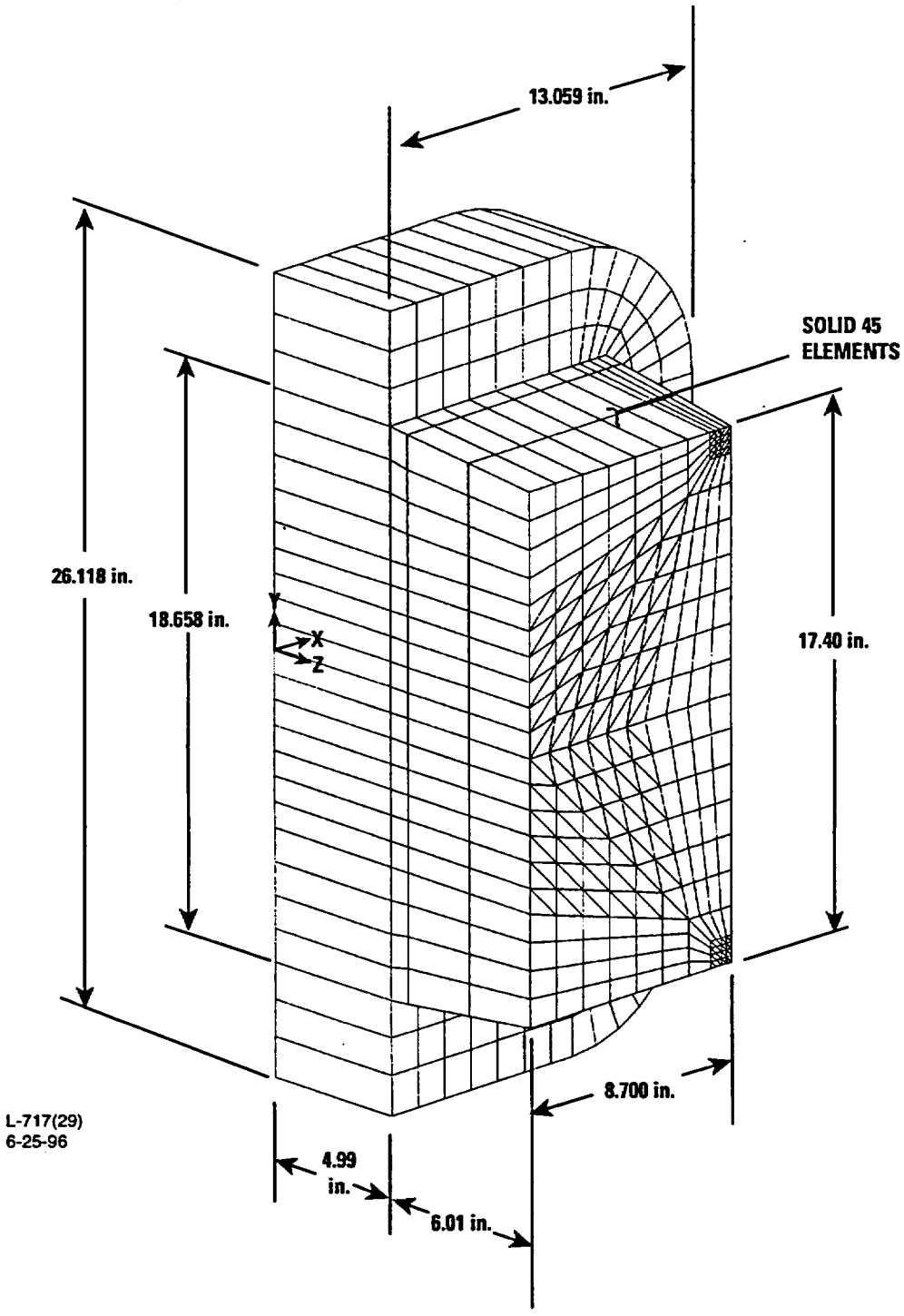

Fig. 2.10.2-8. CLOSURE component of the ANSYS flat model of the GA-4 cask

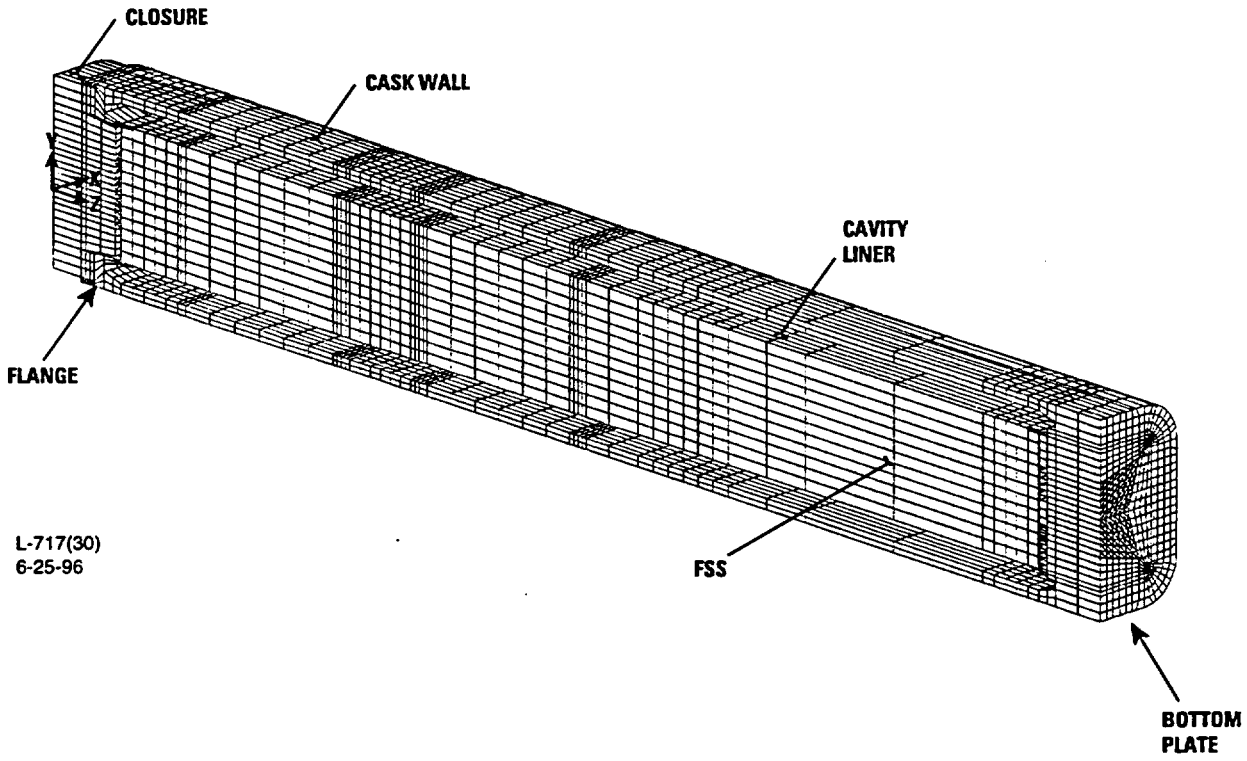

Fig. 2.10.2-9. ANSYS flat model of the GA-4 cask

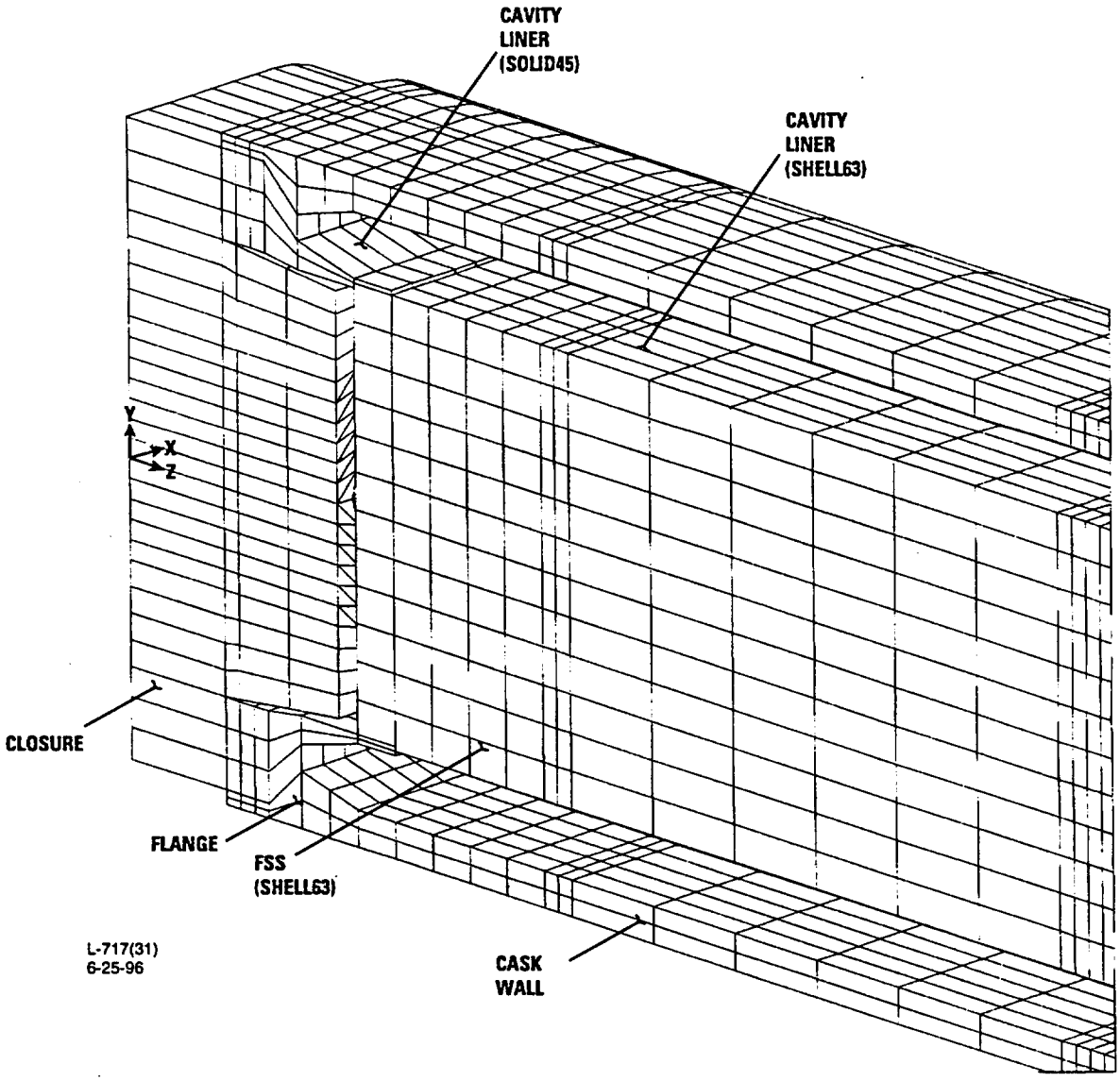

Fig. 2.10.2-10. Isometric view of the closure end of the ANSYS flat model of the GA-4 cask

2.10.2.1.3 Corner Model Geometry. The corner model has a corner of the cask closest to the ground with the cask axis parallel to the ground. The model uses 15,776 nodes and 28,674 elements to describe the geometry. To facilitate post-processing of ANSYS results, the finite element model was broken into various components representative of the actual geometry. The major components selected for definition were the FSS, the cavity liner, the constant thickness portion of the cask wall, the bottom, the flange, and closure. Additional portions of the model included the contact elements, the mass elements and the bolt and tie-to-ground elements. The corner model has bolts simulated at six locations. The components, element and material types, number of nodes and elements for each and the volumes associated with each of the components are summarized in Table 2.10.2-2. ANSYS model plots were used to show each of the major components in Figs. 2.10.2-11 through 2.10.2-16. Symmetry boundary conditions were assumed in the Y-Z plane (fixed in the X direction) at the model's symmetry boundary for the entire length of the cask. The ANSYS corner model is presented in Fig. 2.10.2-17 and an isometric view of the closure end showing the FSS and cavity liner in Fig. 2.10.2-18 (the gap elements between the cavity liner and containment wall were removed in this view). The model's weight is compared with the actual cask in Table 2.10.2-3. The total weight is representative of both the flat and corner models. The model densities and lumped masses for the side drop conditions were chosen to match the per length weight distribution of the cask.

TABLE 2.10.2-2
DETAILS OF ANSYS CORNER MODEL OF GA-4 CASK

Component Label	Element No. — Type	Material Type	Number of Nodes	Number of Elements	Volume (in.^{3})
FSS	2-SHELL63	8	715	1296	3665.36
LINER (Cavity Liner)	2-SHELL63 9-SOLID45	4	3105	2640	2,417.92
CASKWALL	9-SOLID45	3	7425	4752	11,658.4
BOTTOM	9-SOLID45 10-SOLID45	5	2035	1664	3434.88
FLANGE	9-SOLID45	2	1620	1056	1011.91
CLOSURE	9-SOLID45 10-SOLID45	1	1520	1412	2619.08
Bolts and Ties-to-ground	6-LINK8	6-Ties 9-Bolts	16	10	26.5335
Miscellaneous	3-MASS21 5-CONTAC52	1 7,10	2532 5320	12,084 3760	N/A N/A
SUM	N/A	N/A	N/A	28,674	24,834.1
Whole Model	N/A	N/A	15,776	28,674	24,834.1

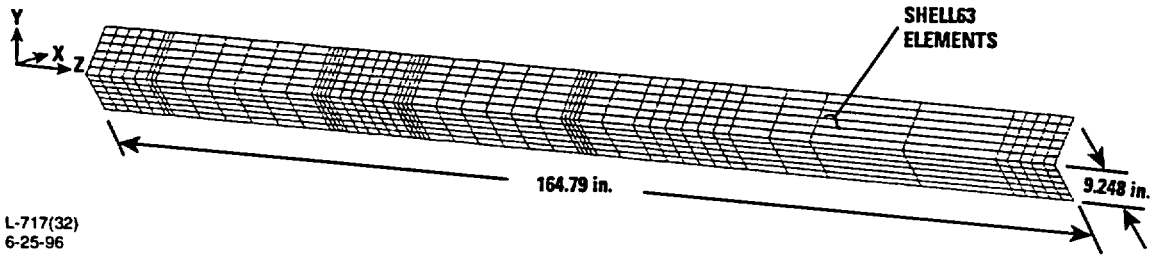

Fig. 2.10.2-11. FSS component of the ANSYS corner model of the GA-4 cask

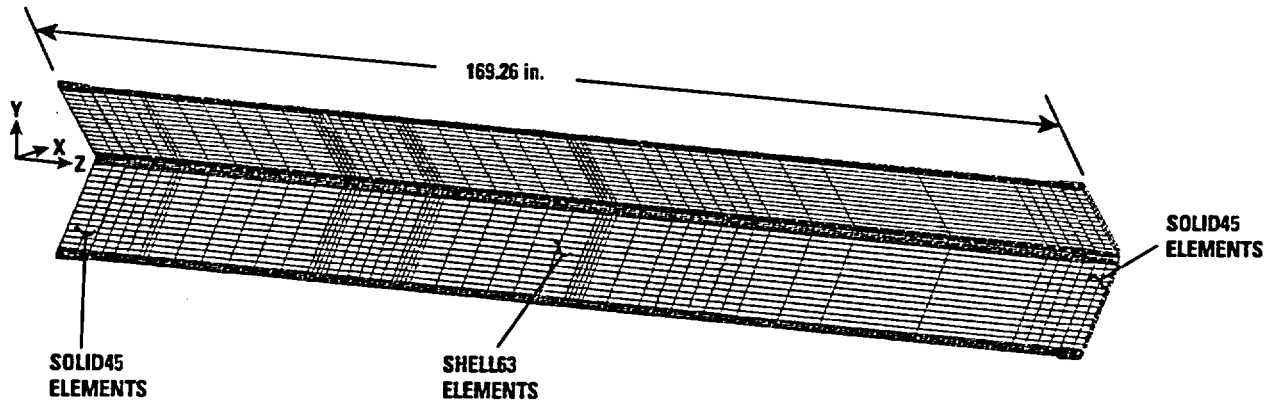

Fig. 2.10.2-12. LINER component of the ANSYS corner model of the GA-4 cask

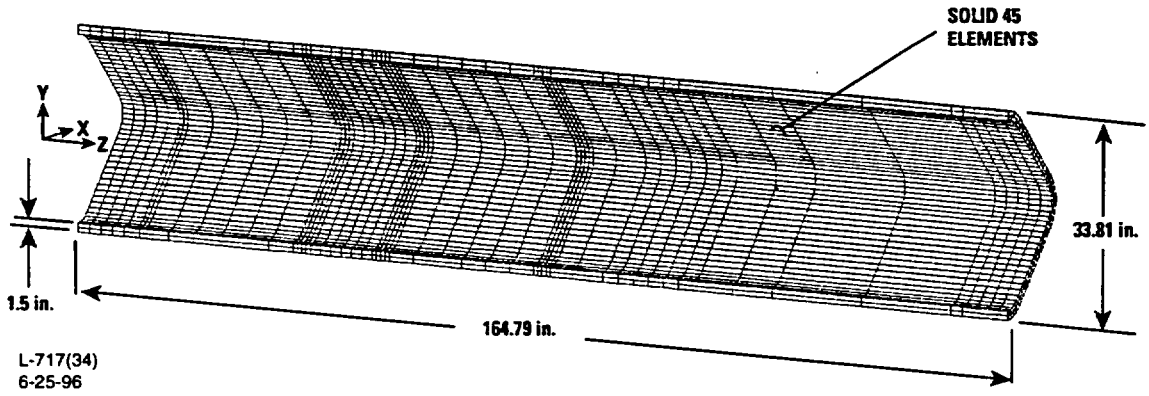

Fig. 2.10.2-13. CASKWALL component of the ANSYS corner model of the GA-4 cask

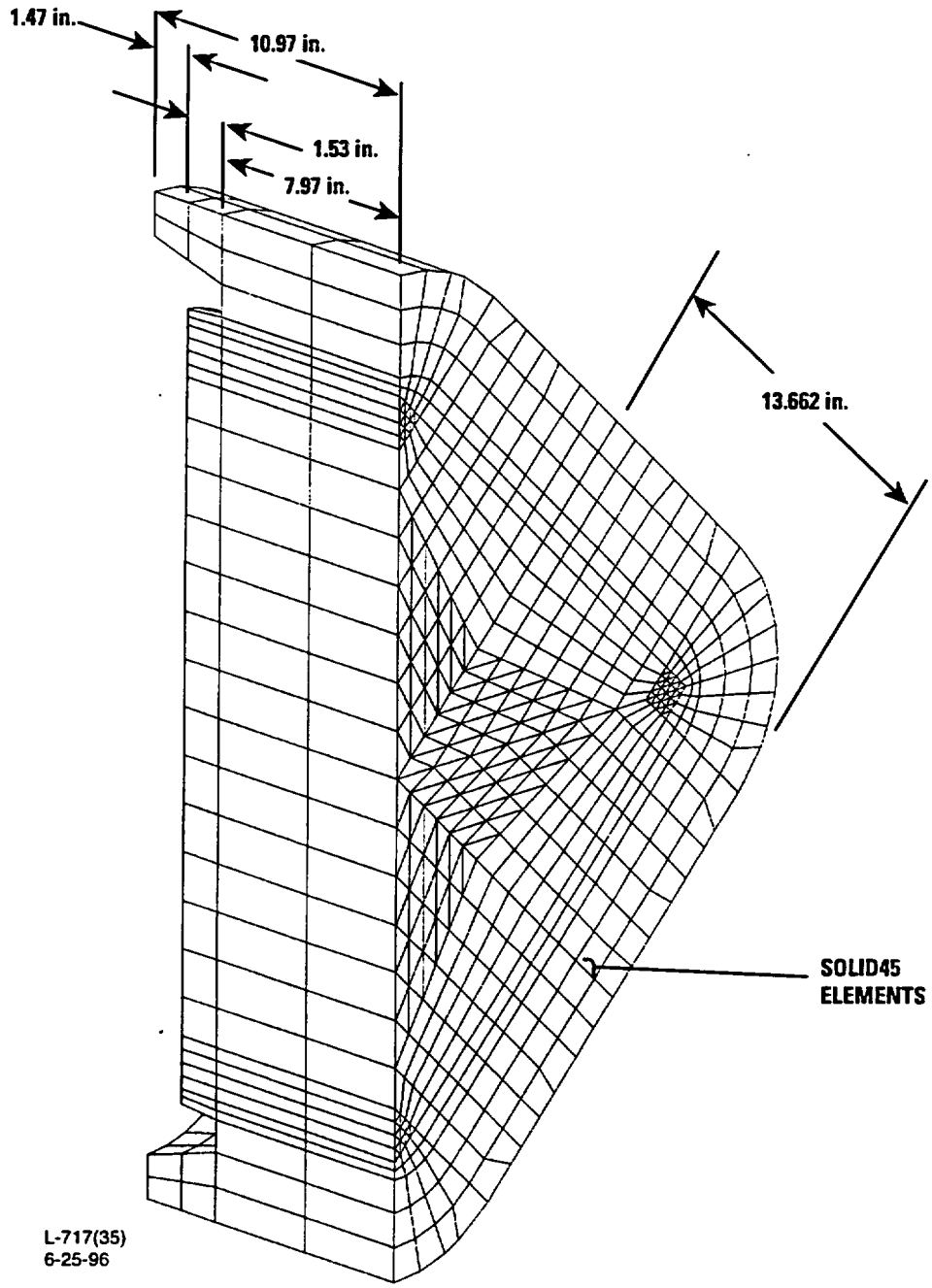

Fig. 2.10.2-14. BOTTOM component of the ANSYS corner model of the GA-4 cask

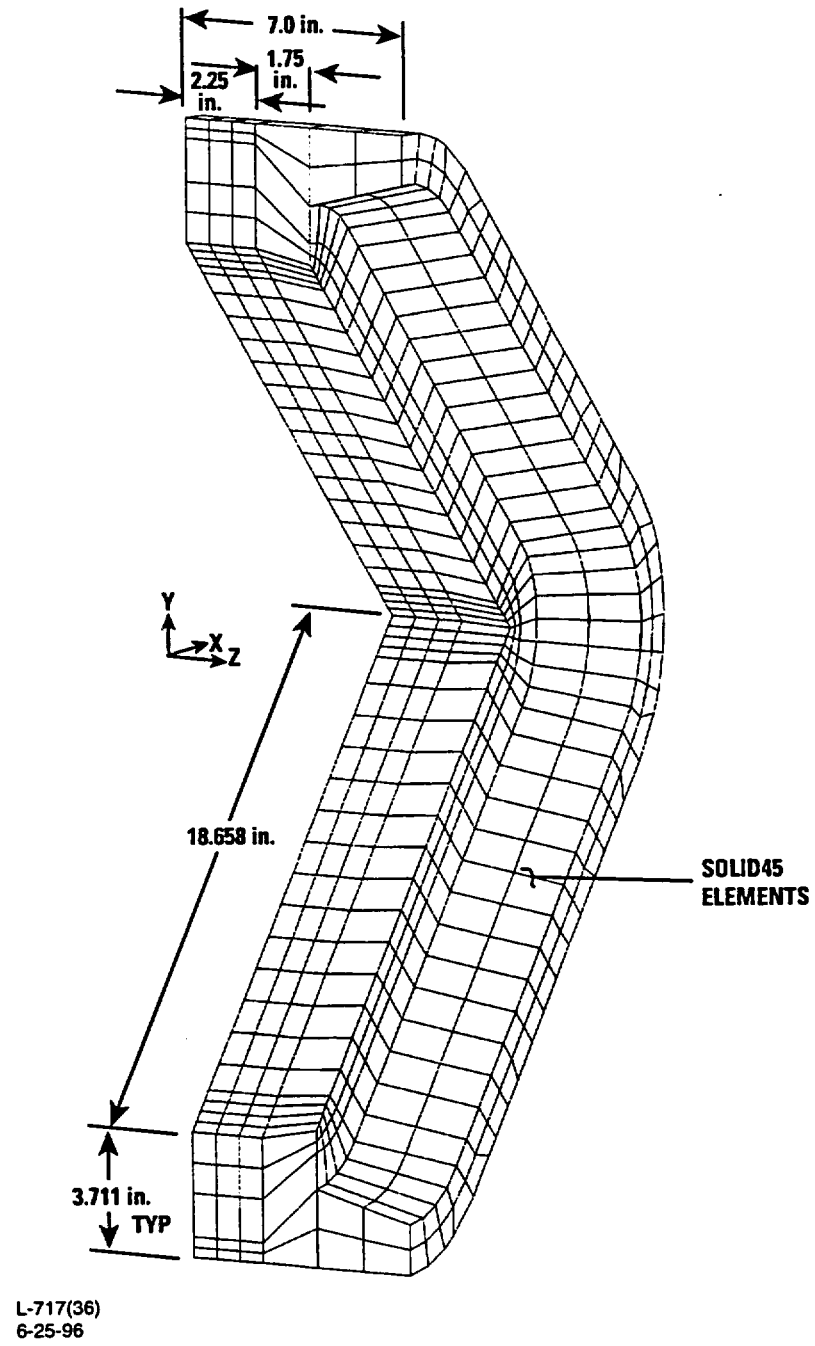

Fig. 2.10.2-15. FLANGE component of the ANSYS corner model of the GA-4 cask

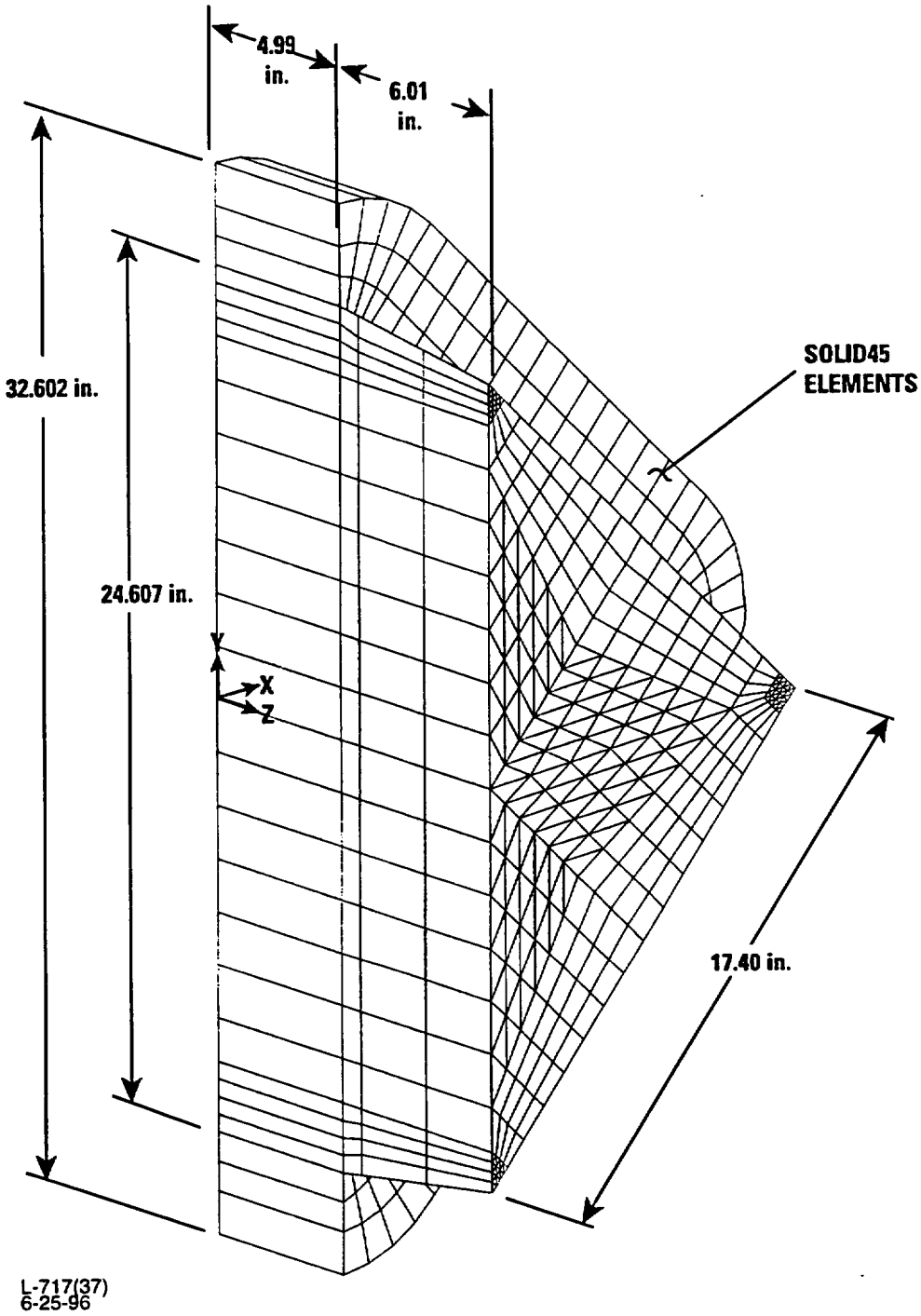

Fig. 2.10.2-16. CLOSURE component of the ANSYS corner model of the GA-4 cask

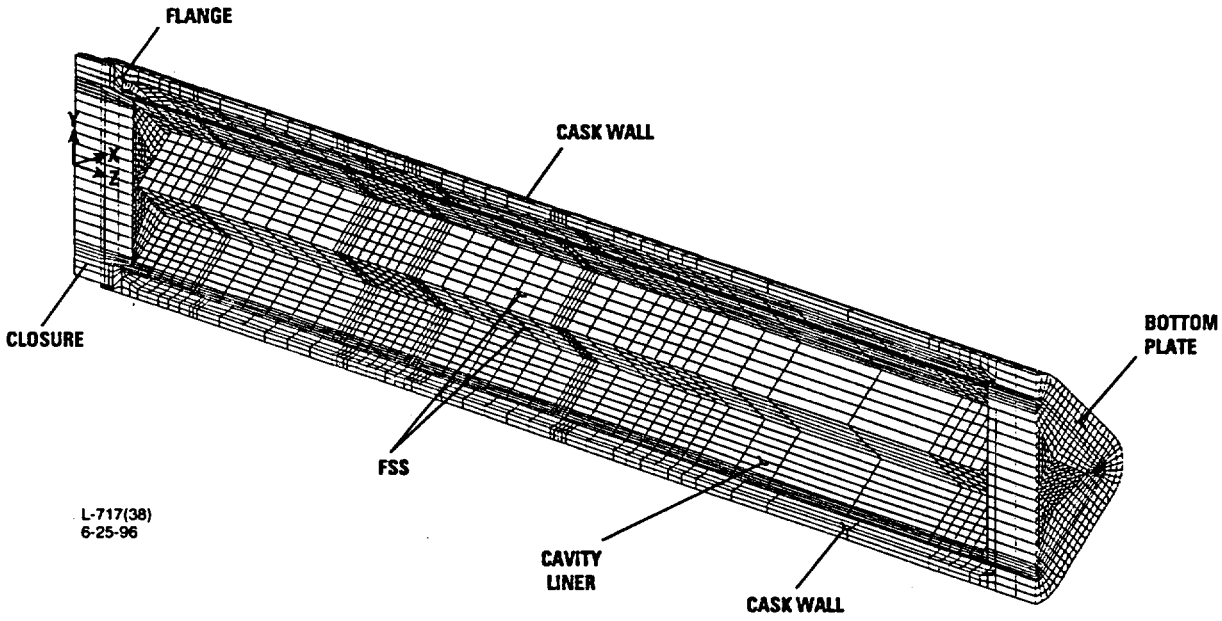

Fig. 2.10.2-17. ANSYS corner model of the GA-4 cask

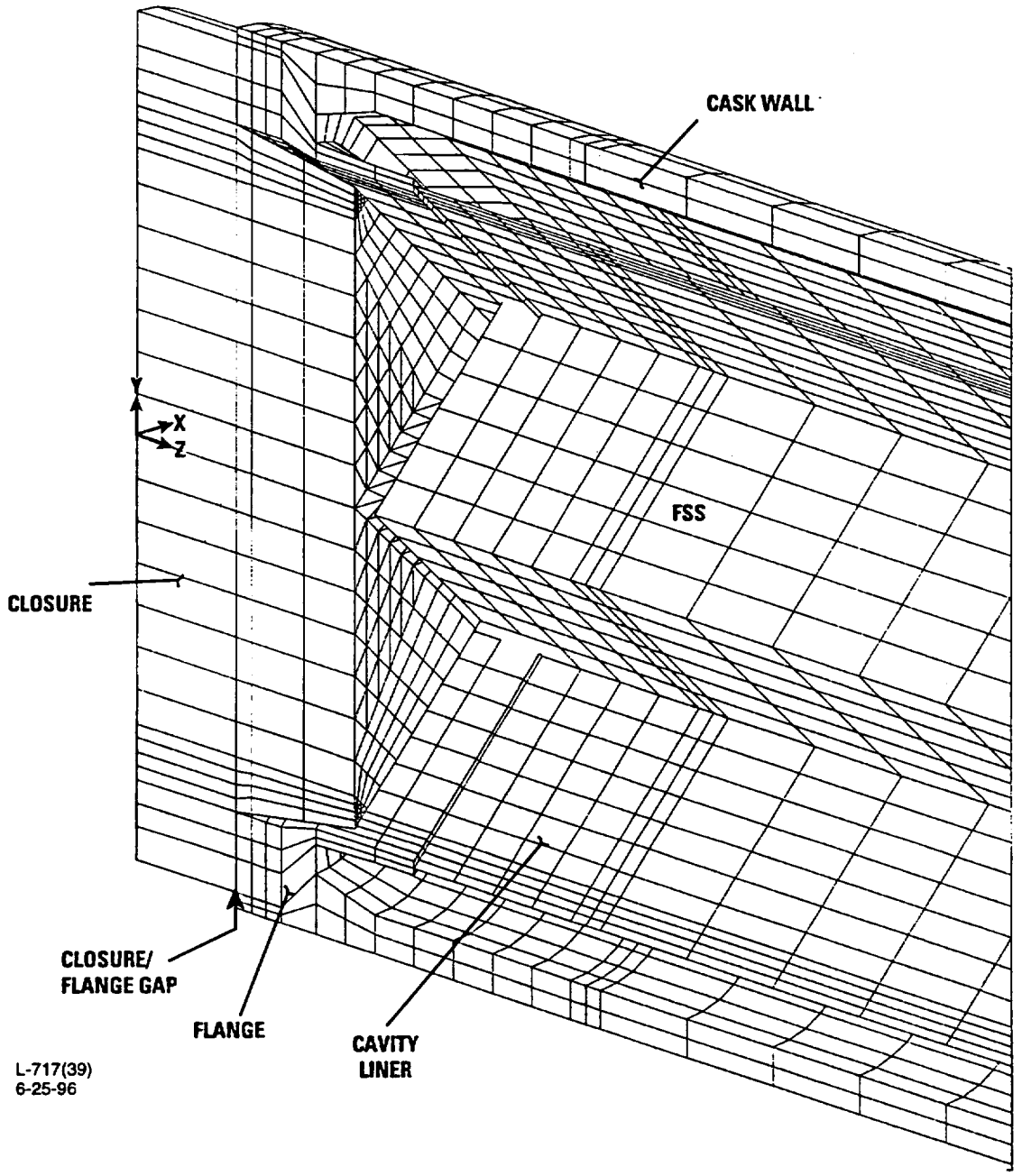

Fig. 2.10.2-18. Isometric view of the closure end of the ANSYS corner model of the GA-4 cask

TABLE 2.10.2-3
WEIGHT DISTRIBUTION BASED ON ANSYS-DEVELOPED VOLUMES

Location	Component	Model Mass Density[b] ($lb\text{-}s^2/in.^4$)	Model Volume[c] ($in.^3$)	Model Weight[c][e] (lb)	Actual Weight[c] (lb)
MIDSECTION[a]					
Cask Body					
	Neutron shield (plus pads)[b]	–	–	–	1,948.5
	1.5 in. wall	1.1342E-03	11,658.	5,109.	3,330.5
Subtotal		N/A	11,658.	5,109.	5,279.
Internals					
	FSS[d]	–	3,665.	–	375.5
	Cavity liner[d]	–	2,418.	–	650.
	Fuel[d]	–	–	–	3324.
	DU[d]	–	–	16,729.	12,267.5
Subtotal		N/A	6,083.	16,729.	16,617.
Total Midsection		N/A	17,742.	21,838.	21,896.
CASK ENDS					
Top End					
	Flange	2.0192E-03	1,011.	789	See total
	Closure	2.0192E-03	2,619.	2,043.	See total
Subtotal		N/A	3,630.	2,833.	2,683.
Bottom end Subtotal		2.1344E-03	3,435.	2,833.	2,683.
Total cask ends			7,065.	5,666.	5,366.
Total cask model		N/A	24,807.	27,500.	27,263.

[a] Includes model between axial dimensions of 12.0 and 176.79 in.
[b] Includes weight of neutron shield skin, neutron shield and neutron shield hardware, which are not explicitly modeled. The mass of the components is included by increasing the density of the containment wall.
[c] Model volume and weights are for half of the actual cask.
[d] The FSS, cavity liner, fuel and DU were included as lumped masses attached to the inner nodes of the containment wall where the DU is supported.
[e] The weight of the cask midsection was adjusted to provide the correct weight distribution of 132.5 lb/in. (265 lb/in. for the total cask, see Table 2.2-1).

2.10.2.1.4 Material and Section Properties. Table 2.10.2-4 presents the material properties as a function of the element's material number for the ANSYS cask models. Tables 2.10.2-1 and 2.10.2-2 give the material numbers for the various portions of the model. The elastic modulus of stainless steel type XM-19 at a temperature of 180°F (avg. axial cask wall temperature) was used for all model components, except the bolts which were simulated as bolting material alloy N07718 and the FSS which used a reduced stainless steel modulus to account for the holes in it. The material properties were considered constant for the analysis, since temperature effects were not evaluated with the ANSYS model. The densities used for the modeling were chosen to provide the proper weight distribution along the axial length of the cask, as shown in Table 2.10.2-3.

Table 2.10.2-5 summarizes additional element characteristics needed for the ANSYS model. In particular, the SHELL63 elements require a shell thickness. These elements, which were used for the FSS and cavity liner were assumed to be a uniform thickness. The FSS was input as 0.6 in. thick with a reduced modulus to provide the proper membrane stiffness in the axial direction. The portion of the cavity liner modeled with SHELL63 elements had a 0.375-in. thickness.

LINK8 elements require cross-sectional area input and it is possible to include an initial strain. The bolts were modeled with LINK8 spar elements. The modeled bolt element length is 7.28 in. long and the initial strain for the bolts was calculated as 1.488E-03 in Section 2.10.2.1.4.1. The tie-to-ground elements were soft springs in order to demonstrate the model's equilibrium. They had a small cross-sectional area and a 10-in. length. The tie-to-ground did not have an initial strain input. The interface gap elements (CONTAC52) joined the cask flange and the closure in both the radial and axial directions and provided load transference capability from the cask wall to the FSS and cavity liner. The initial setting on the interface gaps was 0.0, indicating a closed condition. The gap element stiffness was adequate to prevent penetration of the closure and cask flange and transmit the loads from the cask wall to its internals.

2.10.2.1.4.1 Closure Bolts' Initial Strain Calculation. The initial strain in the closure bolts caused by torquing was calculated for input to the ANSYS model. The value of initial strain used for the LINK8 elements was modified to give the correct force acting on the bolts.

Using the initial stress calculated in Section 2.6.5.3, the tensile force acting in each of the closure bolts is given by:

$$F_{bolt} = (\sigma_{initial})(A_x),$$

where

$\sigma_{initial}$ = the initial stress in the closure bolt (34,805 psi), and

A_x = the closure bolt cross-sectional area (0.606 in.^{2}).

Substituting in the equation for F_{bolt}, we have,

$$F_{bolt} = (34{,}805 \text{ psi})(0.606 \text{ in.}^2),$$

$$= 21{,}092 \text{ lb.}$$

TABLE 2.10.2-4
ANSYS MODEL MATERIAL IDENTIFICATION

Material Number	Elastic Modulus (psi)	Poisson's Ratio	Mass Density ($lb\text{-}s^2/in.^4$)	Comments
1	27.68E+06	0.3	2.0192E-03	
2	27.68E+06	0.3	2.0192E-03	
3	27.68E+06	0.3	1.1342E-03	
4	27.68E+06	0.3	0.000E+00	
5	27.68E+06	0.3	2.0795E-03	
6	27.00E+06	0.3	0.000E+00	Tie-to-ground
7	N/A	N/A	N/A	Initial gap = zero
8	10.345E+06	0.3	0.000E+00	A reduced elastic modulus was used to represent the effect of the holes in the FSS
9	28.65E+06	0.3	7.760E-04	Closure bolts
10	N/A	N/A	N/A	Initial gap = zero

TABLE 2.10.2-5
ANSYS ELEMENT CHARACTERISTICS

Item	ANSYS Element Type	A_x ($in.^2$)	Initial Strain	Thickness (in.)	Stiffness (lb/in.)
FSS	SHELL63	--	--	0.6 [a]	--
Cavity liner	SHELL63	--	--	0.375	--
Bolts	LINK8	0.606 [a]	1.488E-03	--	--
Tie-to-ground restraints	LINK8	0.01	0.0	--	--
Flange/closure interface bolts	CONTAC52	--	--	--	20.0E+06
Gap elements between cavity liner and cask wall	CONTAC52	--	--	--	20.0E+06

[a]Value for elements on the line of symmetry is half the value given in the table.

The initial strain for the LINK8 elements was calculated using the force applied to the bolt. The initial strain is given by the following expression:

$$\varepsilon_{initial} = F_{bolt}/(A_x E),$$

where F_{bolt} and A_x are given above, and E is the elastic modulus (28.65×10^6 psi) for the bolts. Substituting in the equation for $\varepsilon_{initial}$, we have,

$$\varepsilon_{initial} = 21{,}092 \text{ lb}/[(0.606 \text{ in.}^2)(28.65 \times 10^6 \text{ psi})],$$

$$= 1.215 \times 10^{-3} \text{ in./in.}$$

This initial strain was adjusted in the LINK8 elements to closely match the preload force in the bolts. The initial strain used for the LINK8 bolts in the ANSYS models was 1.488×10^{-3}, which resulted in an average bolt axial force of 21,560 lb.

2.10.2.1.5 Boundary Conditions. The flat and corner models assumed symmetry boundary conditions for the nodes on the plane of symmetry. The nodes associated with SOLID45 elements were fixed in the x-direction and the SHELL63 elements were fixed in the x-direction and in the y and z-rotational directions. Two soft, LINK8 elements in the y-direction were used to secure the model to fixed points at each end of the cask. The LINK8 elements were oriented to monitor the force imbalance in the global y-direction. One node in the center of the closure's outer surface was fixed in the z-direction. For the simulated end drops, there was a resultant force (small) at this location.

2.10.2.2 Loading Conditions. The loadings were also developed using the FORTRAN coding which generated the geometry, material property and boundary condition input to ANSYS. The loads input to ANSYS included pressures, nodal forces, accelerations (both linear and rotational, depending upon the particular base case), and lumped masses. Pressures were used to simulate the uniform internal and external pressure base cases and as the impact and inertial loads for the end drop base cases. Nodal forces were used to simulate the impact forces and moments transmitted to the cask through the ILSS ribs for the end, side and oblique drop base cases. Linear accelerations are applied to balance the impact forces for the end and side drop simulations. Both linear and rotational accelerations are added to the oblique drop case to balance the impact forces. Lumped masses were used to simulate the effect of the FSS, cavity liner, fuel and DU during the side and oblique drop base case simulations. The loads applied to the models for each of the base case simulations are described in the following subsections. Figures 2.10.2-19 through 2.10.2-21 show free body diagrams for the end, side and oblique drop base cases, respectively.

2.10.2.2.1 Pressure Loads. For both the flat and corner models a uniform pressure was applied to the cask wall. The two models gave the same results for similar locations, but the two geometries were simulated for easier superposition of the stress results with those of the drop cases.

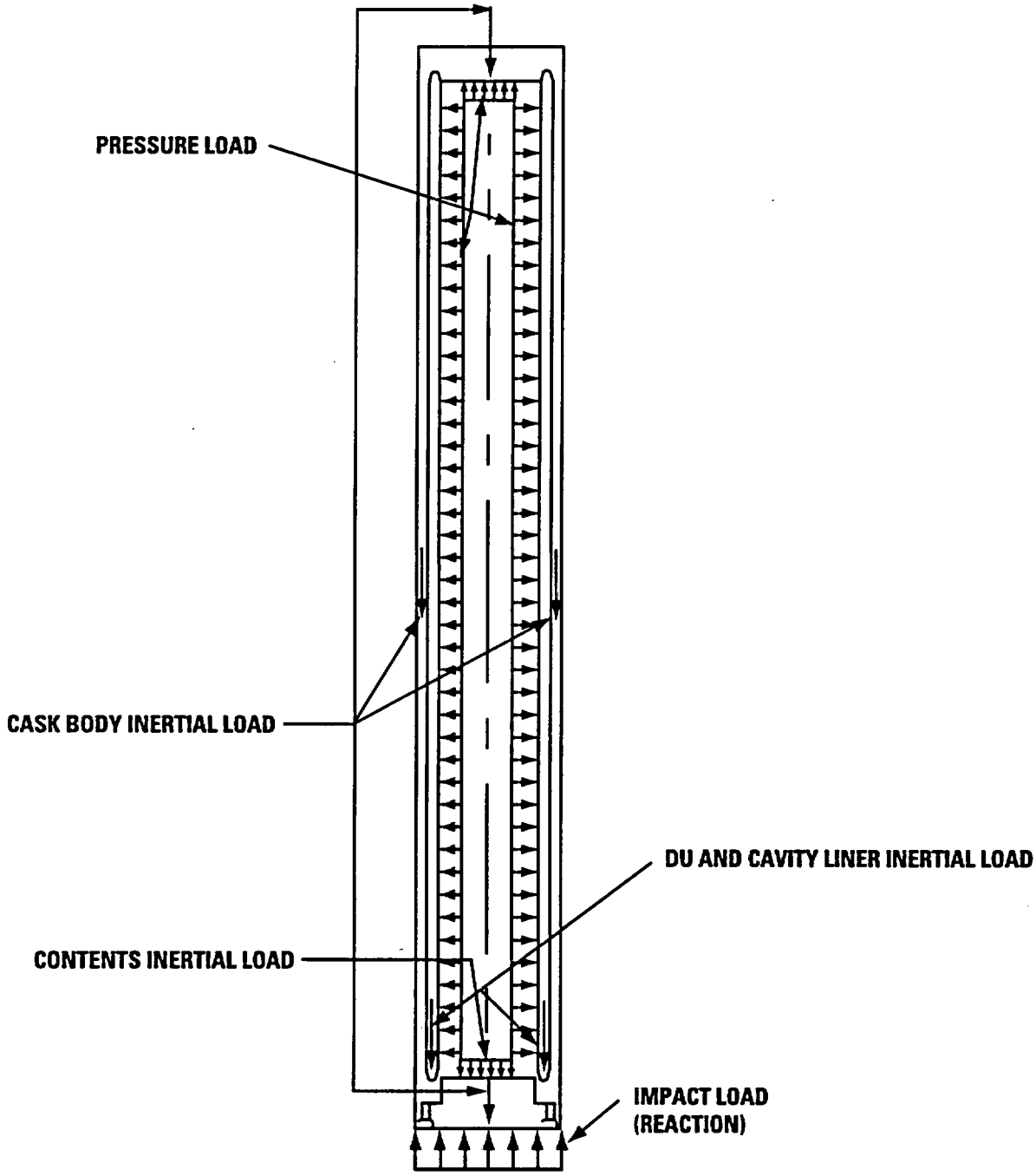

Fig. 2.10.2-19. End drop base case analysis free body diagram

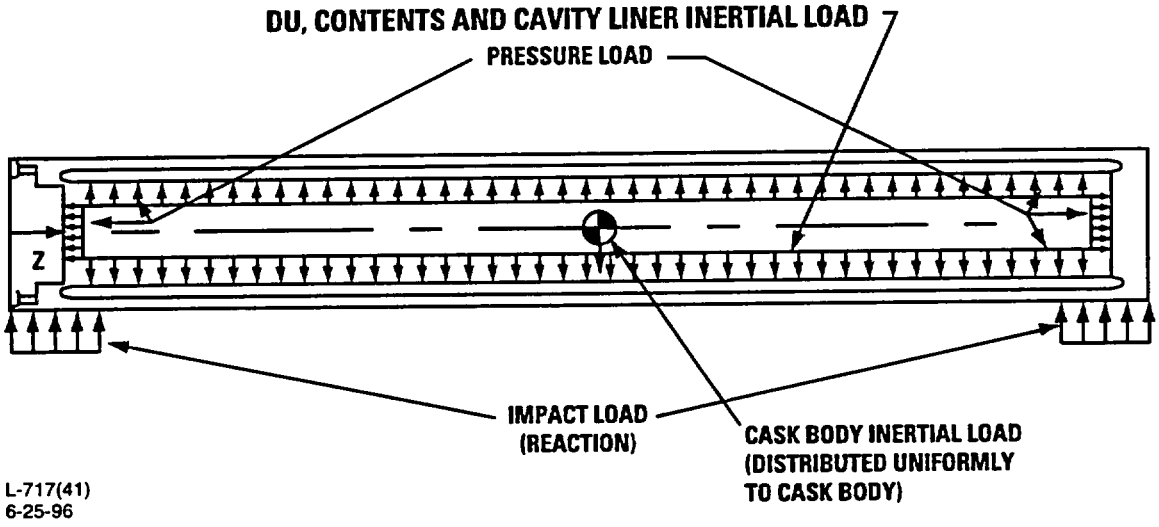

Fig. 2.10.2-20. Side drop base case analysis free body diagram

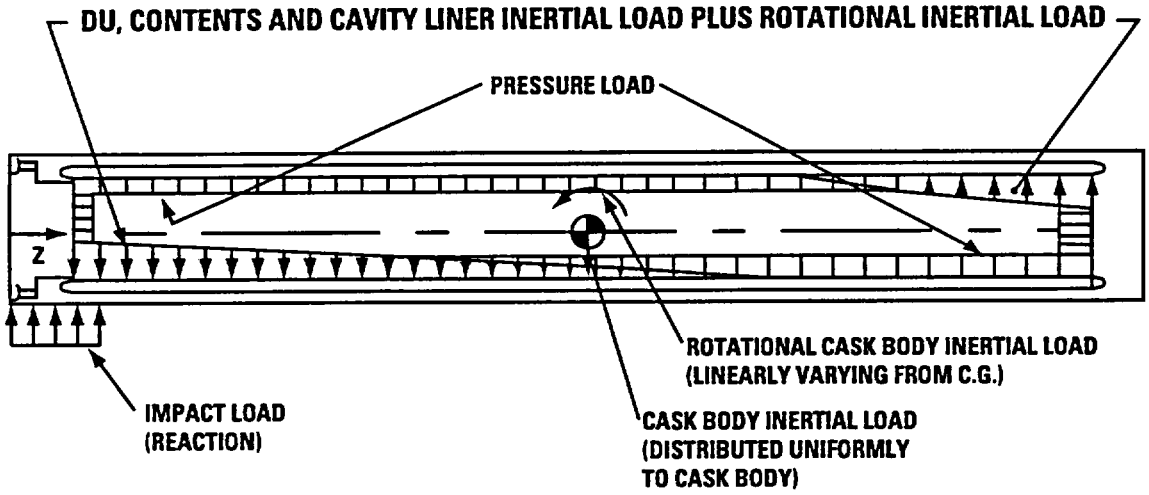

L-717(40)
8-20-96

Fig. 2.10.2-21. Oblique drop base case analysis free body diagram

2.10.2.2.1.1 Internal. The internal pressure MNOP base case had a uniform pressure of 80 psig applied to the inner surface of the cask wall, the closure and the bottom plate. At the closure end all of the flange and closure surfaces from the cask interior to the seal at the flange/closure interface were subjected to the uniform pressure load. The details of this loading are shown in Fig. 2.10.2-22.

2.10.2.2.1.2 External. The external pressure base case had uniform pressure of 290 psi applied to the external surface of the cask side wall, closure and bottom plate. At the closure end all of the flange and closure surfaces from the cask exterior to the seal at the flange/closure interface were subjected to the uniform pressure load. The details of this loading are shown in Fig. 2.10.2-23.

2.10.2.2.2 Dynamic Drop Simulations. The ANSYS model was subjected to statically equivalent loads which simulated three basic drop conditions. The drop conditions analyzed were the end drop, side drop and oblique drop. The end drop assumed that the cask was dropped onto a flat unyielding surface with the cask's axis perpendicular to the drop surface. Both the side and oblique drops simulated impacts with the cask axis parallel to the drop surface. The side drop case assumed that both impact limiters simultaneously struck the ground, while the oblique drop case assumed that only the closure end impact limiter hit. The impact forces calculated by GACAP for selected drop simulations were used as input to the ANSYS models. These impact forces were balanced by linear and angular (for the oblique drop) global accelerations about the model's center-of-gravity and the static solution routine for ANSYS was run. The accelerations needed to balance the input forces were in good agreement with the GACAP results. The forces for the end and oblique drop cases were scaled to give an effective linear acceleration of 10g. The ANSYS end drop input scaled the GACAP results for the 30-ft end drop, while the oblique drop input scaled the slapdown results for a 30-ft drop with a drop angle of 15°. The forces for the side drop case were from a 30-ft drop with both impact limiters simultaneously striking the ground.

2.10.2.2.2.1 30-ft End Drop for Flat and Corner Models. The loadings for this base case are the same for the two different geometries. The only difference is that the corner model's symmetry line cuts two of the ILSS ribs in half. This means that the load applied to these ribs in the model was half the load applied to the other ribs. The total rib load is the same since the flat model has 18 rib locations and the corner model has 17 full and 2 half rib locations.

The 30-ft end drop loading condition assumes the impact occurs on the closure impact limiter with the cask axis perpendicular to the unyielding surface. The 30-ft drop with impact angle of 90° loading condition given in Table 2.10.4-6 was scaled to get the loads for this case. The impact force associated with this case is 3.36×10^6 lb with a vertical acceleration of 61g (Table 2.10.4-2).

The loads applied to the ANSYS model simulate the forces resulting from the vertically accelerated mass of the cask and the impact force experienced by the ILSS. The DU, cavity liner, FSS and fuel are modeled as massless components, therefore the effect of their accelerated masses are simulated as pressure loads. Since the other components of the model include mass density as a material property, their load is calculated by ANSYS using the linear

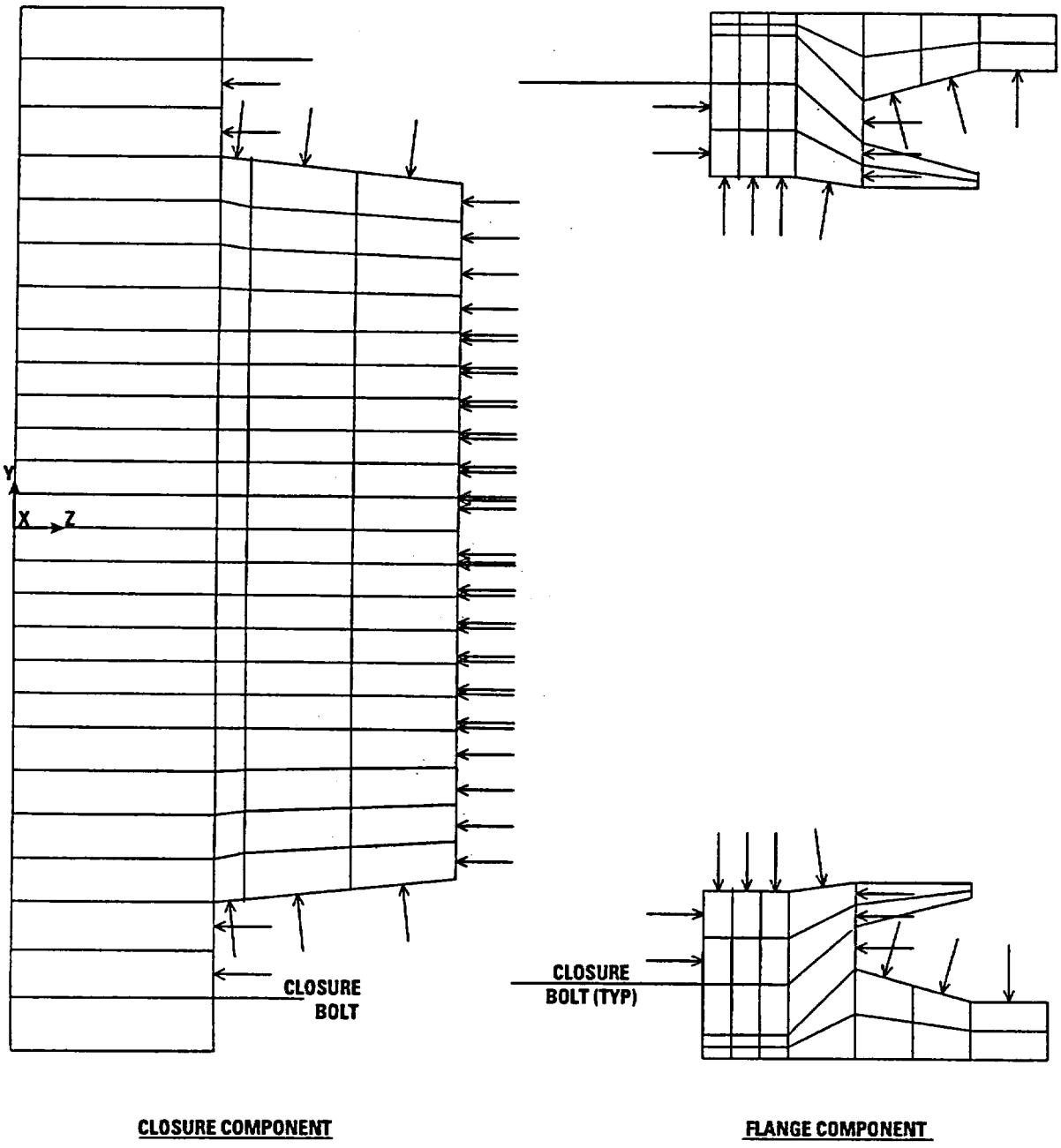

Fig. 2.10.2-22. Details of internal pressure loading on ANSYS model of GA-4 cask

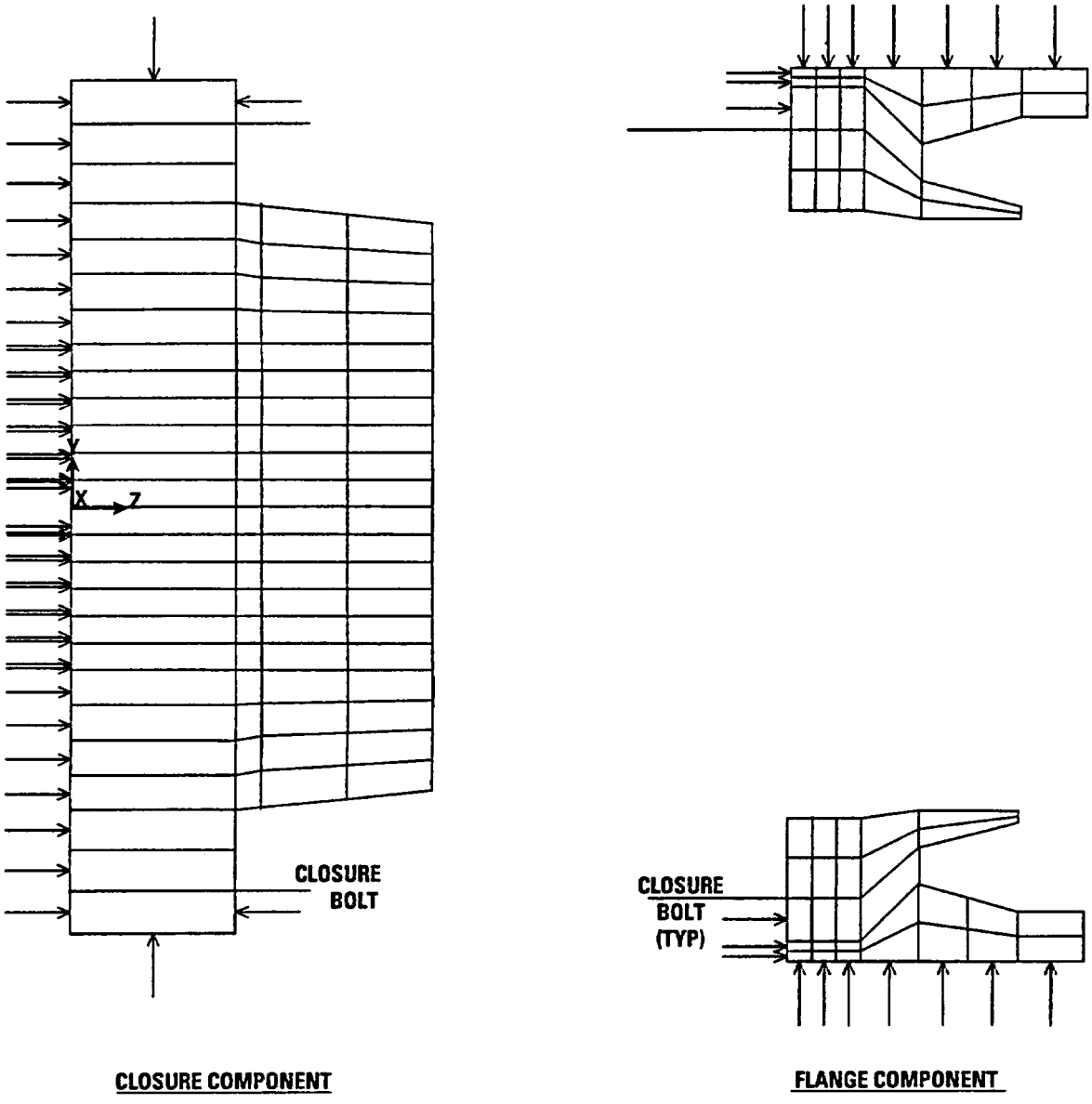

Fig. 2.10.2-23. Details of external pressure loading on ANSYS model of GA-4 cask

acceleration input. The impact force acting on the top of the closure-end impact limiter is simulated as a uniform pressure on the closure and as vertically directed forces applied to nodes on the cask flange and wall. These nodes represent the ILSS rib connections to the cask wall. Each of these loads is described in more detail below:

1) Forces caused by the acceleration of the DU, cavity liner, FSS and fuel masses. These forces were applied as uniform pressure loads acting on the flange and closure. The inner horizontal surface of the flange was assumed to carry the load of the DU, cavity liner and FSS. Similarly, the inner surface of the closure was assumed to carry the load caused by the acceleration of the fuel. Using the sketch of the ANSYS' model flange given in Fig. 2.10.2-24, the area for load application was calculated as follows:

$$A_{flange} = (11.328 \text{ in.} - 10.23 \text{ in.})\,(4)\,(7.826 \text{ in.}) + \pi/2\,[(11.328 \text{ in.} - 7.826 \text{ in.})^2 - (10.23 \text{ in.} - 7.826 \text{ in.})^2],$$

$$= 44.558 \text{ in.}^2$$

The weight supported by half the flange is:

$$W_{flange} = (wt_{DU} + wt_{cav\ liner} + wt_{FSS})/2,$$

$$= (24{,}535 \text{ lb} + 1{,}300 \text{ lb} + 751 \text{ lb})/2,$$

$$= 13{,}293 \text{ lb.}$$

Therefore, the pressure load applied to the flange is,

$$P_{flange} = W_{flange}/A_{flange},$$

$$P_{flange} = 13{,}293 \text{ lb}/44.558 \text{ in.}^2,$$

$$= 298 \text{ psi for 1g acceleration.}$$

The ANSYS analyses used 301 psi/g, a slightly more conservative load.

Performing similar calculations for the fuel load, we have,

$$A_{closure} = 2\,(L)^2,$$

using L = 8.7 in., the half-width of modeled closure plug, as shown in the sketch of Fig. 2.10.2-25, and substituting in the expression for $A_{closure}$ gives

$$A_{closure} = 151.4 \text{ in.}^2,$$

The weight supported by the closure is that of the fuel, 6,648 lb, therefore the pressure applied to the closure is:

$$P_{closure} = 1/2(wt_{fuel})/A_{closure\ end},$$

$$P_{closure} = 1/2\ (6{,}648 \text{ lb})/151.4 \text{ in.}^2,$$

$$= 22 \text{ psi for 1g acceleration.}$$

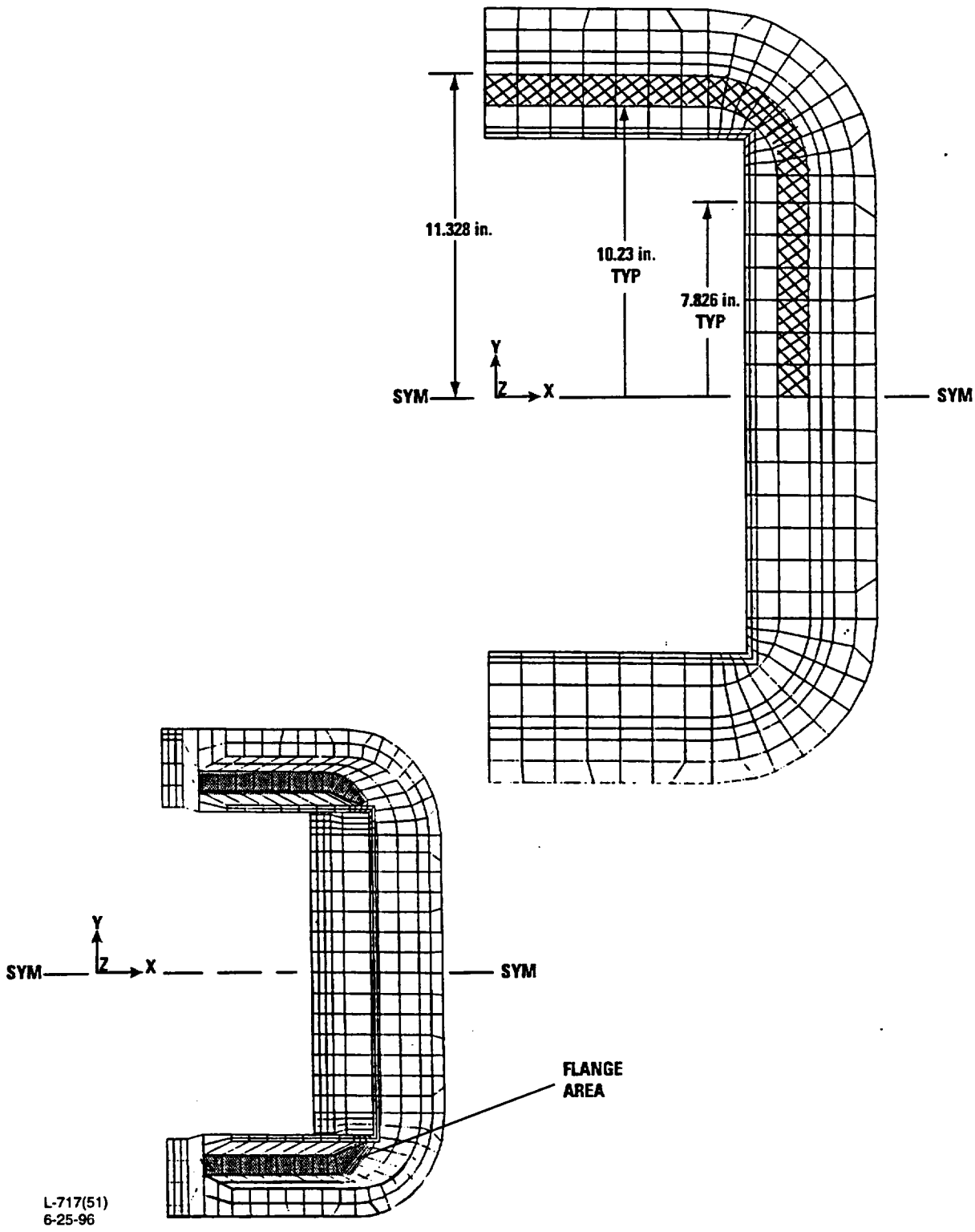

Fig. 2.10.2-24. ANSYS model flange area used for load calculations

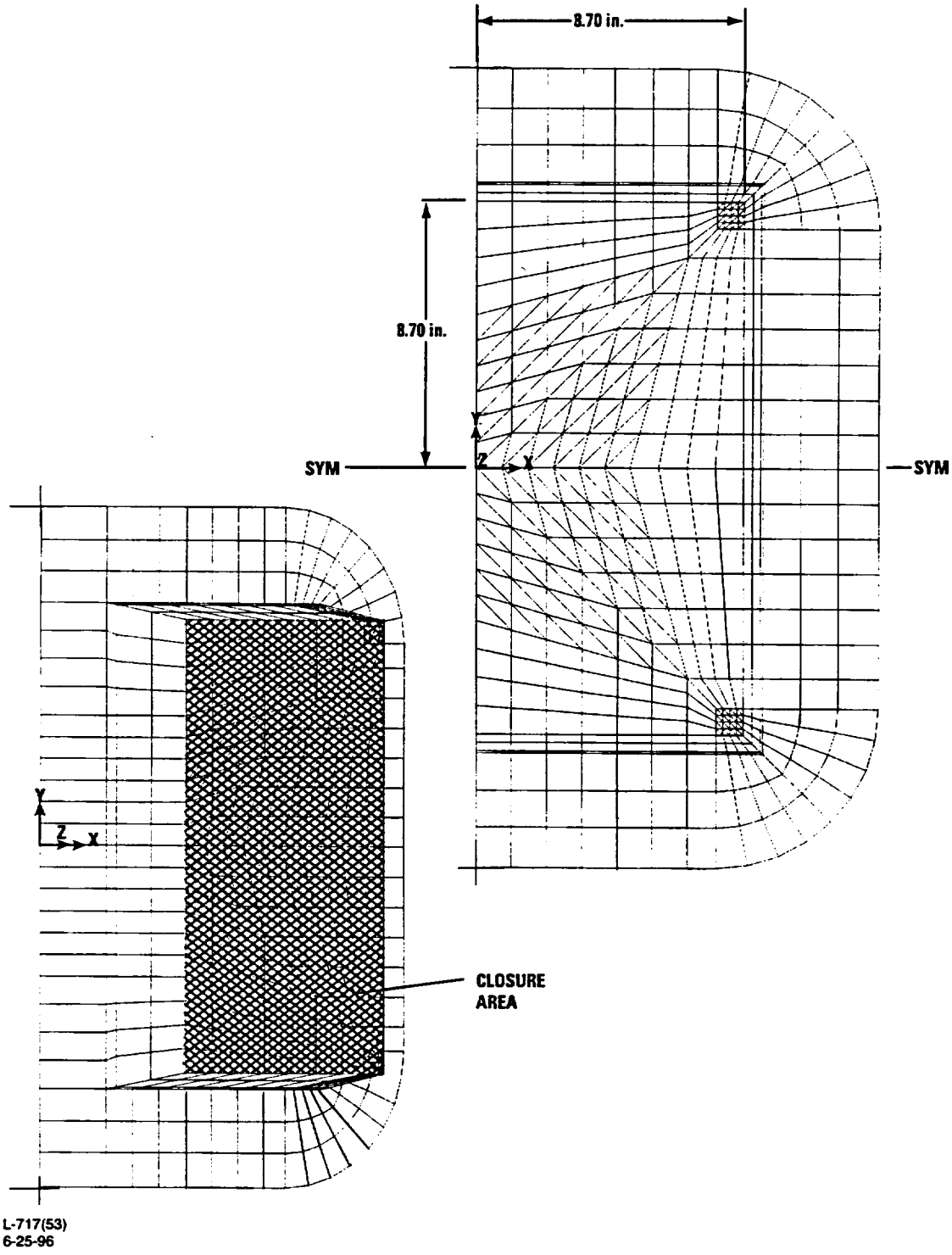

Fig. 2.10.2-25. ANSYS model closure area used for load calculations

2) Forces caused by the mass density of the ANSYS model. The mass densities used for the other components are given in Table 2.10.2-3. Using standard input for ANSYS the linear acceleration for the model is input.

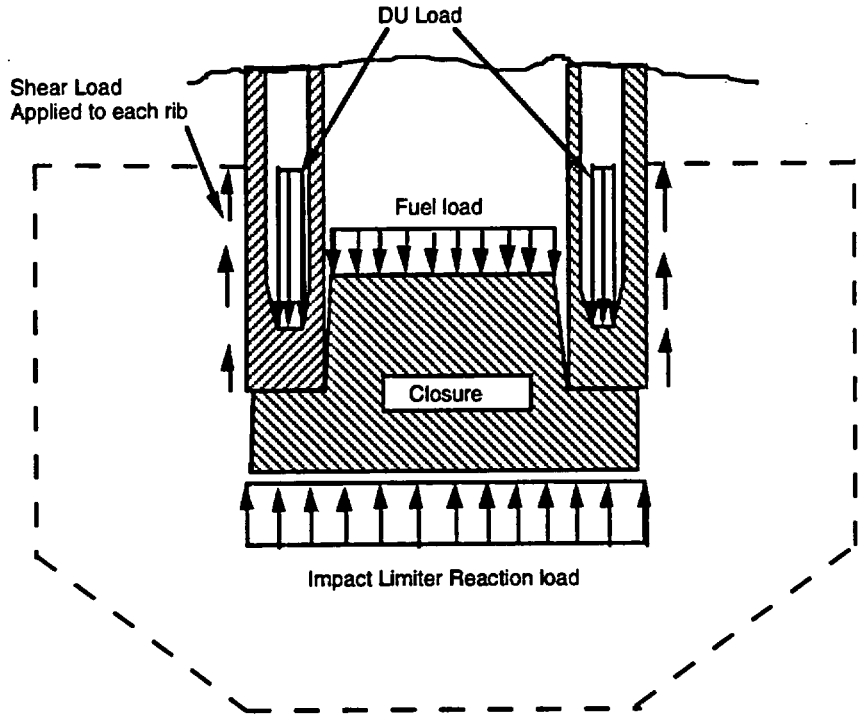

Fig. 2.10.2-26. End drop base case load distribution

3) The impact force acting on the closure-end impact limiter. The impact limiter force reaction was applied to the cask body and the ILSS ribs, as shown in Fig. 2.10.2-27. The total impact force is divided into the portion applied to the cask closure outer surface after crushing of the impact limiter's honeycomb and that which is transferred through the ILSS ribs to the cask as shearing forces at the cask wall. The load applied to the closure is assumed to be a uniform pressure and the remaining load is assumed to be shared by each of the ILSS ribs equally. The loads transmitted by the ribs are applied to the ANSYS model as vertical forces on the nodes which represent the attachment locations of the ILSS ribs. The load applied to the entire cask closure is 1.242×10^6 lb for the 30-ft end drop (impact angle of 90°), as derived in Section 2.10.3.6.2. For the ANSYS model, the load is 6.21×10^5 lb. Since this load resulted from a vertical acceleration of 61g, the load for 1g is 1.02×10^4 lb. Calculating the area of the closure cross section shown in Fig. 2.10.2-25, we have

$$A_{\text{cask end}} = (27.32 \text{ in.})(27.32 \text{ in.}) - (4)(5.84 \text{ in.})^2 + \pi\,(5.84 \text{ in.})^2,$$

$$= 717.1 \text{ in.}^2 \text{ (full cask geometry).}$$

Using the load applied to the cask end, the uniform pressure for ANSYS input is calculated as

$P_{cask\ end}$ = 1.02×10^4 lb/((1/2) 717.1 in.^{2}),

= 28.4 psi for 1g acceleration.

From Section 2.10.3.6.2, the force remaining for this case is 58,800 lb for each rib. Since this load is for the 61g acceleration the load per rib for the 1g case is 964 lb.

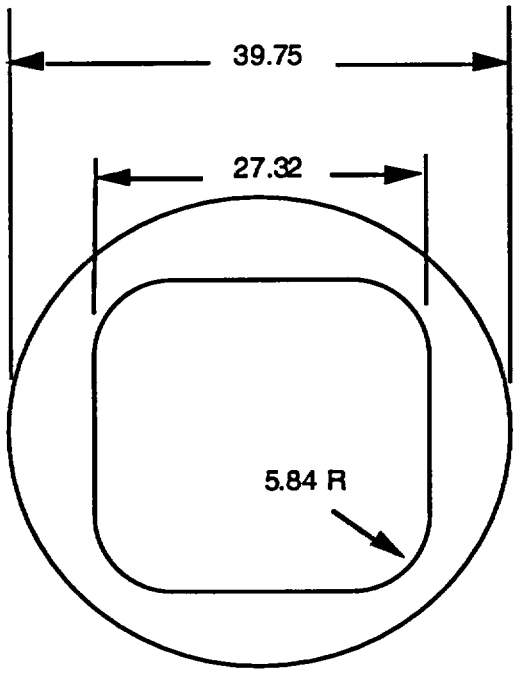

Fig. 2.10.2-27. View of cask body geometry and the ILSS outer diameter

The ANSYS base case model assumed that the vertical acceleration was 10g. Therefore, the forces and pressures input were ten times the values derived for 1g acceleration and the z-direction acceleration was input as 3864 in./ s^2 and no rotational acceleration was applied.

2.10.2.2.2.2 30-ft Side Drop for the Flat Model. This loading case represents a free drop from 30 feet with the cask centerline parallel to the ground and the flat side of the cask facing down. The impact limiters at each end are equally loaded with the impact force and the entire cask is subjected to a transverse, linear acceleration of 47.7g. There is no rotational acceleration.

The purpose of including the FSS and cavity liner in the cask model was to include the out-of-plane (Z direction) stiffness effect in the over-all cask structure. An actual loading of the cavity liner structure was not necessary because a detailed frame analysis of the cavity liner and FSS is presented in Section 2.10.9. The loading imposed on the ANSYS model conservatively assumed that the cavity liner supports the DU immediately above it, and that the load distribution applied to the supporting DU is 25% and 50% of the total load for the cavity liner wall and the FSS, respectively (as shown in Fig. 2.10.2-28). This load distribution was conservative, because results from the cavity liner model (see Section 2.10.9), which used the deflected

shape of the containment wall for support, produced equal loads in the cavity liner wall and FSS leg of approximately 33% of the total load.

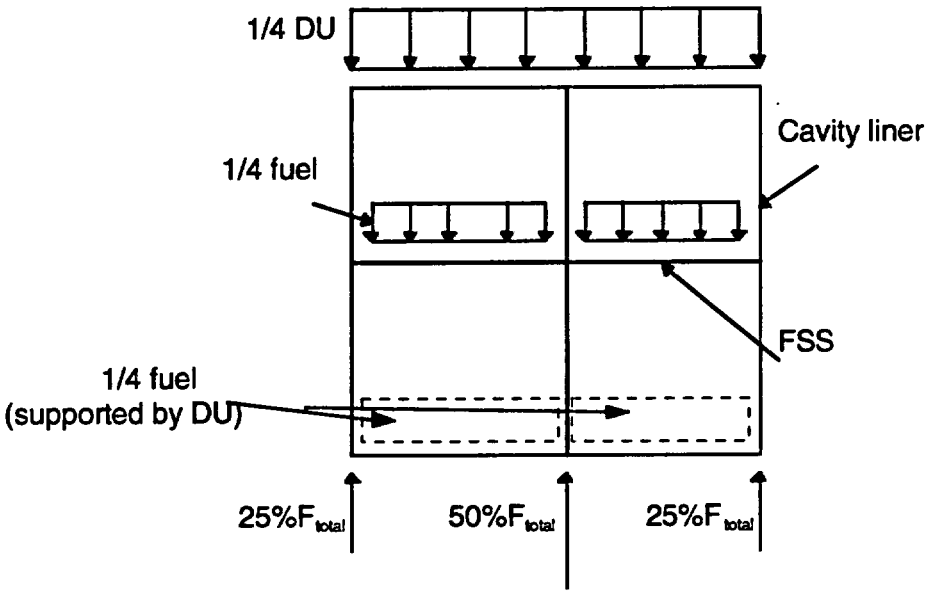

Fig. 2.10.2-28. Cavity liner, FSS, fuel and DU load distribution for the flat model of the GA-4 cask

The loading (F_{total}) applied to the DU structure through the cavity liner/FSS structure (excluding the lower fuel elements which are directly supported off of the DU) is as follows:

$$F_{total} = W_{cavity\ liner} + W_{FSS} + W_{1/4DU} + W_{1/2\ fuel},$$

$$= 11{,}509\ lb\ (11{,}566\ lb\ was\ conservatively\ used\ in\ the\ ANSYS\ models),$$

where

W_i = weight of component "i." In particular,

$W_{cavity\ liner}$ = 1300 lb,

W_{FSS} = 751 lb,

$W_{1/4DU}$ = 6134 lb (6185 lb was conservatively used in the ANSYS models), and

$W_{1/2\ fuel}$ = 3324 lb (3330 lb was conservatively used in the ANSYS models).

Using F_{total}, the loads transmitted by the cavity liner and the FSS are calculated:

$$F_{cavity\ liner} = (0.25)\ F_{total},$$

$$= (0.25)\ (11{,}566\ lb),$$

$$= 2{,}892\ lb,$$

and $F_{FSS} = (0.50)\ F_{total},$

= (0.50)(11,566 lb),

= 5,783 lb.

Therefore, the following is the loading which was used to simulate the effect of the internals on the lower cask wall as shown in Fig. 2.10.2-29:

The DU loading on the model was input as a lumped mass at the model nodes of the containment wall which supports it. The bottom fuel element loading in the cavity liner was assumed to be supported by the DU, and therefore added to the DU lumped mass on the bottom section of the model. The concentrated load from the cavity liner/FSS was distributed in the above mentioned lumped masses immediately below the load location. The total design weight of the cask is 55,000 lb. Since half the cask was modeled, the total model weight is 27,500 lb with 21,838 lb in the cask body, as detailed in Table 2.10.2-3. The remaining weight of 5,666 lb is divided equally between the closure and bottom plate regions.

The ANSYS ILSS reaction loading on the cask at the closure and bottom plate regions was developed using the following assumptions:

1. The total cask weight is 55,000 lb, the 30-ft side drop g-loading is 47.7g (per Section 2.10.4).

2. The reaction loads act at 7.81 in. from each end of the cask.

3. The ANSYS loads at the bottom end will be distributed uniformly along the ILSS.

4. The ANSYS model does not include the portion of the ILSS that extends beyond the cask flange (cantilevered section of the ILSS at the closure end).

5. At the closure end, the ANSYS model load will be distributed uniformly over the model length of the ILSS with the load that would have acted on the missing 5 in. of ILSS will be applied as a concentrated load on the first three elements of the flange (ring of elements) modeled by ANSYS.

The total load on the cask under the 30-ft side drop event is

F = ma,

= (55,000 lb x 47.7g),

= 2,623,500 lb.

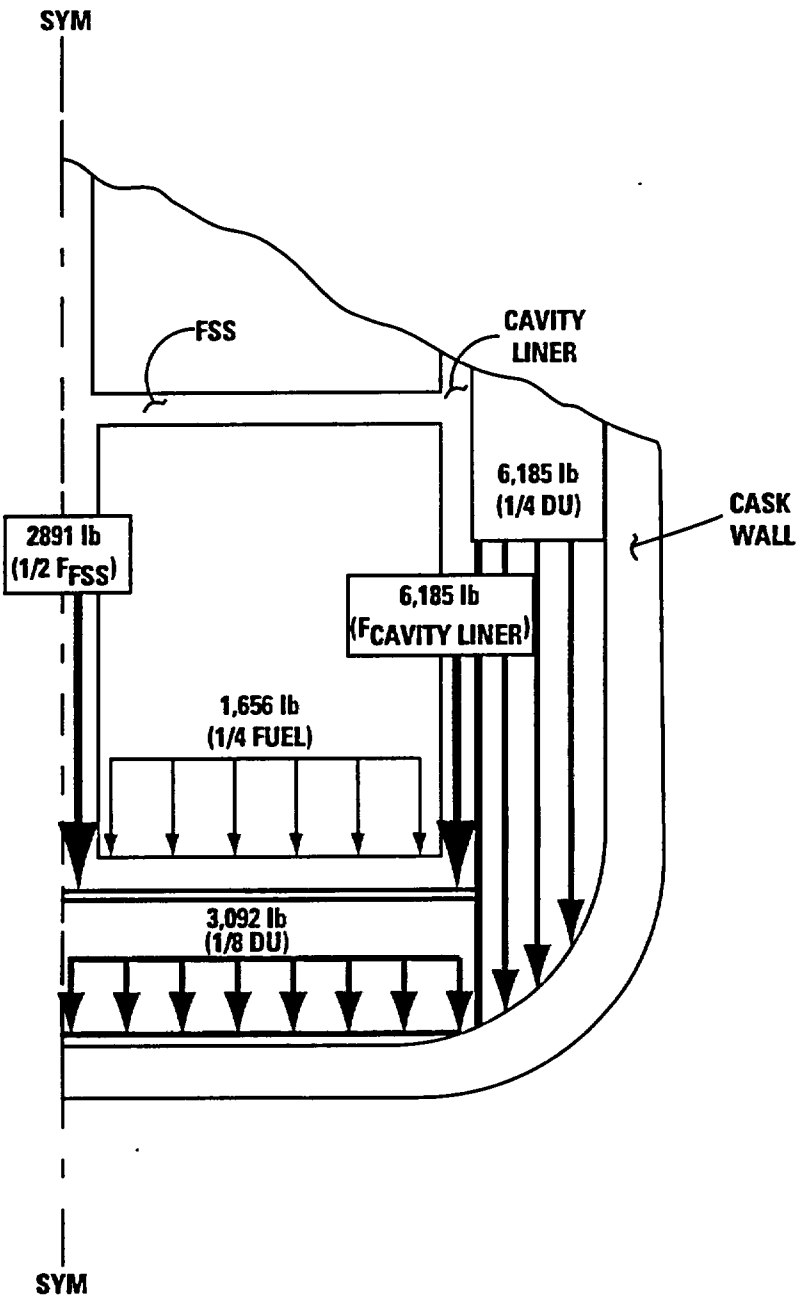

Fig. 2.10.2-29. Cask internals' loading on lower cask wall for ANSYS flat model

The load per end is 1,311,750. lb, as shown in Fig. 2.10.2-30.

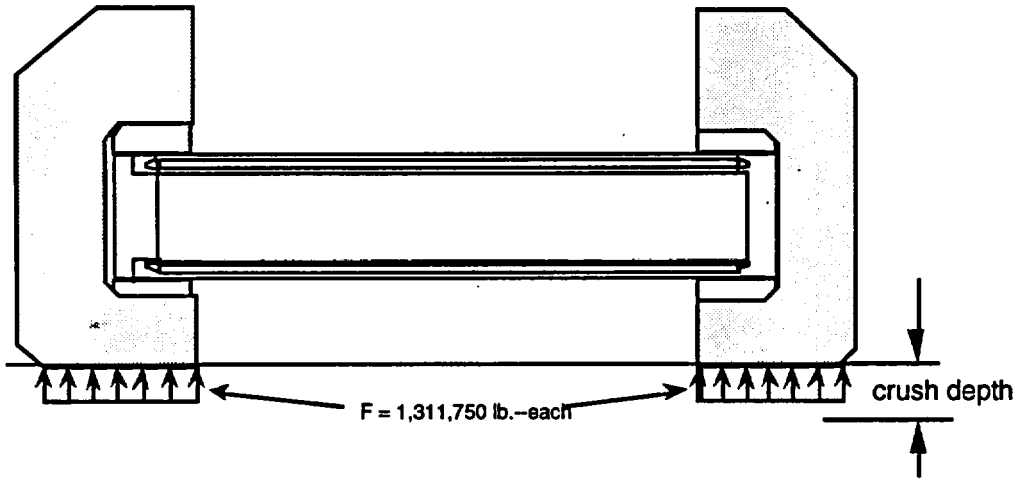

Fig. 2.10.2-30. Side drop impact limiter developed force

The reaction load on the cask is assumed to be applied through the rib structure of the ILSS which distributes the reaction load around the circumference of the cask, as presented in Section 2.10.3. This loading produces a line load on the cask under each rib on the surface of the cask model at the closure and bottom plate regions. The geometry of the ILSS rib structure is presented in Fig. 2.10.2-31 showing the centroid of the reaction ($F_{reaction}$) location of the impact limiter in view (a) of the figure.

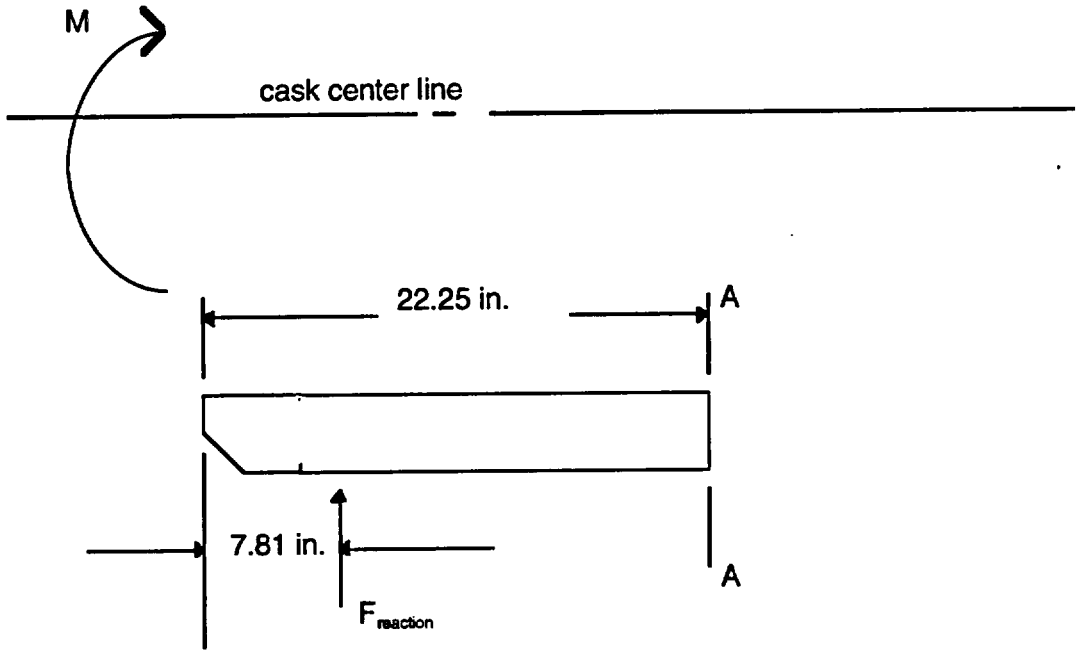

a) Typical ILSS rib geometry at impact location showing load CG location

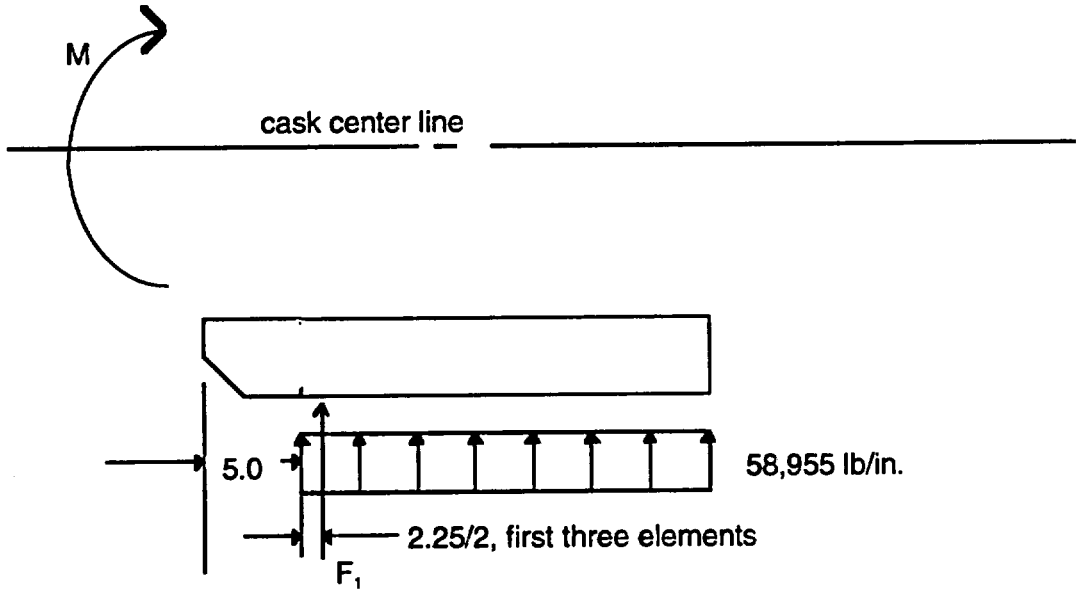

b) Closure end loading on ILSS rib structure

Fig. 2.10.2-31. ILSS loading during 30-ft side drop

The load per in. of ILSS is 1,311,750/22.25 = 58,955 lb/in. The moment at the cask bottom plate end that is required to position the reaction load at the 7.81 in. location, see Fig. 2.10.2-31) is developed as follows:

$M_{GACAP\ MODEL}$ = $M_{ANSYS\ MODEL}$,

(1,311,750)(22.25 – 7.81) = (1,311,750)(22.25/2) + M_{ANSYS},

M_{ANSYS} = 4,348,451 in.-lb (bottom plate end).

As mentioned, the loading on the closure end is modified because the cantilevered section of the ILSS is not included in the ANSYS model, therefore a lumped force is applied at the flange in the ANSYS model, as shown in Fig. 2.10.2-31(b). The moment required at the closure end is developed below.

Calculating the force needed to compensate for the missing 5 in. of cask wall, we have:

F_1 = (5 in.)(58,955 lb/in.),

= 294,775 lb.

Now, equating the GACAP results moment (LHS), to the moment applied to the ANSYS model by the forces, we can find the remaining moment which must be applied.

1,311,750 lb (22.25 in. – 7.81 in.) = 294,775 lb(22.25 in. – 5.0 in. – 2.25 in./2)

+1,016,995 lb([22.25 in. – 5 in.]/2)+M_{ANSYS}.

Solving this equation, we therefore find,

M_{ANSYS} = 5,416,841 in.-lb at the closure end.

This end moment was applied to the model using a couple at the ribs where the impact limiter bolts are attached. The applied reaction force distribution around the circumference of the cask model is developed using the ILSS model presented in Section 2.10.3.6.1c. The loading is applied on the nodes simulating the rib attachment locations (ten degrees on center around the cask circumference). The model was tied to the ground by two spar elements (LINK8) to prevent rigid-body translation in the y-direction. These elements were located at each end of the cask.

2.10.2.2.2.3 Oblique Drop. This loading case represents a free drop which will give a transverse, linear acceleration of 10g at the cask's CG. The cask centerline is parallel to the ground and the flat side of the cask was facing down. The oblique drop is a side drop with only the closure end impact limiter reacting the impact force. The impact limiter at the closure end was loaded with an impact force scaled from the GACAP results for the 30-ft drop secondary impact given in Table 2.10.4-1. To balance the applied impact force and the linear vertical acceleration, a rotational of acceleration of 0.23g about the model's CG was introduced. This rotational acceleration matches the CG rotational acceleration determined from the GACAP analysis given in Section 2.10.4.

The load on the closure end impact limiter of the cask under a unit (10g) oblique drop loading event is given by

$$F_{oblique} = (1{,}450{,}000 \text{ lb}/26.3\text{g})(10\text{g}),$$
$$= 551{,}331 \text{ lb.}$$

The reaction load on the cask was assumed to be applied through the rib structure of the ILSS producing a line load on the cask under each rib acting at the closure region. As mentioned, the loading on the closure end is modified because the cantilevered section of the ILSS is not included in the ANSYS model. The geometry of the ILSS rib structure and the assumed reaction location of F_1 are shown in Fig. 2.10.2-32.

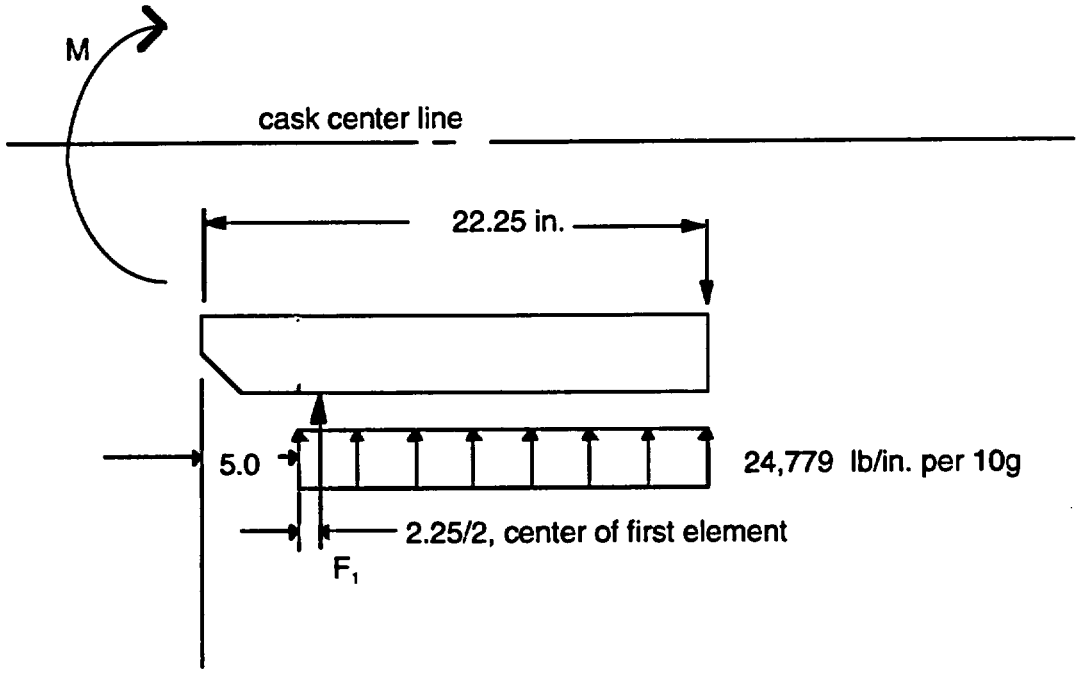

Fig. 2.10.2-32. ILSS loading on the closure end of the cask during the oblique drop case

The load per inch of ILSS/cask wall interface is 551,331 lb/ 22.25 in. = 24,779 lb/in. for the oblique drop normalized to a lateral linear acceleration of 10g.

As mentioned in Section 2.10.2.2.2.2, the loading on the closure end is modified because the cantilevered section of the ILSS is not included in the ANSYS model, therefore a lumped force is applied at the flange in the ANSYS model, as shown in Fig. 2.10.2-32. The moment required at the closure end is developed below.

Calculating the force needed to compensate for the missing 5 in. of cask wall, we have

$$F_1 = (5 \text{ in.})(24{,}779 \text{ lb/in.}),$$
$$= 123{,}895 \text{ lb.}$$

Now, equating the GACAP results moment (LHS), to the moment applied to the ANSYS model by the forces, we can find the remaining moment which must be applied.

$$551{,}331 \text{ lb}(22.25 \text{ in.} - 7.81 \text{ in.}) = 123{,}895 \text{ lb}\,(22.25 \text{ in.} - 5.0 \text{ in.} - 2.25 \text{ in./2}) + 427{,}436 \text{ lb}((22.25 \text{ in.} - 5 \text{ in.})/2) + M_{ANSYS}$$

Solving this equation, we therefore find,

M_{ANSYS} = 2,274,190 in.-lb at the closure end.

This end moment was applied to the model using a couple at the ribs where the impact limiter bolts are attached. The applied reaction force distribution around the circumference of the cask model is developed using the ILSS model presented in Section 2.10.3. The loading is applied on the nodes simulating the rib attachment locations (ten degrees on center around the cask circumference). The model was tied to the ground by two spar elements (LINK8) to prevent rigid-body translation in the y-direction. These elements were located at each end of the cask.

The lumped mass input derived in Section 2.10.2.2.2.2 was used for this model as well as the 30-ft side drop model. The lumped masses simulated the effect of the internals on the GA-4 cask.

2.10.2.2.2.4 30-ft Side Drop for Corner Model. This loading case represents a free drop from 30 feet with the cask centerline parallel to the ground and the flat side of the cask facing down. The impact limiters at each end are equally loaded with the impact force and the entire cask is subjected to a transverse, linear acceleration of 47.7g. There is no angular acceleration.

The purpose of including the FSS and cavity liner in the cask model was to include the out-of-plane (z-direction) stiffness effect in the over-all cask structure. An actual loading of the cavity liner structure was not necessary because a detailed frame analysis of the cavity liner and FSS is presented in Section 2.10.9.

Using the internal loading on the cask wall developed in Section 2.10.2.2.2.2 for the flat orientation, the loading for the corner model was derived. The loads caused by the cask internals were multiplied by the factor 0.707, to account for the change in load direction caused by rotating the cask cross section 45°. As with the flat model, the DU loading on the model was input as lumped masses on the model nodes. The bottom fuel element was assumed to be supported by the DU and, therefore, its mass was added to the DU lumped mass at the bottom of the model's cross section. The concentrated loads from the cavity liner and FSS were added to the lumped masses on the cask wall which were immediately below the load location. The total design weight of the cask is 55,000 lb. Therefore, the remaining weight equal to 10,950 lb (55,000 – 44,050) was divided equally between the closure and bottom plate regions.

Therefore, the following simulation of the internals load on the cask wall was developed as follows:

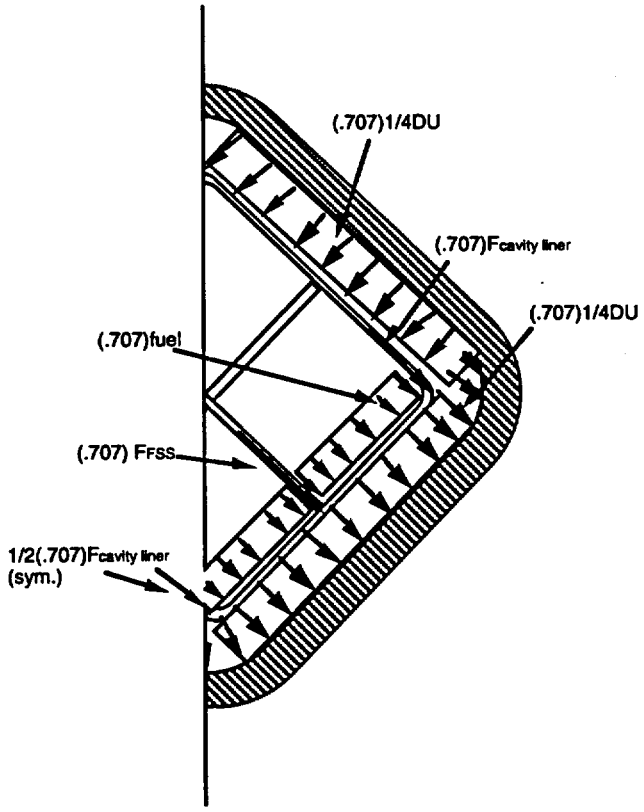

Fig. 2.10.2-33. Cask internals' loading on lower cask wall for ANSYS corner model

The ANSYS ILSS reaction loading on the cask at the closure was the same as presented for the flat model (Section 2.10.2.2.2.2) and the same moments were applied.

2.10.2.2.2.5 30-ft Oblique Drop for Corner Model. This loading case represents a free drop which will give a transverse, linear acceleration of 10g at the cask's CG. The cask centerline was parallel to the ground and the corner of the cask was facing down.

The ANSYS ILSS reaction loading on the cask at the closure was the same as presented for the flat model (Section 2.10.2.2.2.3) and the same moments were applied.

The lumped mass input derived in Section 2.10.2.2.2.4 was used for this model, as well, as for the 30-ft side drop. The lumped masses simulated the effect of the internals on the GA-4 cask.

2.10.2.3 Finite Element Analysis Procedure. The structural evaluation of the GA-4 shipping cask wall was performed using the results of two ANSYS models subjected to similar loading conditions. Because the shipping cask is not axisymmetric about its centerline, but about two of its cross sections, two three-dimensional models were developed, as explained in Section 2.10.2.1. These models were used to simulate the internal and external pressure loads, the 30-ft end and side drops, and a 10g oblique drop.

ANSYS analyses were conducted for each of the models and for each of the cases described above. The individual runs considered are classified as either normal condition, hypothetical accident condition, or special requirement condition. These runs are described in Sections 2.10.2.3.1 and 2.10.2.3.2.

After each of the ANSYS analyses was performed, a stress summary table was developed for the important cross sections of the cask wall. These cross sections are shown in Fig. 2.10.2-1. The cross sections' axial positions were the same for the flat and corner models. The specific points used for the stress summaries are detailed in Tables 2.10.2-6 through 2.10.2-10 for the flat model and in Tables 2.10.2-11 through 2.10.2-15 for the corner model. The directionally dependent stress components were tabulated. To evaluate the cask wall for the different normal, hypothetical accident, and special requirement conditions, the results for the applicable base cases were superposed at the stress component level and the principal stresses, stress intensities and design margins were obtained using an Excel table. For example, to obtain the stresses for a loaded cask subjected to a thirty degree angle, 30-ft high drop, the end drop base case stresses were multiplied by 1.23 and combined with the oblique drop base case which had been multiplied by 2.14. The seventy-two load cases used to evaluate the cask wall adequacy are described in Sections 2.10.2.3.3 through 2.10.2.3.5. Different impact angles were used to find the worst case (lowest design margin) for the cask wall.

To minimize the number of load cases evaluated, the stresses caused by differential thermal expansion were not included. The effects of the thermal stresses given in Sections 2.6.1.3 and 2.6.2 are evaluated in Section 2.10.6.1. The thermal stress in the cask wall is 300 psi tension for the hot environment and 5,000 psi tension for the cold environment (cask and contents at –20°F).

2.10.2.3.1 Normal and Hypothetical Accident Condition Base Cases. The following are the base cases (BC) which were analyzed for the flat and corner models:

BC-1. Internal pressure of 80 psig for both flat and corner cases.

BC-2. Statically equivalent loads, simulating the impact and inertial loads of a 30-ft end drop on the top end of the cask with an impact angle of 90°.

BC-3. Statically equivalent loads, simulating the impact and inertial loads of a 30-ft side drop on both impact limiters with an impact angle of 0°.

BC-4. Statically equivalent loads, simulating the impact and inertial loads of a secondary impact oblique drop normalized to 10g on the top end impact limiter with an impact angle of 0°.

TABLE 2.10.2-6
STRESS SUMMARY POINTS FOR THE FLAT MODEL AT CROSS SECTION A OF FIG. 2.10.2-1 (AXIAL HEIGHT OF 12.0 IN.)

Position Label			Node	Coordinates (in.)	
Axial	Transverse	Wall	Number	X	Y
A	1	inside	1383	0.0	12.162
		middle	1390	0.0	12.912
		outside	1397	0.0	13.662
A	2	inside	1417	7.826	12.162
		middle	1419	7.826	12.912
		outside	1421	7.826	13.662
A	3	inside	1466	10.892	10.892
		middle	1465	11.422	11.422
		outside	1464	11.953	11.953
A	4	inside	9981	12.162	7.826
		middle	9983	12.912	7.826
		outside	9985	13.662	7.826
A	5	inside	9947	12.162	0.0
		middle	9954	12.912	0.0
		outside	9961	13.662	0.0
A	6	inside	27109	12.162	−7.826
		middle	27111	12.912	−7.826
		outside	27113	13.662	−7.826
A	7	inside	18594	10.892	−10.892
		middle	18593	11.422	−11.422
		outside	18592	11.953	−11.953
A	8	inside	18545	7.826	−12.162
		middle	18547	7.826	−12.912
		outside	18549	7.826	−13.662
A	9	inside	18511	0.0	−12.162
		middle	18518	0.0	−12.912
		outside	18525	0.0	−13.662

TABLE 2.10.2-7
STRESS SUMMARY POINTS FOR THE FLAT MODEL AT CROSS SECTION B OF FIG. 2.10.2-1 (AXIAL HEIGHT OF 22.75 IN.)

Position Label			Node	Coordinates (in.)	
Axial	Transverse	Wall	Number	X	Y
B	1	inside	2748	0.0	12.162
		middle	2755	0.0	12.912
		outside	2762	0.0	13.662
B	2	inside	2965	7.826	12.162
		middle	2967	7.826	12.912
		outside	2969	7.826	13.662
B	3	inside	3053	10.892	10.892
		middle	3052	11.422	11.422
		outside	3051	11.953	11.953
B	4	inside	11529	12.162	7.826
		middle	11531	12.912	7.826
		outside	11533	13.662	7.826
B	5	inside	11312	12.162	0.0
		middle	11319	12.912	0.0
		outside	11326	13.662	0.0
B	6	inside	28657	12.162	-7.826
		middle	28659	12.912	-7.826
		outside	28661	13.662	-7.826
B	7	inside	20181	10.892	-10.892
		middle	20180	11.422	-11.422
		outside	20179	11.953	-11.953
B	8	inside	20093	7.826	-12.162
		middle	20095	7.826	-12.912
		outside	20097	7.826	-13.662
B	9	inside	19876	0.0	-12.162
		middle	19883	0.0	-12.912
		outside	19890	0.0	-13.662

TABLE 2.10.2-8
STRESS SUMMARY POINTS FOR THE FLAT MODEL AT CROSS SECTION C OF FIG. 2.10.2-1 (AXIAL HEIGHT OF 51.32 IN.)

Position Label			Node	Coordinates (in.)	
Axial	Transverse	Wall	Number	X	Y
C	1	inside	2937	0.0	12.162
		middle	2944	0.0	12.912
		outside	2951	0.0	13.662
C	2	inside	3019	7.826	12.162
		middle	3021	7.826	12.912
		outside	3023	7.826	13.662
C	3	inside	3188	10.892	10.892
		middle	3187	11.422	11.422
		outside	3186	11.953	11.953
C	4	inside	11583	12.162	7.826
		middle	11585	12.912	7.826
		outside	11587	13.662	7.826
C	5	inside	11501	12.162	0.0
		middle	11508	12.912	0.0
		outside	11515	13.662	0.0
C	6	inside	28711	12.162	−7.826
		middle	28713	12.912	−7.826
		outside	28715	13.662	−7.826
C	7	inside	20316	10.892	−10.892
		middle	20315	11.422	−11.422
		outside	20314	11.953	−11.953
C	8	inside	20147	7.826	−12.162
		middle	20149	7.826	−12.912
		outside	20151	7.826	−13.662
C	9	inside	20065	0.0	−12.162
		middle	20072	0.0	−12.912
		outside	20079	0.0	−13.662

TABLE 2.10.2-9
STRESS SUMMARY POINTS FOR THE FLAT MODEL AT CROSS SECTION D OF FIG. 2.10.2-1 (AXIAL HEIGHT OF 65.25 IN.)

Position Label			Node	Coordinates (in.)	
Axial	Transverse	Wall	Number	X	Y
D	1	inside	3399	0.0	12.162
		middle	3406	0.0	12.912
		outside	3413	0.0	13.662
D	2	inside	3481	7.826	12.162
		middle	3483	7.826	12.912
		outside	3485	7.826	13.662
D	3	inside	3650	10.892	10.892
		middle	3649	11.422	11.422
		outside	3648	11.953	11.953
D	4	inside	12045	12.162	7.826
		middle	12047	12.912	7.826
		outside	12049	13.662	7.826
D	5	inside	11963	12.162	0.0
		middle	11970	12.912	0.0
		outside	11977	13.662	0.0
D	6	inside	29173	12.162	-7.826
		middle	29175	12.912	-7.826
		outside	29177	13.662	-7.826
D	7	inside	20778	10.892	-10.892
		middle	20777	11.422	-11.422
		outside	20776	11.953	-11.953
D	8	inside	20609	7.826	-12.162
		middle	20611	7.826	-12.912
		outside	20613	7.826	-13.662
D	9	inside	20527	0.0	-12.162
		middle	20534	0.0	-12.912
		outside	20541	0.0	-13.662

TABLE 2.10.2-10
STRESS SUMMARY POINTS FOR THE FLAT MODEL AT CROSS SECTION E OF FIG. 2.10.2-1 (AXIAL HEIGHT OF 93.88 IN.)

Position Label			Node	Coordinates (in.)	
Axial	Transverse	Wall	Number	X	Y
E	1	inside	3861	0.0	12.162
		middle	3868	0.0	12.912
		outside	3875	0.0	13.662
E	2	inside	3943	7.826	12.162
		middle	3945	7.826	12.912
		outside	3947	7.826	13.662
E	3	inside	4112	10.892	10.892
		middle	4111	11.422	11.422
		outside	4110	11.953	11.953
E	4	inside	12507	12.162	7.826
		middle	12509	12.912	7.826
		outside	12511	13.662	7.826
E	5	inside	12425	12.162	0.0
		middle	12432	12.912	0.0
		outside	12439	13.662	0.0
E	6	inside	29635	12.162	−7.826
		middle	29637	12.912	−7.826
		outside	29639	13.662	−7.826
E	7	inside	21240	10.892	−10.892
		middle	21239	11.422	−11.422
		outside	21238	11.953	−11.953
E	8	inside	21071	7.826	−12.162
		middle	21073	7.826	−12.912
		outside	21075	7.826	−13.662
E	9	inside	20989	0.0	−12.162
		middle	20996	0.0	−12.912
		outside	21003	0.0	−13.662

TABLE 2.10.2-11
STRESS SUMMARY POINTS FOR THE CORNER MODEL AT CROSS SECTION A OF FIG. 2.10.2-1 (AXIAL HEIGHT OF 12.0 IN.)

Position Label			Node	Coordinates (in.)	
Axial	Transverse	Wall	Number	X	Y
A	3	inside	10030	0.0	15.404
		middle	10029	0.0	16.154
		outside	10028	0.0	16.904
A	4	inside	9981	3.0660	14.134
		middle	9983	3.5963	14.664
		outside	9985	4.1267	15.194
A	5	inside	1383	8.5998	8.5998
		middle	1390	9.1302	9.1302
		outside	1397	9.6605	9.6605
A	6	inside	1417	14.134	3.0660
		middle	1419	14.664	3.5963
		outside	1421	15.194	4.1267
A	7	inside	1466	15.404	0.0
		middle	1465	16.154	0.0
		outside	1464	16.904	0.0
A	8	inside	18545	14.134	–3.0660
		middle	18547	14.664	–3.5963
		outside	18549	15.194	–4.1267
A	9	inside	18511	8.5998	–8.5998
		middle	18518	9.1302	–9.1302
		outside	18525	9.6605	–9.6605
A	10	inside	27109	3.0660	–14.134
		middle	27111	3.5963	–14.664
		outside	27113	4.1267	–15.194
A	11	inside	27158	0.0	–15.404
		middle	27157	0.0	–16.154
		outside	27156	0.0	–16.904

TABLE 2.10.2-12
STRESS SUMMARY POINTS FOR THE CORNER MODEL AT CROSS SECTION B OF FIG. 2.10.2-1 (AXIAL HEIGHT OF 22.75 IN.)

Position Label			Node	Coordinates (in.)	
Axial	Transverse	Wall	Number	X	Y
B	3	inside	11617	0.0	15.404
		middle	11616	0.0	16.154
		outside	11615	0.0	16.904
B	4	inside	11529	3.0660	14.134
		middle	11531	3.5963	14.664
		outside	11533	4.1267	15.194
B	5	inside	2748	8.5998	8.5998
		middle	2755	9.1302	9.1302
		outside	2762	9.6605	9.6605
B	6	inside	2965	14.134	3.0660
		middle	2967	14.664	3.5963
		outside	2969	15.194	4.1267
B	7	inside	3053	15.404	0.0
		middle	3052	16.154	0.0
		outside	3051	16.904	0.0
B	8	inside	20093	14.134	–3.0660
		middle	20095	14.664	–3.5963
		outside	20097	15.194	–4.1267
B	9	inside	19876	8.5998	–8.5998
		middle	19883	9.1302	–9.1302
		outside	19890	9.6605	–9.6605
B	10	inside	28657	3.0660	–14.134
		middle	28659	3.5963	–14.664
		outside	28661	4.1267	–15.194
B	11	inside	28745	0.0	–15.404
		middle	28744	0.0	–16.154
		outside	28743	0.0	–16.904

TABLE 2.10.2-13
STRESS SUMMARY POINTS FOR THE CORNER MODEL AT CROSS SECTION C OF FIG. 2.10.2-1 (AXIAL HEIGHT OF 51.32 IN.)

Position Label			Node	Coordinates (in.)	
Axial	Transverse	Wall	Number	X	Y
C	3	inside	11752	0.0	15.404
		middle	11751	0.0	16.154
		outside	11750	0.0	16.904
C	4	inside	11583	3.0660	14.134
		middle	11585	3.5963	14.664
		outside	11587	4.1267	15.194
C	5	inside	2937	8.5998	8.5998
		middle	2944	9.1302	9.1302
		outside	2951	9.6605	9.6605
C	6	inside	3019	14.134	3.0660
		middle	3021	14.664	3.5963
		outside	3023	15.194	4.1267
C	7	inside	3188	15.404	0.0
		middle	3187	16.154	0.0
		outside	3186	16.904	0.0
C	8	inside	20147	14.134	-3.0660
		middle	20149	14.664	-3.5963
		outside	20151	15.194	-4.1267
C	9	inside	20065	8.5998	-8.5998
		middle	20072	9.1302	-9.1302
		outside	20079	9.6605	-9.6605
C	10	inside	28711	3.0660	-14.134
		middle	28713	3.5963	-14.664
		outside	28715	4.1267	-15.194
C	11	inside	28880	0.0	-15.404
		middle	28879	0.0	-16.154
		outside	28878	0.0	-16.904

TABLE 2.10.2-14
STRESS SUMMARY POINTS FOR THE CORNER MODEL AT CROSS SECTION D OF FIG. 2.10.2-1 (AXIAL HEIGHT OF 65.25 IN.)

Position Label			Node	Coordinates (in.)	
Axial	Transverse	Wall	Number	X	Y
D	3	inside	12214	0.0	15.404
		middle	12213	0.0	16.154
		outside	12212	0.0	16.904
D	4	inside	12045	3.0660	14.134
		middle	12047	3.5963	14.664
		outside	12049	4.1267	15.194
D	5	inside	3399	8.5998	8.5998
		middle	3406	9.1302	9.1302
		outside	3413	9.6605	9.6605
D	6	inside	3481	14.134	3.0660
		middle	3483	14.664	3.5963
		outside	3485	15.194	4.1267
D	7	inside	3650	15.404	0.0
		middle	3649	16.154	0.0
		outside	3648	16.904	0.0
D	8	inside	20609	14.134	–3.0660
		middle	20611	14.664	–3.5963
		outside	20613	15.194	–4.1267
D	9	inside	20527	8.5998	–8.5998
		middle	20534	9.1302	–9.1302
		outside	20541	9.6605	–9.6605
D	10	inside	29173	3.0660	–14.134
		middle	29175	3.5963	–14.664
		outside	29177	4.1267	–15.194
D	11	inside	29342	0.0	–15.404
		middle	29341	0.0	–16.154
		outside	29340	0.0	–16.904

TABLE 2.10.2-15
STRESS SUMMARY POINTS FOR THE CORNER MODEL
AT CROSS SECTION E OF FIG. 2.10.2-1
(AXIAL HEIGHT OF 93.88 IN.)

Position Label			Node	Coordinates (in.)	
Axial	Transverse	Wall	Number	X	Y
E	3	inside	12676	0.0	15.404
		middle	12675	0.0	16.154
		outside	12674	0.0	16.904
E	4	inside	12507	3.0660	14.134
		middle	12509	3.5963	14.664
		outside	12511	4.1267	15.194
E	5	inside	3861	8.5998	8.5998
		middle	3868	9.1302	9.1302
		outside	3875	9.6605	9.6605
E	6	inside	3943	14.134	3.0660
		middle	3945	14.664	3.5963
		outside	3947	15.194	4.1267
E	7	inside	4112	15.404	0.0
		middle	4111	16.154	0.0
		outside	4110	16.904	0.0
E	8	inside	21071	14.134	-3.0660
		middle	21073	14.664	-3.5963
		outside	21075	15.194	-4.1267
E	9	inside	20989	8.5998	-8.5998
		middle	20996	9.1302	-9.1302
		outside	21003	9.6605	-9.6605
E	10	inside	29635	3.0660	-14.134
		middle	29637	3.5963	-14.664
		outside	29639	4.1267	-15.194
E	11	inside	29804	0.0	-15.404
		middle	29803	0.0	-16.154
		outside	29802	0.0	-16.904

2.10.2.3.2 External Pressure Base Case. The following is the external pressure base case which was analyzed for both the flat and corner models.

BC-5. External pressure of 290 psig.

2.10.2.3.3 Normal Condition Load Cases. The base case results were combined as detailed in Table 2.10.2-16 to evaluate the following normal condition load cases for both the flat and corner models:

1. MNOP with 1-ft end drop at a drop angle of 90°.
2. MNOP with 1-ft side drop at a drop angle of 0°.
3. MNOP with 1-ft drop at a drop angle of 15°.
4. MNOP with 1-ft drop at a drop angle of 30°.
5. MNOP with 1-ft drop at a drop angle of 45°.
6. MNOP with 1-ft drop at a drop angle of 60°.
7. MNOP with 1-ft drop at a drop angle of 75°.
8. MNOP with 1-ft drop at a drop angle of 78 (cask and contents CG over point of impact).
9. 1-ft end drop at a drop angle of 90°.
10. 1-ft side drop at a drop angle of 0°.
11. 1-ft drop at a drop angle of 15°.
12. 1-ft drop at a drop angle of 30°.
13. 1-ft drop at a drop angle of 45°.
14. 1-ft drop at a drop angle of 60°.
15. 1-ft drop at a drop angle of 75°.
16. 1-ft drop at a drop angle of 78 (cask and contents CG over point of impact).

All load combinations are applicable to the hot environment condition since the thermal stresses in the cask wall are so low (<300 psi tension). The cold environment condition is discussed in Section 2.10.6.1.

2.10.2.3.4 Hypothetical Accident Condition Load Cases. The base case results were combined as detailed in Table 2.10.2-17 to evaluate the following hypothetical accident condition load cases for both the flat and corner models:

17. MNOP with 30-ft end drop at a drop angle of 90°.
18. MNOP with 30-ft side drop at a drop angle of 0°.
19. MNOP with 30-ft drop at a drop angle of 15°.
20. MNOP with 30-ft drop at a drop angle of 30°.
21. MNOP with 30-ft drop at a drop angle of 45°.
22. MNOP with 30-ft drop at a drop angle of 60°.
23. MNOP with 30-ft drop at a drop angle of 75°.

24. MNOP with 30-ft drop at a drop angle of 78 (cask and contents CG over point of impact).
25. MNOP with 30-ft slapdown at a drop angle of 15°.
26. 30-ft end drop at a drop angle of 90°.
27. 30-ft side drop at a drop angle of 0°.
28. 30-ft drop at a drop angle of 15°.
29. 30-ft drop at a drop angle of 30°.
30. 30-ft drop at a drop angle of 45°.
31. 30-ft drop at a drop angle of 60°.
32. 30-ft drop at a drop angle of 75°.
33. 30-ft drop at a drop angle of 78 (cask and contents CG over point of impact).
34. 30-ft slapdown with a drop angle of 15°.
35. Fire test conditions. Internal pressure of 90.2 psig.
    Maximum containment boundary temperature of 780°F.

2.10.2.3.5 Special Requirement for Irradiated Nuclear Fuel Shipments Load Case. The following base case results were used to evaluate the special requirement load case for both the flat and corner models:

36. Uniform external pressure of 290 psig.

TABLE 2.10.2-16
NORMAL CONDITION LOAD CASES GIVEN AS
SUMMATIONS OF SCALED BASE CASE RESULTS

Load Case Number	Load Case Description		Applicable Base Case Factor				
			Pressure		Dynamic Base Case		
	Drop Height (ft)	Impact Angle (deg.)	Internal	External	End Drop	Side Drop	Oblique Drop
Normal Condition Load Cases							
1	1	90	1.0	0.0	1.49	0.00	0.00
2	1	0	1.0	0.0	0.00	0.33	0.00
3	1	15	1.0	0.0	0.20	0.00	0.74
4	1	30	1.0	0.0	0.27	0.00	0.47
5	1	45	1.0	0.0	0.37	0.00	0.37
6	1	60	1.0	0.0	1.12	0.00	0.65
7	1	75	1.0	0.0	0.99	0.00	0.26
8	1	78	1.0	0.0	0.99	0.00	0.26
9	1	90	0.0	0.0	1.49	0.00	0.00
10	1	0	0.0	0.0	0.00	0.33	0.00
11	1	15	0.0	0.0	0.20	0.00	0.74
12	1	30	0.0	0.0	0.27	0.00	0.47
13	1	45	0.0	0.0	0.37	0.00	0.37
14	1	60	0.0	0.0	1.12	0.00	0.65
15	1	75	0.0	0.0	0.99	0.00	0.26
16	1	78	0.0	0.0	0.99	0.00	0.26

TABLE 2.10.2-17
ACCIDENT CONDITION AND SPECIAL REQUIREMENT LOAD CASES
GIVEN AS SUMMATIONS OF SCALED BASE CASE RESULTS

Load Case Number	Load Case Description		Applicable Base Case Factor				
			Pressure		Dynamic Base Case		
	Drop Height (ft)	Impact Angle (deg.)	Internal	External	End Drop	Side Drop	Oblique Drop
Hypothetical Accident Condition Load Cases							
17	30	90	1.0	0.0	6.10	0.00	0.00
18	30	0	1.0	0.0	0.00	1.00	0.00
19	30	15	1.0	0.0	0.58	0.00	2.15
20	30	30	1.0	0.0	1.23	0.00	2.14
21	30	45	1.0	0.0	2.31	0.00	2.31
22	30	60	1.0	0.0	3.78	0.00	2.18
23	30	75	1.0	0.0	5.54	0.00	1.49
24	30	78	1.0	0.0	5.68	0.00	1.21
25	30	15	1.0	0.0	0.00	0.00	2.63
26	30	90	0.0	0.0	6.10	0.00	0.00
27	30	0	0.0	0.0	0.00	1.00	0.00
28	30	15	0.0	0.0	0.58	0.00	2.15
29	30	30	0.0	0.0	1.23	0.00	2.14
30	30	45	0.0	0.0	2.31	0.00	2.31
31	30	60	0.0	0.0	3.78	0.00	2.18
32	30	75	0.0	0.0	5.54	0.00	1.49
33	30	78	0.0	0.0	5.68	0.00	1.21
34	30	15	0.0	0.0	0.00	0.00	2.63
35	N/A	N/A	1.1275	0.0	0.00	0.00	0.00
Special Requirement for Irradiated Fuel Shipments Load Case							
36	N/A	N/A	0.0	1.0	0.00	0.00	0.00

2.10.3 Impact Limiter Design and Tests

2.10.3.1 Introduction. The design for the GA-4 cask includes identical honeycomb impact limiters on the top and bottom of the cask body to protect it during normal conditions of transport or hypothetical accident condition drops onto an unyielding surface. The impact limiters were designed so that they would protect the trunnions or any other part of the cask from contacting the impact surface during a 30-ft free drop. To evaluate the response of the cask during a drop, we used load-deflection curves for the impact limiters at different impact angles. GA developed a computer code to determine impact limiter load-deflection curves.

GA also developed a test program to provide data on the behavior of the honeycomb impact limiters. GA tested the final impact limiter design at different angles using 1/4-scale test articles, providing a complete characterization of the impact limiter behavior. Section 2.10.13 provides the results of half-scale model drop tests which verified the impact limiter design.

This section presents the impact limiter design as well as the results of the 1/4-scale impact limiter tests.

2.10.3.2 Impact Limiter Structural Design. Figures 2.10.3-1 and 2.10.3-2 show the design of the GA-4 impact limiters. The design uses standard aluminum honeycomb. Because the standard honeycomb structure is unidirectional while the impact limiter absorbs energy in three dimensions, the impact limiter contains three basic parts (shown in Fig. 2.10.3-2). For a more detailed discussion of the impact limiter design see Chapter 1, Section 1.2.1.2.

Part 1 covers the end section at the bottom or top of the cask. The cell orientation of the honeycomb is parallel to the length of the cask. The outer 1.6 in. is lower strength honeycomb.

Part 2, the corner section around the cask, consists of twenty-four 15° segments. The honeycomb cell orientation of each segment lines up radially with the center of the cask at an angle of 30° from the length of the cask.

Part 3 makes a circumferential section around the sides of the cask. It consists of twenty-four 15° segments. The cells of each segment line up radially with the center of the cask and are perpendicular to the length of the cask.

To facilitate decontamination, all impact limiter surfaces are covered with a stainless steel sheet with smooth welded joints.

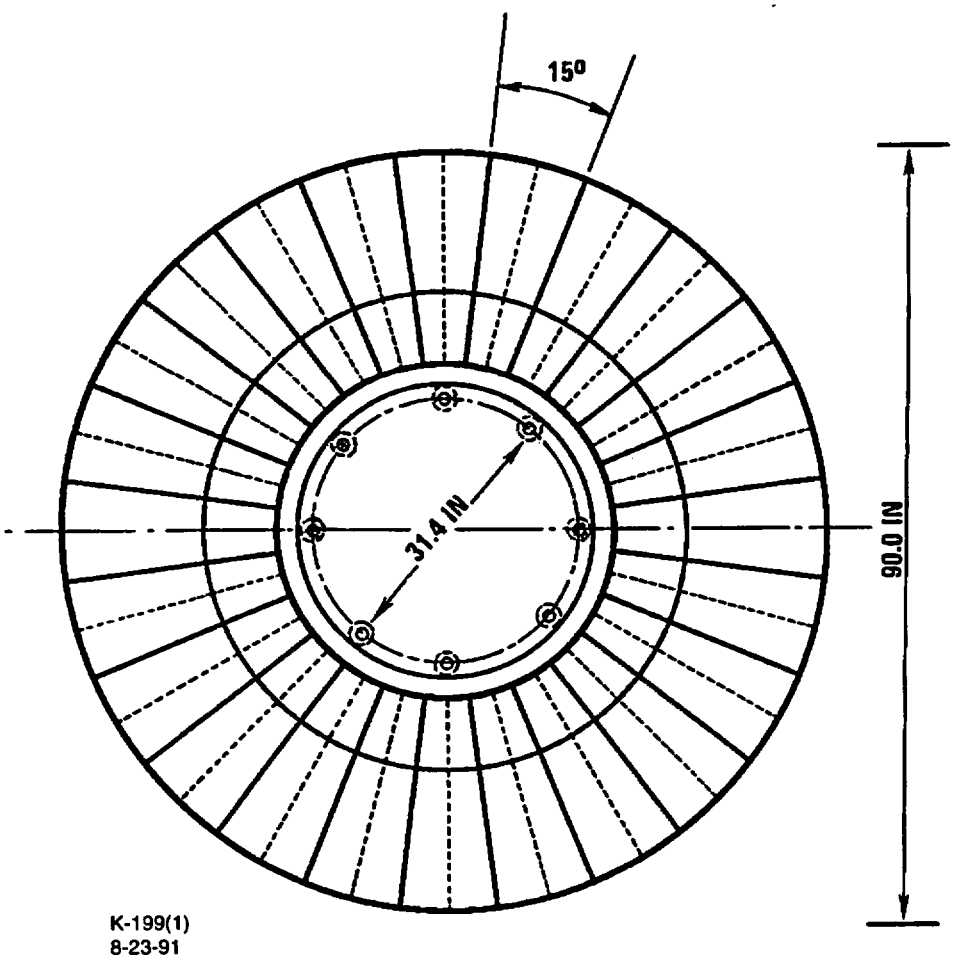

Fig. 2.10.3-1. GA-4 impact limiter design, top view (does not show lifting attachments)

Security-Related Information Figure
Withheld Under 10 CFR 2.390.

Fig. 2.10.3-2. GA-4 impact limiter design, cross-sectional view showing different honeycomb parts

2.10.3.3 Analytical Procedure for Obtaining Load-deflection Curves. In order to obtain the load-versus-deflection curve for impact limiters with standard unidirectional honeycomb, GA developed the computer code ILMOD which calculates the footprint of the crushed impact limiter for any orientation and depth. It then assigns a crush strength to each part of the impact limiter footprint and calculates the total load. The code calculates the complete impact limiter load-versus-deflection tables for all crush orientations. Section 2.10.1.4 describes the ILMOD code in more detail.

We developed the load-versus-deflection curves for crush orientations from side (0°) to end (90°).

ILMOD calculated the minimum and maximum crush force developed by the impact limiter by assigning each honeycomb section a minimum and a maximum crush strength, which vary from the nominal honeycomb crush strengths depending on the following characteristics:

1. Manufacturing Tolerances and Temperature Effect on Honeycomb Crush Strength. The manufacturer of the honeycomb has guaranteed the crush strength of the honeycomb to be within ±12.5% of the nominal value over the temperature range of –20°F to 200°F. This range includes all variances due to manufacturing and material tolerances.

2. Strain Rate Effects on Crush Strength of Honeycomb. The expected velocity at impact during a 30-ft drop is 44 ft/sec, or 527.45 in./sec. The crushing strength of the honeycomb increases a maximum of 10 percent above the static crush value at these strain rates.

   Taking these effects into account, the minimum and maximum crush strengths for the different parts are:

   For 1400 psi honeycomb
   F_c max = 1400 x 1.125 x 1.1 = 1732.5 psi
   F_c min = 1400 x (1–.125) x 1.1 = 1347.5 psi,

   For 725 psi honeycomb
   F_c max = 725 x 1.125 x 1.1 = 897.19 psi
   F_c min = 725 x (1–.125) x 1.1 = 697.81 psi,

   For 220 psi honeycomb
   F_c max = 220 x 1.125 x 1.1 = 272.25 psi
   F_c min = 220 x (1–.125) x 1.1 = 211.75 psi.

ILMOD uses an effective angle factor to modify the crush strength of the honeycomb depending on the angle between the honeycomb cell direction and the direction of crush.

The impact limiter tests show that using an effective angle factor of 1 for all honeycomb sections fit the test data best, except at high deflections during a side drop, 0°, in

which the test data fit better if the effective angle factor is set to 0.56 for honeycomb sections in which the honeycomb cell is oriented more than 60° from the crush direction.

Figures 2.10.3-3 to 2.10.3-9 show the ILMOD-developed minimum and maximum load versus deflection curves for different orientations. As reported there, these curves envelop the variations of the nominal honeycomb crush strength due to temperature, manufacturing tolerance, and strain rate effects.

2.10.3.4 Honeycomb Impact Limiter Tests. Four 1/4-scale versions of the impact limiter designs were tested at different crush angles to provide data on the load-versus-deflection curve of the impact limiter. Three impact limiters were tested twice, on opposite sides. The tests performed range from end (90°) to side crush (0°). Table 2.10.3-1 shows the tests performed.

The tests were performed on a compression testing machine. The impact limiters were directly backed by a solid aluminum test fixture. The test set-up was instrumented during the entire event to provide a complete record of the load applied to the specimen as a function of deflection. Graphs of the load-versus-deflection data were produced. Figures 2.10.3-10 and 2.10.3-11 show the test set-up and an impact limiter model after a side crush test.

The 1/4-scale models tested are directly scaled from the actual design except for the following minor details that will not affect the behavior of the impact limiter:

- Outer skins were not welded together on the 1/4-scale models because ease of decontamination is not required. Some doublers were bonded on the seams of the circumferential skin to provide continuity. Even without welds, skins remained attached after testing and no splits or tears developed demonstrating that confinement by the skins was maintained without welds.

- Lifting attachments were not modeled on the 1/4-scale models. These small attachments will not modify the behavior of the impact limiters.

- The adhesive used between the bolt opening tubes and the top honeycomb was changed after the 1/4-scale model fabrication to facilitate larger-scale impact limiter fabrication. This bond plays a minimal role on the impact limiter behavior.

- The 1/4-scale models did not include the 1.6-in. thick 220 psi crush strength honeycomb located on the outer flat surface of the impact limiters. This was included in the design for the 1-ft end drop to reduce the g-level. The 1/4-scale test load-deflection curve is conservative for the 30-ft end drop. Since there is significant margin against bottoming out during the end drop as shown in Tables 2.10.4-8 through 2.10.4-10, substituting 220 psi crush strength honeycomb is acceptable.

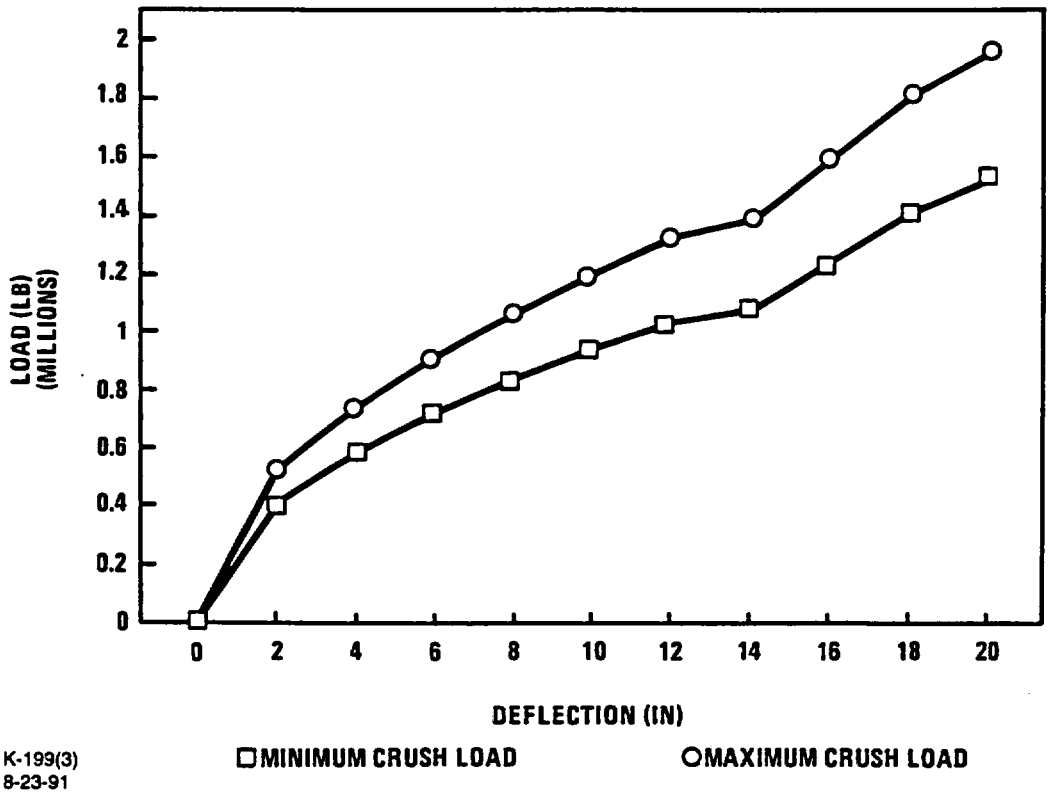

Fig. 2.10.3-3. Side drop (0°) force-versus-deflection curve

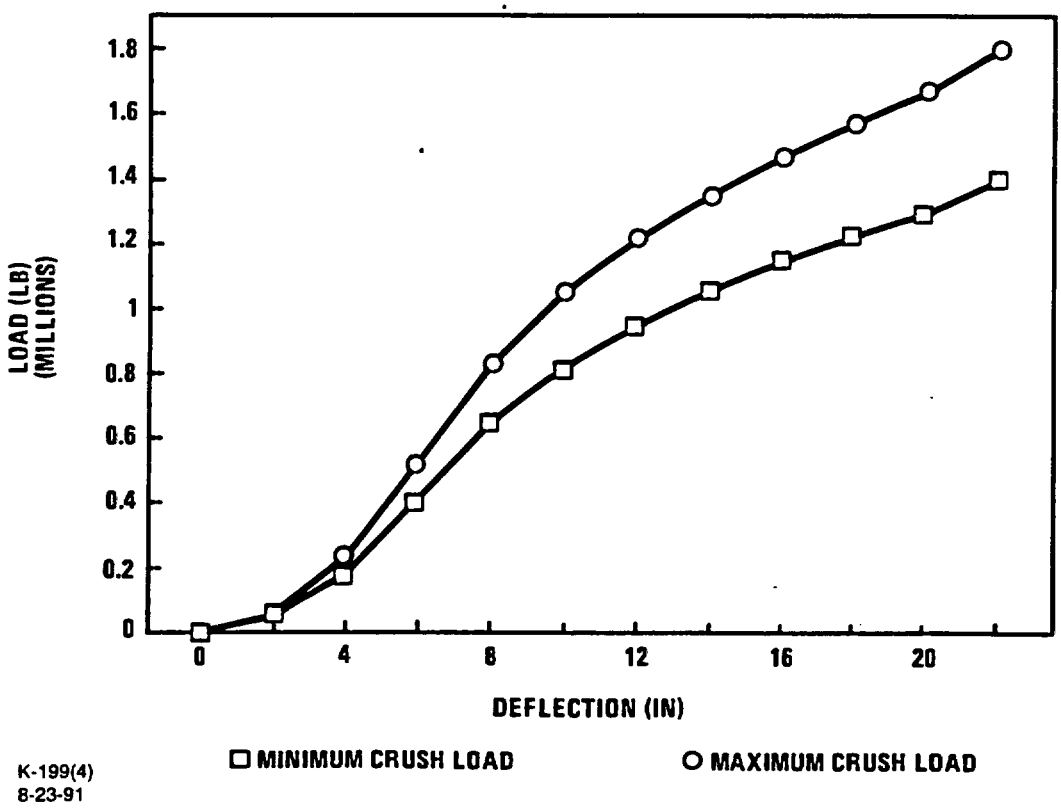

Fig. 2.10.3-4. 15° drop force-versus-deflection curve

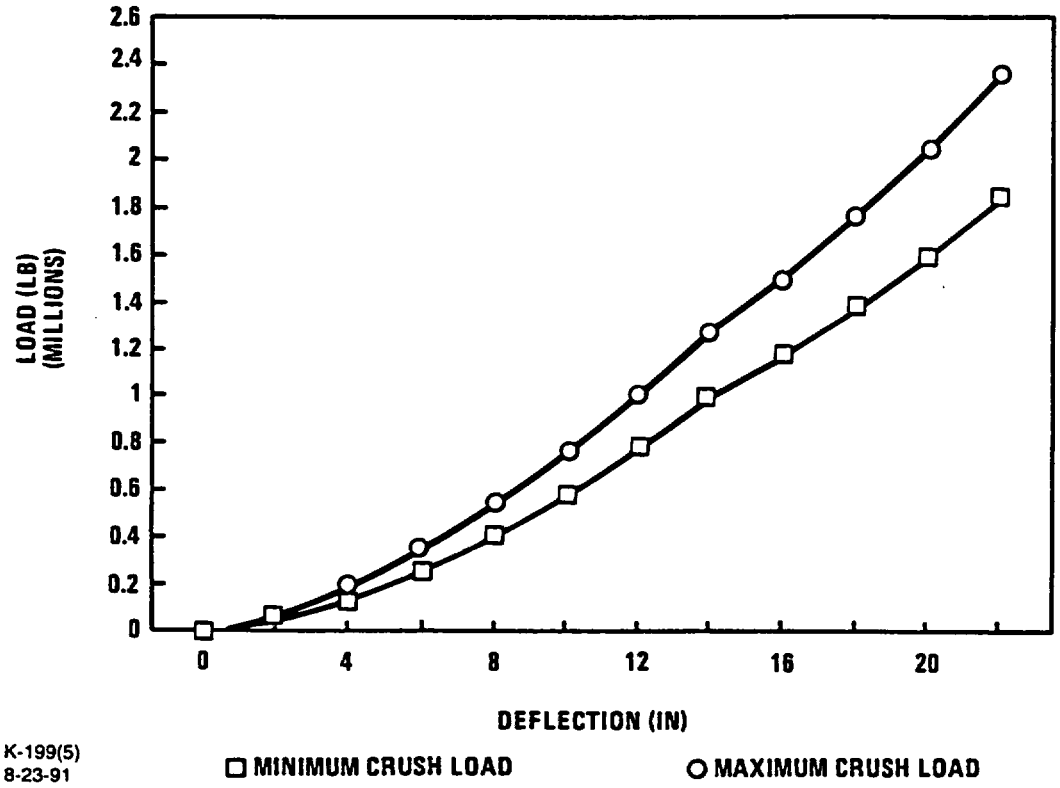

Fig. 2.10.3-5. 30° drop force-versus-deflection curve

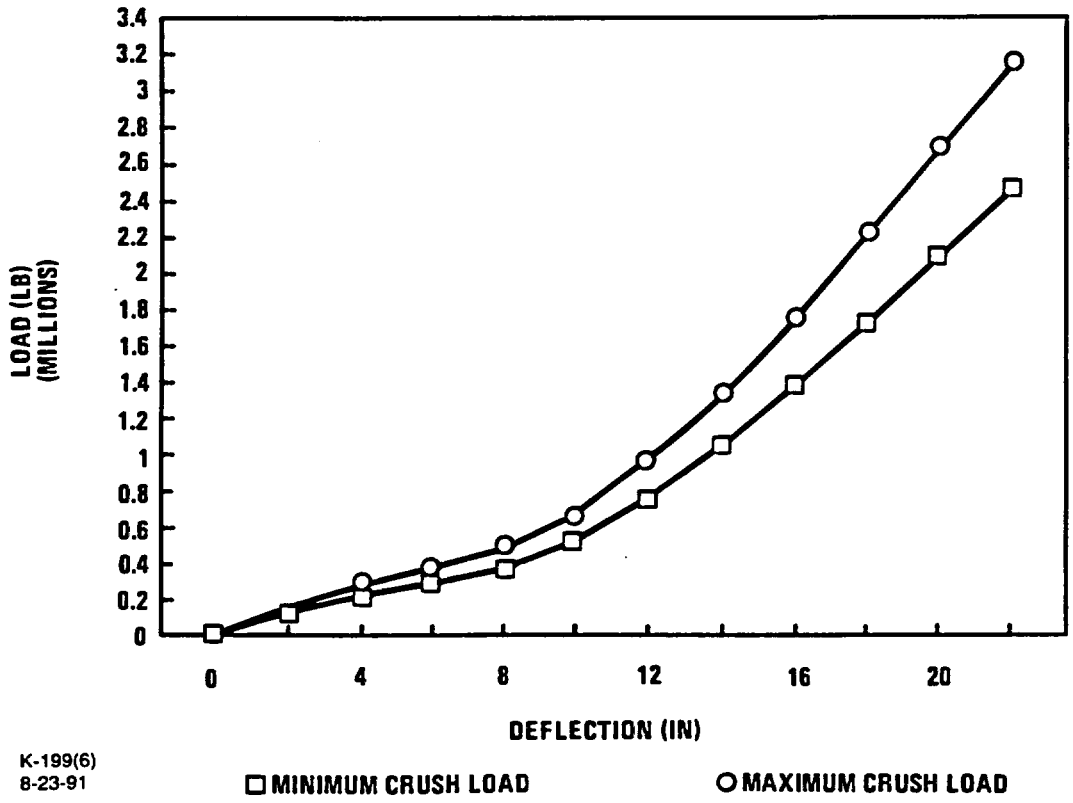

Fig. 2.10.3-6. 45° drop force-versus-deflection curve

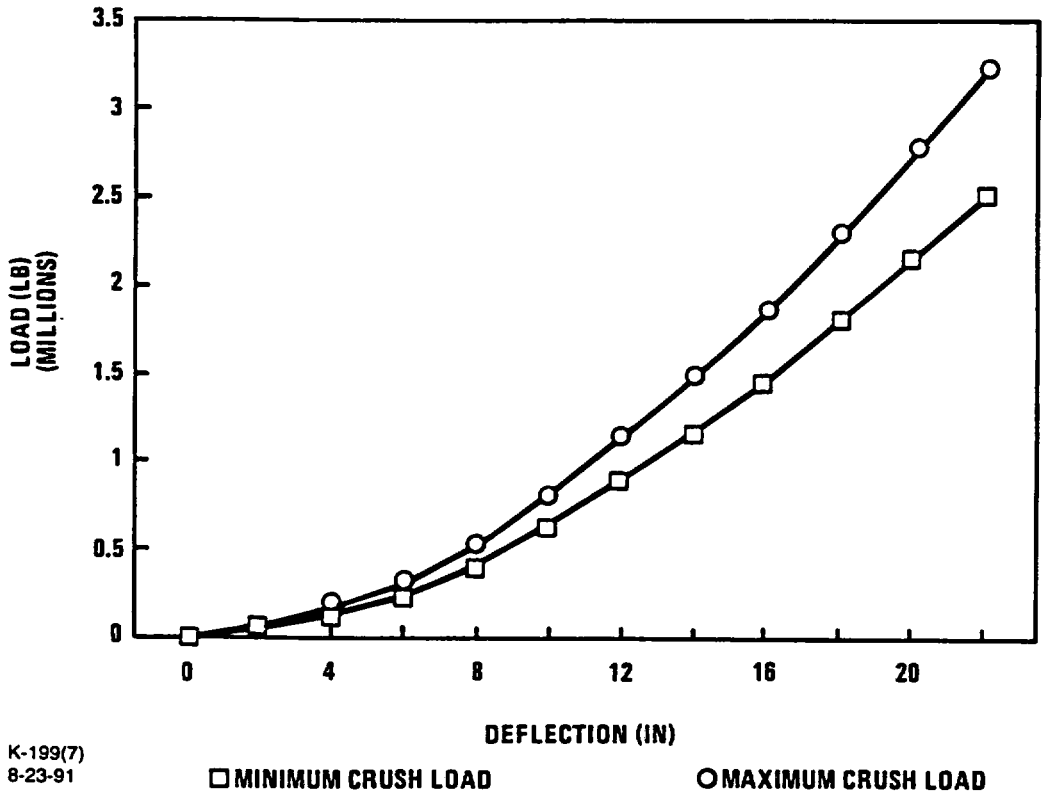

Fig. 2.10.3-7. 60° drop force-versus-deflection curve

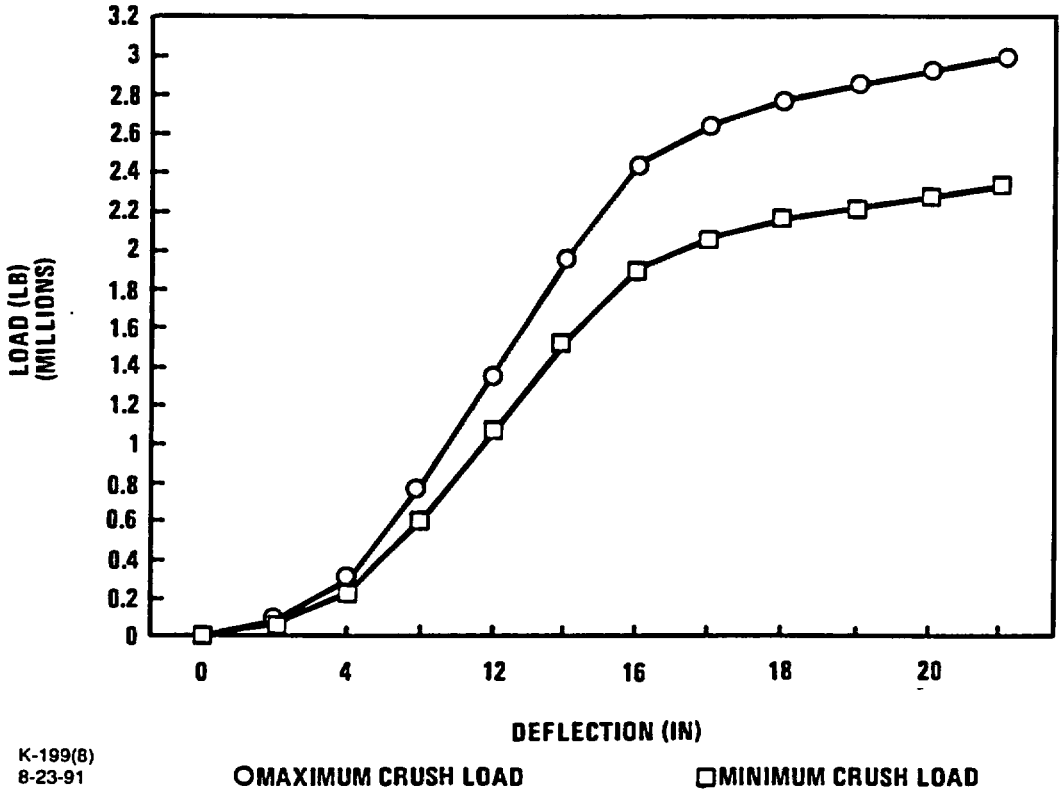

Fig. 2.10.3-8. 75° drop force-versus-deflection curve

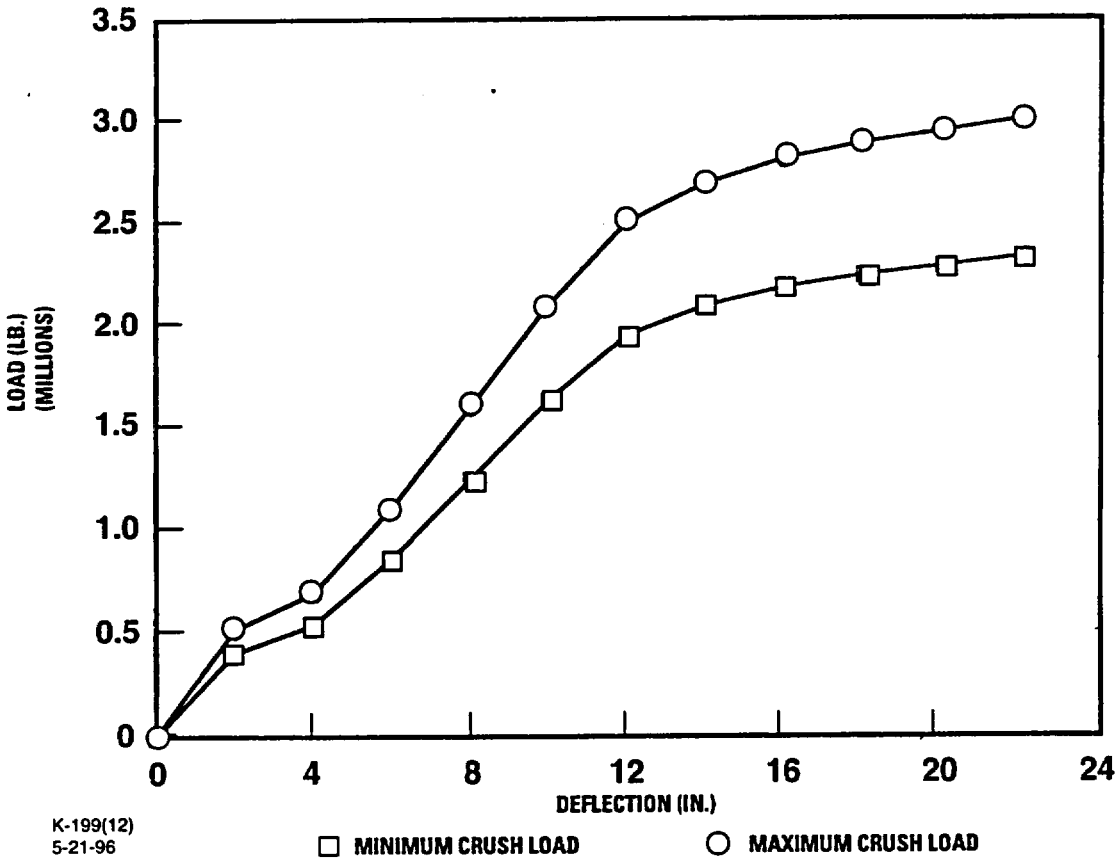

Fig. 2.10.3-8a. 78° drop force-versus-deflection curve

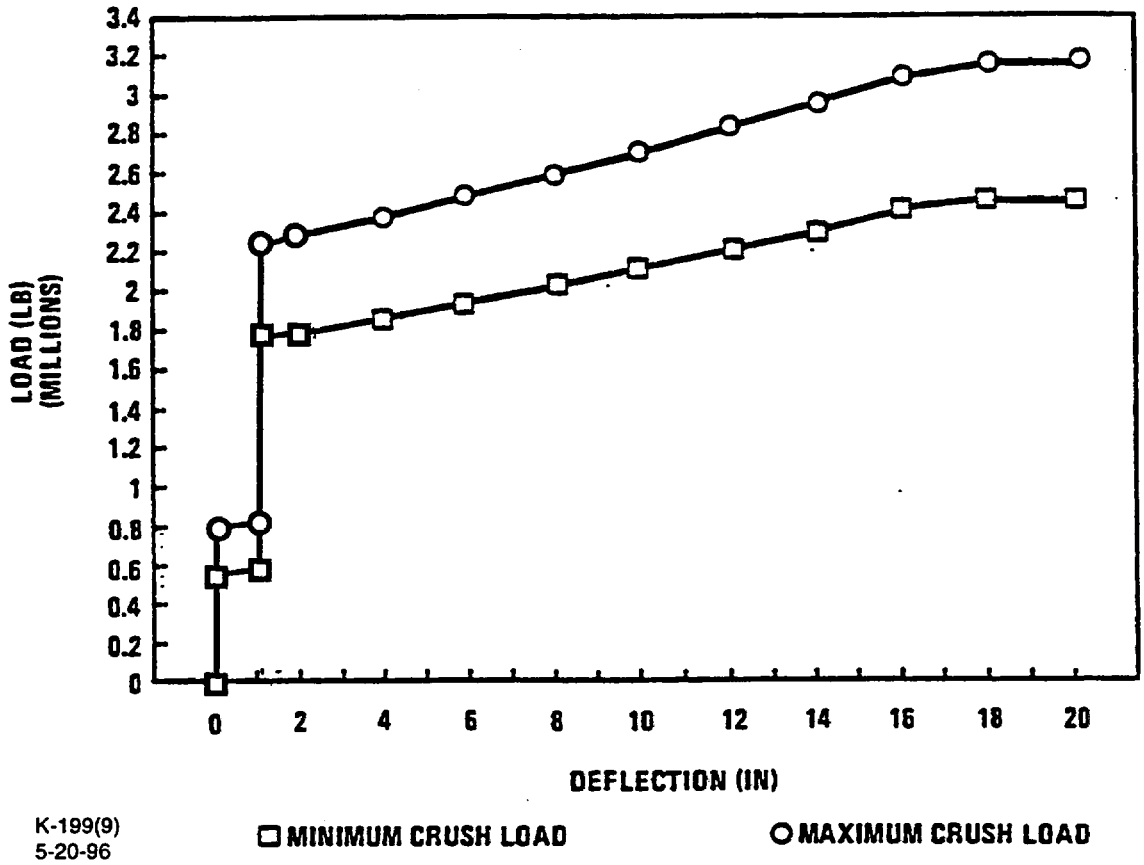

Fig. 2.10.3-9. End drop (90°) force-versus-deflection curve

TABLE 2.10.3-1
TESTS PERFORMED ON 1/4-SCALE MODEL IMPACT LIMITERS

Impact Limiter Number	Test on Impact Limiter	Test Crush Orientation (Degrees)	Energy Dissipated during Tests (lb-in.)
1	1 2	60 15	626,178 480,743
2	1 2	0 (side) 45	324,570 464,708
3	1 2	75 30	698,051 218,119
4	1	90 (end)	717,358

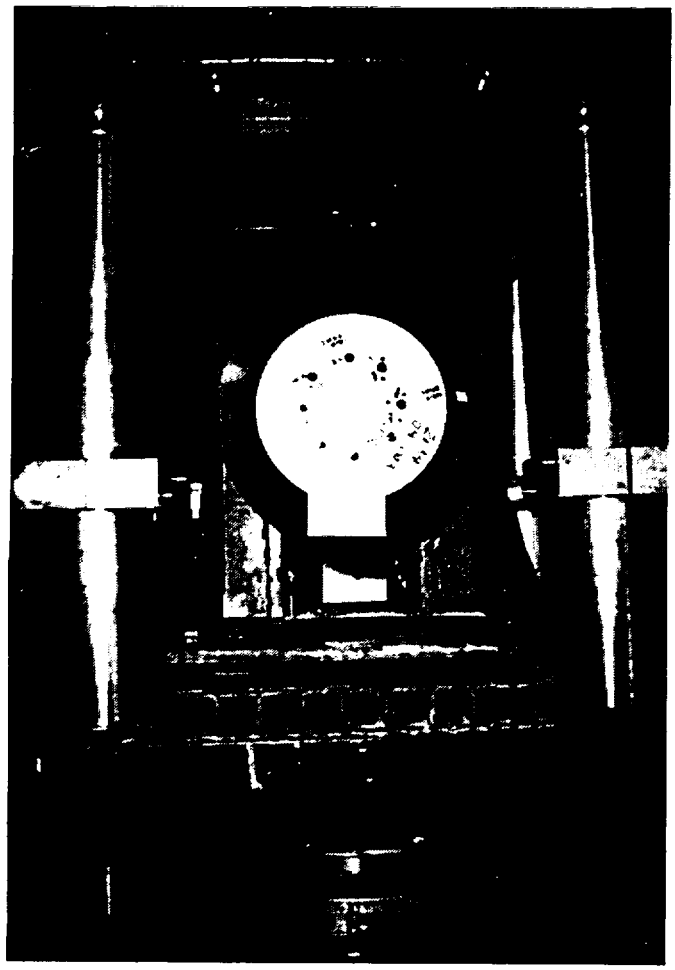

K-199(25)
9-1-92/Mac

Fig. 2.10.3-10. 1/4-scale impact limiter test set-up

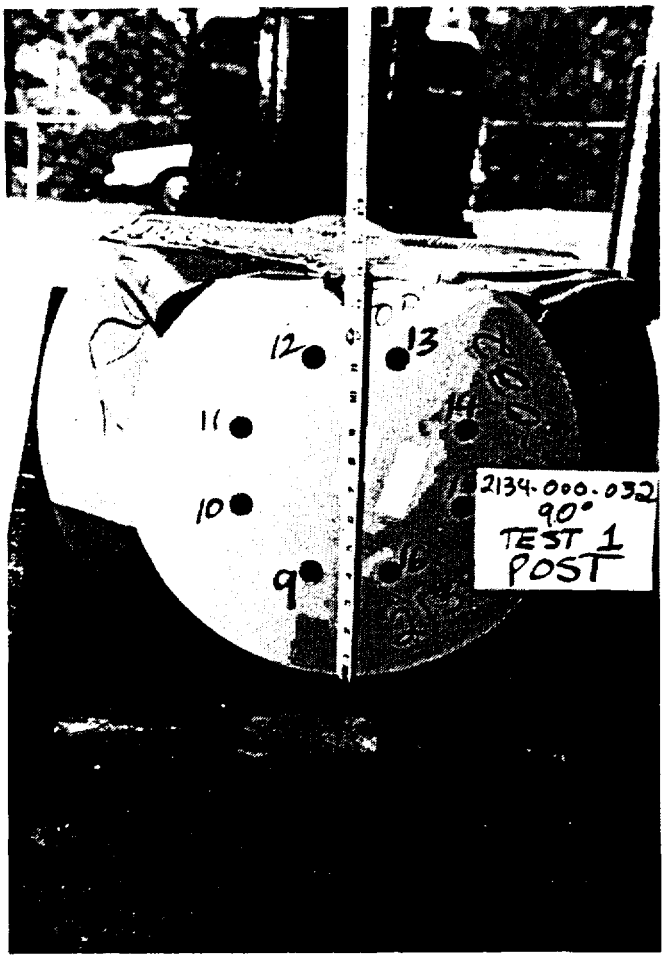

K-199(24)
9-1-92/Mac

Fig. 2.10.3-11. 1/4-scale impact limiter after a 0° (side) crush

- A 1.5° taper was added to the inner surface of the impact limiter to facilitate installation and removal from the cask. This minor change does not affect the behavior of the impact limiters.

The test results are shown in Figs. 2.10.3-12 through 2.10.3-18. All tests showed an even crush, and no splits or tears developed on the impact limiter face sheets. The load-versus-deflection curves for the second test on each of the impact limiters are used only to get an idea of the effectiveness of the impact limiter and the general shape of the curve, since it is hard to determine the extent, if any, of the internal damage on the honeycomb pieces after the first test. For example, after the 75° test, the outer diameter of the impact limiter had grown from 22.48 in. to 23.06 in. This suggests that the impact limiter had suffered some damage during the test, even in areas where there was no crushing. As shown in Section 2.10.3-5, the results of the 30° test (the second test after the 75° test) are lower than expected. Therefore, it is reasonable that the reduced performance of the impact limiter is due to the damage from the first test. It is harder to determine if the second load-versus-deflection curve for the other impact limiters are suspect, since the damage on the sides opposite the initial tests was not so obvious as after the 75° test. A comparison with the expected curves (see Section 2.10.3.5) shows good agreement, which indicates that the damage of the initial tests did not affect the performance of the impact limiter durings the second test.

Table 2.10.3-1 also shows the energy dissipated by the impact limiters during the tests before the impact limiters bottomed out. Section 2.10.4.1 shows that the GA-4 impact limiters need to absorb less than 20.6×10^6 lb-in. energy during an end or near-end 30-ft drop (90° to 75°); less than 16.1×10^6 lb-in. during a 60° drop (initial hit); and less than 15×10^6 lb-in. during other angle, side, or slapdown drops. Converting these to 1/4-scale values (divide by 64) and taking out the strain effect factor (divide by 1.1) these values become 292,614 lb-in., 228,693 lb-in. and 213,068 lb-in. respectively. Table 2.10.3-1 shows that the impact limiters absorbed more than the required energy.

The test load-versus-deflection curves show an increase in the crushing force that indicates bottoming out of the honeycomb at depths well past 70 percent of the total thickness. It is especially true at angles other than 90° (end test, perpendicular to flat end of cask). Table 2.10.3-2 shows the deflection and the percentage of the initial honeycomb thickness at which the test impact limiters bottomed out.

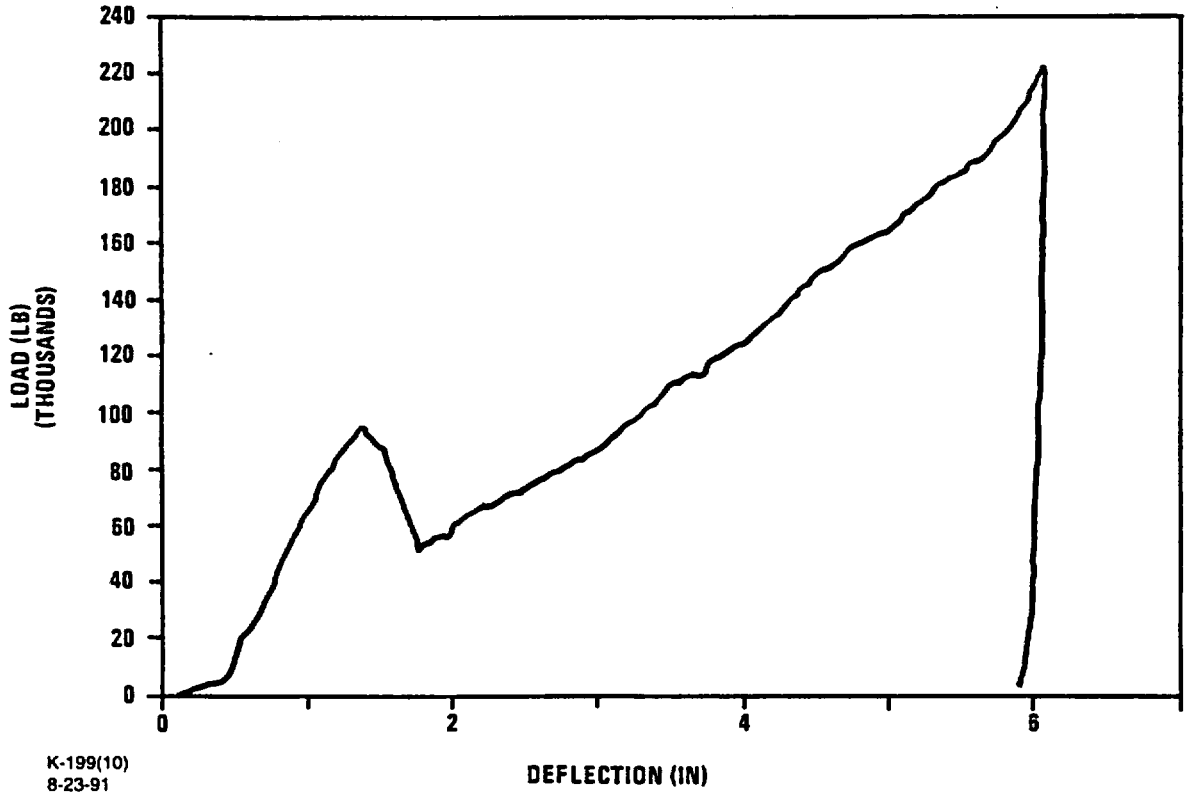

Fig. 2.10.3-12. 1/4-scale test results, 60° test (test 1 on model)

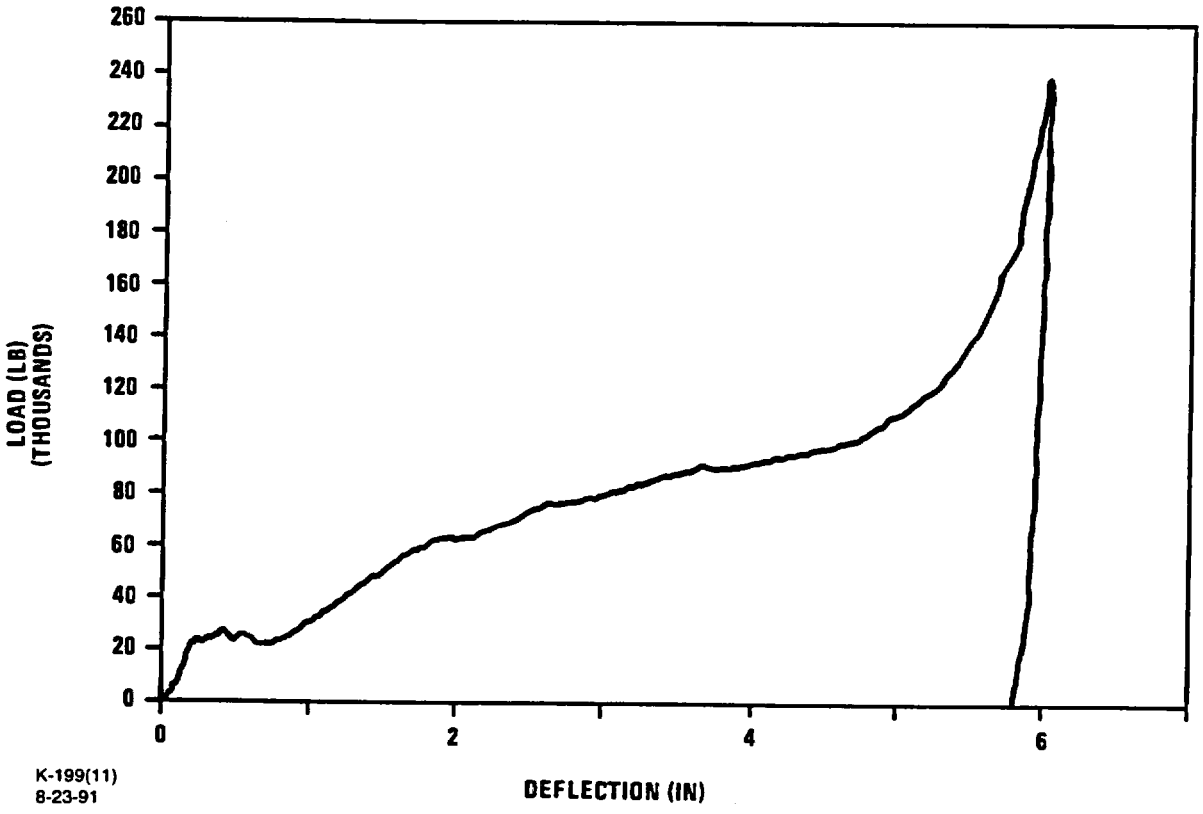

Fig. 2.10.3-13. 1/4-scale test results, 15° test (test 2 on model)

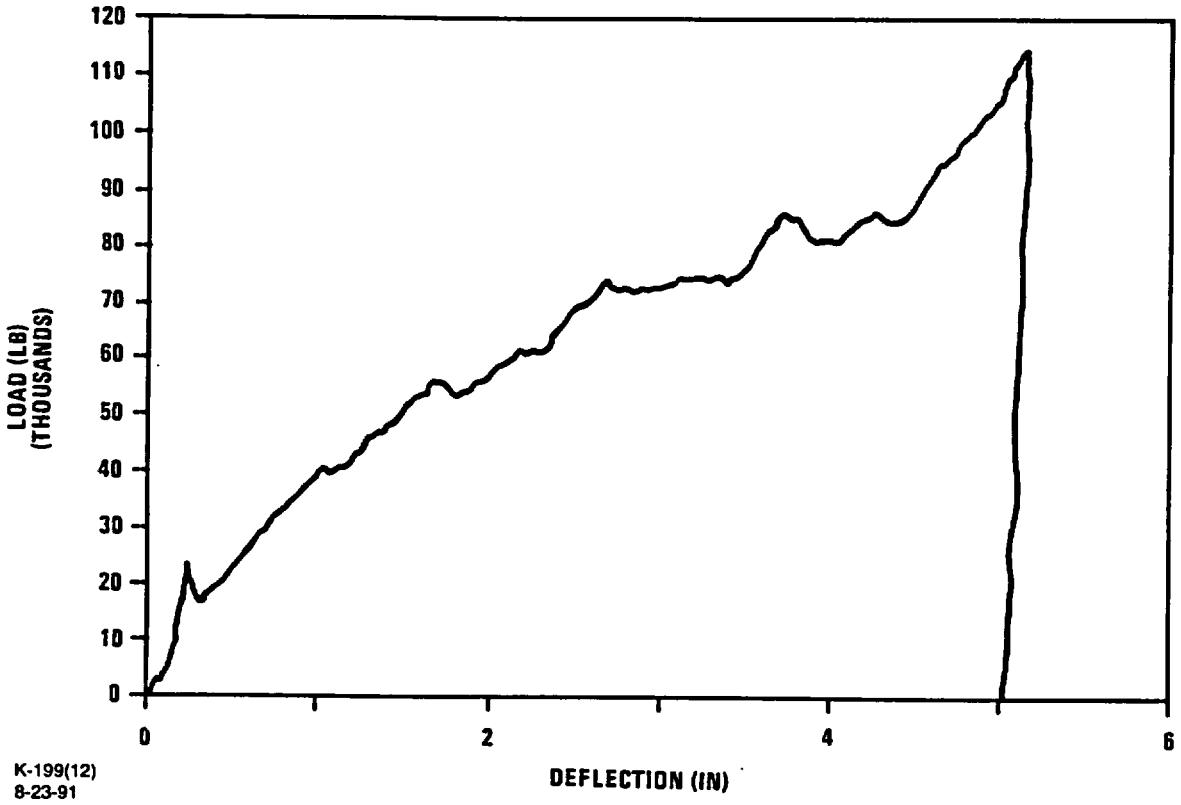

Fig. 2.10.3-14. 1/4-scale test results, 0° (side) test (test 1 on model)

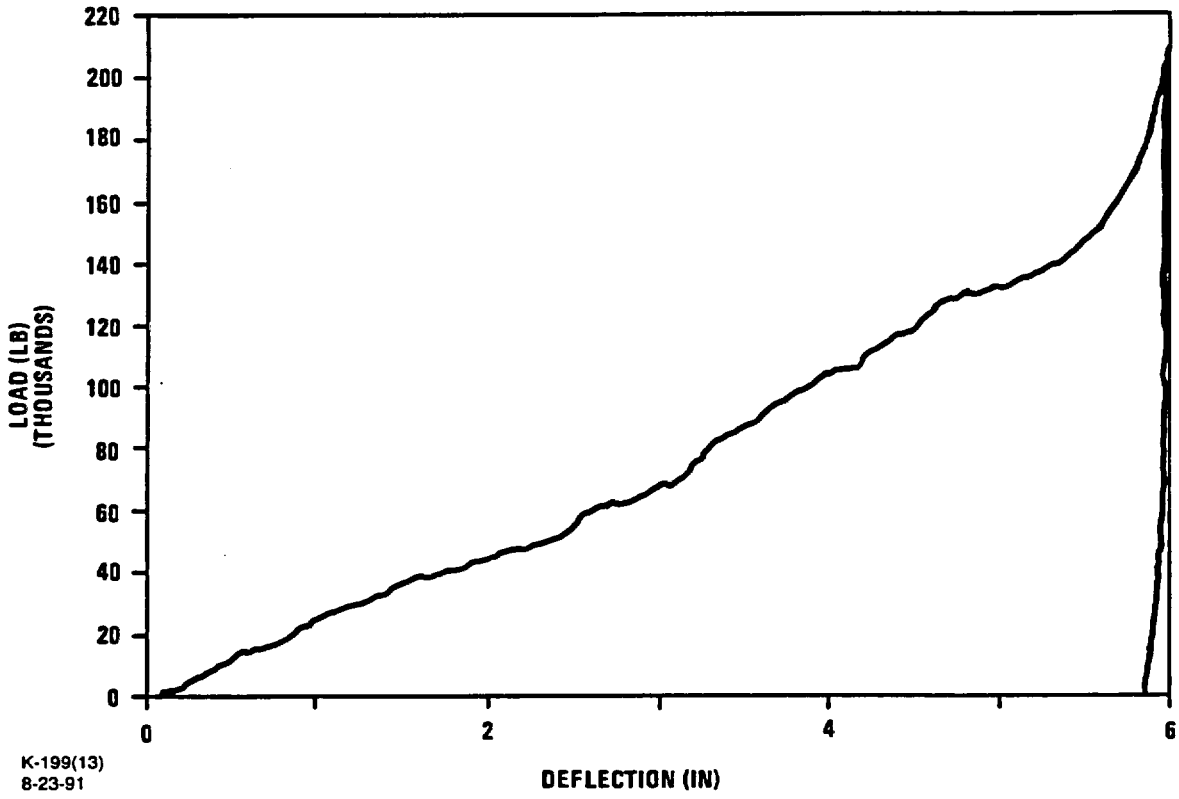

Fig. 2.10.3-15. 1/4-scale test results, 45° test (test 2 on model)

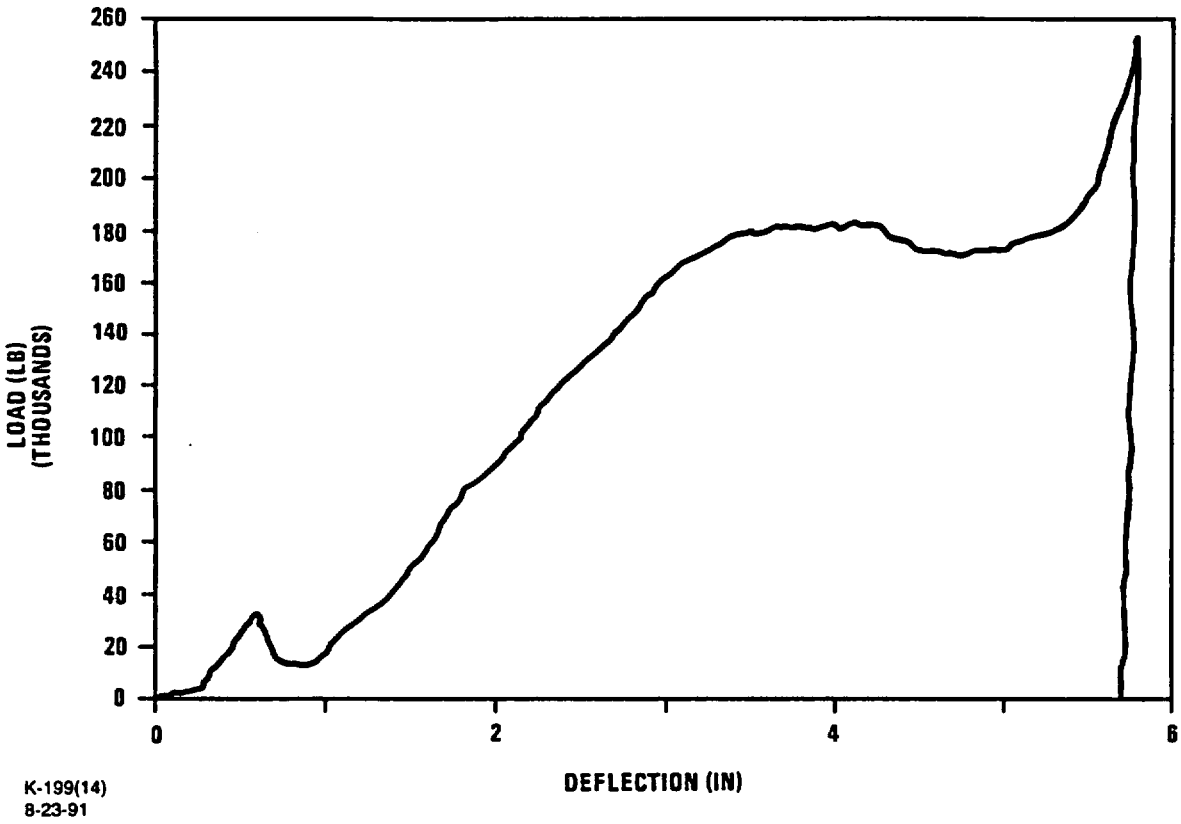

Fig. 2.10.3-16. 1/4-scale test results, 75° test (test 1 on model)

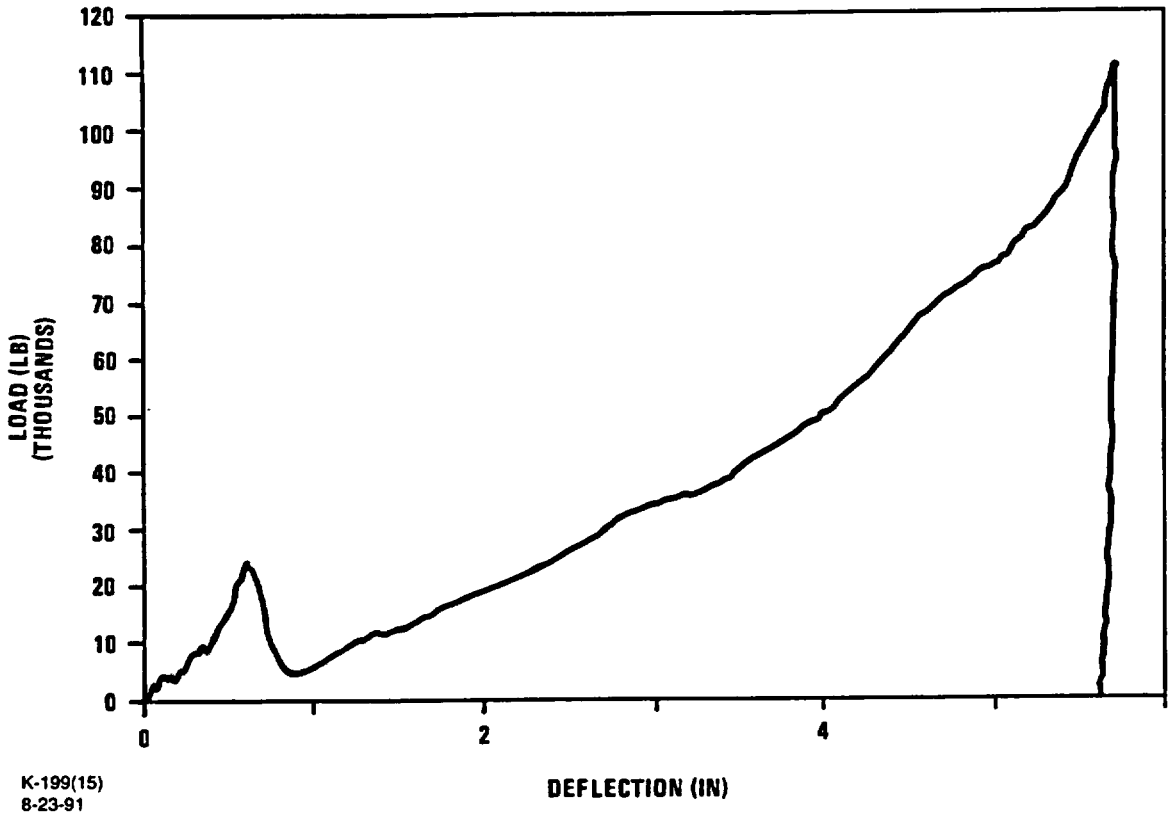

Fig. 2.10.3-17. 1/4-scale test results, 30° test (test 2 on model)

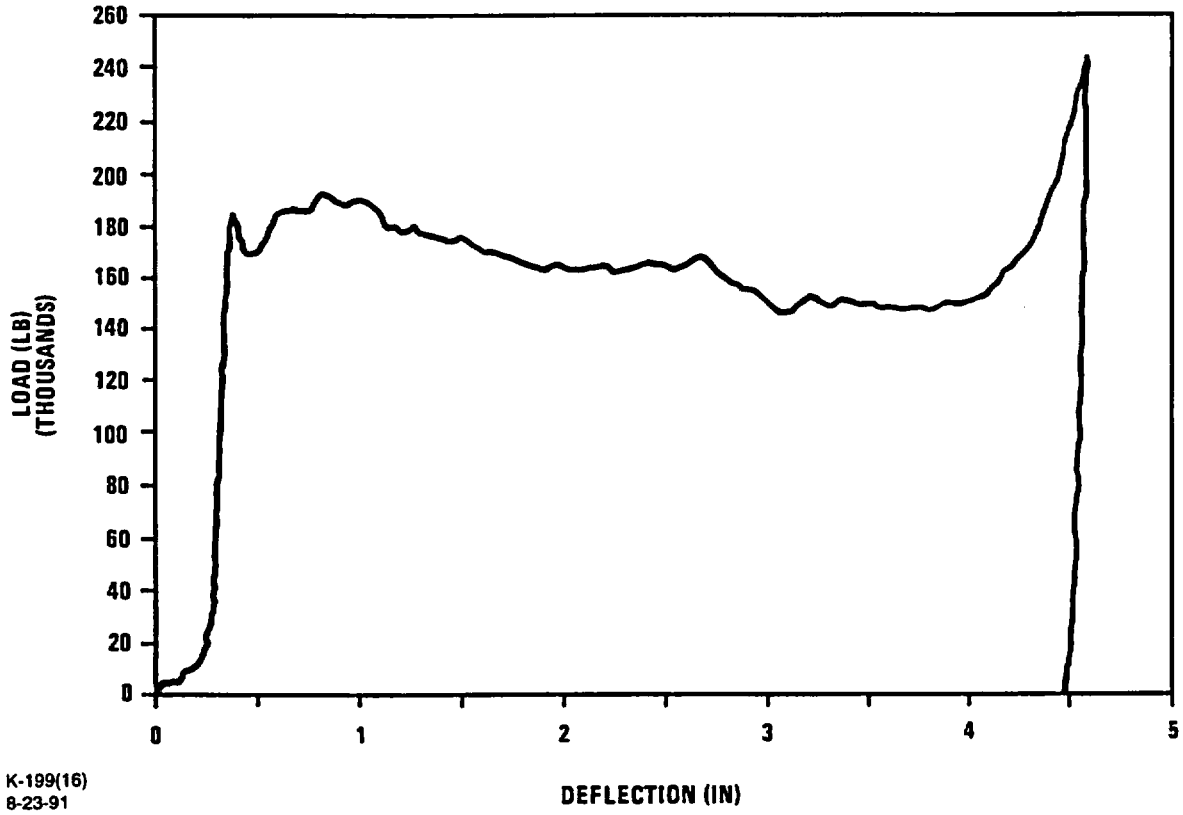

Fig. 2.10.3-18. 1/4-scale test results, 90° (end) test (test 1 on model)

TABLE 2.10.3-2
DISPLACEMENTS AT WHICH THE OPTIMIZED TEST IMPACT LIMITERS BOTTOMED OUT

Test Angle (Degrees)	Displacement (Inches)	% of Initial Honeycomb Thickness
0	5.00	80
15	5.25	76
30	5.5	78
45	5.75	80
60	5.75	80
75	5.25	78
90	4.25	74

2.10.3.5 Comparison of Test and Analytical Results. Figures 2.10.3-19 through 2.10.3-25 compare the impact limiter test force-versus-deflection curves with the ILMOD analytical curves, compare the maximum impact limiter deflection with the impact limiter deflection at which the honeycomb begins to bottom out, and show the energy absorbed by the impact limiters during a 30-ft drop. Figure 2.10.3-24a, 78° CG-over-corner, shows only ILMOD data since the 1/4-scale tests were conducted at 15° increments at angles from 0° to 90°. Figure 2.10.3-24 compares test results at 75° with ILMOD.

The maximum and minimum ILMOD curves show the effects of manufacturing tolerances and temperature on the honeycomb crush strength.

The 1/4-scale test data was scaled to full scale as follows:

- Forces were multiplied by 16 and the displacement values by 4 to convert them to full-scale.
- The static test forces were also multiplied by 1.1 to account for the dynamic strain rate effects.

The test load-versus-deflection curves show good correlations with the ILMOD analytical test results. In particular, the 0° side orientation, which is shown to produce the highest stress (Section 2.7), has exceptionally good correlation.

In addition, the impact limiters show ample margin against bottoming out. The minimum margin is 2.7 in. for the 60° 30-ft drop. Tables 2.10.4-8 through 2.10.4-10 show in tabular form the crush depths and margins against the initiation of bottoming out. It should be noted that in most cases, for example the side drop, only a small portion of the honeycomb involved in the crush footprint is at the point of bottoming out. Most of the remaining honeycomb in the crush footprint can sustain significantly more crushing before bottoming out. Consequently, the crush force rises gradually after the initiation of bottoming out, rather than sharply as it does in an end drop where all of the honeycomb in the crush footprint has the same thickness and crush deflection.

The largest differences between the test and analytical results occur during the end crush. The test showed a higher initial crush load, dropping to the analytical value later in the crush. The higher load is partly attributable to the buckling of the impact-limiter-bolt guide tubes in the end of the impact limiter. To reduce this tube buckling load, GA changed the tube material from 1/8 hard Type 304 stainless steel with a yield of 90 ksi to 304 Stainless Steel annealed with a minimum yield of 30 ksi. In addition, the tube wall thickness was decreased from .07-in.-thick to .035-in.-thick. This change reduces the guide tube buckling loads to a level that is small compared to the honeycomb crush load, while still maintaining the necessary energy absorption capability during an end crush. The remaining difference between test and analytical results is ignored since the design margins for the cask and neutron shield structure for the 1-ft end drop are high.

The crush forces from the 30° test are lower than the ILMOD data. As discussed in Section 2.10.3.4, this is almost certainly due to the fact that this was the second test of the impact limiter and the first 75° test weakened the impact limiter. After the 75° test, the outer diameter of the impact limiter had grown from 22.48 in. to 23.06 in.

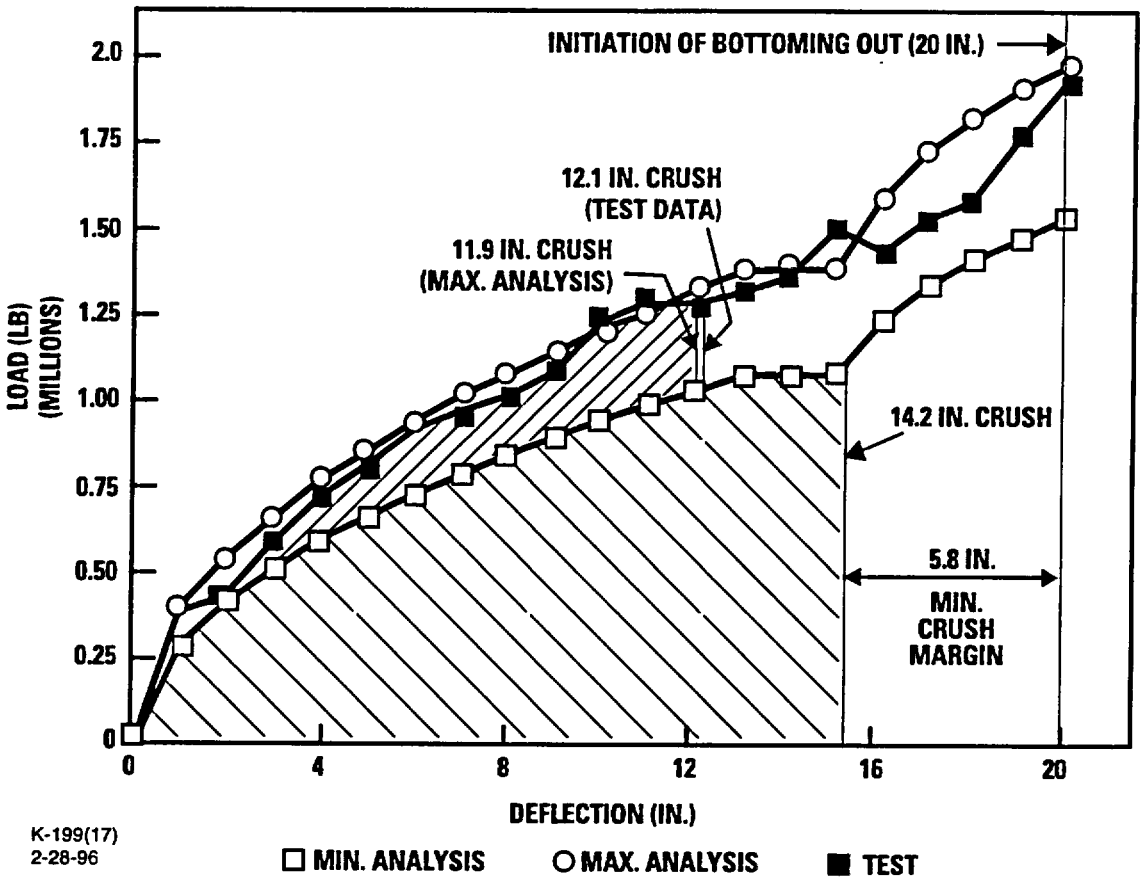

Fig. 2.10.3-19. Test and analysis results comparison (0°, side), 30-ft drop energy and crush margin

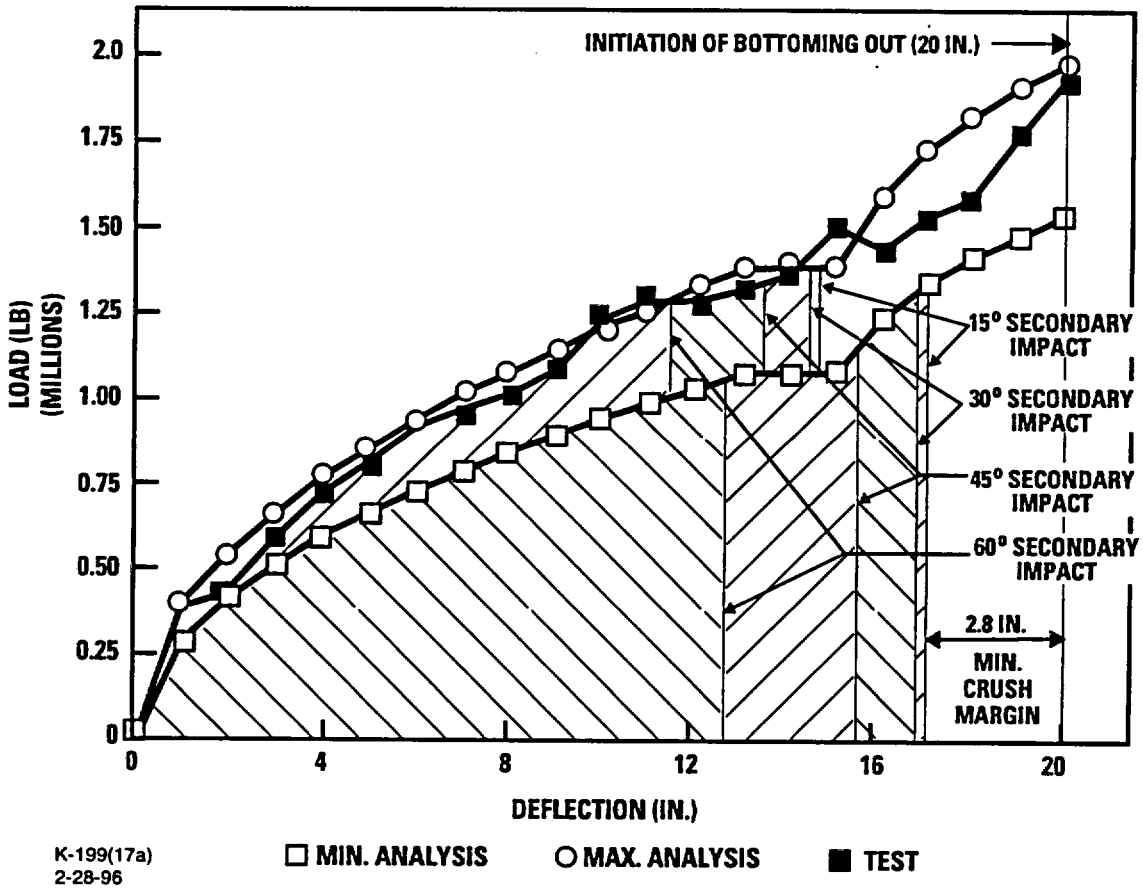

Fig. 2.10.3-19a. Test and analysis results comparison (slapdown impacts), 30-ft drop energy and crush margin

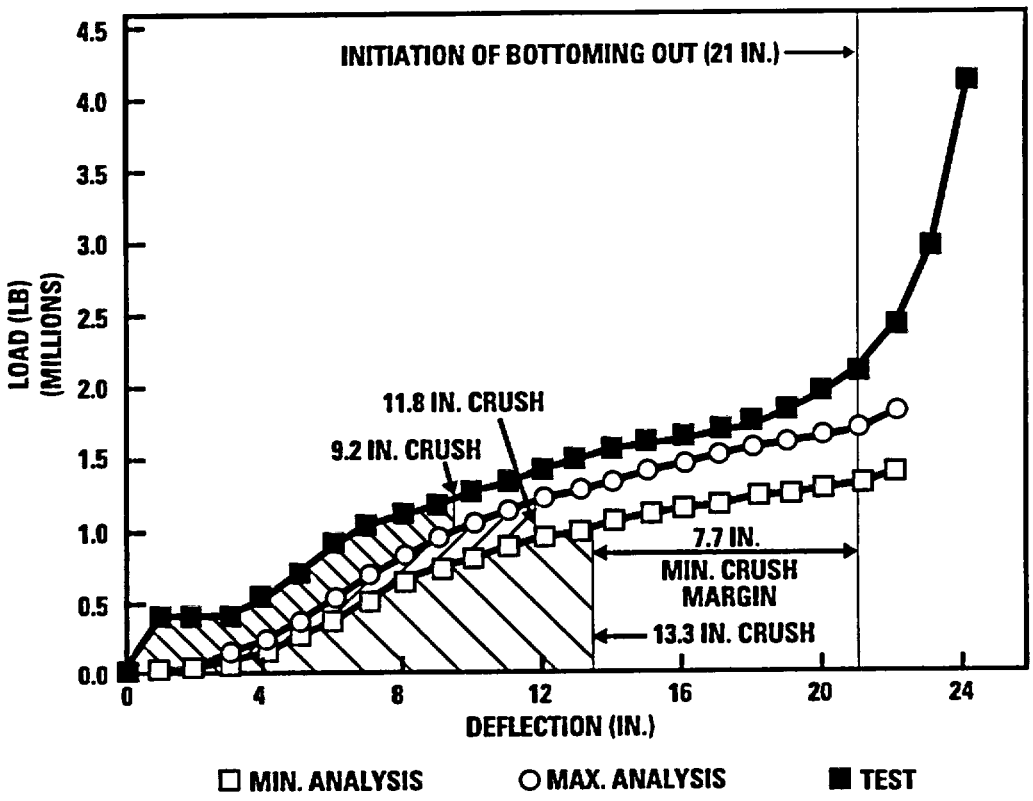

K-199(18)
3-19-96

Fig. 2.10.3-20. Test and analysis results comparison (15°), 30-ft drop energy and crush margin

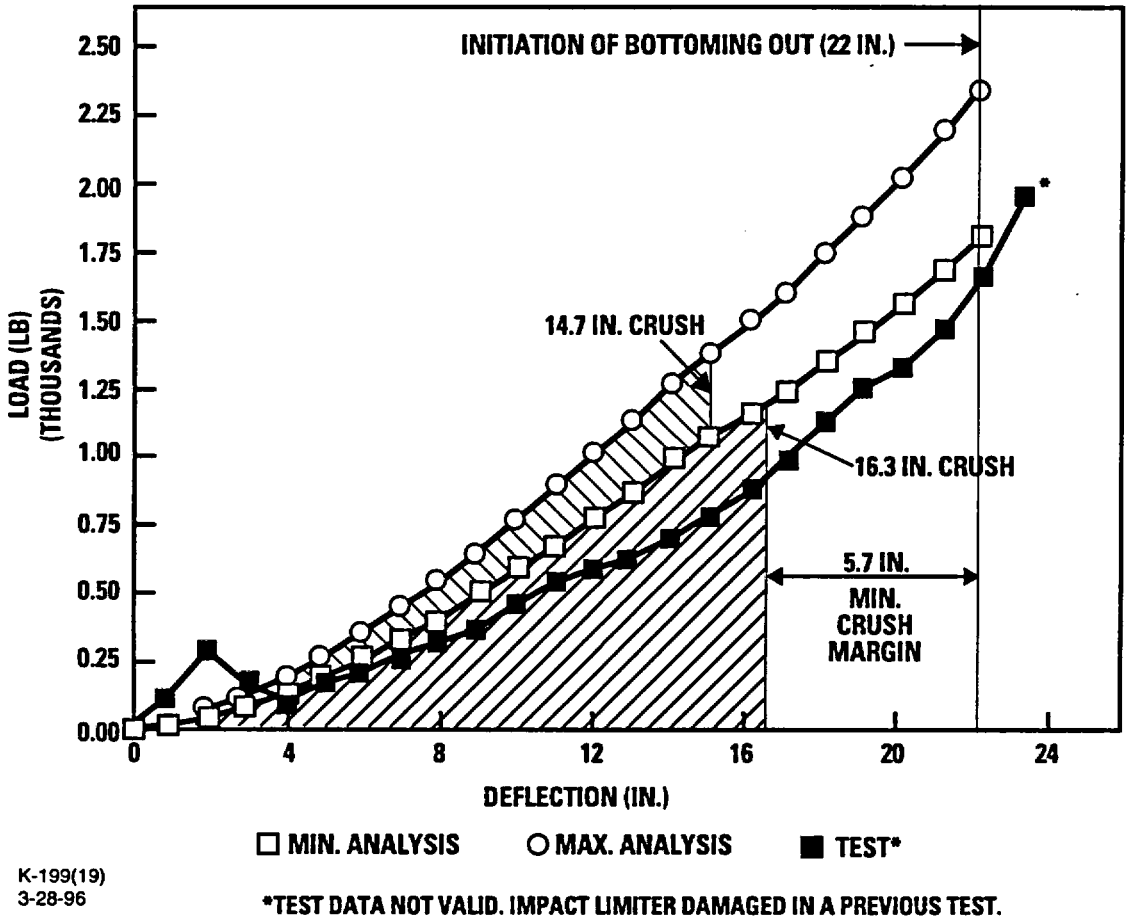

Fig. 2.10.3-21. Test and analysis results comparison (30°), 30-ft drop energy and crush margin

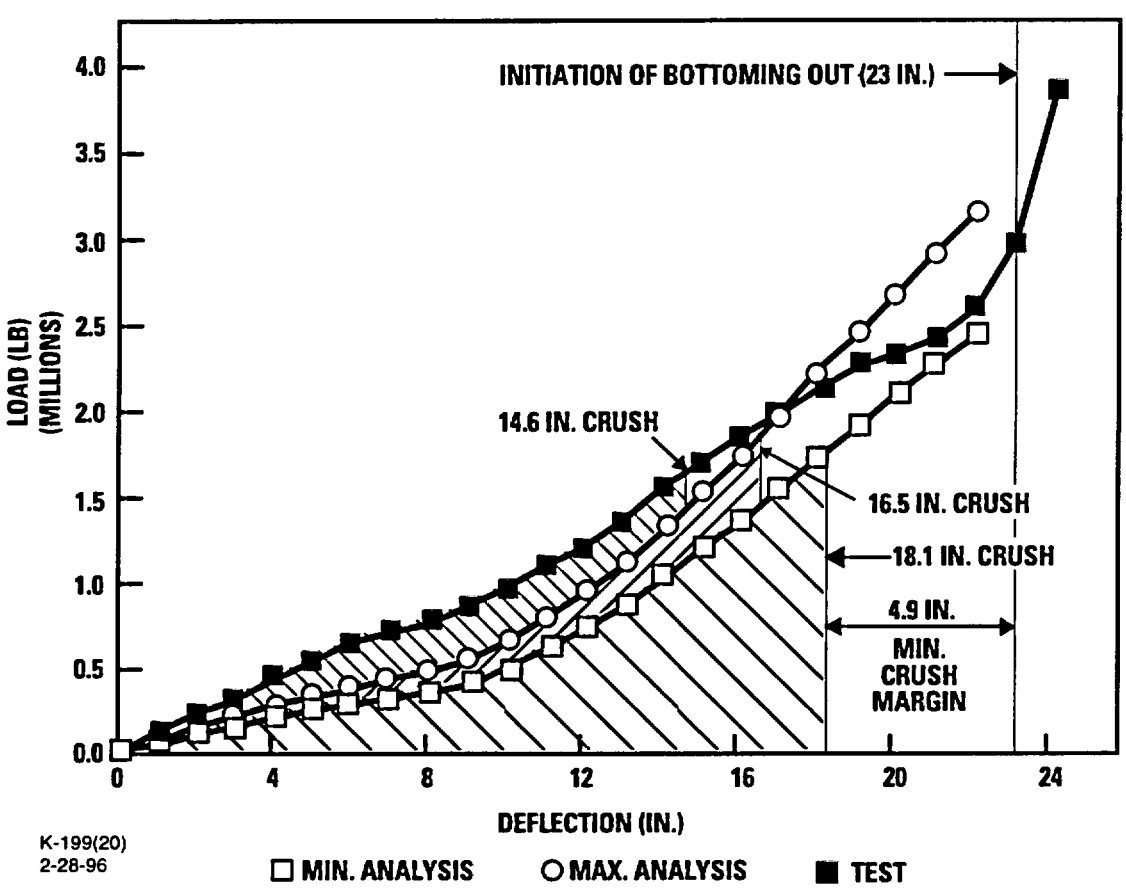

Fig. 2.10.3-22. Test and analysis results comparison (45°), 30-ft drop energy and crush margin

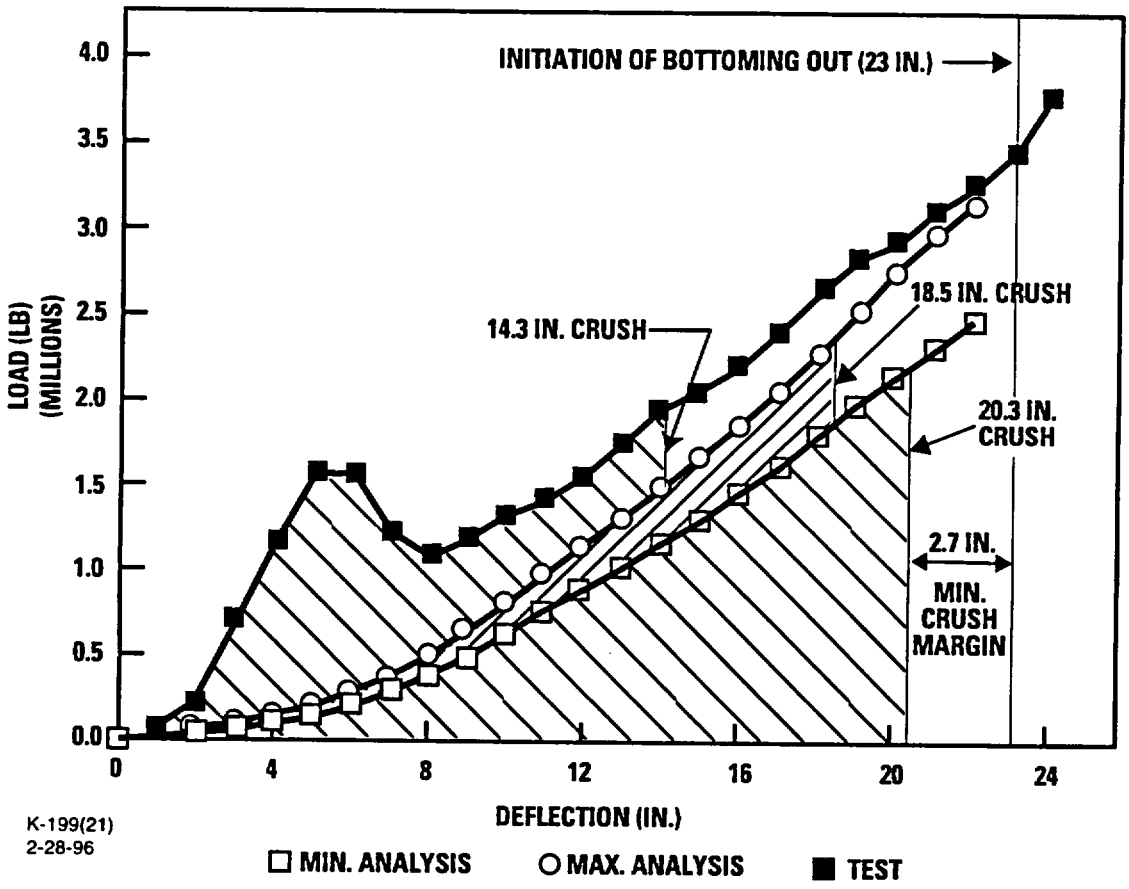

Fig. 2.10.3-23. Test and analysis results comparison (60°), 30-ft drop energy and crush margin

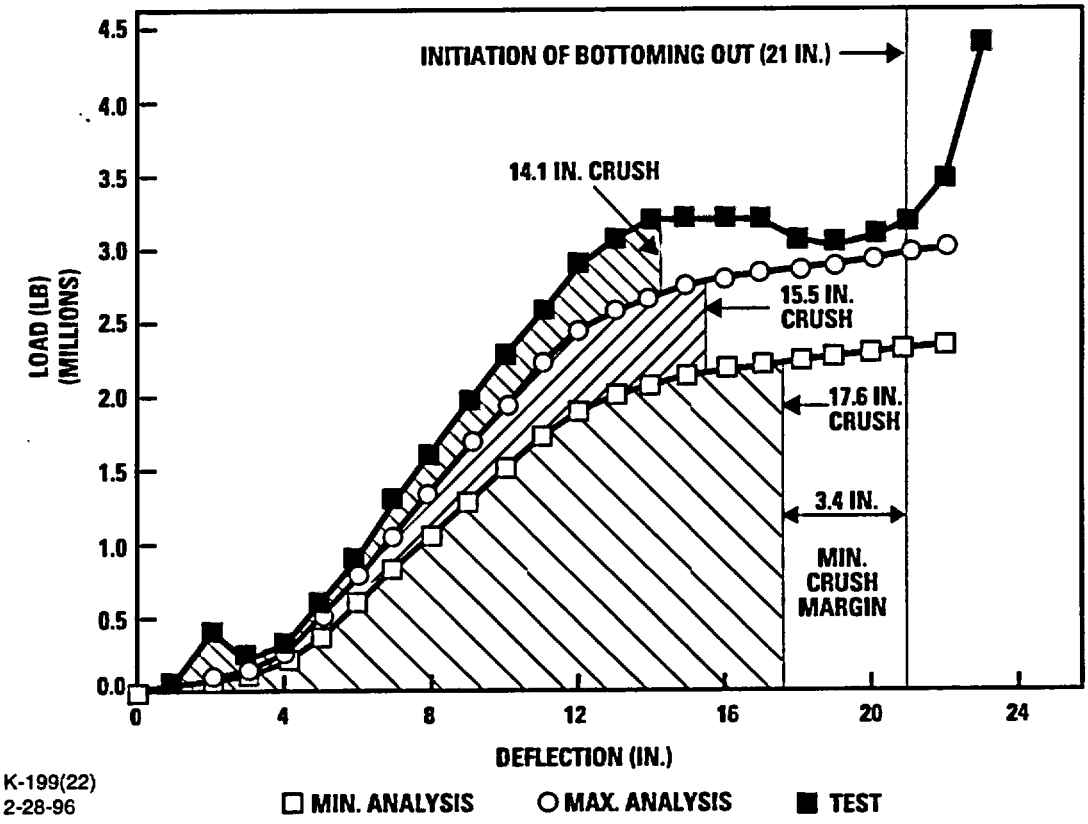

Fig. 2.10.3-24. Test and analysis results comparison (75°), 30-ft drop energy and crush margin

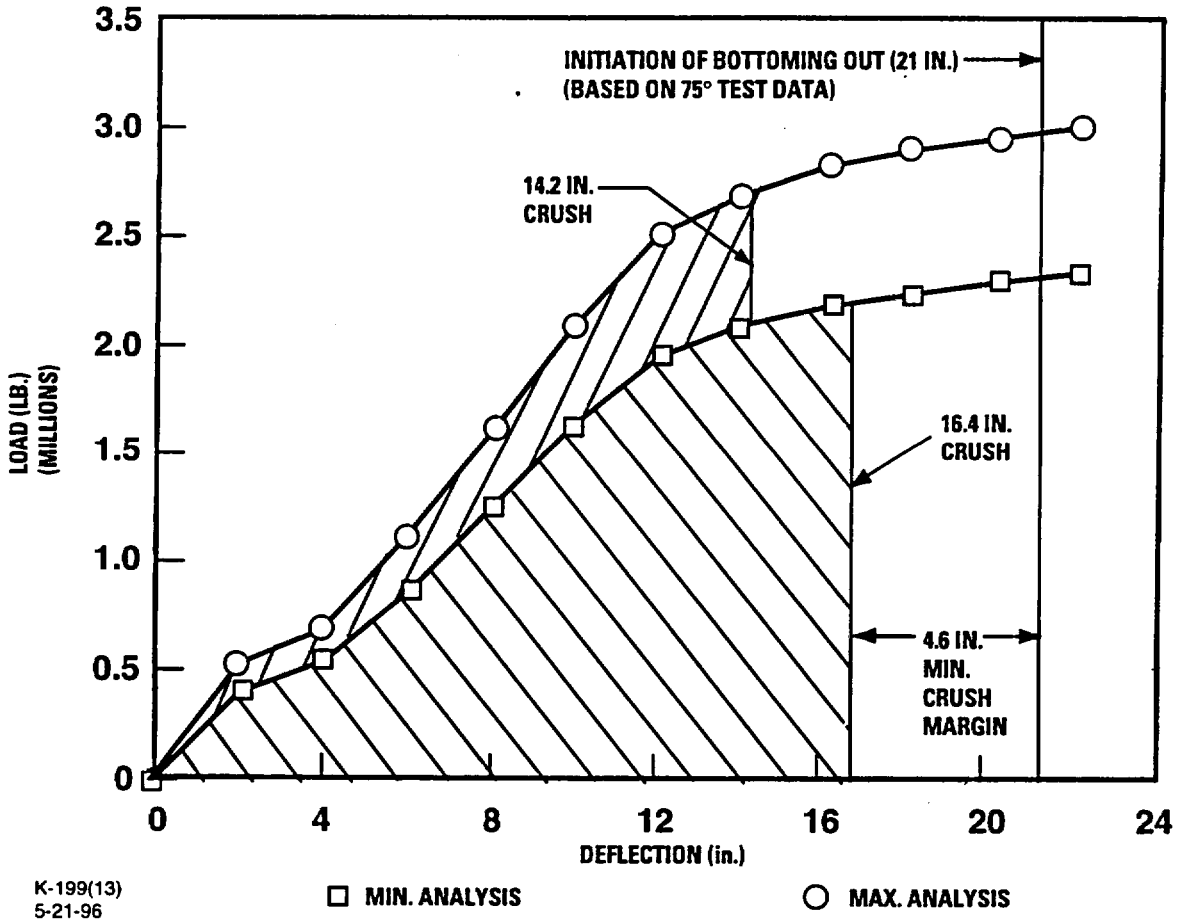

Fig. 2.10.3-24a. Analysis results (78°), 30-ft drop energy and crush margin

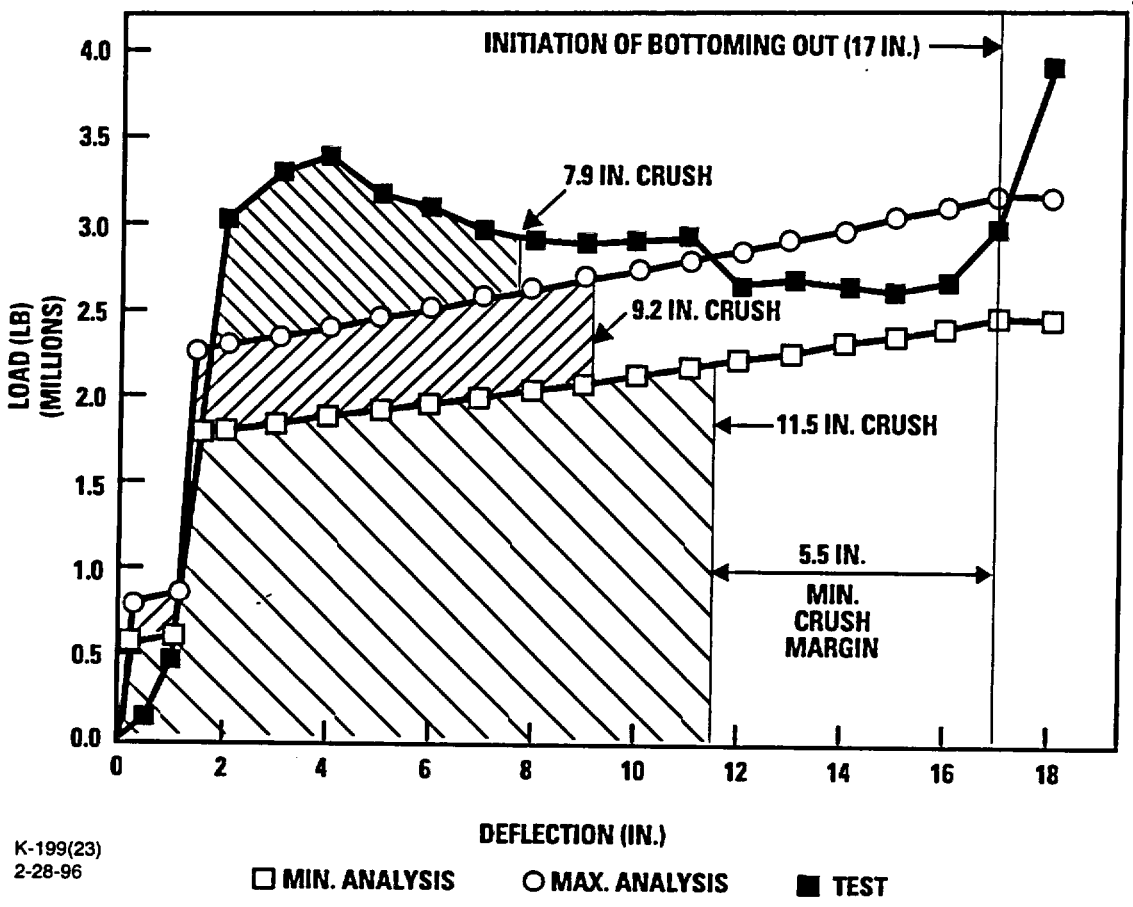

Fig. 2.10.3-25. Test and analysis results comparison (90°), 30-ft drop energy and crush margin

For all other tests, the test data are within or slightly above the ILMOD data. To be conservative, GA analyzed the impact limiters (see Section 2.10.4) using all three sets of data: the maximum and minimum ILMOD data and the test data.

In addition, the test was performed without the 1.6-in-thick 220 psi crush strength honeycomb at the outer end surface. Therefore, the calculated force-versus-deflection curve is used for the 1-ft drop and 30-ft drop analyses.

2.10.3.6 Impact Limiter Support Structure (ILSS). The impact limiter support structures are the structures around the bottom and top ends of the cask that transfer the loads from the impact limiters to the cask body. Each structure consists of a 0.4-in.-thick outer shell which is plug welded to thirty-six ribs, which in turn are double fillet welded to the exterior of the cask body. Each rib is 0.75 in. thick except for a 1.0-in. length at the attachment to the cask body where the rib thickness increases to 0.88 in. All material is ASME SA-240 Type XM-19. Figure 2.10.3-26 shows a cross section through an ILSS, and Fig. 2.10.3-27 shows a longitudinal section through the upper ILSS. The length of each ILSS is 22.25 in., of which 21.76 in. are enclosed by each impact limiter. The ribs are drilled out to reduce weight. The drill hole pattern is shown in Fig. 2.10.3-28. Each ILSS also serves as part of the neutron shield tank system as discussed in Section 2.10.11.

In the following sections, the cask is analyzed for 30-ft side and secondary slapdown impacts (Section 2.10.3.6.1), an end impact (Section 2.10.3.6.2), and other oblique impacts (Section 2.10.3.6.3). The side and secondary slapdown impacts consider two orientations: (1) a corner of the square cross section faces the ground at impact, and (2) flat side faces the ground at impact.

The analyses presented in this section demonstrate the adequacy of the ILSS to transfer the loads from the impact limiter to the cask body. Section 2.10.6 demonstrates the adequacy of the cask body to carry these loads.

The half-scale tests confirm the adequacy of the ILSS design. The test data show that the ILSSs did not deform during any of the tests. Further, none of the impact limiter housings (the inner shells of the impact limiters) deformed during any of the 30-ft drop tests.

The effects of the increased neutron-shield fluid pressure during a drop are evaluated in Section 2.10.11.4. The analyses show that the maximum neutron-shield-fluid pressure is 416 psi for a 30-ft end drop at the maximum temperature condition. This pressure includes the increase in pressure due to thermal expansion of the fluid. The analyses show that the ILSS top and bottom end plates can withstand this pressure and meet all design requirements. During a 30-ft drop, the effect of the fluid pressure is to act opposite to the impact limiter loads and thus will reduce the loads on the ILSS outer shell. Because it is less than the impact force, it may be conservatively neglected.

2.10.3.6.1 Side Drop and Secondary Slapdown. The maximum load on an impact limiter during a 30-ft side drop is 1310 kips (Table 2.10.4-1, 2620 kips/2), and the maximum secondary impact (slapdown) load is 1450 kips which occurs during the 15° angle drop (Table 2.10.4-1). Since both loads occur at approximately a zero degree impact angle (horizontal), the 1450-kip load is the critical load.

Two loading conditions are evaluated, each selected to conservatively bound the actual loading condition: (1) the maximum compressive loads transferred from the impact limiter to the cask body and (2) the maximum shear load transferred from the impact limiter to the ILSS.

Security-Related Information Figure
Withheld Under 10 CFR 2.390.

Fig. 2.10.3-26. Section view of GA-4 ILSS

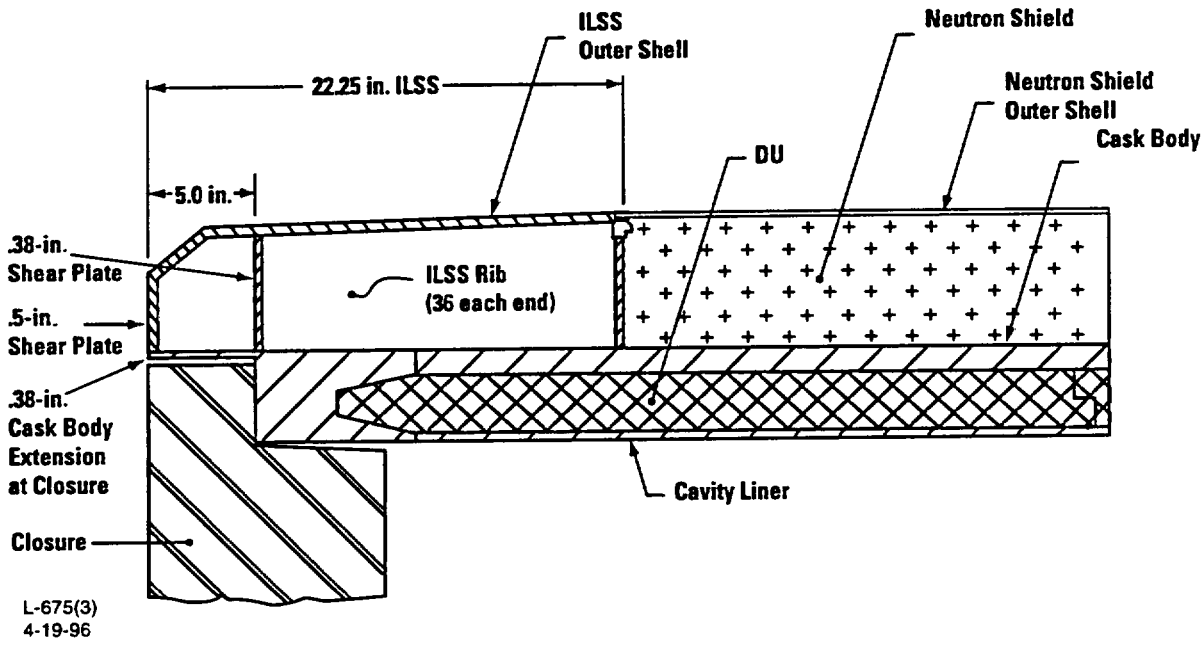

Fig. 2.10.3-27. Longitudinal section through ILSS at middle of flat side of cask

Security-Related Information Figure
Withheld Under 10 CFR 2.390.

Fig. 2.10.3-28. Cross-sectional view of ILSS ribs

Figure 2.10.3-29 shows the upper ILSS loading condition (from ILMOD, described in Section 2.10.1.4) that produces the maximum shear load. The inboard portion of the load (all of the 60.5-kips/in. load and a small portion of the 12.4-kips/in. load) is transferred through compression directly into the ILSS. The outboard portion of the load (almost all of the 12.4-kips/in. load) is not directly backed by the ILSS and consequently must be carried by the impact limiter honeycomb to the end of the ILSS. The moment from this outboard load is reacted by tension in the impact limiter bolts and compression between the impact limiter and the ends of the cask (Section 2.10.3.7). Two shear plates (0.5-in. end shear plate and 0.38-in. shear plate, Fig. 2.10.3-27) are incorporated into the upper ILSS to transfer this load to the cask body. These plates are shown in Section 2.10.3.6.1a to be capable of transferring all of the load outboard of the ILSS to the cask body. Buckling of these shear plates will not occur since they are welded to the ILSS ribs and are therefore deflection controlled. The outer shell is in membrane tension where the impact load is applied, therefore it will not buckle.

At the bottom end of the cask, a 0.38-in. shear plate is not needed since the impact limiter loads are transferred directly to the solid 9.5-in.-thick bottom plate through the ribs. However, at the closure end this shear plate is welded to a 5-in.-long, 0.38-in.-thick cylindrical extension of the cask body. Section 2.10.3.6.1a shows that the outer 5-in. of the ILSS is sufficiently strong to transfer the loads into the cask body.

In Section 2.10.3.6.1c the ILSS is shown to have adequate strength to transfer the compressive loads from the impact limiter to the cask body. The analysis conservatively ignores that the load, which is outboard of the ILSS, is carried by the 0.5-in. shear plate directly into the cask body. Instead, it assumes that all of the load is transferred through the ILSS shell and ribs, increasing the 60.5-kips/in. load shown in Fig. 2.10.3-29 to 66.6 kips/in.

a. Maximum Shear Load. This section evaluates the capability of the ILSS to transfer the maximum shear load from the impact limiter to the cask body. As discussed above, this is of primary concern at the closure end where the load must be transferred to the cask body through the 5-in.-long ILSS shell that protects the closure lid (Figs. 2.10.3-27 and 2.10.3-29). The critical loading is for a drop on the flat side of the cask.

Shear Plates. The portion of the upper-end ILSS surrounding the closure lid has two shear plates, one 0.5-in. thick and the other 0.38-in. thick, separated by 4.5 in. (Figs. 2.10.3-27 and 2.10.3-29).

End Shear Plate. Assuming that all of the load is carried by the plates and none is carried by the ribs, the stress and design margin (D.M.) for the 0.5-in. plate are shown below. Calculating the membrane stress, σ_m we have

$$\sigma_m = P/A = 23.1 \text{ ksi};$$

where

P = load in 0.5-in. plate (Fig. 2.10.3-29),

= load outboard of plate + load on first 2.5 in. of ILSS,

= (26.16 in. – 3.2 in. + 5.0 in./2) 12.4 kips/in. = 315.7 kips;

Security-Related Information Figure
Withheld Under 10 CFR 2.390.

Fig. 2.10.3-29. Impact limiter side loads on ILSS due to 30-ft slapdown (15°) load of 1450 kips

A = cross section area,

= thickness x cask body width,

= 0.5 x 27.32 = 13.66 in.^{2}

The maximum bending stress on the end shear plate due to the maximum neutron shield tank pressure of 173.6 psi (Section 2.10.11.4) on a side slapdown drop is conservatively calculated as follows. The maximum end drop pressure case is not considered since the impact force is opposite to the pressure force.

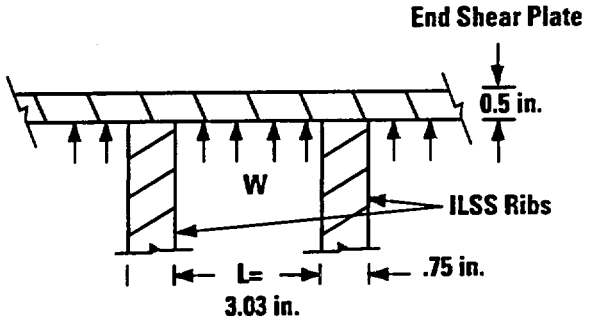

$\sigma_b = \frac{Mc}{I}$, K-199(11) 5-21-96

= 3.2 ksi (side slapdown),

where

M = $\frac{wL^2}{12}$ (fixed ends ignoring side fixity at the outer shell and cask body extension),

= 772 in.-lb,

L = 3.03 in.,

c = 0.50/2 = 0.25 in.,

I = $\frac{5.81(.5)^3}{12}$ (using 5.81 in. to represent the height),

.061 in.^{4}, and

w = 173.6 psig x 5.81,

= 1009 lb/in.

Combining this bending stress with the maximum compression from Section 2.10.3.6.1a

$\sigma_{total} = \sigma_m + \sigma_b$

= 23.1 ksi + 3.2 ksi,

= 26.3 ksi.

Evaluating the design margin, we have:

D.M. = $(S_{allow}/\sigma_{total}) - 1$,

= 2.8,

where

S_{allow} = $P_m + P_b$ allowable = 99.5 ksi (hypothetical accident conditions)

The actual D.M. is higher since some of the load is transferred to the sides of the cask by shear and some of the load is carried by the ribs.

0.38-in. Shear Plate. Similarly, assuming that all of the load is carried by the plates and none is carried by the ribs, the stress and design margin (D.M.) for the 0.38-in. shear plates are shown below.

σ_m = P/A = 117.6/8.07 = 14.6 ksi;

where

P = load in 0.38-in. plate (Figs. 2.10.3-27 and 2.10.3-29),

= load on second 2.5 in. of ILSS,

= (0.7 in.)(12.4 kips/in.) + (1.8 in.)(60.5 kips/in.),

= 117.6 kips;

A = cross section area,

= thickness x cask body width x factor of 28/36
(shear plates removed at location of impact limiter bolt tube),

= 0.38 in. x 27.32 in. (28/36) = 8.07 $in.^2$, and

D.M. = $(S_{allow}/\sigma_m) - 1$,

= 3.8;

where

S_{allow} = P_m allowable = 69.7 ksi at 200°F (hypothetical accident conditions).

The actual D.M. is higher since some of the load is transferred to the sides of the cask by shear and some of the load is carried by the ribs.

b. Cask Body Extension at Closure (Figs. 2.10.3-27 and 2.10.3-29). This section shows that the 5-in.-long, 0.38-in.-thick extension of the cask body can carry all of the moment applied to the outer 5 in. of the ILSS and the neutron shield fluid pressure without the help of the ILSS ribs and outer shell. This assumption is very conservative since the actual loads are shared by all three components: the cask body, ILSS ribs, and ILSS shell.

Shear. Assuming that all of the shear is carried by the cask body extension at the closure, the maximum shear stress is computed as follows:

τ = 1.5 x P/A_s = 31.35 ksi, (flat orientation),

= 15.7 ksi, (corner orientation);

where

P = load on outer 5.0 in.,

= 324 kips + 1.8 in. (60.5 kips/in.) (See free body diagram, Fig. 2.10.3-29),

= 433 kips;

A_s = area of 0.38-in.-thick cask body shell,

= 0.38 [2 x 27.32],

= 20.76 in.^{2} (flat orientation, conservatively taking the area of the vertical legs only)

= 0.38 [2 x 27.32 + 2 x (27.32 – 0.38)],

= 41.24 in.^{2}, (corner orientation).

Moment. Assuming that all of the moment is carried in the cask body extension at the closure and none by the ILSS, the bending stress is computed as follows:

$$\sigma_b = \frac{Mc}{I} = 4.7 \text{ ksi, (flat orientation)}$$

= 6.6 ksi, (corner orientation);

where

M = moment on outer 5 in. of ILSS,

= 315.7 x 5 + (3.2 – 2.5)(12.4)(1.8 + .70/2) + 1.8 (60.5)(1.8/2),

= 1695 kip-in.;

I = 1/12[(27.32)(27.32)^3 – (27.32 – 2(.38))^4],

= 4954 in.^{4} (flat and corner orientations);

c = 27.32/2 = 13.66 in. (flat orientation),

= 27.32/(2 x 0.707) = 19.32 in. (corner orientation).

Neutron Shield Fluid Pressure. The pressure exerts a load on both the 0.5-in. end shear plate and the .38-in.-thick cask body extension at the closure. From Section 2.10.11.4, the maximum pressure during a 30-ft end drop is 472 psi and 173.6 psi for the 30-ft side slapdown drop. This is conservative since it assumes that the expansion tank is filled during the drop on the closure end.

The maximum bending stress on the cask body extension at the closure can be conservatively calculated as follows.

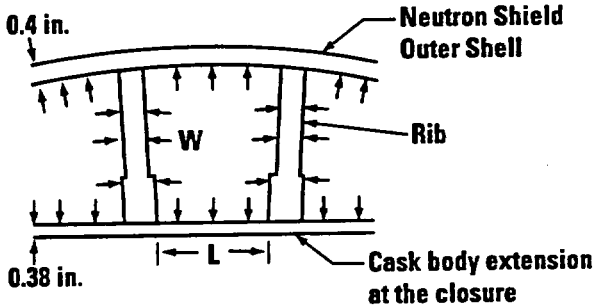

K-215(10)
5-20-96

$$\sigma_b = \frac{Mc}{I},$$

$$= 6.6 \text{ ksi (end drop)},$$

$$= 2.4 \text{ ksi (side drop)};$$

where

$$M = \frac{wL^2}{12} \text{ (fixed ends ignoring side fixity at the shear plates)},$$

$$= 794.6 \text{ in.-lb} \quad \text{(end drop)},$$

$$= 292.20 \text{ in.-lb} \quad \text{(side drop)};$$

$$L = 2.01 \text{ in.},$$

$$c = .38/2 = .19,$$

$$I = \frac{5.0(.38)^3}{12},$$

$$= .023 \text{ in.}^4;$$

$$w = 472 \text{ psig x } 5.0 \text{ in. (end drop)},$$

$$= 2360 \text{ lb/in.},$$

$$= 173.6 \text{ x } 5.0 \text{ in.},$$

$$= 868 \text{ lb/in. (side drop)}.$$

The side drop impact shear and bending stresses and the neutron shield dynamic pressure stresses calculated in this section are combined to obtain the stress intensities shown in Tables 2.10.3-16 and 2.10.3-17.

Tables 2.10.3-16 and 2.10.3-17 show that the design margins are 2.1 for the corner orientation and 0.6 for the flat orientation.

c. Maximum Compressive Load. This section evaluates the capability of the ILSS to distribute the load from the impact limiter to the cask body assuming that none of the load is transmitted through the shear plates directly to the cask body. The analysis assumes that the compressive load is uniform along the length of the ILSS. This is conservative because much of the load is concentrated at the ends of the ILSS (as discussed in the section above) and carried directly to the cask body by the shear plate(s). The compressive loads per inch are

$$F = \text{(Total load)/(contact length between ILSS and impact limiter)},$$

$$= (1450 \text{ kips}) / (21.76 \text{ in.}) = 66.6 \text{ kips/in.}$$

To determine the load distribution to each rib, a two-dimensional ANSYS model representing a 1-in. axial section of the ILSS was developed. The model and its element numbers are shown in Fig. 2.10.3-30. Node numbers are shown in Fig. 2.10.3-31. A 66.6-kip load was used as a uniform pressure acting over one side of the 39.75-in.-diameter ILSS. Four cask orientations were analyzed. The same model was used for all analyses, only the orientation of the applied load was changed. The loads were rotated about the cask axis to simulate the different clocking positions about the cask's axis. The flat case simulated the impact of the cask's flat face on the ground. This is also the 0° clocking position. The other three cases had clocking angles of 15°, 30° and 45° about the cask's axis. The 45° clocking position simulates the corner of the, cask impacting the ground. The model with the applied loads are shown in Fig. 2.10.3-32 for the four orientations. The uniform pressure load was applied as nodal forces on the cylindrical ILSS. The forces were applied to the outer shell nodes—nodes 1 through 41 for the flat orientation and nodes 11 through 51 for the corner orientation. This section shows the results for flat and corner orientations and Section 2.10.3.6.5 shows the results for the other angular orientations.

The ribs and shell are modeled using beam elements. The cask body is assumed to be rigid, and each rib is assumed to be rigidly attached to the cask body.

The shell (outer skin) elements have a thickness of 0.4 in. and a bending modulus of

$$I = \frac{.4^3(1)}{12} = .00533 \text{ in.}^4$$

The rib elements have a thickness of 0.88 in. for a 1-in. height at the attachment to the cask body, and a thickness of 0.75 in. outboard of this location. The ribs are considered fixed at the cask body. The area and moment of inertia of the ribs are adjusted to account for the drilled holes as follows:

For the 0.75-in. section

A = average cross-sectional area,
= $L[t \times p - A_{hole}]/p$,
= $1.0\ [.75 \times .688 \text{ in.} - \pi \times (0.312 \text{ in.})^2]/0.688 \text{ in.}$,
= 0.305 in.^2;

where

L = length of section through ILSS = 1.0 in.,
t = thickness = 0.75 in.,
p = pitch between holes = .688 in.,
A_{hole} = area of hole = πr^2,
r = radius = 0.624/2 = 0.312 in.; and
I = average bending modulus,
= $L[p \times t^3/12 - \pi r^4/4]/p$,

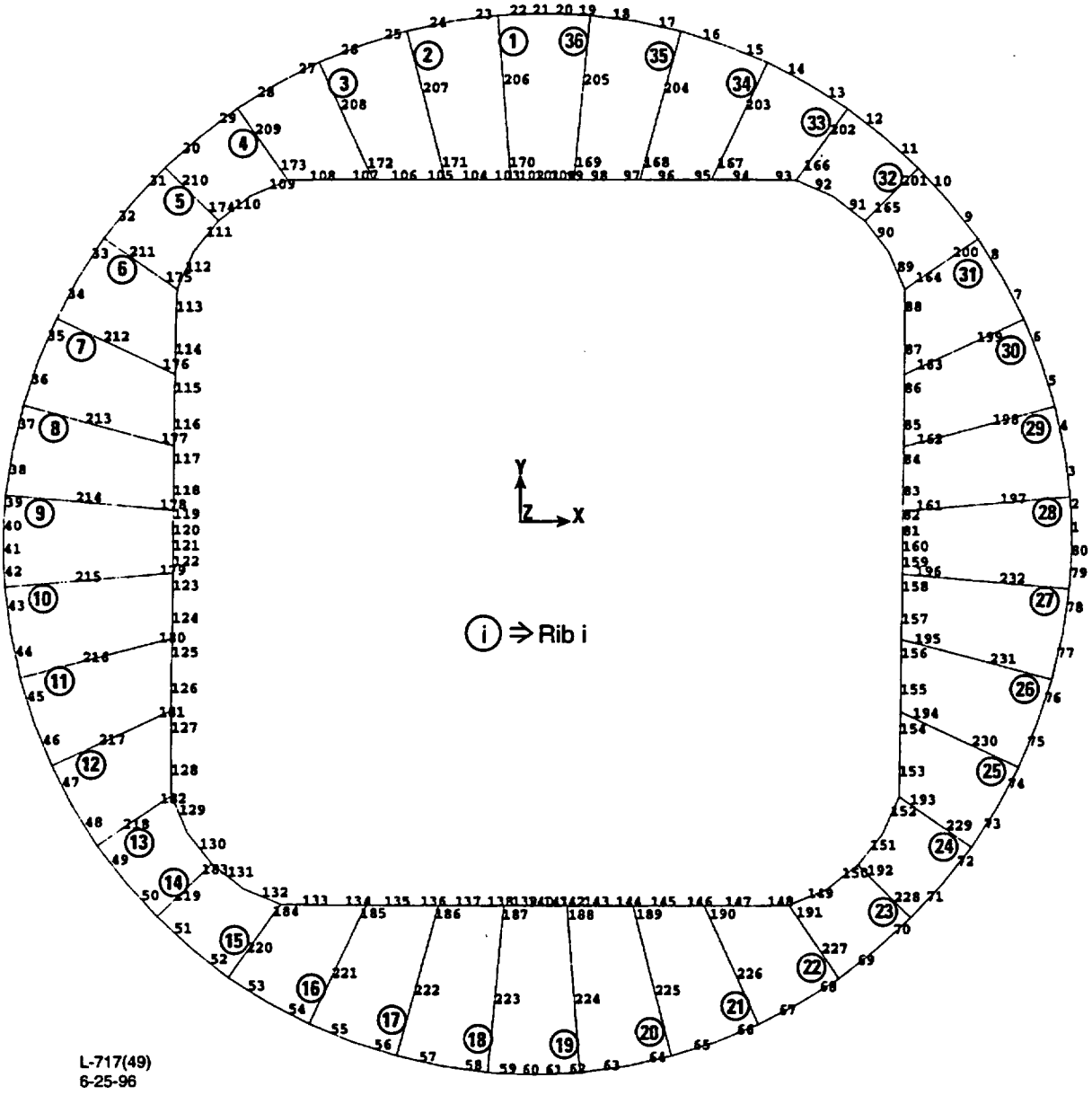

Fig. 2.10.3-30. Element numbers and rib numbers for ILSS ANSYS model

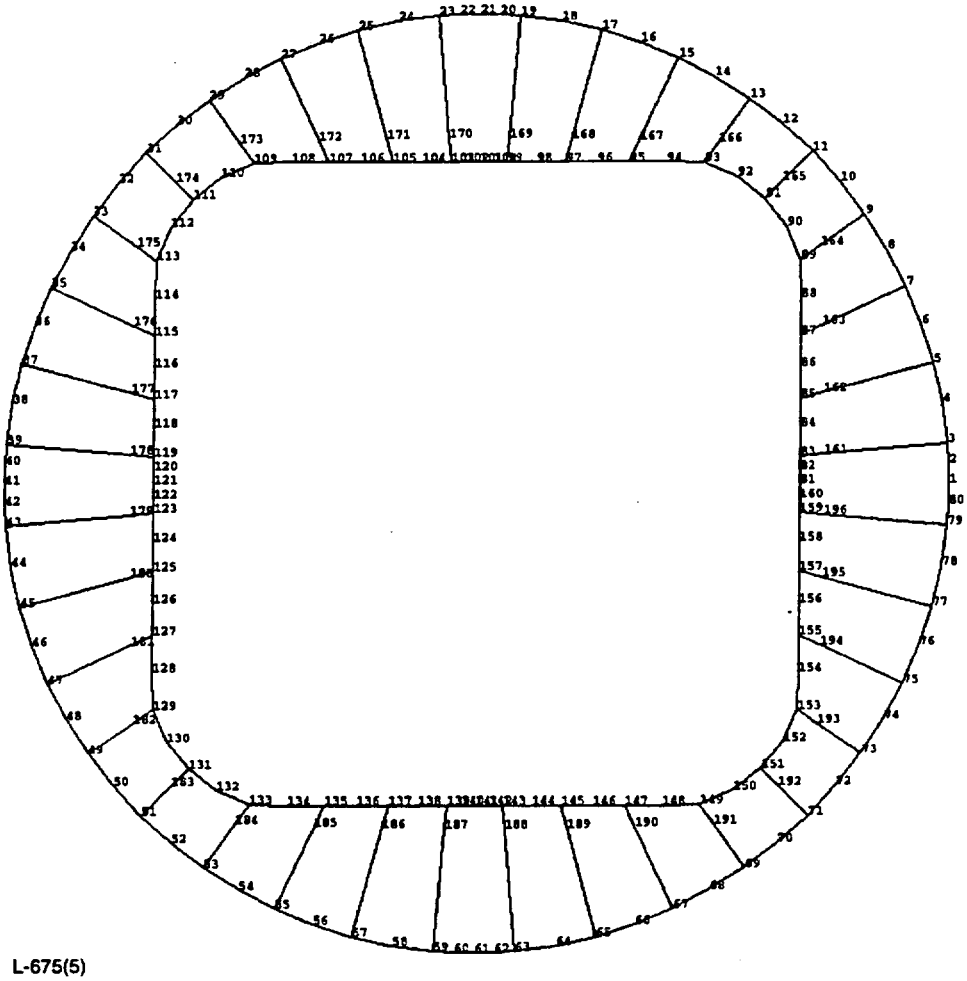

L-675(5)
5-10-96

Fig. 2.10.3-31. Node numbers for flat orientation for ILSS ANSYS model

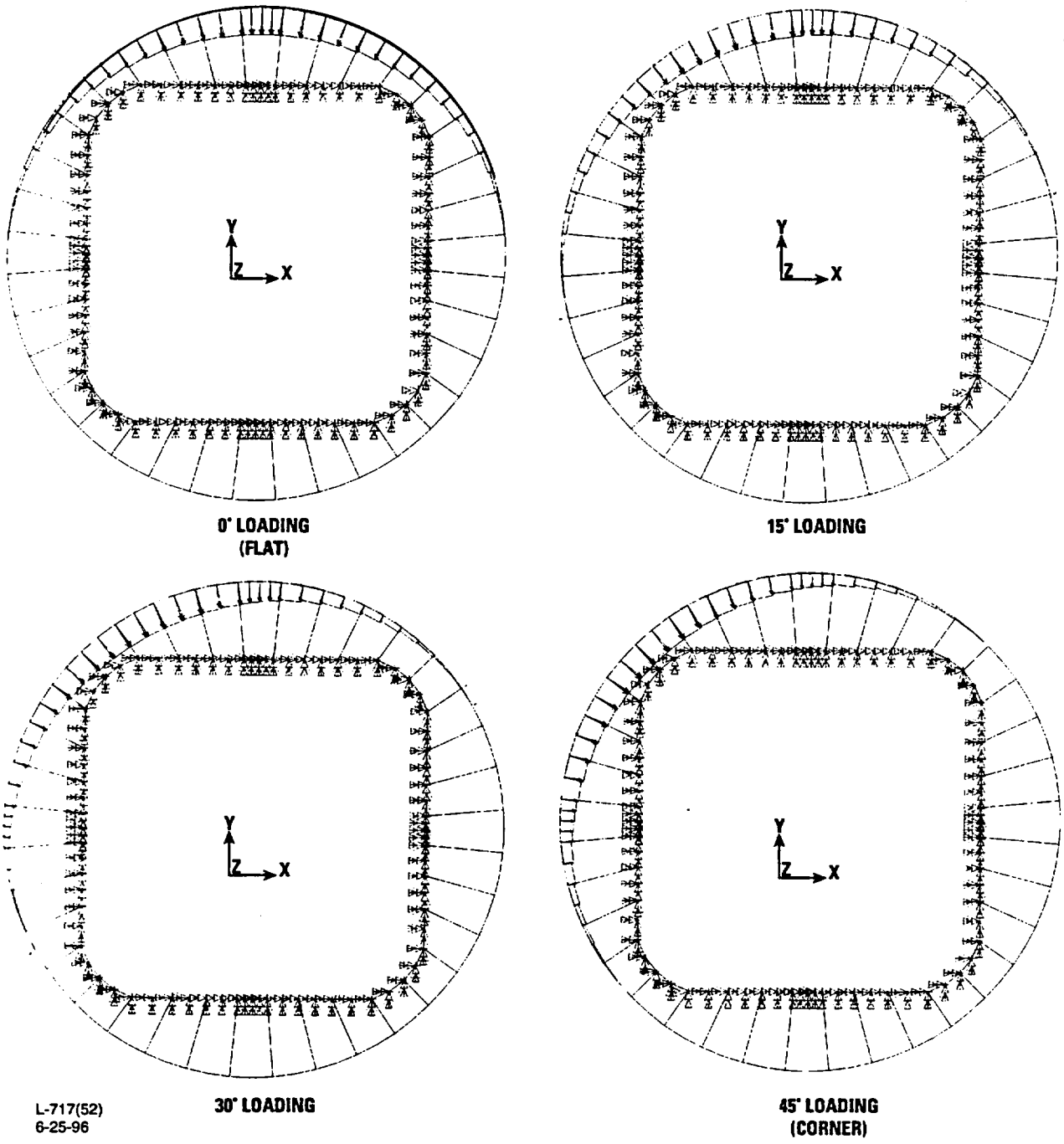

Fig. 2.10.3-32. Loading for the four clocking angular orientations

$= 1.0[.688 \text{ in.} \times (.75 \text{ in.})^3/12 - \pi \times (0.312 \text{ in.})^4/4]/.688 \text{ in.},$

$= 0.0243 \text{ in.}^4$

For the 0.88-in. section (0.875-in. rib width and 0.624-in. hole size was conservatively used in the analysis)

$A = 1.0[.875 \text{ in.} \times .688 \text{ in.} - \pi \times (0.312 \text{ in.})^2]/.688 \text{ in.},$

$= 0.430 \text{ in.}^2$; and

$I = 1.0[.688 \text{ in.} \times (.875 \text{ in.})^3/12 - \pi \times (0.312 \text{ in.})^4/4]/.688 \text{ in.},$

$= 0.045 \text{ in.}^4$

The material properties used are

$E = 29.0 \times 10^6$ psi

$\nu = 0.3$, and

$G = 11.15 \times 10^6$ psi.

The model had 196 nodes and 232 elements and was loaded with a uniform 1.0 ksi pressure across the projected diameter of the outer shell, then scaled to the full 66.6 kip/in. load. The loading conditions are shown in Fig. 2.10.3-32.

The total load on the model was 39.35 kips. The desired load is 66.6 kips (66.6 kips/in. x 1.0 in.). Therefore, the ANSYS results were increased by the factor 66.6/39.35 = 1.69. Since the ANSYS loads were scaled to the desired 66.6 kips load, the following stress analyses are representative of the full load.

These results show that the pressure loading is distributed by the shell to all of the ribs (Tables 2.10.3-3 and 2.10.3-4). The ribs directly resisting the pressure are in compression, and the ribs that are remote from the pressure loading are in tension. The maximum compression occurs in the rib which is nearest the center of the pressure load. Rib compression diminishes as the ribs become more oblique to the pressure loading, and become tension on ribs that are on the side opposite of the pressure loading. As the angle of inclination increases (and the compression on the ribs diminishes), the component of pressure loading normal to the sides of the ribs increases. This component bends the ribs outward, away from the center of pressure. Accordingly, the shear force and bending moment on the ribs increase, becoming a maximum on the ribs that are perpendicular to the direction of the pressure load.

The distribution of the pressure loading by the shell to the ribs results in tensile membrane forces in the shell. These shell tensile forces are maximum near the center of the pressure load, and diminish as the inclination angle of the shell to the pressure load increases. The decrease is largely due to the buildup of compressive forces in the shell that result from the angle of inclination to the pressure. As the angle of inclination increases, these compressive

TABLE 2.10.3-3 SCALED ANSYS RESULTS FOR ILSS - FLAT SIDE SLAPDOWN DROP

Rib No.	Element Nos. .875/.75 Thick Ribs	Element Axial Force lb	Element Shear Force lb	Element Moment at Top of Rib in.-lb	Element Moment at Stepped Thickness in.-lb	Element Moment at Base of Rib in.-lb
1	170/206	-6,968	58	166	134	193
2	171/207	-6,447	162	377	387	549
3	172/208	-5,487	376	699	733	1,109
4	173/209	-4,326	1,059	1,078	1,321	2,380
5	174/210	-3,138	1,646	1,252	1,665	3,311
6	175/211	-1,984	1,199	1,154	1,561	2,760
7	176/212	-823	493	838	1,038	1,531
8	177/213	113	291	604	769	1,059
9	178/214	608	208	458	611	818
10	179/215	688	160	316	507	667
11	180/216	661	169	319	481	650
12	181/217	649	219	328	505	723
13	182/218	589	441	373	627	1,068
14	183/219	478	503	335	556	1,059
15	184/220	402	266	234	369	634
16	185/221	381	76	121	170	247
17	186/222	385	28	54	80	108
18	187/223	390	11	30	27	38
Shell	Element No.	Element Axial Force lb	Element Shear Force lb	Element Moment in.-lb		
	21	7,480	-163	-1,038		
	22	7,370	-1,937	-276		
	23	7,401	3,109	1,841		
	24	7,022	355	-1,049		
	25	6,555	2,767	1,557		
	26	5,713	-371	-928		
	27	5,036	2,221	1,134		
	28	3,828	-396	-720		
	29	3,536	1,607	653		
	30	2,108	-404	-538		
	31	2,270	1,032	257		
	41	-4,050	-17	115		

TABLE 2.10.3-4 SCALED ANSYS RESULTS FOR ILSS - CORNER SLAPDOWN DROP

RibNo.	Element Nos. .875/.75 Thick Ribs	Element Axial Force lb	Element Shear Force lb	Element Moment at Top of Rib in.-lb	Element Moment at Stepped Thickness in.-lb	Element Moment at Base of Rib in.-lb
5	174/210	-7,189	0	0	0	0
6	175/211	-6,997	335	285	474	809
7	176/212	-6,295	280	461	607	887
8	177/213	-5,203	275	601	698	973
9	178/214	-3,846	279	672	768	1,047
10	179/215	-2,378	306	738	836	1,142
11	180/216	-1,014	355	769	910	1,265
12	181/217	94	491	821	1,047	1,537
13	182/218	708	1,012	911	1,381	2,394
14	183/219	727	1,217	815	1,340	2,557
15	184/220	539	718	624	1,002	1,719
16	185/221	473	246	382	556	802
17	186/222	475	130	246	366	496
18	187/223	474	91	197	274	365
19	188/224	468	65	125	209	273
20	189/225	455	61	115	174	236
21	190/226	448	62	90	145	207
22	191/227	431	76	60	112	188
23	192/228	416	0	0	0	0
Shell	Element No.	Element Axial Force lb	Element Shear Force lb	Element Moment in.-lb		
	29	8,070	3,261	2,047		
	30	8,449	-328	-1,103		
	31	8,575	3,224	1,946		
	32	8,445	-409	-1,103		
	33	8,395	3,024	1,761		
	34	7,775	-420	-1,057		
	35	7,205	2,625	1,468		
	36	6,169	-391	-912		
	37	5,230	2,090	1,117		
	38	3,903	-315	-699		
	39	2,720	1,539	737		
	48	-5,512	-158	308		

forces eventually overcome the shell tensile forces. Similarly, the bending of the shell between ribs is maximum at the center of the pressure loading, and diminishes as the angle of the loading to the shell increases. Therefore maximum stresses in the shell occur at or near the center of the pressure loads.

Table 2.10.3-3 gives the forces on the ribs and several shell elements for the flat side pressure load, and Table 2.10.3-4 gives the values for the corner side pressure load. The values in the tables include the 1.69 scaling factor applied to the ANSYS results. The moments on the ribs are given at the top of the rib, at the step from 0.75 in. to 0.88 in., and at the base of the rib where it is welded to the cask. The moments on the shell are given at the centerline of the ribs and midway between the ribs. The membrane, bending and shear stresses are calculated using hand calculations which account for the presence of the holes in the ribs using the rib and shell moments of inertia and areas. The stress intensities for the ribs and the shell segments with the highest stresses are shown in Tables 2.10.3-5 through 2.10.3-14.

Rib Evaluation. The maximum compressive force occurs on Rib 5 during the corner loading. This force is 7,189 lb. Since there is no shear or bending on this rib during this loading, the corresponding membrane stress and stress intensity are both 23.6 ksi. However, the maximum stress intensity for the corner orientation is 23.9 ksi in Rib 14. The maximum membrane stress intensity occurs on Rib 5 with the flat side loading, because of the combination of the compressive force and shear force. This stress intensity of 33.7 ksi is well below the allowable membrane stress of 69.7 ksi at 200°F (Table 2.1-4).

The maximum membrane plus bending stress intensity also occurs on Rib 5 due to flat side loading. This stress intensity is 48.2 ksi, and occurs at the step in the rib where the section increases from 0.75 in. to 0.88 in. It is well below the allowable limit of 99.5 ksi (Table 2.1-4).

The maximum compressive stress, which occurs on the 0.75-in.-thick portion of the rib, is also below the buckling limit for the rib. The buckling limit is conservatively determined by neglecting the increased thickness at the base of the rib, and by using the maximum stress in either the .75-in.-thick portion of the rib or the .88-in.-thick portion, whichever is higher. Four cases are considered to bound all of the possible cases: 1) the maximum height rib with the maximum axial load (Rib 1 in a flat side drop), 2) the maximum height rib with axial load and bending (Rib 9 in a corner side drop), 3) the rib with the maximum axial stress (Rib 5 in a flat side drop), and, 4) the rib with the maximum axial load (Rib 5 in a corner drop). The buckling criteria for axial compression plus bending is given in Section 2.1.2.6.3. The results of the buckling analysis are summarized in Table 2.10.3-15.

Loads and Stresses

Rib 1

Loads on rib—flat drop

P = 6.97 kips (Table 2.10.3-3),

M = 0.134 kip-in. (Table 2.10.3-3);

TABLE 2.10.3-5 ILSS, FLAT SIDE SLAPDOWN, MEMBRANE STRESSES AT STEP IN RIBS (psi)

Rib	Element	Combined Stress Components						Principal Stresses			Stress	Stress	Stress	Design
		Sx	Sy	Sz	Sxy	Syz	Sxz	S1	S2	S3	Int.	Type	Limit	Margin
1	206	-22846	0	0	566	0	0	14	0	-22860	22874	P_m	69700	2.05
2	207	-21138	0	0	1580	0	0	118	0	-21256	21373	P_m	69700	2.26
3	208	-17991	0	0	3668	0	0	719	0	-18710	19430	P_m	69700	2.59
4	209	-14185	0	0	10332	0	0	5439	0	-19624	25064	P_m	69700	1.78
5	210	-10290	0	0	16059	0	0	11718	0	-22007	33725	P_m	69700	1.07
6	211	-6505	0	0	11698	0	0	8889	0	-15394	24283	P_m	69700	1.87
7	212	-2698	0	0	4810	0	0	3646	0	-6344	9991	P_m	69700	5.98
8	213	370	0	0	2839	0	0	3030	0	-2660	5690	P_m	69700	11.25
9	214	1992	0	0	2029	0	0	3257	0	-1264	4521	P_m	69700	14.42
10	215	2257	0	0	1561	0	0	3054	0	-798	3852	P_m	69700	17.09
11	216	2168	0	0	1649	0	0	3057	0	-889	3946	P_m	69700	16.66
12	217	2128	0	0	2137	0	0	3451	0	-1323	4774	P_m	69700	13.60
13	218	1932	0	0	4302	0	0	5376	0	-3443	8819	P_m	69700	6.90
14	219	1568	0	0	4907	0	0	5754	0	-4185	9939	P_m	69700	6.01
15	220	1317	0	0	2595	0	0	3336	0	-2019	5355	P_m	69700	12.02
16	221	1251	0	0	741	0	0	1595	0	-345	1940	P_m	69700	34.93
17	222	1264	0	0	273	0	0	1320	0	-57	1377	P_m	69700	49.62
18	223	1279	0	0	107	0	0	1288	0	-9	1297	P_m	69700	52.73

Sx is the radial stress in the rib due to membrane and Sxy is the shear stress due to the transverse shear load on the rib.

TABLE 2.10.3-6 ILSS, FLAT SIDE SLAPDOWN, MEMBRANE + BENDING STRESSES AT STEP IN RIBS (psi)

Rib	Element	Combined Stress Components						Principal Stresses			Stress	Stress	Stress	Design
		Sx	Sy	Sz	Sxy	Syz	Sxz	S1	S2	S3	Int.	Type	Limit	Margin
1	206	-24914	0	0	566	0	0	13	0	-24927	24940	P_m+P_b	99500	2.99
2	207	-27110	0	0	1580	0	0	92	0	-27202	27294	P_m+P_b	99500	2.65
3	208	-29303	0	0	3668	0	0	452	0	-29755	30207	P_m+P_b	99500	2.29
4	209	-34571	0	0	10332	0	0	2852	0	-37423	40275	P_m+P_b	99500	1.47
5	210	-35984	0	0	16059	0	0	6124	0	-42108	48232	P_m+P_b	99500	1.06
6	211	-30594	0	0	11698	0	0	3960	0	-34554	38514	P_m+P_b	99500	1.58
7	212	-18717	0	0	4810	0	0	1164	0	-19880	21044	P_m+P_b	99500	3.73
8	213	-11497	0	0	2839	0	0	663	0	-12160	12823	P_m+P_b	99500	6.76
9	214	-7437	0	0	2029	0	0	518	0	-7954	8472	P_m+P_b	99500	10.74
10	215	-5567	0	0	1561	0	0	408	0	-5975	6383	P_m+P_b	99500	14.59
11	216	-5255	0	0	1649	0	0	474	0	-5729	6204	P_m+P_b	99500	15.04
12	217	-5665	0	0	2137	0	0	715	0	-6380	7096	P_m+P_b	99500	13.02
13	218	-7743	0	0	4302	0	0	1916	0	-9660	11576	P_m+P_b	99500	7.60
14	219	-7012	0	0	4907	0	0	2525	0	-9537	12062	P_m+P_b	99500	7.25
15	220	-4378	0	0	2595	0	0	1206	0	-5584	6790	P_m+P_b	99500	13.65
16	221	-1373	0	0	741	0	0	324	0	-1697	2021	P_m+P_b	99500	48.24
17	222	29	0	0	273	0	0	288	0	-259	547	P_m+P_b	99500	180.86
18	223	863	0	0	107	0	0	876	0	-13	889	P_m+P_b	99500	110.91

Sx is the radial stress in the rib due to membrane and bending and Sxy is the shear stress due to the transverse shear load on the rib.

TABLE 2.10.3-7 ILSS, FLAT SIDE SLAPDOWN, MEMBRANE + BENDING STRESSES AT BASE OF RIBS (psi)

Rib	Element	Combined Stress Components						Principal Stresses			Stress	Stress	Stress	Design
		Sx	Sy	Sz	Sxy	Syz	Sxz	S1	S2	S3	Int.	Type	Limit	Margin
1	170	-18078	0	0	483	0	0	13	0	-18091	18104	P_m+P_b	99500	4.50
2	171	-20329	0	0	1350	0	0	89	0	-20418	20507	P_m+P_b	99500	3.85
3	172	-23541	0	0	3133	0	0	410	0	-23951	24361	P_m+P_b	99500	3.08
4	173	-33197	0	0	8825	0	0	2200	0	-35398	37598	P_m+P_b	99500	1.65
5	174	-39487	0	0	13717	0	0	4297	0	-43784	48081	P_m+P_b	99500	1.07
6	175	-31444	0	0	9992	0	0	2906	0	-34350	37257	P_m+P_b	99500	1.67
7	176	-16797	0	0	4108	0	0	951	0	-17748	18699	P_m+P_b	99500	4.32
8	177	-10036	0	0	2425	0	0	555	0	-10591	11146	P_m+P_b	99500	7.93
9	178	-6543	0	0	1733	0	0	431	0	-6974	7405	P_m+P_b	99500	12.44
10	179	-4879	0	0	1333	0	0	341	0	-5220	5560	P_m+P_b	99500	16.89
11	180	-4784	0	0	1408	0	0	384	0	-5167	5551	P_m+P_b	99500	16.92
12	181	-5523	0	0	1825	0	0	549	0	-6071	6620	P_m+P_b	99500	14.03
13	182	-9012	0	0	3675	0	0	1309	0	-10320	11629	P_m+P_b	99500	7.56
14	183	-9182	0	0	4192	0	0	1626	0	-10808	12434	P_m+P_b	99500	7.00
15	184	-5233	0	0	2217	0	0	813	0	-6046	6859	P_m+P_b	99500	13.51
16	185	-1510	0	0	633	0	0	230	0	-1740	1971	P_m+P_b	99500	49.48
17	186	-152	0	0	233	0	0	169	0	-321	491	P_m+P_b	99500	201.74
18	187	537	0	0	92	0	0	552	0	-15	567	P_m+P_b	99500	174.35

Sx is the radial stress in the rib due to membrane and bending and Sxy is the shear stress due to the transverse shear load on the rib.

TABLE 2.10.3-8 ILSS, CORNER SLAPDOWN, MEMBRANE STRESSES AT STEP IN RIBS (psi)

Rib	Element	Combined Stress Components						Principal Stresses			Stress	Stress	Stress	Design
		Sx	Sy	Sz	Sxy	Syz	Sxz	S1	S2	S3	Int.	Type	Limit	Margin
5	210	-23571	0	0	0	0	0	0	0	-23571	23571	P_m	69700	1.96
6	211	-22941	0	0	3270	0	0	457	0	-23398	23855	P_m	69700	1.92
7	212	-20638	0	0	2736	0	0	357	0	-20994	21351	P_m	69700	2.26
8	213	-17060	0	0	2682	0	0	412	0	-17472	17883	P_m	69700	2.90
9	214	-12610	0	0	2727	0	0	564	0	-13174	13738	P_m	69700	4.07
10	215	-7796	0	0	2983	0	0	1010	0	-8806	9816	P_m	69700	6.10
11	216	-3326	0	0	3467	0	0	2182	0	-5508	7690	P_m	69700	8.06
12	217	309	0	0	4786	0	0	4943	0	-4634	9577	P_m	69700	6.28
13	218	2321	0	0	9875	0	0	11103	0	-8783	19886	P_m	69700	2.50
14	219	2383	0	0	11870	0	0	13121	0	-10739	23860	P_m	69700	1.92
15	220	1767	0	0	7001	0	0	7940	0	-6173	14113	P_m	69700	3.94
16	221	1550	0	0	2403	0	0	3299	0	-1750	5049	P_m	69700	12.80
17	222	1558	0	0	1265	0	0	2265	0	-706	2971	P_m	69700	22.46
18	223	1555	0	0	892	0	0	1961	0	-406	2367	P_m	69700	28.45
19	224	1533	0	0	632	0	0	1760	0	-227	1987	P_m	69700	34.08
20	225	1492	0	0	598	0	0	1702	0	-210	1912	P_m	69700	35.46
21	226	1469	0	0	604	0	0	1685	0	-216	1901	P_m	69700	35.66
22	227	1412	0	0	744	0	0	1732	0	-320	2051	P_m	69700	32.98
23	228	1363	0	0	0	0	0	1363	0	0	1363	P_m	69700	50.12

Sx is the radial stress in the rib due to membrane and Sxy is the shear stress due to the transverse shear load on the rib.

TABLE 2.10.3-9 ILSS, CORNER SLAPDOWN, MEMBRANE + BENDING STRESSES AT STEP IN RIBS (psi)

Rib	Element	Combined Stress Components						Principal Stresses			Stress	Stress	Stress	Design
		Sx	Sy	Sz	Sxy	Syz	Sxz	S1	S2	S3	Int.	Type	Limit	Margin
5	210	-23571	0	0	0	0	0	0	0	-23571	23571	P_m+P_b	99500	3.22
6	211	-30255	0	0	3270	0	0	349	0	-30604	30954	P_m+P_b	99500	2.21
7	212	-30004	0	0	2736	0	0	247	0	-30251	30499	P_m+P_b	99500	2.26
8	213	-27836	0	0	2682	0	0	256	0	-28092	28348	P_m+P_b	99500	2.51
9	214	-24456	0	0	2727	0	0	300	0	-24757	25057	P_m+P_b	99500	2.97
10	215	-20698	0	0	2983	0	0	421	0	-21119	21540	P_m+P_b	99500	3.62
11	216	-17368	0	0	3467	0	0	666	0	-18034	18701	P_m+P_b	99500	4.32
12	217	-15842	0	0	4786	0	0	1334	0	-17176	18509	P_m+P_b	99500	4.38
13	218	-18996	0	0	9875	0	0	4204	0	-23199	27403	P_m+P_b	99500	2.63
14	219	-18295	0	0	11870	0	0	5839	0	-24133	29972	P_m+P_b	99500	2.32
15	220	-13689	0	0	7001	0	0	2946	0	-16636	19582	P_m+P_b	99500	4.08
16	221	-7031	0	0	2403	0	0	743	0	-7773	8516	P_m+P_b	99500	10.68
17	222	-4095	0	0	1265	0	0	359	0	-4454	4813	P_m+P_b	99500	19.67
18	223	-2672	0	0	892	0	0	270	0	-2942	3213	P_m+P_b	99500	29.97
19	224	-1686	0	0	632	0	0	211	0	-1896	2107	P_m+P_b	99500	46.22
20	225	-1200	0	0	598	0	0	247	0	-1447	1694	P_m+P_b	99500	57.73
21	226	-775	0	0	604	0	0	330	0	-1104	1434	P_m+P_b	99500	68.38
22	227	-319	0	0	744	0	0	601	0	-921	1522	P_m+P_b	99500	64.39
23	228	1363	0	0	0	0	0	1363	0	0	1363	P_m+P_b	99500	71.98

Sx is the radial stress in the rib due to membrane and bending and Sxy is the shear stress due to the transverse shear load on the rib.

TABLE 2.10.3-10 ILSS, CORNER SLAPDOWN, MEMBRANE + BENDING STRESSES AT BASE OF RIBS (psi)

Rib	Element	Combined Stress Components						Principal Stresses			Stress	Stress	Stress	Design
		Sx	Sy	Sz	Sxy	Syz	Sxz	S1	S2	S3	Int.	Type	Limit	Margin
5	174	-16719	0	0	0	0	0	0	0	-16719	16719	P_m+P_b	99500	4.95
6	175	-24138	0	0	2793	0	0	319	0	-24457	24776	P_m+P_b	99500	3.02
7	176	-23265	0	0	2337	0	0	232	0	-23498	23730	P_m+P_b	99500	3.19
8	177	-21562	0	0	2291	0	0	241	0	-21803	22043	P_m+P_b	99500	3.51
9	178	-19124	0	0	2329	0	0	280	0	-19404	19683	P_m+P_b	99500	4.06
10	179	-16630	0	0	2548	0	0	382	0	-17012	17394	P_m+P_b	99500	4.72
11	180	-14661	0	0	2961	0	0	576	0	-15236	15812	P_m+P_b	99500	5.29
12	181	-14726	0	0	4088	0	0	1059	0	-15784	16843	P_m+P_b	99500	4.91
13	182	-21625	0	0	8435	0	0	2901	0	-24526	27427	P_m+P_b	99500	2.63
14	183	-23166	0	0	10139	0	0	3811	0	-26977	30787	P_m+P_b	99500	2.23
15	184	-15462	0	0	5980	0	0	2043	0	-17505	19548	P_m+P_b	99500	4.09
16	185	-6701	0	0	2052	0	0	579	0	-7279	7858	P_m+P_b	99500	11.66
17	186	-3717	0	0	1080	0	0	291	0	-4008	4299	P_m+P_b	99500	22.15
18	187	-2449	0	0	762	0	0	218	0	-2667	2884	P_m+P_b	99500	33.50
19	188	-1570	0	0	540	0	0	168	0	-1738	1906	P_m+P_b	99500	51.21
20	189	-1234	0	0	511	0	0	184	0	-1418	1602	P_m+P_b	99500	61.12
21	190	-973	0	0	516	0	0	222	0	-1195	1418	P_m+P_b	99500	69.19
22	191	-831	0	0	635	0	0	344	0	-1174	1518	P_m+P_b	99500	64.54
23	192	967	0	0	0	0	0	967	0	0	967	P_m+P_b	99500	101.89

Sx is the radial stress in the rib due to membrane and bending and Sxy is the shear stress due to the transverse shear load on the rib.

TABLE 2.10.3-11 ILSS, FLAT SIDE SLAPDOWN, MEMBRANE STRESSES IN OUTER SHELL (psi)

Element	Combined Stress Components						Principal Stresses			Stress	Stress	Stress	Design
	Sx	Sy	Sz	Sxy	Syz	Sxz	S1	S2	S3	Int.	Type	Limit	Margin
21	0	18699	0	-408	0	0	18708	0	-9	18717	P_m	69700	2.72
22	0	18426	0	-4842	0	0	19621	0	-1195	20815	P_m	69700	2.35
23	0	18503	0	7773	0	0	21335	0	-2832	24167	P_m	69700	1.88
24	0	17554	0	889	0	0	17599	0	-45	17644	P_m	69700	2.95
25	0	16388	0	6918	0	0	18917	0	-2530	21447	P_m	69700	2.25
26	0	14281	0	-927	0	0	14341	0	-60	14401	P_m	69700	3.84
27	0	12590	0	5553	0	0	14689	0	-2099	16789	P_m	69700	3.15
28	0	9570	0	-990	0	0	9671	0	-101	9773	P_m	69700	6.13
29	0	8841	0	4017	0	0	10393	0	-1553	11946	P_m	69700	4.83
30	0	5271	0	-1010	0	0	5458	0	-187	5645	P_m	69700	11.35
31	0	5674	0	2581	0	0	6673	0	-998	7671	P_m	69700	8.09
41	0	-10125	0	-41	0	0	0	0	-10125	10126	P_m	69700	5.88

TABLE 2.10.3-12 ILSS, FLAT SIDE SLAPDOWN, MEMBRANE + BENDING STRESSES IN OUTER SHELL (psi)

Element	Combined Stress Components						Principal Stresses			Stress	Stress	Stress	Design
	Sx	Sy	Sz	Sxy	Syz	Sxz	S1	S2	S3	Int.	Type	Limit	Margin
21	0	57652	0	-408	0	0	57655	0	-3	57658	P_m+P_b	99500	0.73
22	0	28769	0	-4842	0	0	29562	0	-793	30355	P_m+P_b	99500	2.28
23	0	87565	0	7773	0	0	88250	0	-685	88934	P_m+P_b	99500	0.12
24	0	56920	0	889	0	0	56934	0	-14	56948	P_m+P_b	99500	0.75
25	0	74819	0	6918	0	0	75453	0	-634	76087	P_m+P_b	99500	0.31
26	0	49091	0	-927	0	0	49109	0	-17	49126	P_m+P_b	99500	1.03
27	0	55149	0	5553	0	0	55703	0	-554	56256	P_m+P_b	99500	0.77
28	0	36576	0	-990	0	0	36602	0	-27	36629	P_m+P_b	99500	1.72
29	0	33341	0	4017	0	0	33818	0	-477	34295	P_m+P_b	99500	1.90
30	0	25472	0	-1010	0	0	25512	0	-40	25552	P_m+P_b	99500	2.89
31	0	15318	0	2581	0	0	15741	0	-423	16164	P_m+P_b	99500	5.16
41	0	-14436	0	-41	0	0	0	0	-14436	14437	P_m+P_b	99500	5.89

TABLE 2.10.3-13 ILSS, CORNER SLAPDOWN, MEMBRANE STRESSES IN OUTER SHELL (psi)													
Element	Combined Stress Components						Principal Stresses			Stress	Stress	Stress	Design
	Sx	Sy	Sz	Sxy	Syz	Sxz	S1	S2	S3	Int.	Type	Limit	Margin
29	0	20175	0	8151	0	0	23056	0	-2882	25938	P_m	69700	1.69
30	0	21122	0	-821	0	0	21154	0	-32	21186	P_m	69700	2.29
31	0	21438	0	8059	0	0	24130	0	-2692	26821	P_m	69700	1.60
32	0	21113	0	-1023	0	0	21162	0	-49	21212	P_m	69700	2.29
33	0	20988	0	7561	0	0	23427	0	-2440	25867	P_m	69700	1.69
34	0	19438	0	-1050	0	0	19494	0	-57	19551	P_m	69700	2.57
35	0	18012	0	6561	0	0	20149	0	-2137	22285	P_m	69700	2.13
36	0	15422	0	-977	0	0	15483	0	-62	15545	P_m	69700	3.48
37	0	13076	0	5224	0	0	14906	0	-1831	16737	P_m	69700	3.16
38	0	9758	0	-788	0	0	9821	0	-63	9884	P_m	69700	6.05
39	0	6801	0	3847	0	0	8535	0	-1734	10269	P_m	69700	5.79
48	0	-13780	0	-395	0	0	11	0	-13792	13803	P_m	69700	4.05

TABLE 2.10.3-14 ILSS, CORNER SLAPDOWN, MEMBRANE + BENDING STRESSES IN OUTER SHELL (psi)													
Element	Combined Stress Components						Principal Stresses			Stress	Stress	Stress	Design
	Sx	Sy	Sz	Sxy	Syz	Sxz	S1	S2	S3	Int.	Type	Limit	Margin
29	0	96970	0	8151	0	0	97651	0	-680	98331	P_m+P_b	99500	0.01
30	0	62499	0	-821	0	0	62510	0	-11	62521	P_m+P_b	99500	0.59
31	0	94451	0	8059	0	0	95134	0	-683	95817	P_m+P_b	99500	0.04
32	0	62486	0	-1023	0	0	62503	0	-17	62520	P_m+P_b	99500	0.59
33	0	87081	0	7561	0	0	87733	0	-652	88384	P_m+P_b	99500	0.13
34	0	59085	0	-1050	0	0	59104	0	-19	59122	P_m+P_b	99500	0.68
35	0	73093	0	6561	0	0	73677	0	-584	74262	P_m+P_b	99500	0.34
36	0	49641	0	-977	0	0	49660	0	-19	49680	P_m+P_b	99500	1.00
37	0	54971	0	5224	0	0	55463	0	-492	55955	P_m+P_b	99500	0.78
38	0	35994	0	-788	0	0	36012	0	-17	36029	P_m+P_b	99500	1.76
39	0	34464	0	3847	0	0	34889	0	-424	35313	P_m+P_b	99500	1.82
48	0	-25335	0	-395	0	0	6	0	-25341	25348	P_m+P_b	99500	2.93

TABLE 2.10.3-15 BUCKLING FOR COMBINED AXIAL COMPRESSION AND BENDING - ILSS RIBS

Drop Height	Drop Orientation	Rib No.	M_1, in.-lb	M_2, in.-lb	$C_m = .6-.4(M_1/M_2)$ or .4	f_a	f_b	f_a/F_a	f_b/F_b	$C_m(f_b)/((1-1.46f_a/F_e)F_b)$	$f_a/0.6S_y + (f_b)/F_b$	Design Margin	$f_a/F_a + C_m(f_b)/((1-1.46f_a/F_e)F_b)$	Design Margin
30-ft	Corner	1	672	1047	0.4	12.6	11.9	0.33	0.20	0.08	0.64	0.57	0.41	1.45
30-ft	Corner	5	0	0	0	23.6	0	0.61	0.00	0.00	0.82	0.22	0.61	0.64
30-ft	Flat	1	166	193	0.4	22.8	2.1	0.59	0.03	0.02	0.83	0.21	0.60	0.65
30-ft	Flat	5	1252	3311	0.45	10.3	32.2	0.27	0.53	0.24	0.89	0.12	0.51	0.97

Stresses on rib

f_a = P/A,

= 22.85 ksi;

where

A = 0.305 $in.^2$,

f_b = Mc/I,

= 2.1 ksi,

where

c = .375 in.

I = 0.0243 $in.^4$ (.75-in.-thick portion of rib)

Rib 9

Loads on rib—corner drop

P = 3.85 kips (Table 2.10.3-4),

M = 0.768 kip-in. (Table 2.10.3-4).

Stresses on rib

f_a = P/A,

= 12.6 ksi;

where

A = .305 $in.^2$

f_b = Mc/I,

= 11.9 ksi,

where

c = 0.375 in.,

I = 0.0243 $in.^4$

Rib 5

Loads on rib—flat drop

P = 3.14 kips (Table 2.10.3-3),

M = 3.31 kip-in. (Table 2.10.3-3).

Stresses on rib

f_a = P/A,

= 10.3 ksi;

where

$A = 0.305 \text{ in.}^2$,

$f_b = Mc/I$,

$= 32.2$ ksi,

where

$c = 0.44$ in.

$I = 0.045 \text{ in.}^4$ (.88-in.-thick portion of rib)

Loads on rib—corner drop

$P = 7.19$ kips,

$M = 0$.

Stresses on rib

$f_a = P/A$,

$= 23.6$ ksi;

where

$A = 0.305 \text{ in.}^2$,

$f_b = 0$.

The following buckling equations for axial compression plus bending are taken from Section 2.1.2.6.1

$$\frac{f_a}{F_a} + \frac{C_m(f_b)}{\left(1 - \frac{1.46\ f_a}{F_e}\right)F_b} \leq 1 \quad \text{and}$$

$$\frac{f_a}{0.6\ S_y} + \frac{f_b}{F_b} \leq 1$$

where

$C_m = 0.6 - 0.4\ (M_1/M_2)$ but not less than 0.4,

$F_e = \frac{\pi^2 E}{(k\ell/r)^2}$ (accident conditions),

$= 385$ ksi (Rib 1),

$= 1924$ ksi (Rib 5);

$k\ell/r$ = 26.6 (Rib 1)

= 11.9 (Rib 5);

ℓ = unbraced length,

= 5.76 in. (Rib 1),

= 2.57 in. (Rib 5);

k = 1.3 (conservative for base of rib fixed and other end is partially restrained against rotation and displacement by shell stiffness);

$r = \sqrt{\frac{I}{A}}$,

= 0.282;

I = 0.0243 in.^{4} (per 1.0 in. length of rib),

A = 0.305 in.^{2} (per 1.0 in. length of rib),

E = 27.6 x 10^6 psi (200°F),

$F_a = S_y\left[\frac{1-\lambda^2/4}{1.12(1.11+0.75\lambda+0.83\lambda^2-0.81\lambda^3)}\right]$ for $\lambda < 1$

= 28.7 ksi (Rib 1),

= 34.0 ksi (Rib 5),

S_y = 47.8 ksi (190°F);

$\lambda = \sqrt{\frac{S_y}{E}}\left(\frac{k\ell}{r}\right)\left(\frac{1}{\pi}\right)$,

= 0.35 (Rib 1),

= 0.16 (Rib 5);

$F_b = fS_y$,

= 60.23,

$f = \frac{A'y_1}{I/c} = 1.26$,

A' = area of 0.688 in. length of rib = 0.210 in.^{2},

y_1 = distance to centroid of half section = .268 in.,

I = moment of inertia of 0.688 in. length of rib = 0.01675 in.^{4}, and

c = distance to extreme fiber = 0.375.

Table 2.10.3-15 shows that for the maximum axial and bending loads on the ribs, the minimum design margin against buckling is 0.25 for Rib 5 for the flat drop orientation.

Shell Evaluation. The axial membrane force in the 0.4-in. outer shell is a maximum of 8575 lb tension and 5512 lb compression (as shown in Table 2.10.3-4 for element no. 31, and element no. 48, respectively), both of which occur during the corner drop. The maximum tensile forces in the shell exist near the rib directly under the pressure loading while the compressive forces in the shell occur away from the pressure loading on the opposite side of the cask. The shear stress in the shell results from the pressure applied to it between ribs, as well as differential end moments resulting from rib rotation. The maximum membrane stress intensity considers the parabolic shear distribution across the thickness of the shell, and has a value of 32.3 ksi, which is well below the allowable limit of 69.7 ksi. The largest bending stress in the shell occurs at a rib which is close to the center of the pressure loading where there is tension in the shell. Due to ANSYS modeling, the bending moments and shears are conservatively evaluated at the centerline of the rib rather than more realistically at the face of the rib. The bending moment in the shell at the rib produces tension on the outer surface of the shell and compression at the inside surface. The largest moment at the centerline of the ribs is (element no. 29) 2047 in.-lb, which results in a bending stress of 76.8 ksi. Midway between ribs, where the bending moment produces compression on the outside of the shell, the largest moment determined at the centerline of a rib is –1103 in.-lb and the bending stress is 41.4 ksi. The maximum membrane plus bending stress intensity of 98.3 ksi occurs at a rib and is below the limit of 99.5 ksi. The minimum margin, evaluated at the centerline of a rib, equals (99.5/98.3) – 1 or 0.01.

Welds. The plug welds connecting the shell to the ribs transfer shear, moment and tension between these elements, while the fillet welds at the base of the ribs transfer these forces to the cask body. The largest weld stresses occur at Rib 5 during the flat side drop where the moment and shear to be transferred is maximum, but there is no tension, only compression. These stresses are calculated and found to be acceptable as follows:

Plug welds at top of ribs

M_{max} = 1.25 kip-in./in. (Table 2.10.3-3);
V_{max} = 1.65 kip/in. (Table 2.10.3-3).

The length of each rib between end plates in the impact limiter support structures is 21.5 in.

Therefore, M = 1.25 x 21.5 = 26.9 kip-in/rib and
V = 1.65 x 21.5 = 35.5 kips/rib

The minimum cumulative length of weld between the rib and shell is 11 in., which conservatively ignores the rounded corners of the welds. (See Drawing 031348, Sheet 14 in Section 1.3.2 and the following sketch. Note that the minimum length of weld is at the bottom end ILSS.)

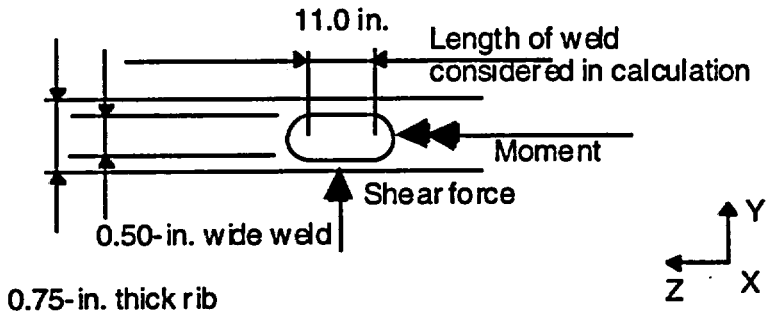

The shear force is transmitted from the shell to the rib by the total area of the weld and results in a stress of

$$\tau_y = 35.5 \text{ kip}/11.0 \text{ in.} \times 0.5 \text{ in.} = 6.45 \text{ ksi.}$$

The moment is transmitted from the shell to the rib through bearing on the rib and shear in the weld as shown in the following free body diagram.

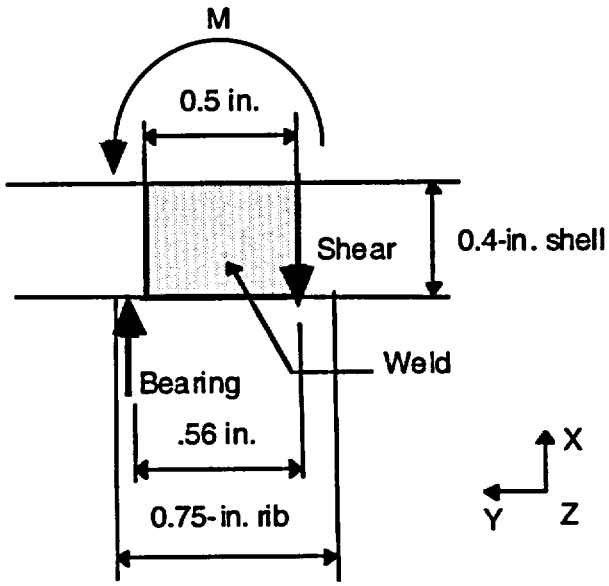

The shear stress on the weld due to the moment is

$$\tau_x = 26.9 \text{ kip-in}/(0.56 \text{ in.} \times 11 \text{ in.} \times 0.4 \text{ in.}) = 10.92 \text{ ksi.}$$

The combined stress is

$$(\tau_x^2 + \tau_y^2) = (6.45^2 + 10.92^2)^5 = 12.7 \text{ ksi.}$$

The allowable stress for a Type VIII Cat E weld with Visual Examination, following Table 2.1-3 and ASME Code Subsection NG-5231, is .42 S_u with a weld quality factor n = 0.45. Therefore, the allowable stress on the weld is .42 x 99.5 ksi x .45 = 18.8 ksi, which is greater than the actual stress of 12.7 ksi.

$$\text{D.M.} = \frac{18.8}{12.7} - 1 = 0.48.$$

The bearing stress on the rib results from the bearing force due to the moment and the compression transferred by the shell. The bearing force is found from the above figure to be 26.9 kips-in/.56 in. = 48.0 kips. The compression force at the location of maximum moment is found from the ANSYS analysis to be 3.14 kip/in. (Table 2.10.3-3 for Rib no. 5) Since the length of each rib between end plates is 21.5 in., the compression force is 3.14 x 21.5 = 67.5 kips. The total bearing force is therefore 67.5 + 48.0 = 115.5 kips. This force may conservatively be considered to be applied to the length of the rib portion outboard of the plug weld, so the effective bearing area = 21.5 in. x .12 in. = 2.58 in.^{2} The resulting bearing stress = 115.5/2.58 = 44.8 ksi.

$$\text{D.M.} = \frac{99.5}{44.8} - 1 = 1.22.$$

Fillet welds at base of ribs. These welds transfer the shear and moment in the rib into the cask body. The highest stress in the welds occur where the moment at the base of the rib is highest, which occurs in Rib 5 during the flat side drop. At this location: M_{max} = 3.31 kip-in./in. and V_{max} = 1.65 kip/in. (Table 2.10.3-3).

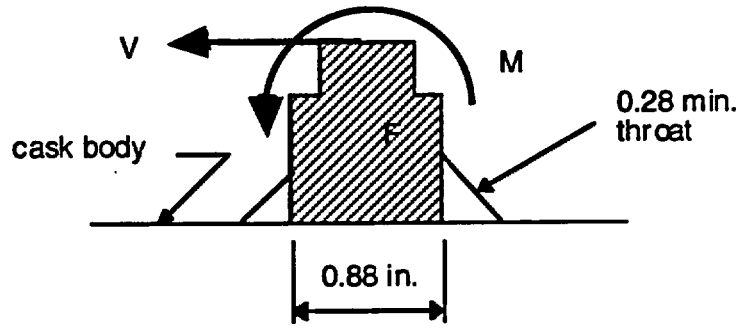

The load on the weld is as follows:

$$[(3.31 \text{ kip-in./0.88 in})^2 + (1.65 \text{ kip /2 welds})^2]^{0.5} = 3.85 \text{ kip/in. of weld.}$$

The resulting stress on the 0.28-in. minimum throat weld is 3.85/.28 = 13.8 ksi.

With a weld quality factor of 0.4 for a visually examined Type V Category E weld per ASME Code, Table NG-3352-1, the allowable load on the weld is .42 x 99.5 ksi x 0.4 = 16.7 ksi, which is greater than the design stress of 13.8 ksi.

$$\text{D.M.} = \frac{16.7}{13.8} - 1 = 0.21$$

2.10.3.6.2 Stresses Due to End Drops. The maximum impact limiter load due to a 30-ft end drop is 3360 kips (Table 2.10.4-2). This load was computed using the maximum strength honeycomb and is shared by the ILSS and the cask body during bottom-end drop, and the ILSS, cask body, and closure for a closure-end drop.

The load reacted directly by the cask body at the bottom end and the cask body and closure at the top end is computed as follows:

$$F_{cb} = P \times A_{cb} = 1242 \text{ kips},$$

where

P = honeycomb crush strength = 1732 psi,

A_{cb} = cross-sectional area of cask body (to outside dimension of cask body, 27.32 in.),

$$= 27.32^2 - (4 - \pi)\, 5.84^2 = 717 \text{ in.}^2$$

The force on the ILSS (ribs and shell outboard of the cask body) is therefore

$$F_{ILSS} = 3360 - 1242 = 2118 \text{ kips}.$$

Bearing Stress on ILSS Surface:

$$\sigma = F_{ILSS}/A_{ILSS} = 2118/524 = 4 \text{ ksi},$$

where

A_{ILSS} = frontal area of ILSS,

$$= \pi r^2 - A_{cb},$$

$$= \pi(39.75/2)^2 - 717 = 524 \text{ in.}^2$$

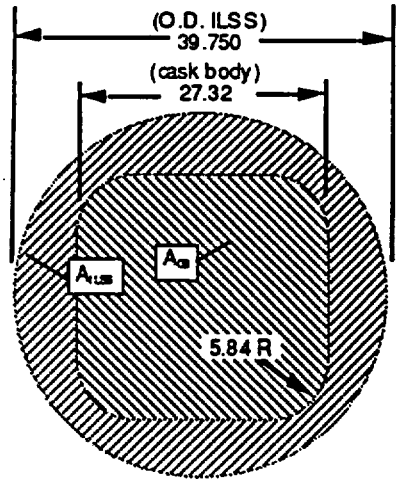

Bearing Stress on ILSS Ribs. Even if it is assumed that the entire end load on the ILSS (2118 kips) is transferred to the ribs through direct bearing, the stresses are still well below allowables. It is assumed that each of the 36 ribs is equally loaded and the bearing is calculated for the shortest rib.

$$\sigma_b = \frac{F_R}{A_b},$$

$$= \frac{58.8}{1.59},$$

$$= 37.0 \text{ ksi};$$

$$\text{D.M.} = \frac{99.5}{37} - 1,$$

$$= 1.69.$$

where

$F_R = \frac{F_{ILSS}}{\text{no. of ribs}}$,

$= 2118 \text{ kips}/36$,

$= 58.8$ kips, and

A_b = area of shortest rib,

$= 2.12 \text{ in.} \times .75 \text{ in.}$,

$= 1.59 \text{ in.}^2$

Stresses in the Outer Shell-to-rib Plug Welds (Fig. 2.10.3-33)

The force in the outer shell is transferred to the ribs by bearing on the front of the ribs and shear along tops of the ribs. The analysis conservatively assumes that all of the load in the outer shell is transferred to the ribs through shear in the plug welds at the top of the ribs. The force per rib is

$F_R = F_{ILSS}/\text{no. of ribs} = 2118 \text{ kips}/36 = 58.8 \text{ kips/rib}$

The bottom-end ILSS has 11 inches of 0.5-in.-wide plug welds per rib. The closure-end ILSS has additional weld area; therefore, the maximum weld stresses occur at the bottom ILSS and are computed as follows:

$\tau = F_R/A = 58.8/(11 \times .5) = 10.7$ ksi.

The allowable for a Type VIII Cat E weld with progressive PT or MT examination, following ASME Code Subsection NG-5231, uses a weld quality factor n = 0.45; therefore, the allowable shear stress on the weld is $41.8 \times .45 = 18.8$ ksi.

$\text{D.M.} = \frac{18.8}{10.7} - 1 = .76.$

Shear Stresses in the Rib and Rib-to-cask-body Fillet Welds (Fig. 2.10.3-33)

The shear load from the outer shell to the ribs is transmitted to the cask body in shear. The shear flow in the rib is

Shear flow = F_R/(ILSS length) = 58.8/22.25 = 2.64 kips/in.

Considering only the minimum section of the ribs, the section with the largest drilled holes, the effective thickness of the ribs is

Effective thickness = minimum width – maximum diameter = 0.75 – 0.63 = .12 in.

The resulting shear stress is

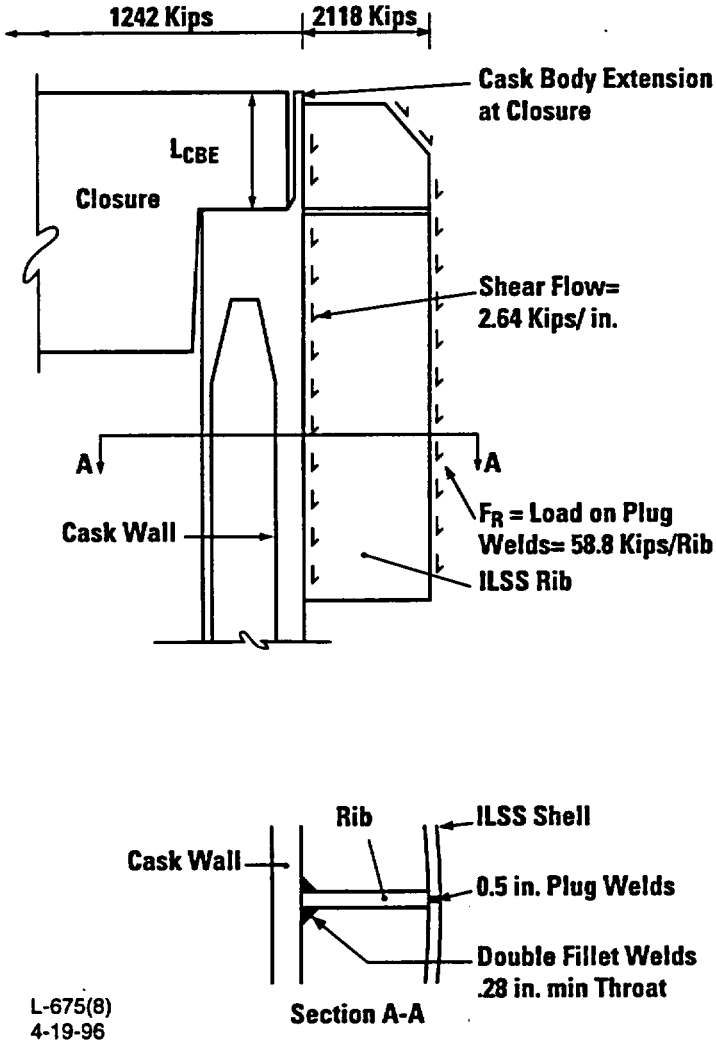

Fig. 2.10.3-33. Loading on ILSS ribs due to end drop

τ = (shear flow)/(effective thickness) = 2.64/0.12 = 22.0 ksi.

The allowable for pure primary shear stress is .42 S_u = 41.8 ksi (at 200°F). The corresponding design margin is

D.M. = (41.8/22.0) – 1 = 0.90.

The shear flow in the ribs is transferred to the cask body with double fillet welds which are visually examined. The minimum throat thickness of the welds is 0.28 in. Therefore, the weld stress is

τ = (shear flow)/(throat thickness x 2) = 2.64/(0.28 x 2) = 4.7 ksi.

The weld quality factor taken from ASME Code Table NG-3352-1 is 0.4 for a visually examined Type V, Category E weld. The allowable stress in the weld is 41.8 ksi x 0.4 = 16.7 ksi. The design margin is

D.M. = (16.7/4.7) – 1 = 2.55

Compression in Cask Body Extension at Closure

σ_{CB} = F_{CB}/A_{CB} + shear flow x L_{CBE}/A_{CBE},
= 1.73 ksi + 12.75 ksi,
= 14.5 ksi;

where
F_{CB} = load on cask body = 1242 kips,
A_{CB} = cross-sectional area of cask body = 717 in.^{2},
shear flow = 2.64 kips/in. on one ILSS rib,
L_{CBE} = length of cask body extension = 5 in.,
A_{CBE} = 0.375 in. x 2.76 in.,
= 1.035 in.^{2}.

2.10.3.6.3 Oblique Drops. The impact forces due to the 30-ft oblique angle drops are determined using GACAP (Section 2.10.4) and summarized in Tables 2.10.4-1 through 2.10.4-4. From these tables, it is seen that the maximum slapdown impact force is 1450 kips, which is used in Section b above. This force does not act concurrently with end drop force components. However, primary impact forces for all angles other than 0° and 90° have components, which are evaluated to show whether the stresses are higher than those for either the end drop force or maximum slapdown impact force acting alone. The evaluation considers angles from 15° to 78°. The maximum impact forces and their components are shown below:

Angle (°)	Impact Force (kips)	End Drop Component (kips)	Side Drop Component (kips)
0	1450	0	1450
15	1230	318	1188
30	1360	680	1178
45	1800	1273	1273
60	2400	2078	1200
75	3160	3052	818
78	2720	2661	565
90	3360	3360	0

The above components are used to determine the stresses for oblique angles shown in Tables 2.10.3-16 through 2.10.3-23. The major effects of end and side components in combinations that increase the stresses or stress intensities over that due to one component acting alone are in the following areas:

a. Stresses in the cask body extension at the closure. The compression due to bearing adds directly to the compression due to bending as a cantilever. The compressive stress due to the 3360 kip end drop is 14.5 ksi. The compressive stress due to bending in the 1450 kip secondary impact is 4.7 for the flat orientation and 6.6 ksi for the corner orientation. The expansion tank pressure stress during the 30-ft drop is 2.5 ksi for the side drop and 6.8 ksi for the end drop. The shear stress is 15.7 ksi for the corner drop orientation and 31.4 for the flat orientation. Tables 2.10.3-16 and 2.10.3-17 show the combined maximum stress for each drop angle for the corner and flat orientations, respectively.

b. Stress intensities in the outer shell. The axial compressive stress due to bearing combines directly with the hoop membrane and bending tensile stress. Table 2.10.3-18 shows the combined maximum stress in the ILSS outer shell for each oblique drop angle.

c. Stress intensities in welds. Shear stresses in the axial direction can increase the shear stresses due to hoop loads. For the plug welds connecting the outer shell to the rib, the weld stresses due to the axial force component being transferred to the ribs is combined with the weld stresses due to the side component loading on the shell and rib. Table 2.10.3-19 shows the combined maximum stress for each drop angle. For the fillet welds connecting the ribs to the cask body, the shear stress due to axial shear flow and hoop shear stress due to hoop shear and bending are orthogonal. Table 2.10.3-20 shows the combined maximum stress in the rib-to-cask-body fillet welds for each drop angle.

d. Bearing on ribs. The maximum bearing stress occurs either on the end (90°) drop or side (0°) drop or slapdown where the maximum impact forces occur. Other oblique orientations will result in lower bearing stresses since the impact forces in each direction (axial and side) are lower. The analyses in Section 2.10.3.6.1c and 2.10.3.6.2 give the maximum bearing stresses.

TABLE 2.10.3-16 SUMMARY STRESSES IN CASK BODY EXTENSION AT THE CLOSURE AT LOCATION OF MAXIMUM STRESS, CORNER ORIENTATION (psi)

Impact Angle, (Deg)	Stress Components						Principal Stresses			Stress Int.	Stress Type	Stress Limit	Design Margin
	Sx	Sy	Sz	Sxy	Syz	Sxz	S1	S2	S3				
0	0	2400	6600	0	0	15700	19343	2400	-12743	32086	P_m+P_b	99500	2.1
15	0	2600	6800	0	0	12860	16702	2600	-9902	26604	P_m+P_b	99500	2.7
30	0	3300	8300	0	0	12710	17520	3300	-9220	26741	P_m+P_b	99500	2.7
45	0	4600	11300	0	0	13756	20521	4600	-9221	29742	P_m+P_b	99500	2.3
60	0	6100	14500	0	0	13009	22143	6100	-7643	29786	P_m+P_b	99500	2.3
75	0	7300	16900	0	0	8822	20666	7300	-3766	24432	P_m+P_b	99500	3.1
78	0	6700	15300	0	0	6579	17740	6700	-2440	20180	P_m+P_b	99500	3.9
90	0	6600	14500	0	0	0	14500	6600	0	14500	P_m+P_b	99500	5.9

Sz is the stress in the cask axial direction due to end drop loads and side drop cantilever loads, Sy is the stress in the circumferential direction due to expansion tank pressure loads and Sxz is the shear stress due to the cantilever load.

TABLE 2.10.3-17 SUMMARY STRESSES IN CASK BODY EXTENSION AT THE CLOSURE AT LOCATION OF MAXIMUM STRESS, FLAT ORIENTATION (psi)

Impact Angle, (deg)	Stress Components						Principal Stresses			Stress Int.	Stress Type	Stress Limit	Design Margin
	Sx	Sy	Sz	Sxy	Syz	Sxz	S1	S2	S3				
0	0	2400	4700	0	0	31350	33788	2400	-29088	62876	P_m+P_b	99500	0.6
15	0	2600	5300	0	0	25650	28437	2600	-23137	51573	P_m+P_b	99500	0.9
30	0	3300	6700	0	0	25500	29069	3300	-22369	51438	P_m+P_b	99500	0.9
45	0	4600	9600	0	0	27450	32667	4600	-23067	55733	P_m+P_b	99500	0.8
60	0	6100	12900	0	0	25950	33190	6100	-20290	53479	P_m+P_b	99500	0.9
75	0	7300	15900	0	0	17700	27353	7300	-11453	38807	P_m+P_b	99500	1.6
78	0	6700	14500	0	0	13200	22310	6700	-7810	30120	P_m+P_b	99500	2.3
90	0	6600	14500	0	0	0	14500	6600	0	14500	P_m+P_b	99500	5.9

Sz is the stress in the cask axial direction due to end drop loads and side drop cantilever loads, Sy is the stress in the circumferential direction due to expansion tank pressure loads and Sxz is the shear stress due to the cantilever load.

TABLE 2.10.3-18 30-FT DROP STRESSES IN ILSS OUTER SHELL AT LOCATION OF MAXIMUM STRESS

Impact Angle (Deg)	Compressive Stress due to End Loading Bearing, ksi	P_m+P_b due to Side Loading, ksi	Total Stress, ksi	Allowable Stress, S_u ksi	Design Margin
0.0	0.0	98.3	98.3	99.5	0.01
15.0	1.9	80.5	82.4	99.5	0.21
30.0	4.0	79.9	83.9	99.5	0.19
45.0	7.6	86.3	93.9	99.5	0.06
60.0	12.4	81.4	93.7	99.5	0.06
75.0	18.2	55.5	73.6	99.5	0.35
78.0	17.2	41.6	58.7	99.5	0.69
90.0	20.0	0.0	20.0	99.5	3.98

TABLE 2.10.3-19 30-FT DROP STRESSES IN OUTER SHELL TO RIB PLUG WELDS AT LOCATION OF MAXIMUM STRESS

Impact Angle (Deg)	Weld Shear Stress due to End Loading, ksi	Weld Shear Stress due to Side Loading, ksi	Resultant Shear Stress, ksi	Allowable Stress[a], ksi	Design Margin
0.0	0.0	12.7	12.7	18.8	0.48
15.0	1.0	10.4	10.4	18.8	0.80
30.0	2.2	10.3	10.5	18.8	0.79
45.0	4.1	11.1	11.8	18.8	0.59
60.0	6.6	10.5	12.4	18.8	0.52
75.0	9.7	7.2	12.1	18.8	0.56
78.0	9.2	5.4	10.6	18.8	0.77
90.0	10.7	0.0	10.7	18.8	0.76

(a) Allowable stress = $0.42S_u n = 0.42 \times 99.5 \times 0.45 = 18.8$ ksi.

TABLE 2.10.3-20 30-FT DROP STRESSES IN THE RIB-TO-CASK-BODY-WALL FILLET WELDS AT LOCATION OF MAXIMUM STRESS

Impact Angle (Deg)	Weld Shear Stress due to End Loading, ksi	Weld Shear Stress due to Side Loading, ksi	Resultant Shear Stress, ksi	Allowable Stress[a], ksi	Design Margin
0.0	0.0	13.8	13.8	16.7	0.21
15.0	0.4	11.3	11.3	16.7	0.48
30.0	1.0	11.2	11.2	16.7	0.49
45.0	1.8	12.1	12.2	16.7	0.37
60.0	2.9	11.4	11.7	16.7	0.42
75.0	4.3	7.8	8.9	16.7	0.89
78.0	4.0	5.8	7.1	16.7	1.36
90.0	4.7	0.0	4.7	16.7	2.55

(a) Allowable stress = $0.42S_un = 0.42 \times 99.5 \times 0.4 = 16.7$ ksi.

e. Stress intensities in the ribs. The axial load is transferred to the cask body through shear in the rib and the slapdown loads are transferred to the cask body through compression and bending as described in Sections 2.10.3.6.2 and 2.10.3.6.1c, respectively. Table 2.10.3-21 shows the combined stresses for the rib with the highest stress intensity for each drop angle.

2.10.3.6.4 Summary of Results. Conservative analyses and assumptions are used throughout the ILSS design. These analyses show the following minimum margins of safety:

Component	Stress Intensity (ksi)	Loading Condition	Minimum Design Margin
Outer shell	98.3	0° drop	(99.5/98.3) – 1= .01
Ribs	48.4	75° drop	(99.5/48.4) – 1 = 1.06
Cask body extension at closure	62.9	0° drop	(99.5/62.9) – 1 = 0.60
Shell to rib plug welds	12.7	side drop	(18.8/12.7) – 1 = .48
Rib to cask body fillet welds	13.8	side drop	(16.7/13.8) – 1 = .21
Bearing on ribs	37.0	90° end drop	(99.5/37) – 1 = 1.69

2.10.3.6.5 Angular Orientations–Other than Flat Side and Corner Side Drops. The ILSS components that are affected by the angular orientation around the cask axes during a side impact are the ribs and outer shell. The ANSYS analysis described in Section 2.10.3.6.1c was performed for a flat side drop (the flat side of the cask is parallel to the impact surface) and a corner side drop (the cask corner is parallel to the impact surface). The ANSYS analysis was also performed for angular orientations of 15° and 30° from a flat side drop. Tables 2.10.3-22 and 2.10.3-23 compare the stresses in the ribs and shell, respectively, at the critical stress locations for the flat side, corner side, 15° from flat side, and 30° from flat side orientations. As shown by these tables, the flat and corner results envelop the results for the other two orientations.

TABLE 2.10.3-21 ILSS, FLAT SIDE SLAPDOWN, MEMBRANE + BENDING STRESSES AT STEP IN RIBS AT LOCATION OF MAXIMUM STRESS, RIB 5, (psi)

Impact	Combined Stress Components						Principal Stresses			Stress	Stress	Stress	Design
Angle (deg)	Sx	Sy	Sz	Sxy	Syz	Sxz	S1	S2	S3	Int.	Type	Limit	Margin
0	-35984	0	0	16059	0	0	6124	0	-42108	48233	P_m+P_b	99500	1.06
15	-29482	0	0	13321	0	0	5127	0	-34609	39737	P_m+P_b	99500	1.50
30	-29234	0	0	13785	0	0	5475	0	-34709	40184	P_m+P_b	99500	1.48
45	-31591	0	0	16378	0	0	6958	0	-38550	45508	P_m+P_b	99500	1.19
60	-29780	0	0	19020	0	0	9265	0	-39045	48310	P_m+P_b	99500	1.06
75	-20300	0	0	21941	0	0	14025	0	-34325	48350	P_m+P_b	99500	1.06
78	-15213	0	0	20079	0	0	13865	0	-29078	42943	P_m+P_b	99500	1.32
90	0	0	0	22000	0	0	22000	0	-22000	44000	P_m+P_b	99500	1.26

Sx is the radial stress in the rib due to membrane and bending and Sxy is the shear stress due to the transverse shear load on the rib.

Table 2.10.3-22 HIGHEST ILSS RIB STRESSES AT ANGULAR ORIENTATIONS FOR SIDE DROP

Location	Element No.	Orientation	Stress Type	Stress Intensity, ksi	Stress Limit, ksi	Design Margin
Rib 5 @ Step	210	Flat Side	P_m	33.7	69.7	1.07
Rib 5 @ Step	210	Flat Side	P_m+P_b	48.2	99.5	1.06
Rib 5 @ Base	174	Flat Side	P_m+P_b	48.1	99.5	1.07
Rib 5 @ Step	201	15 Deg from Flat Side	P_m	33.2	69.7	1.10
Rib 5 @ Step	201	15 Deg from Flat Side	P_m+P_b	45.2	99.5	1.20
Rib 5 @ Base	165	15 Deg from Flat Side	P_m+P_b	46.0	99.5	1.16
Rib 5 @ Step	201	30 Deg from Flat Side	P_m	29.7	69.7	1.35
Rib 6 @ Step	201	30 Deg from Flat Side	P_m+P_b	39.2	99.5	1.54
Rib 6 @ Base	165	30 Deg from Flat Side	P_m+P_b	40.1	99.5	1.48
Rib 6 @ Step	211	Corner Side	P_m	23.9	69.7	1.92
Rib 6 @ Step	211	Corner Side	P_m+P_b	31.0	99.5	2.21
Rib14 @ Base	183	Corner Side	P_m+P_b	30.8	99.5	2.23

Table 2.10.3-23 HIGHEST ILSS SHELL STRESSES AT ANGULAR ORIENTATIONS FOR SIDE DROP

Location	Element No.	Orientation	Stress Type	Stress Intensity, ksi	Stress Limit, ksi	Design Margin
Shell	23	Flat Side	P_m	24.2	69.7	1.88
Shell	23	Flat Side	P_m+P_b	88.9	99.5	0.12
Shell	25	15 Deg from Flat Side	P_m	25.0	69.7	1.79
Shell	23	15 Deg from Flat Side	P_m+P_b	93.2	99.5	0.07
Shell	27	30 Deg from Flat Side	P_m	25.8	69.7	1.70
Shell	27	30 Deg from Flat Side	P_m+P_b	93.9	99.5	0.06
Shell	31	Corner Side	P_m	26.8	69.7	1.60
Shell	29	Corner Side	P_m+P_b	98.3	99.5	0.01

2.10.3.7 Impact Limiter Bolt Design.

2.10.3.7.1 Load Due to Impact. This section calculates the maximum stresses in the impact limiter bolts resulting from the 30-ft drop event. The half-scale model tests described in Section 2.10.13 confirmed that the impact limiter bolts did not fail and the impact limiters remained on the cask for three 30-ft drop orientations; side drop, 30° slapdown and CG-over-closure corner. These orientations give the maximum loading on the impact limiter bolts as shown in this section.

For most orientations and crush depths, the impact limiter crush force is transmitted to the cask body directly; hence, the forces seen by the impact limiter bolts are relatively small. This is not true at the start of an oblique crush, when the crush area is not backed by the cask. Therefore, the impact limiter bolts are designed conservatively to take the moment produced by the crush of the total unbacked area on the side of the cask during both a nearly vertical and a nearly horizontal oblique drop. Fig 2.10.3-34 shows the unbacked area during a nearly vertical oblique drop.

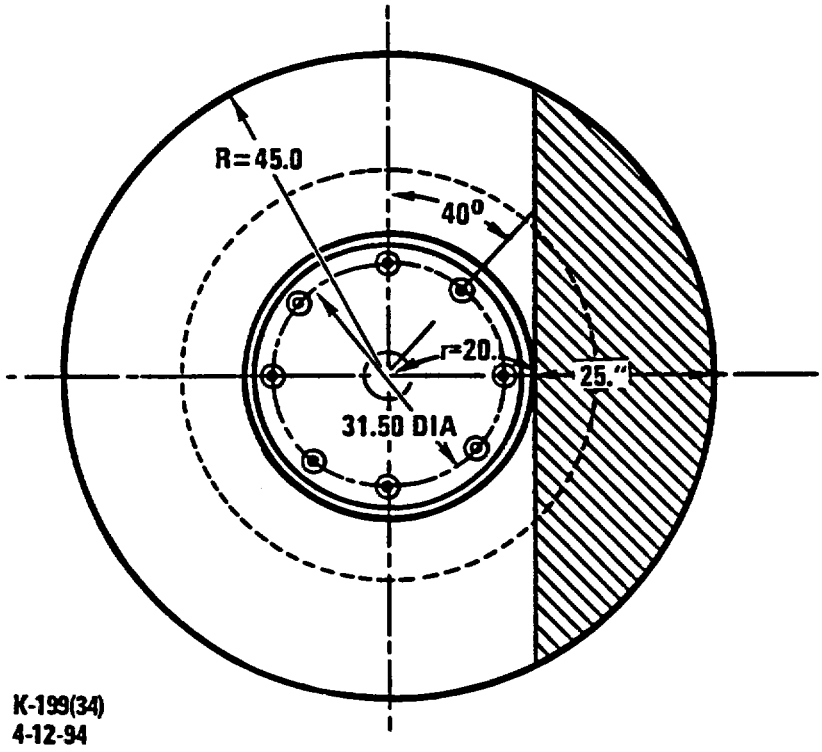

Fig. 2.10.3-34. Area of unbacked footprint during a near-vertical oblique drop used for design of impact limiter bolts

The moment produced by crushing during a near-vertical oblique drop is calculated as follows:

Chord = 80.62 in.

Rise = 25.0 in.

Angle = 127.22°,

Arc = 99.92 in., and

$$\text{Area} = \frac{99.92 \times 45.0 - 80.62(45.0 - 25.0)}{2} = 1442 \text{ in.}^2$$

Center of load = 4 x 25.0/(3π),

= 10.61 in.

M_{max} = Area x crush strength x center of load,

M_{max} = 1442 in.^{2} x (220 x 1.125 x 1.1) lb/in.^{2} x 10.61 in.,

= 4,165,322 in.-lb (near vertical drop orientation)

Another drop orientation that produces a moment on the impact limiter bolts is a near-horizontal oblique drop. A conservative loading condition assumes that the moment on the impact limiter bolts results from crushing of the corner honeycomb (part 2, Fig. 2.10.3-35). The GACAP results (Table 2.10.4-1, Section 2.10.4.1.3) show a maximum side crush of 14.7 in. Since the footprint is formed by the intersection of both conical and cylindrical shapes with a straight plane, the crush area was calculated using ILMOD (Section 2.10.1.4). A crush depth of 16 in. was conservatively used. The area crushed on the corner honeycomb (part 2) due to a 16-in. side crush is 1423 in.^{2} Fig. 2.10.3-35 shows the crush plane profile on the impact limiter after the 16-in. crush.

Part 2 crushed area = 1423 in.^{2}

Center of this load = (26.16 – 3.28)/2 = 11.44 in. (conservative value).

M_{max} = 1423 in.^{2} (220 x 1.125 x 1.1) lb/in.^{2} x 11.44 in.,

= 4,430,000 in.-lb (horizontal drop orientation).

The moment produced by oblique drops which have load components perpendicular to the cask axis and parallel to the cask axis, will be less for the closure bolts than the two bounding cases above. This is true since the moments produced by each load component oppose each other, reducing the total moment, and all directional component impact forces are less than those for either the end or side drop.

The bolts' reaction due to the maximum moment was conservatively analyzed by assuming that the edge of the impact limiter has a pinned boundary condition. Assuming that the impact limiter remains rigid, the force per bolt can be calculated as follows:

Moment of inertia through the centroid of the bolt group:

I_{xx} = 0.5 N $(r_b)^2$,

= 992.25 in.^{2},

where

N = 8 bolts,

r_b = 31.5 in./2 = 15.75 in. (radius of bolt circle).

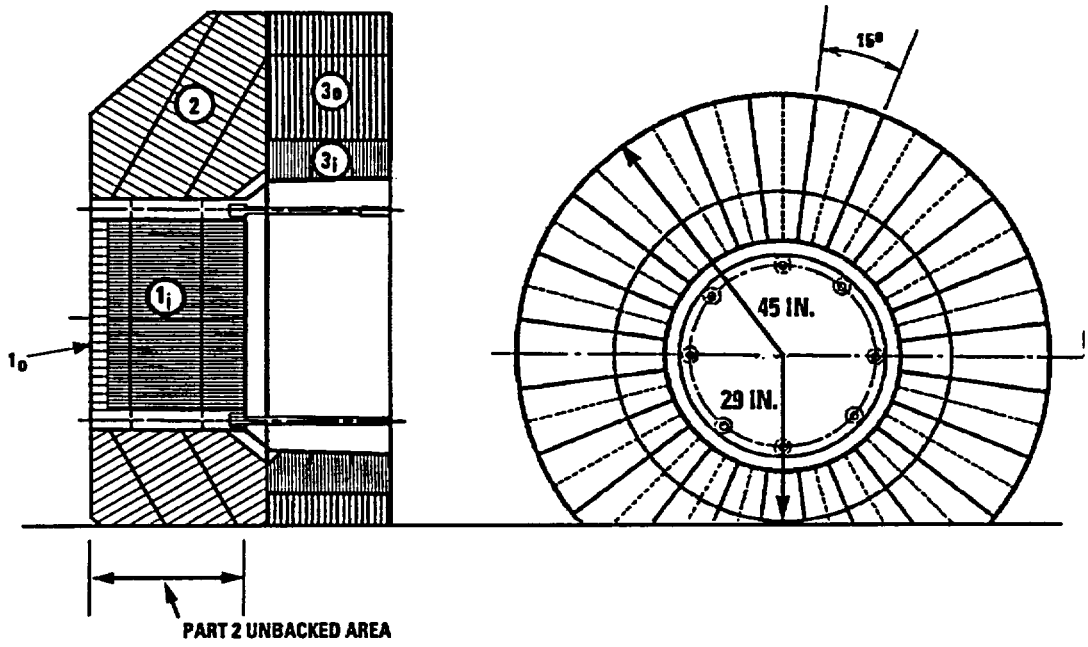

Fig. 2.10.3-35. Crush profile plane at a 16 in. crush height

The moment about the base of the group is

$I_{aa} = I_{xx} + Nr^2$,

where

$r = 19.875$,

$I_{aa} = 992.25 + 8\,(19.875)^2 = 4152$ in.^{2}.

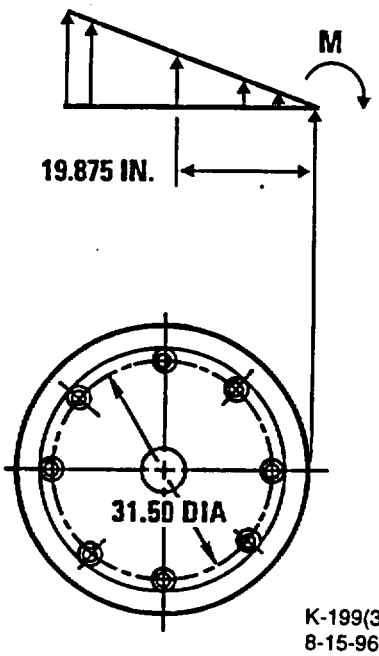

K-199(35)
8-15-96

The maximum force in any bolt then becomes

$f_{axial} = Mc/I_{aa}$

$= 4{,}430{,}000$ in.-lb x 35.625 in./4152 in.^{2} = 38,010 lb,

where

$c = 15.75 + 19.875 = 35.625$ in.

for the 1.125-in.-dia. bolts with a reduced shank dia. = 0.838 in.

$\sigma_{max} = f_{axial}/A_{min} = 38{,}010$ lb/0.551 in.^{2} = 69 ksi < allowable.

The allowable for non-containment bolts (SB-637, Alloy N07718) is

$P_m = 146.3$ ksi (T = 150°F).

D.M. = (146.3/69) – 1 = 1.12

The cask impact limiter attachment method was designed so that there is no interference and minimum shear stress imposed on the impact limiter bolts during the drop events. The impact limiter bolt diameter is 0.838 in., and the impact limiter support structure tube inner diameter is 1.750 – (2 x 0.065) = 1.62 in. This is the size of the hole in the outer plate of the impact limiter support structure. The clearance between the bolt and the edge of the hole in the plate is (1.62 – 0.838)/2 = 0.391 in.

The diametral clearance between the impact limiter housing and the impact limiter support structure is 40.00 – 39.75 = 0.25 in. This clearance is smaller than the clearance between the bolt and the edge of the hole in the plate of the impact limiter support structure. During a side impact, as the impact limiter moves laterally relative to the cask, the impact limiter canister will contact the impact limiter support structure before the bolts contact the edge of the hole in the plate. This will be true even if the impact limiter is installed completely against one side of the cask and then subjected to a side drop on the opposite side. The maximum impact limiter movement is 0.25 in. After moving 0.25 in., the impact limiter attachment bolts will not contact the side of the impact limiter support plate. Therefore, the only loads on the impact limiter bolts will be the tension loads from the moment produced by the crush of the unbacked portion of the impact limiter and the bending produced by the 0.25-in. side movement. The stress on the bolts due to this movement is calculated as follows:

Δ = 0.5 in., maximum impact limiter side movement (conservative value; maximum gap between impact limiter and ILSS is 0.25 in.),

L = length of bolts = 21.14 in. + (1/3)(2) in. = 21.80 in.,

c = .838/2 = .419 in.,

E = 29.0×10^6 psi for SB-637, alloy N07718,

$$\sigma_{bending} = \frac{M_{max}c}{I} = \frac{5.25E\Delta c}{L^2},$$

$$= \frac{5.25(29.0\times10^6)0.5(.419)}{(21.80)^2} = 67{,}116 \text{ psi.}$$

The total stress on the bolt during impact and side movement is

σ_{m+b} = 69 ksi + 67 ksi = 136 ksi.

This stress is less than the $P_m + P_b$ allowable of 179.5 ksi (T = 150°F) for non-containment bolts.

D.M. = (179.5/136) – 1 = .32

2.10.3.7.2 Loads Due to Hypothetical Accident Condition Puncture and Thermal Events. The half-scale model tests described in Section 2.10.13 confirmed that the impact limiters would remain attached to the cask for the puncture orientations tested; puncture on the side of the impact limiter and closure, puncture attacking the impact limiter and gas sample port through the CG, and puncture attacking the side of the cask with the cask axis horizontal. These puncture orientations envelop the most severe orientations. The bolt design is such that in the event an impact limiter bolt failed during a puncture event, the remaining seven bolts would still ensure that the impact limiter remains attached to the cask.

Since it has been shown that the impact limiters will remain attached to the cask after the drop and puncture events, the fire event will not add any loading that would cause the impact limiter to not remain attached. The thermal analysis in Section 3 shows that the temperature of the impact limiter bolts during the fire is 1010°F maximum and below 800°F average. The ASME Code, Section III, Code Case N-47-28 gives properties for the Type N07718 bolt material as follows:

S_y = 128 ksi at 1050°F,

S_m = 42.7 ksi at 1050°F, and

α = 7.86×10^{-6} in./in.– °F at 800°F

The only loading during the fire event is thermal. The maximum differential thermal expansion stresses in the bolts at an average temperature of 800°F is calculated as follows:

$\sigma_{th} = E(\alpha_{xm\text{-}19} - \alpha_{bolt})\Delta T,$

= 26.2 ksi;

where

$E = 25.8 \times 10^6$ psi at 800°F,

$\alpha_{XM\text{-}19} = 9.25 \times 10^{-6}$ in./in.– °F at 800°F,

$\alpha_{bolt} = 7.86 \times 10^{-6}$ in./in.– °F at 800°F, and

$\Delta T = 800°F - 70°F,$

$= 730°F.$

D.M. against yielding $= (128/26.2) - 1,$

$= 3.9.$

This calculation is conservative since it assumes that the cask temperature increases the same amount as the impact limiter bolts, which is not the case.

THIS PAGE LEFT BLANK INTENTIONALLY

2.10.4 GACAP Free Drop Analysis

10 CFR Part 71 requires that the cask be evaluated for a free drop onto a flat, unyielding horizontal surface for both normal and hypothetical accident conditions. The cask should strike the surface in a position that is expected to inflict the maximum damage. We used the GACAP computer code (described in Section 2.10.1.1) to perform the 1-ft and 30-ft drop analyses to obtain accelerations, impact limiter crush forces and impact limiter crush distances for the drop orientations that bound all possible drops.

2.10.4.1 30-ft GACAP Analysis. We evaluated the GA-4 cask for hypothetical accident 30-ft free drops at 0° (side drop), 15°, 30°, 45°, 60°, 75°, 78° (CG-over-corner), and 90° (end drop). For each hypothetical accident 30-ft impact, we analyzed the upper and lower bound expected crush force on the impact limiter behavior. The range of impact limiter behavior covers variations in the normal operating temperature (maximum 200°F and minimum –20°F), and variations on the honeycomb nominal strength. Section 2.10.3 explains in detail the behavior of the impact limiters. Generally, the maximum-value impact limiter force-deflection curve produces the maximum loadings on the cask body. The minimum value curve produces the maximum deflection of the impact limiter. In addition, we ran several critical cases using the load-deflection curves obtained during the impact limiter tests reported in Section 2.10.3.4. We scaled the tests results to full size and multiplied by 1.1 to account for the strain rate effect.

To satisfy the requirements of NRC Regulatory Guide 7.8 for the GA-4 cask, we also considered impacts with the maximum and minimum weights of contents.

In the hypothetical accident condition analyses, a secondary impact or slapdown of the cask on the opposite end follows the initial impact for all oblique drops. For the end, side, and CG over corner drops, all the energy is absorbed during the primary impact.

The GACAP analyses assume the following:

1. The DU is nonstructural (i.e., adds mass but not strength), except that it transfers compressive loads.

2. The cask acts as a rigid body.

3. The cask/cavity liner behaves as a structural unit.

4. The impact limiter support structure and neutron shield structure strengths and stiffnesses are ignored.

5. The cask is symmetric with respect to impacts on the top and bottom ends. (The only difference is a slight change in thickness between the bottom plate and closure. To make the model symmetric, the length of the cask was increased, resulting in slightly conservative results.

6. Only one impact occurs on the primary impact side. The energy remaining after the primary impact is absorbed during the secondary impact.

7. No energy is dissipated through friction.

2.10.4.1.1 GACAP Model. The GACAP model represents the GA-4 cask with 14 beams. Figure 2.10.4-1 shows that 12 beams are positioned within the cavity of the cask and a beam is positioned 6 inches into the bottom and top head at each end of the model.

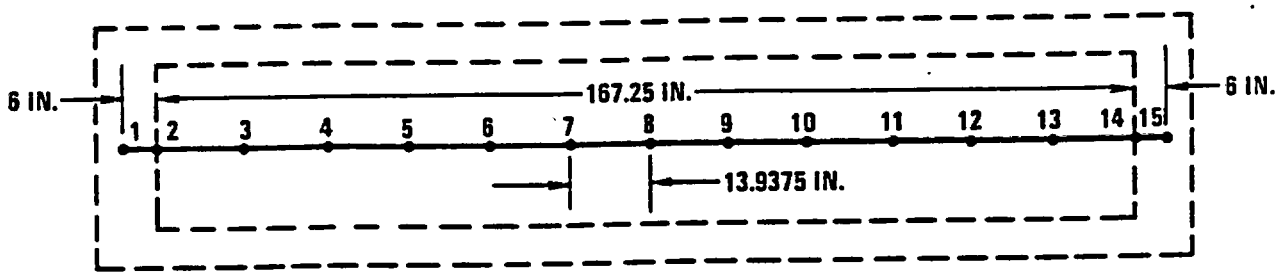

K-234 (18)
9-19-91

Fig. 2.10.4-1. GACAP representation of GA-4 cask, using 14 beams and 15 nodes

The mass distribution for the maximum contents weight condition is as follows:

Maximum package weight = 55,000 lb
Midspan wt/in. = 265.5 lb/in. (Conservative, actual weight, lb/in., from Table 2.2-1 is 265.2 lb/in.)

Mass for nodes 2 to 14:

$m_n = (265.5)(13.9375)/386.4 = 9.578$ lb sec^2/in.

Mass for end nodes 1 and 15:

55,000 – (13)(9.578)(386.4) = 6,889 lb.
Assume equally distributed,
$m_{1,15} = (6,889)/(2)(386.4)$ = 8.915 lb sec^2/in.

The mass distribution for the minimum contents weight condition is as follows:

Minimum package weight = Minimum packaging weight and minimum weight of one fuel assembly,
= 47,170 lb + 1182 lb,
= 48,352 lb,
Midspan wt/in. = = 225.72 lb/in.

Mass of nodes 2 to 14:

$m_n = (225.72)(13.9375)/386.4 = 8.142$ lb sec^2/in.

Mass of end nodes 1 and 15:

48,352 – (13)(8.142)(386.4) = 7,454 lb.
Assume equally distributed between nodes,
$m_{1,15} = 7,454/(2)(386.4) = 9.646$ lb sec^2/in.

We used variations of the same model to run the different drop orientations. The difference between these runs is the location of the impact limiter reaction points. For the side drop analysis, the reaction point is located at the centroid of the impact limiter force at its maximum crushed condition obtained during a side drop (see Fig. 2.10.4-2). During the CG-over-corner, 75°, 60°, 45°, 30°, and 15° drops, the primary impact limiter reaction point is located at the corner of the cask. The secondary impact or slapdown reaction point is located the same as for the side drop, as shown in Fig. 2.10.4-3. This is justified since the secondary impacts always occur at a very low angle, as shown by the GACAP runs. During the end drop, the model used two reaction points located at each corner of the closure, as shown in Fig. 2.10.4-4. The total impact limiter force was equally divided between these two points.

The model represents the cask body, the fuel cavity liner, the closure/flange, and the bottom end sections, with the following dimensions (see Fig. 2.10.4-5):

	Nodes 2 to 14		Nodes 1, 15
Dimension	Cask Body	Fuel Cavity Structure	Closure/Flange, Bottom End
HC	12.162 in.	9.080 in.	9.080 in.
RC	4.336 in.	0.125 in.	0.125 in.
TH	1.5 in.	0.375 in.	4.582 in.

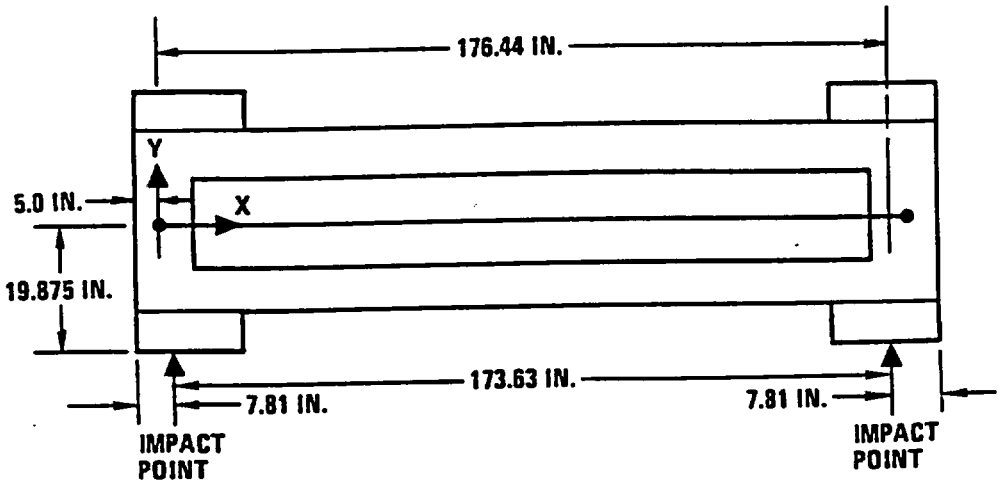

Fig. 2.10.4-2. Impact points used in GACAP analyses for side drop

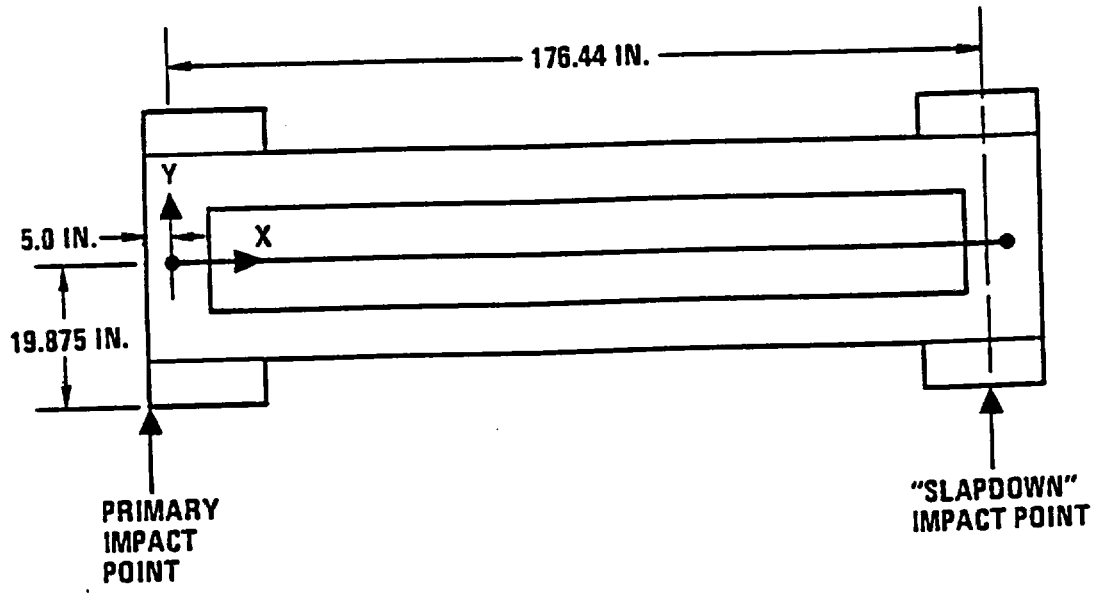

Fig. 2.10.4-3. Impact points used in GA-4 cask GACAP CG over corner and oblique drop analyses

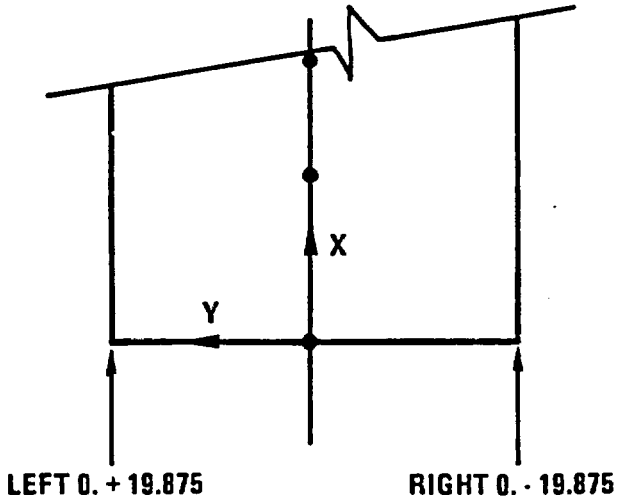

K-234 (16)
9-19-91

Fig. 2.10.4-4. Impact points used in GA-4 cask GACAP end drop analyses

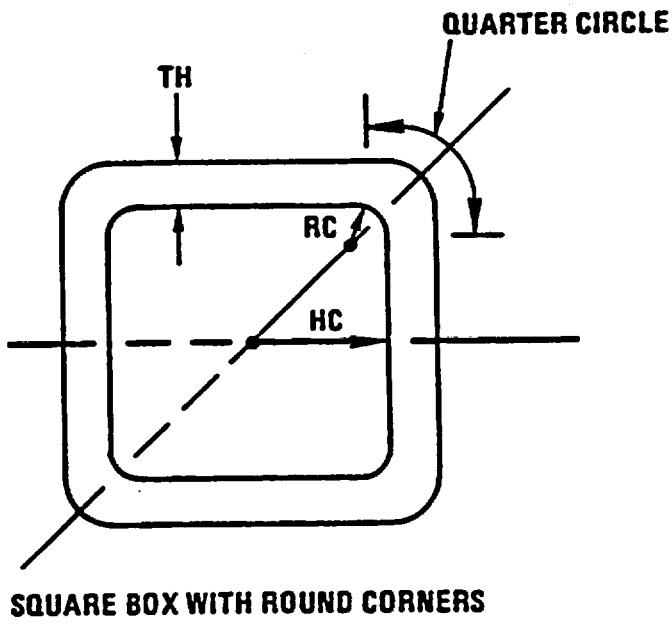

Fig. 2.10.4-5. Nomenclature to describe geometry of structural elements in GACAP runs

2.10.4.1.2 Impact Limiter Load Deflection Data. Section 2.10.3 explains in detail the behavior of the impact limiters. The GACAP runs utilize the ILMOD-developed minimum and maximum impact limiter crush strength data as described in 2.10.3.3. Critical runs were also performed using the 1/4-scale test results (Section 2.10.3.4) scaled to full size and multiplied by the strain rate effect factor of 1.1. These runs envelop the range of impact limiter behavior.

2.10.4.1.3 Results. GACAP calculates the accelerations at all mass points and the center of gravity. In addition, it calculates the impact limiter crush, the maximum impact limiter force and the energy absorbed by the primary and secondary impacts. Tables 2.10.4-1 through 2.10.4-5 summarize the results for the bounding impact limiter strengths and for maximum and minimum contents weight. Figures 2.10.4-6 through 2.10.4-25 show the transverse (perpendicular to cask axis) and axial (parallel to cask axis) accelerations along the length of the cask.

For the side drop, CG over corner drop and end drop, the accelerations are constant throughout the cask. However, as Figs. 2.10.4-6 through 2.10.4-25 show, the accelerations for all oblique primary and slapdown impacts vary along the length of the cask and are maximum for each impact (primary or secondary) at the impact end. The maximum accelerations are higher than the acceleration at the center of gravity. This effect is due to the added rotational accelerations experienced during an oblique primary or slapdown impact.

The accelerations are generally higher for the minimum contents load case. This is due to the fact that the impact limiter load-deflection curves are not linear and the final impact limiter forces that occur during drops with the minimum or maximum design weights are relatively close in magnitude.

The loadings that result in the maximum stress for each component of the cask are summarized in Tables 2.10.4-6 and 2.10.4-7 (maximum g-levels) and are used as follows:

a. Containment Boundary. The stresses in the containment boundary are a maximum with the maximum contents loading for most of the drop orientations. This is true since the increase in acceleration for the minimum contents weight load case is less than the decrease in total cask weight.

b. Fuel Support Structure (FSS) and Cavity Liner. The stresses in the FSS and cavity liner are maximum with the maximum contents loading for all of the drop orientations. This is true since the contents directly load those components and because the accelerations increase less than the weight decreases for the minimum contents loading.

c. Neutron Shield Structure. The stresses in the neutron shield are a maximum with the minimum contents weight load case for all drops since the accelerations are higher and the contents do not affect the loading on the neutron shield.

d. Impact Limiter Support Structure (ILSS). The maximum stresses in the ILSS occur for the maximum contents weight load case since the ILSS is directly loaded from the crush of the impact limiters. The maximum impact limiter crush force occurs for the maximum contents weight load case.

TABLE 2.10.4-1 GA-4 30-FT DROP RESULTS FOR HIGH IMPACT LIMITER STRENGTH AND MAXIMUM WEIGHT CONTENTS

Drop Angle (Deg)	Primary Impact Crush (in.)	Primary Impact Force-F (lb)	Primary Impact-G (CG)	Primary Impact-G Axial	Primary Impact-G Transverse	Primary Impact Energy (lb-in.)	Secondary Impact Crush (in.)	Secondary Impact Force-F (lb)	Secondary Impact-G (CG)	Secondary Impact Energy (lb-in.)
0	11.9	2.62E+06	47.7	0.0	47.7	2.01E+07				
15	11.8	1.23E+06	22.3	5.8	21.5	6.36E+06	14.7	1.45E+06	26.3	1.34E+07
30	14.7	1.36E+06	24.7	12.3	21.4	8.03E+06	14.5	1.43E+06	25.9	1.31E+07
45	16.5	1.79E+06	32.6	23.1	23.1	1.10E+07	13.4	1.36E+06	24.8	1.17E+07
60	18.5	2.40E+06	43.6	37.8	21.8	1.60E+07	11.4	1.21E+06	22.0	7.38E+06
75	15.5	2.70E+06	49.1	47.4	12.7	2.04E+07				
78	14.2	2.72E+06	49.4	48.3	10.3	2.04E+07				
90	9.2	2.65E+06	48.2	48.2	0.0	2.03E+07				

TABLE 2.10.4-2 GA-4 30-FT DROP RESULTS FOR TEST DATA IMPACT LIMITER STRENGTH AND MAXIMUM WEIGHT CONTENTS

Drop Angle (Deg)	Primary Impact Crush (in.)	Primary Impact Force-F (lb)	Primary Impact-G (CG)	Primary Impact-G Axial	Primary Impact-G Transverse	Primary Impact Energy (lb-in.)	Secondary Impact Crush (in.)	Secondary Impact Force-F (lb)	Secondary Impact-G (CG)	Secondary Impact Energy (lb-in.)
0	12.1	2.57E+06	46.8	0.0	46.8	2.02E+07				
15	9.2	1.19E+06	21.7	5.6	20.9	6.35E+06	14.5	1.44E+06	26.3	1.34E+07
45	14.6	1.46E+06	26.5	18.7	18.7	1.07E+07	13.2	1.37E+06	24.9	1.16E+07
60	14.3	1.86E+06	33.9	29.3	16.9	1.58E+07	10.1	1.26E+06	23.0	7.49E+06
75	14.1	3.16E+06	57.4	55.4	14.9	2.02E+07				
90	7.9	3.36E+06	61.0	61.0	0.0	2.02E+07				

TABLE 2.10.4-3 GA-4 30-FT DROP RESULTS FOR LOW IMPACT LIMITER STRENGTH AND MAXIMUM WEIGHT CONTENTS

Drop Angle (Deg)	Primary Impact Crush (in.)	Primary Impact Force-F (lb)	Primary Impact-G (CG)	Primary Impact-G Axial	Primary Impact-G Transverse	Primary Impact Energy (lb-in.)	Secondary Impact Crush (in.)	Secondary Impact Force-F (lb)	Secondary Impact-G (CG)	Secondary Impact Energy (lb-in.)
0	14.2	2.18E+06	39.6	0.0	39.6	2.05E+07				
15	13.3	1.03E+06	18.7	4.9	18.1	6.41E+06	17.2	1.33E+06	24.2	1.34E+07
30	16.3	1.18E+06	21.5	10.7	18.6	8.06E+06	16.9	1.30E+06	23.7	1.31E+07
45	18.1	1.64E+06	29.9	21.1	21.1	1.10E+07	15.7	1.18E+06	21.5	1.17E+07
60	20.3	2.18E+06	39.7	34.4	19.8	1.61E+07	12.8	1.01E+06	18.3	7.45E+06
75	17.6	2.18E+06	39.6	38.2	10.2	2.04E+07				
78	16.4	2.21E+06	40.2	39.3	8.4	2.06E+07				
90	11.5	2.16E+06	39.3	39.3	0.0	2.04E+07				

TABLE 2.10.4-4 GA-4 30-FT DROP RESULTS FOR HIGH IMPACT LIMITER STRENGTH AND MINIMUM WEIGHT CONTENTS

Drop Angle (Deg)	Primary Impact Crush (in.)	Primary Impact Force-F (lb)	Primary Impact-G (CG)	Primary Impact-G Axial	Primary Impact-G Transverse	Primary Impact Energy (lb-in.)	Secondary Impact Crush (in.)	Secondary Impact Force-F (lb)	Secondary Impact-G (CG)	Secondary Impact Energy (lb-in.)
0	11.0	2.51E+06	51.9	0.0	51.9	1.77E+06				
15	11.3	1.18E+06	24.4	6.3	23.6	5.76E+06	13.5	1.36E+06	28.2	1.18E+07
30	14.1	1.30E+06	26.8	13.4	23.2	7.25E+06	13.3	1.36E+06	28.0	1.15E+07
45	15.9	1.67E+06	34.5	24.4	24.4	9.90E+06	12.4	1.31E+06	27.0	1.02E+07
60	17.8	2.22E+06	46.0	39.8	23.0	1.42E+07	10.5	1.13E+06	23.4	6.30E+06
75	14.5	2.65E+06	54.8	52.9	14.2	1.77E+07				
78	13.3	2.64E+06	54.5	53.3	11.3	1.79E+07				
90	8.3	2.60E+06	53.7	53.7	0.0	1.78E+07				

TABLE 2.10.4-5 GA-4 30-FT DROP RESULTS FOR TEST DATA IMPACT LIMITER STRENGTH AND MINIMUM WEIGHT CONTENTS

Drop Angle (Deg)	Primary Impact Crush (in.)	Primary Impact Force-F (lb)	Primary Impact-G (CG)	Primary Impact-G Axial	Primary Impact-G Transverse	Primary Impact Energy (lb-in.)	Secondary Impact Crush (in.)	Secondary Impact Force-F (lb)	Secondary Impact-G (CG)	Secondary Impact Energy (lb-in.)
0	11.2	2.56E+06	53.0	0.0	53.0	1.77E+07				
15	8.7	1.15E+06	23.7	6.1	22.9	5.74E+06	13.3	1.34E+06	27.8	1.17E+07
45	14.0	1.37E+06	28.3	20.0	20.0	9.68E+06	12.1	1.32E+06	27.3	1.02E+07
60	13.4	1.70E+06	35.1	30.4	17.5	1.40E+07	9.2	1.16E+06	23.9	6.41E+06
75	13.3	3.07E+06	63.5	61.3	16.4	1.78E+07				
90	7.0	3.36E+06	69.4	69.4	0.0	1.77E+07				

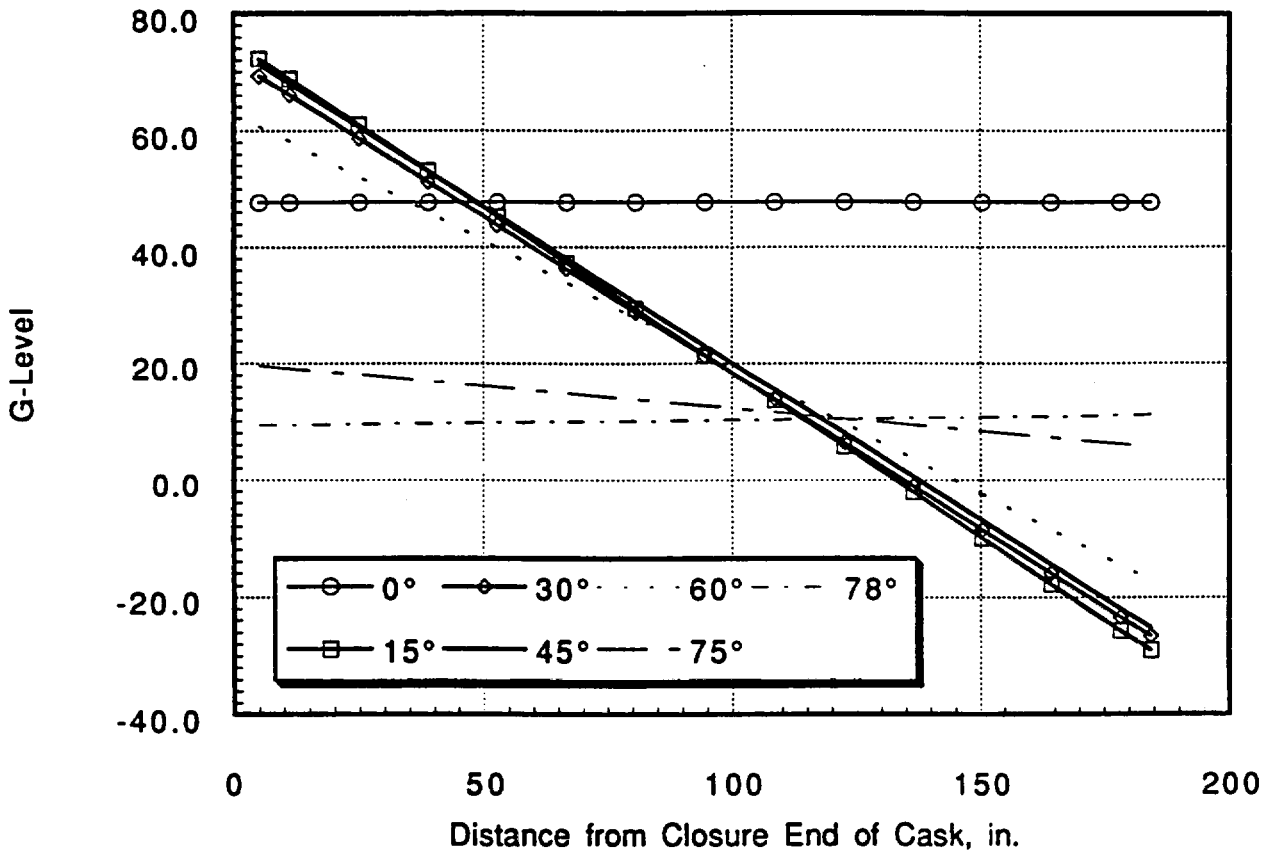

Fig. 2.10.4-6. 30-ft high impact limiter strength, primary impact, transverse g-level

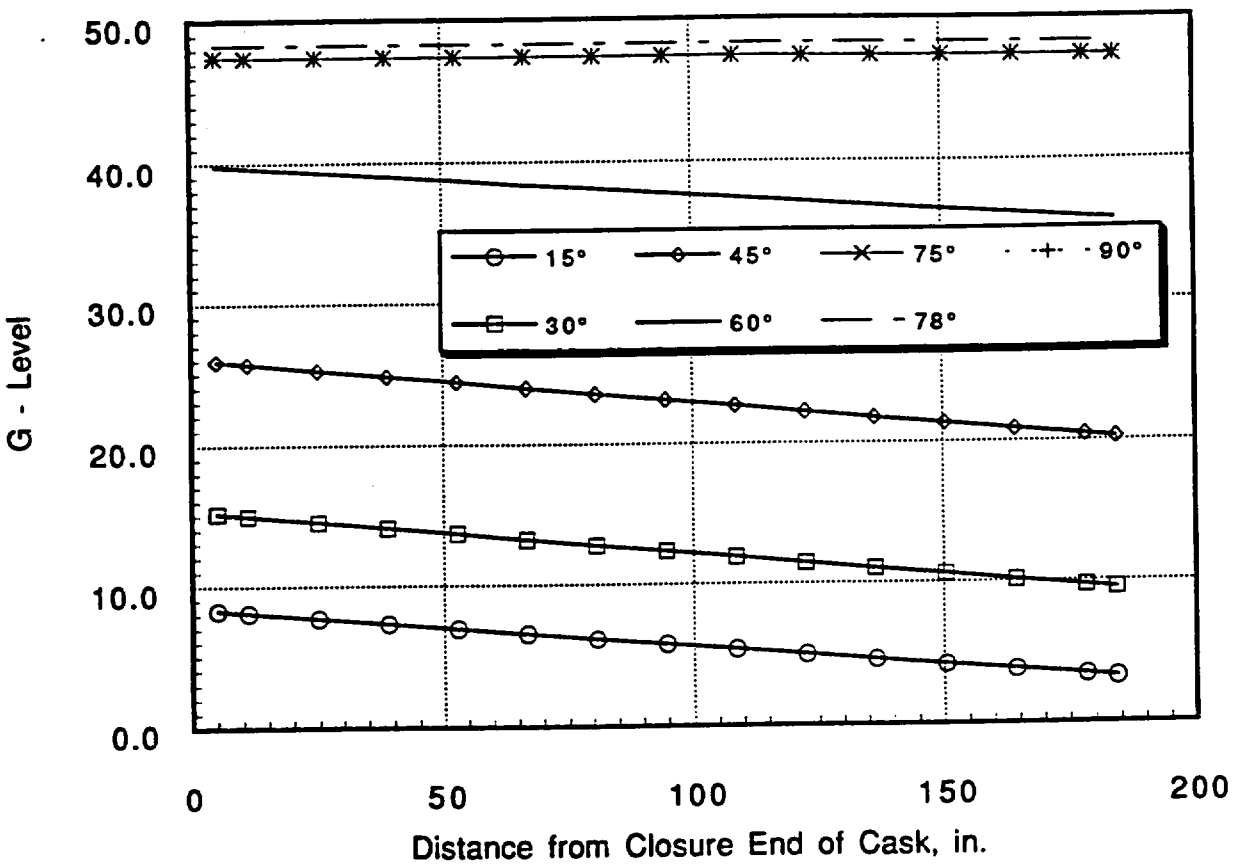

Fig. 2.10.4-7. 30-ft high impact limiter strength, primary impact, axial g-level

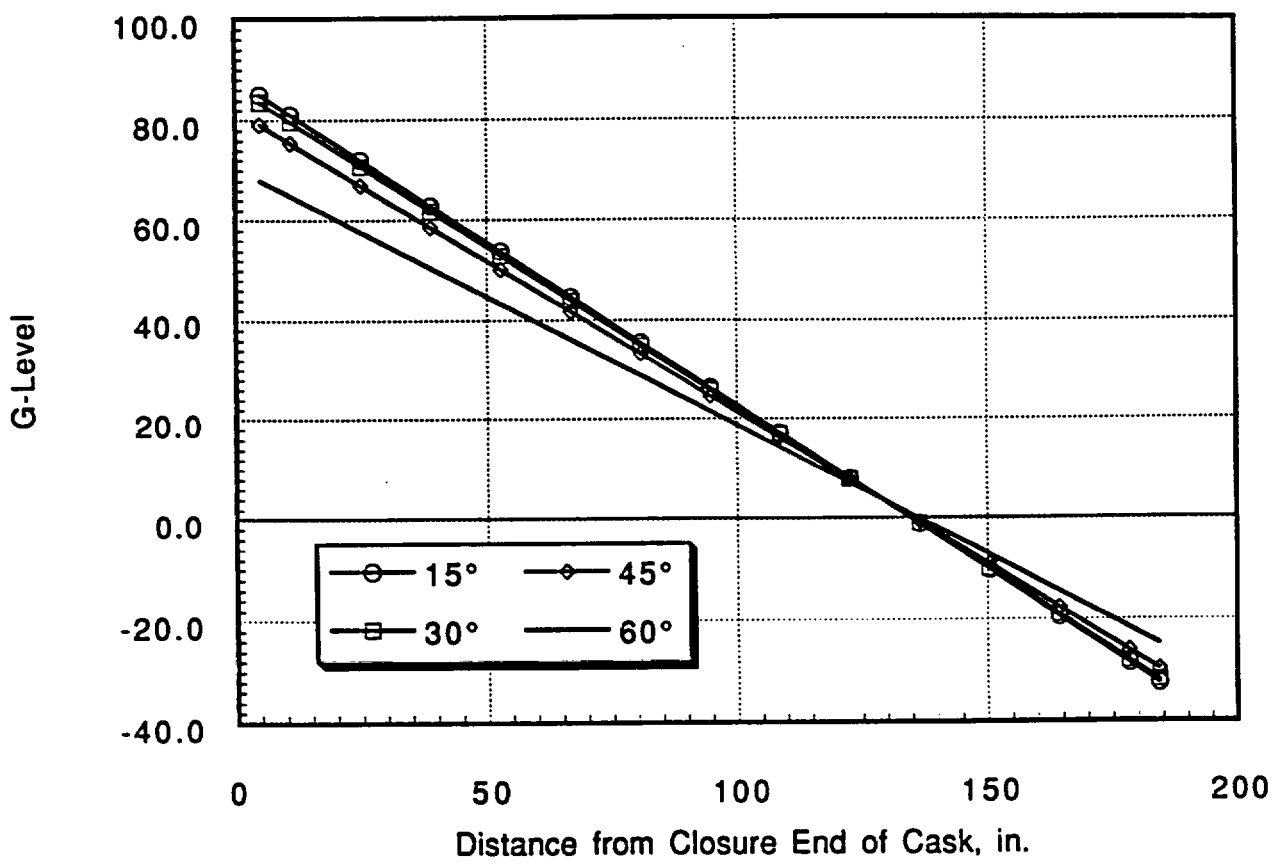

Fig. 2.10.4-8. 30-ft high impact limiter strength, secondary impact, transverse g-level

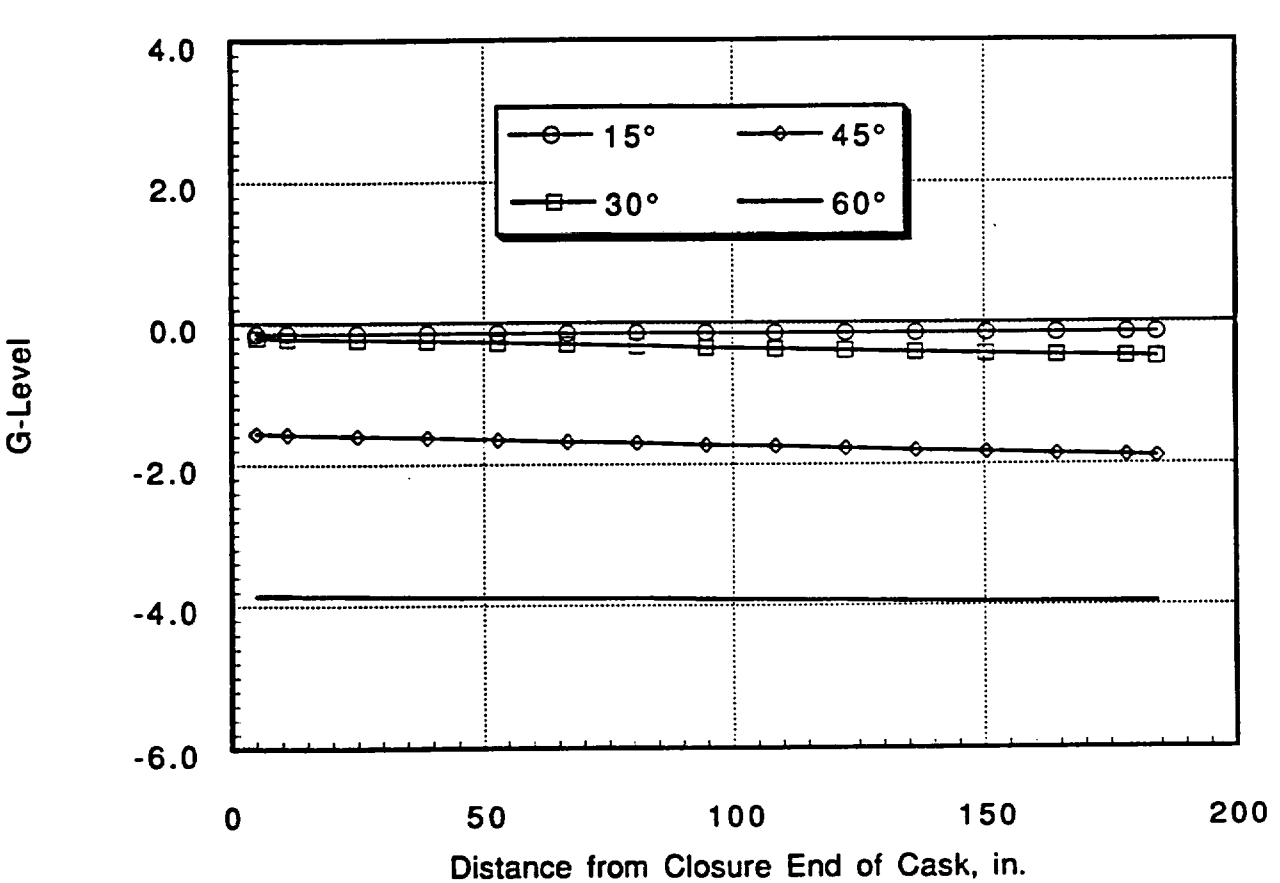

Fig. 2.10.4-9. 30-ft high impact limiter strength, secondary impact, axial g-level

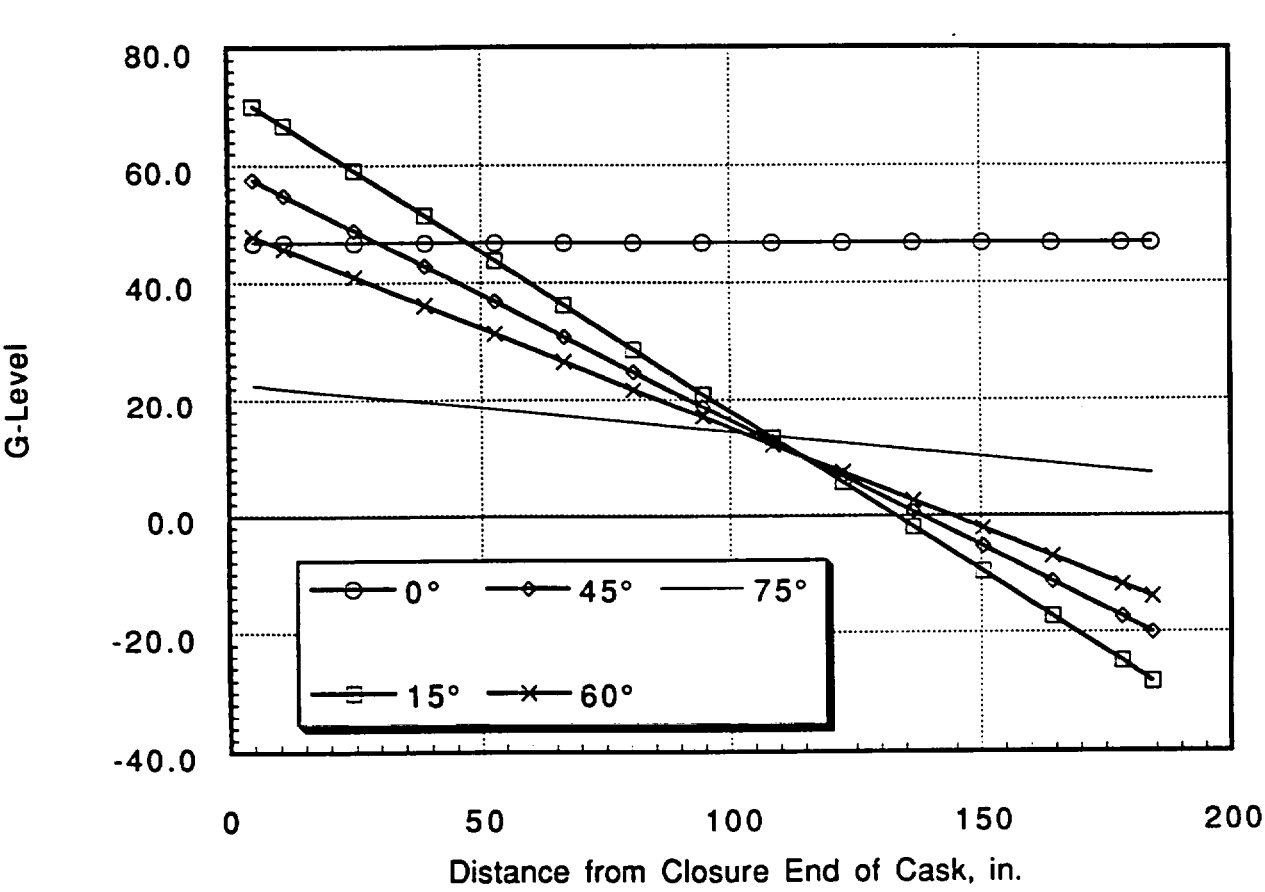

Fig. 2.10.4-10. 30-ft test impact limiter strength, primary impact, transverse g-level

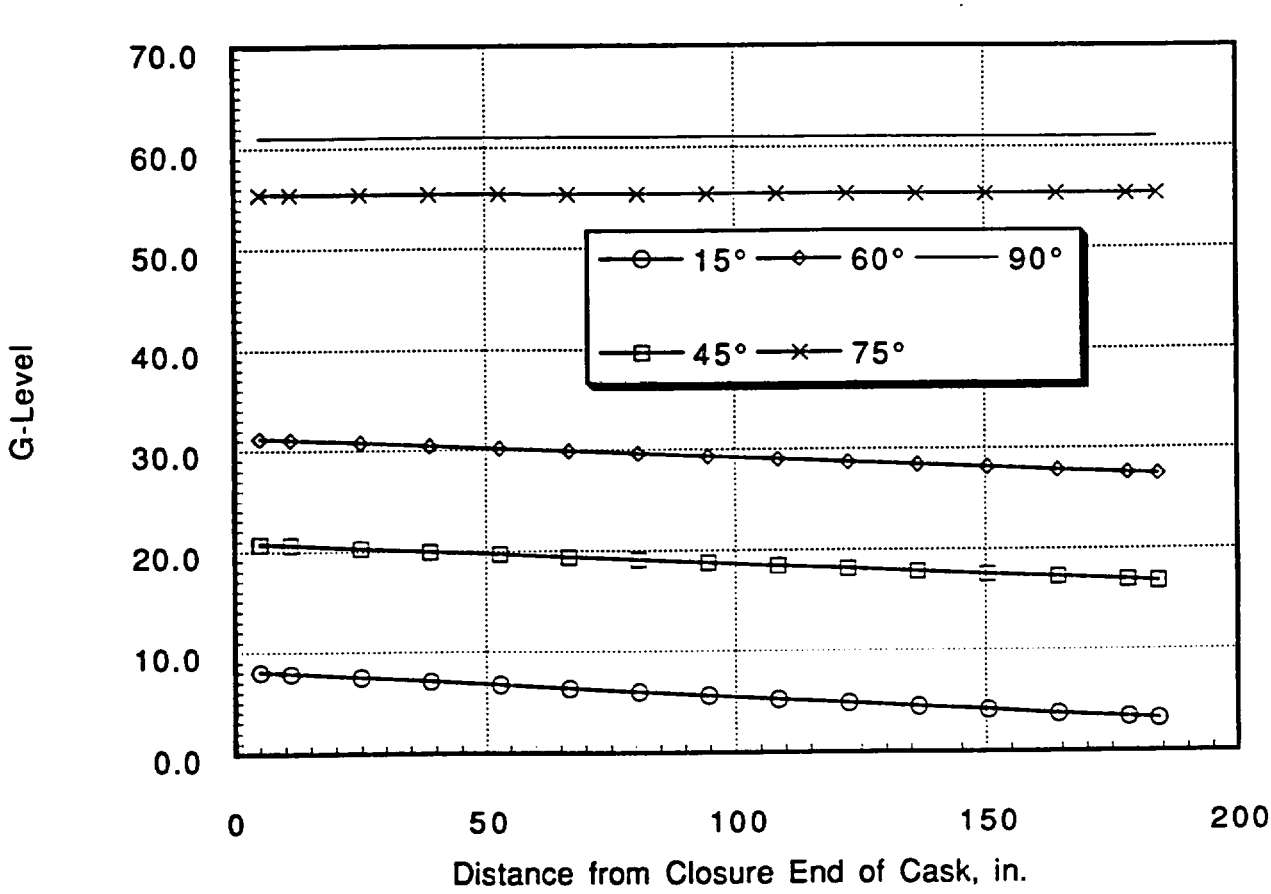

Fig. 2.10.4-11. 30-ft test impact limiter strength, primary impact, axial g-level

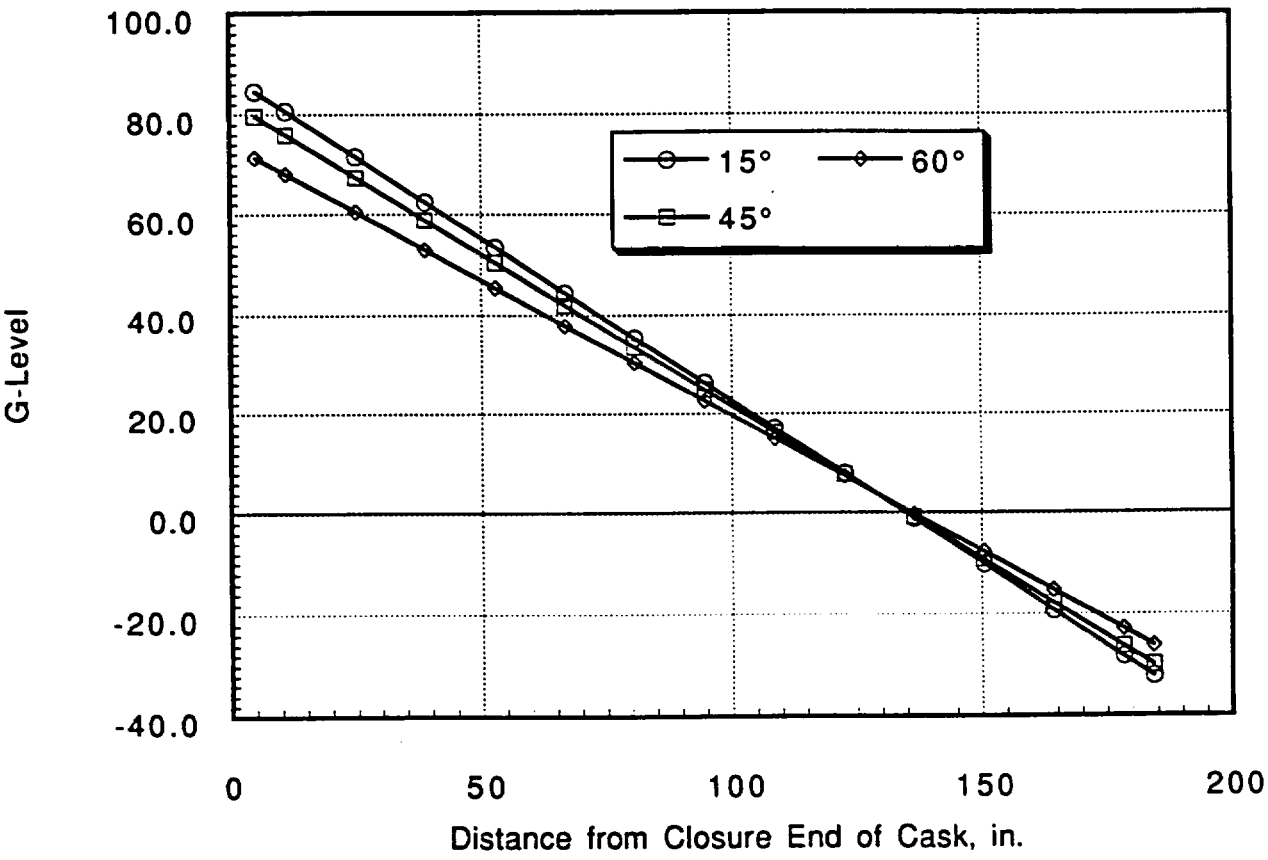

Fig. 2.10.4-12. 30-ft test impact limiter strength, secondary impact, transverse g-level

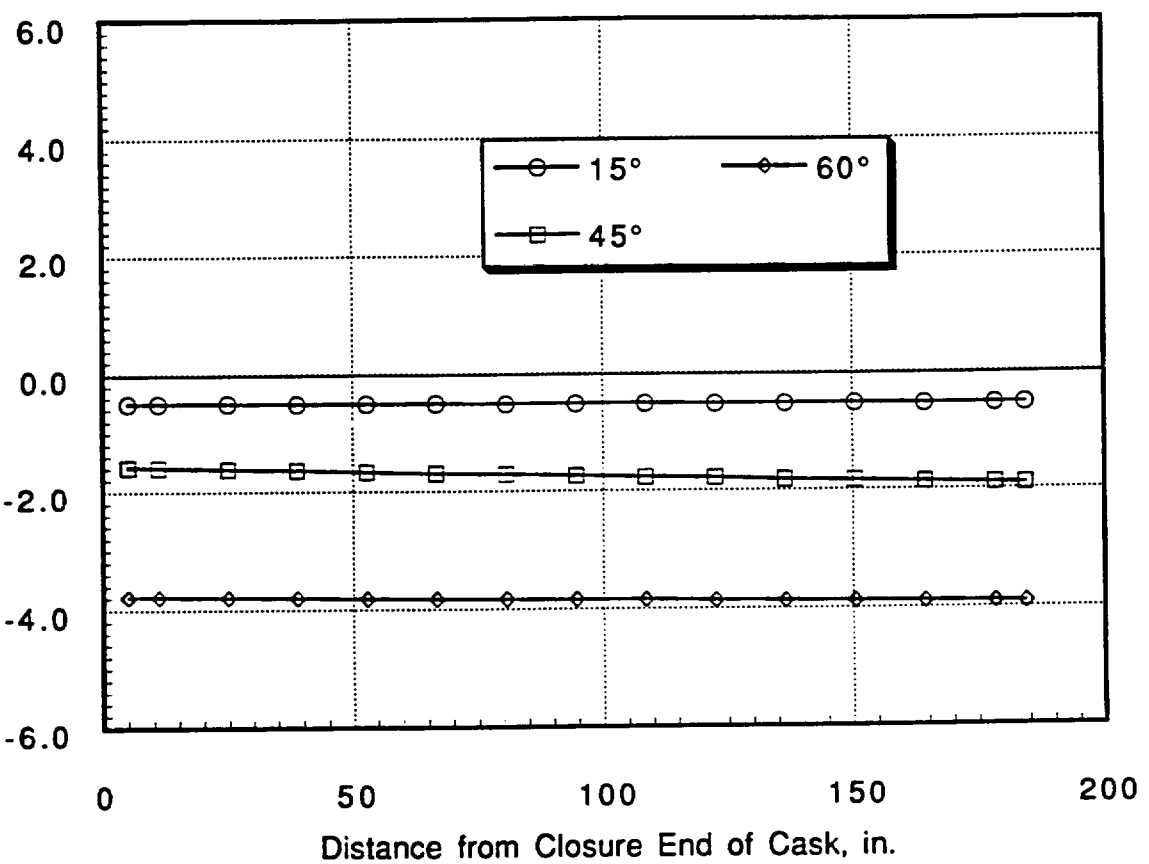

Fig. 2.10.4-13. 30-ft test impact limiter strength, secondary impact, axial g-level

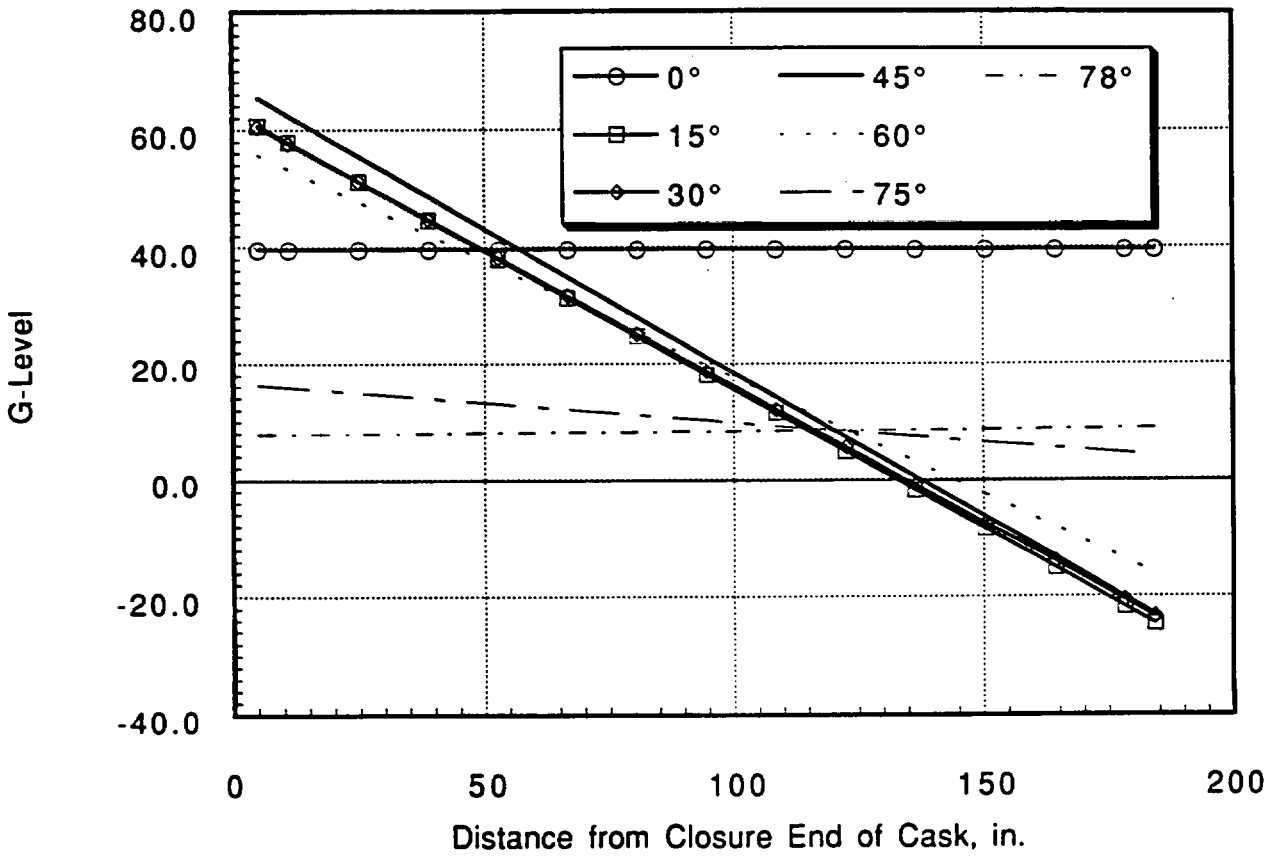

Fig. 2.10.4-14. 30-ft low impact limiter strength, primary impact, transverse g-level

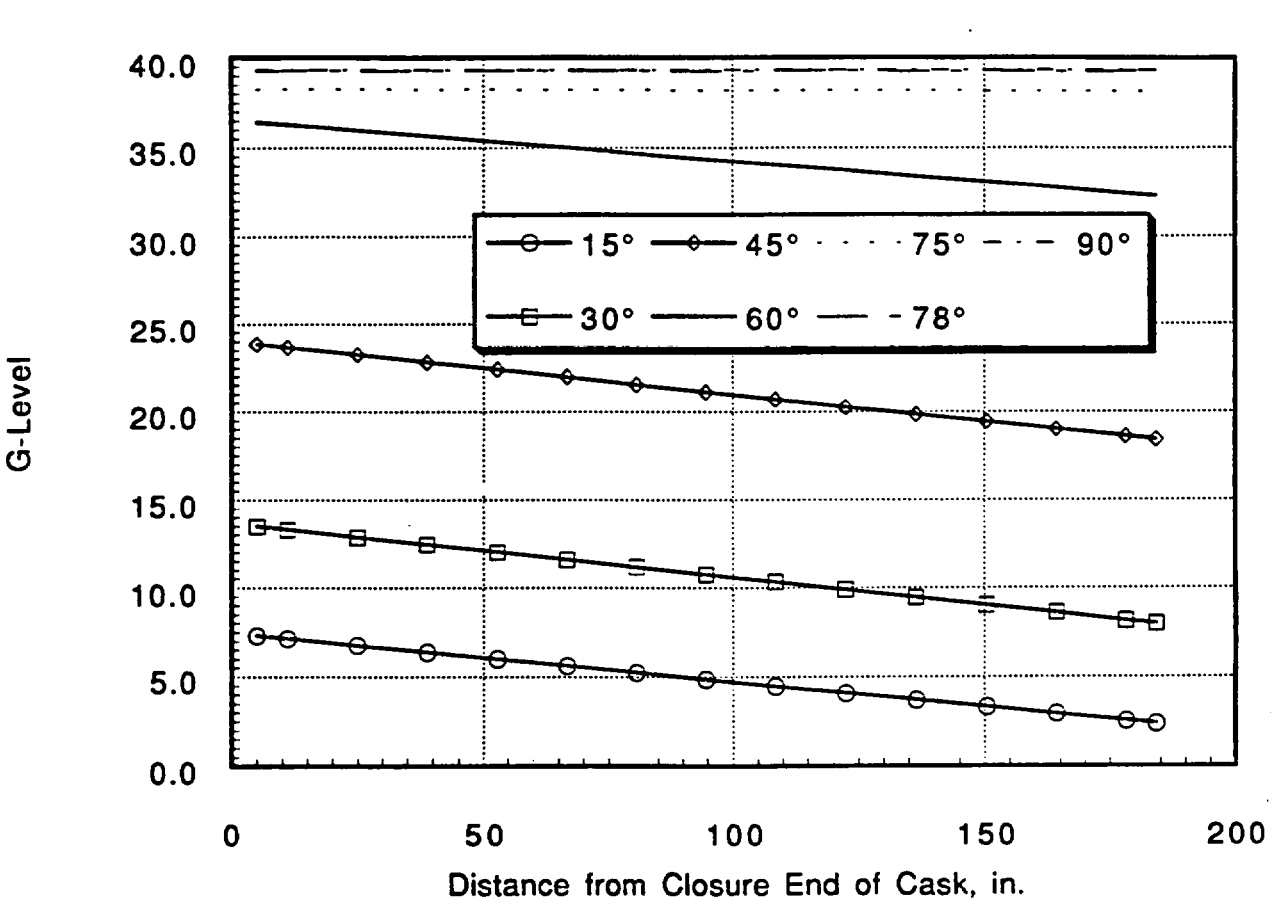

Fig. 2.10.4-15. 30-ft low impact limiter strength, primary impact, axial g-level

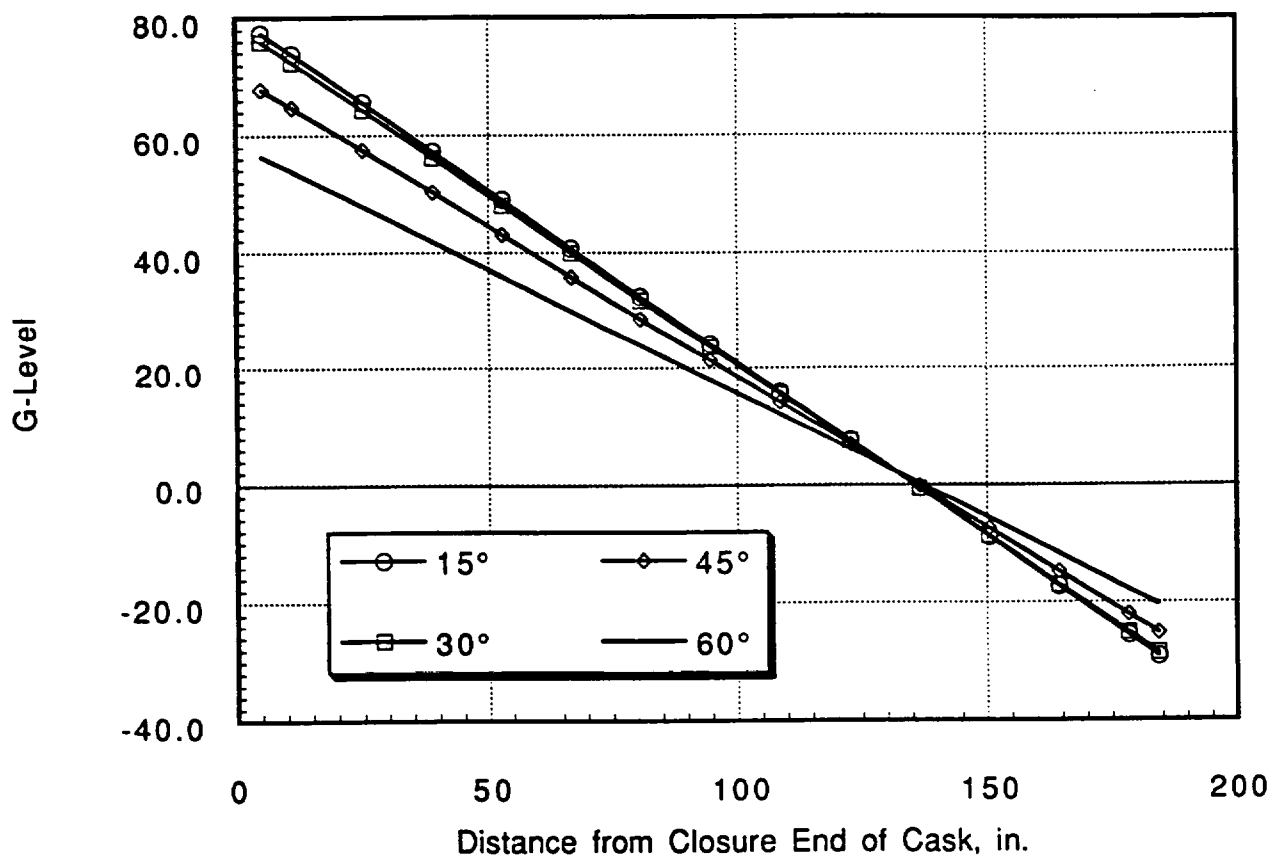

Fig. 2.10.4-16. 30-ft low impact limiter strength, secondary impact, transverse g-level

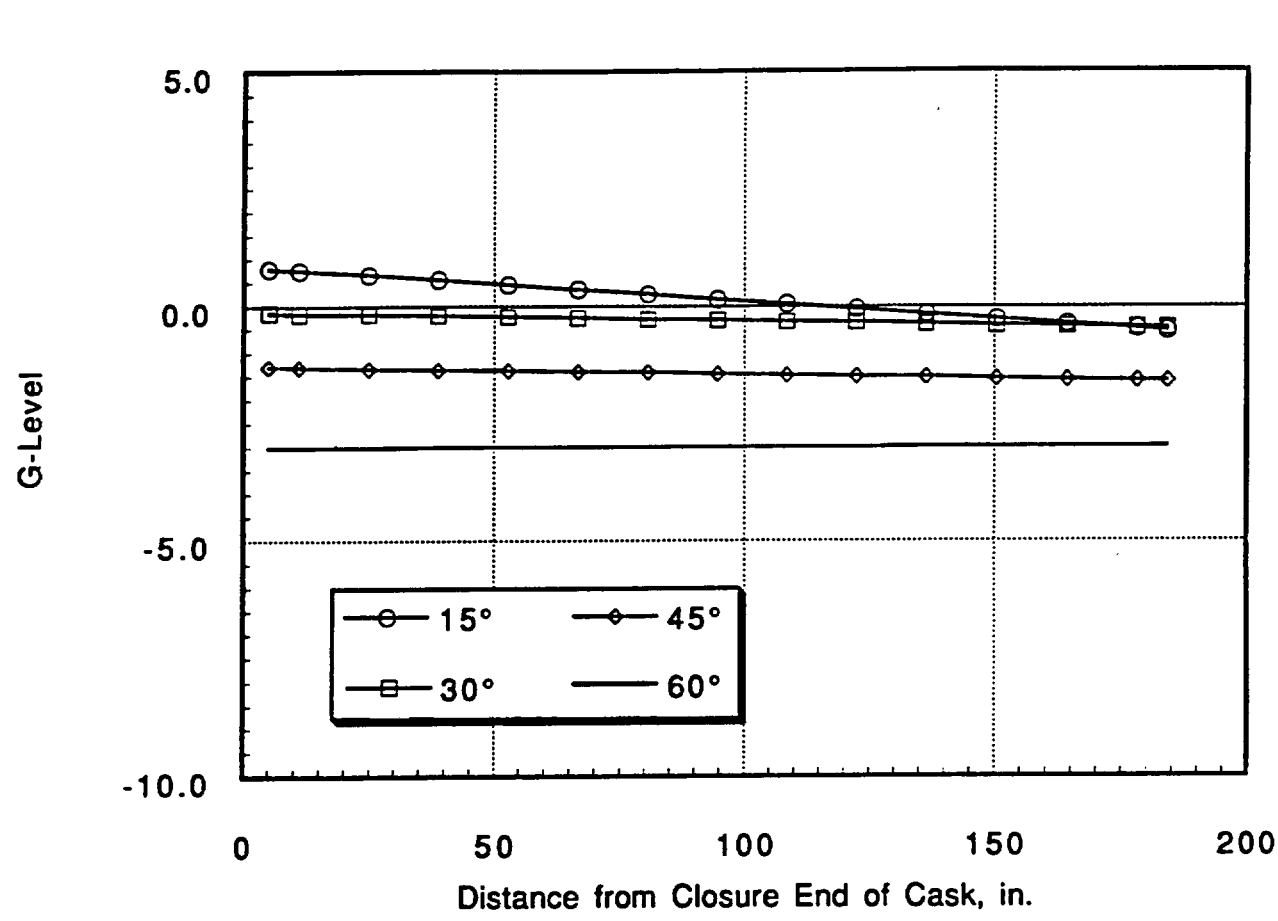

Fig. 2.10.4-17. 30-ft low impact limiter strength, secondary impact, axial g-level

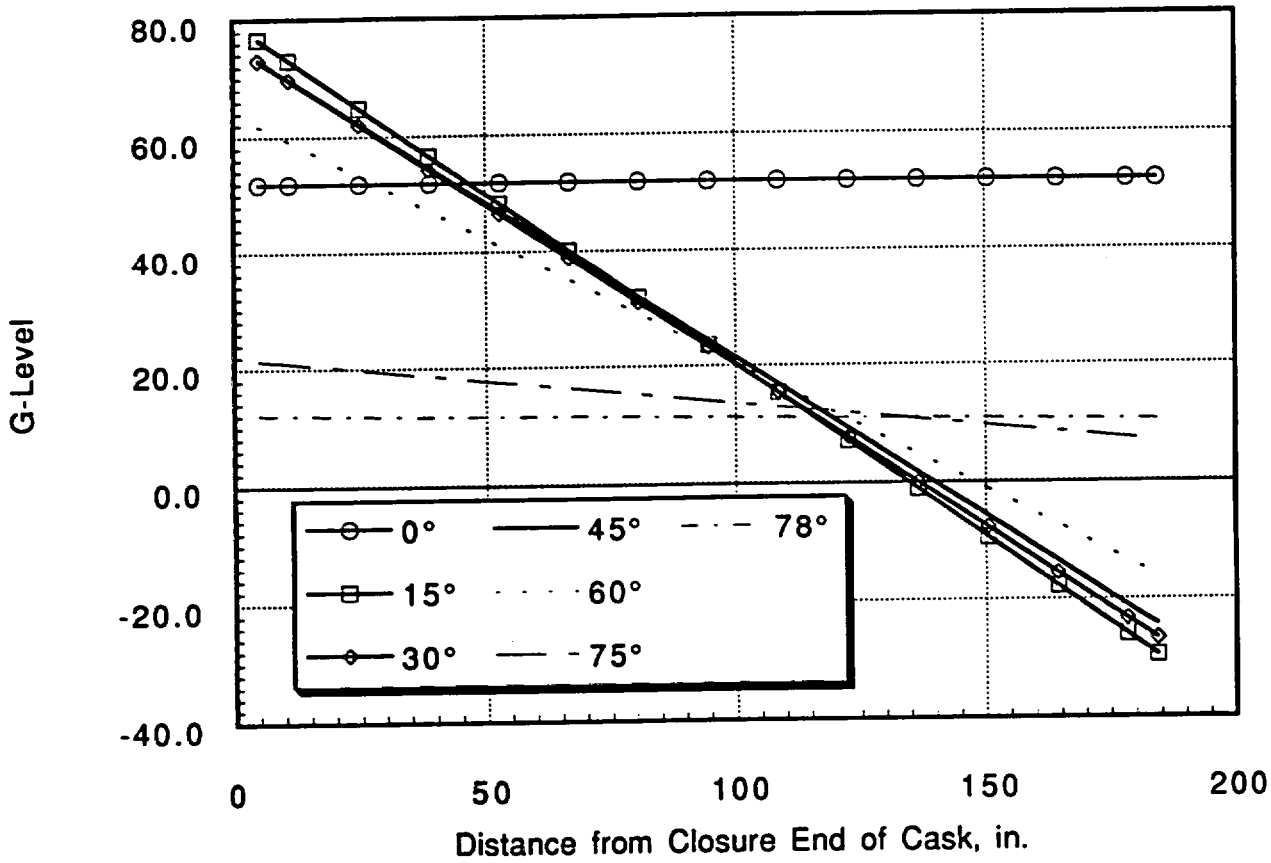

Fig. 2.10.4-18. 30-ft high impact limiter strength and minimum contents weight primary impact, transverse g-level

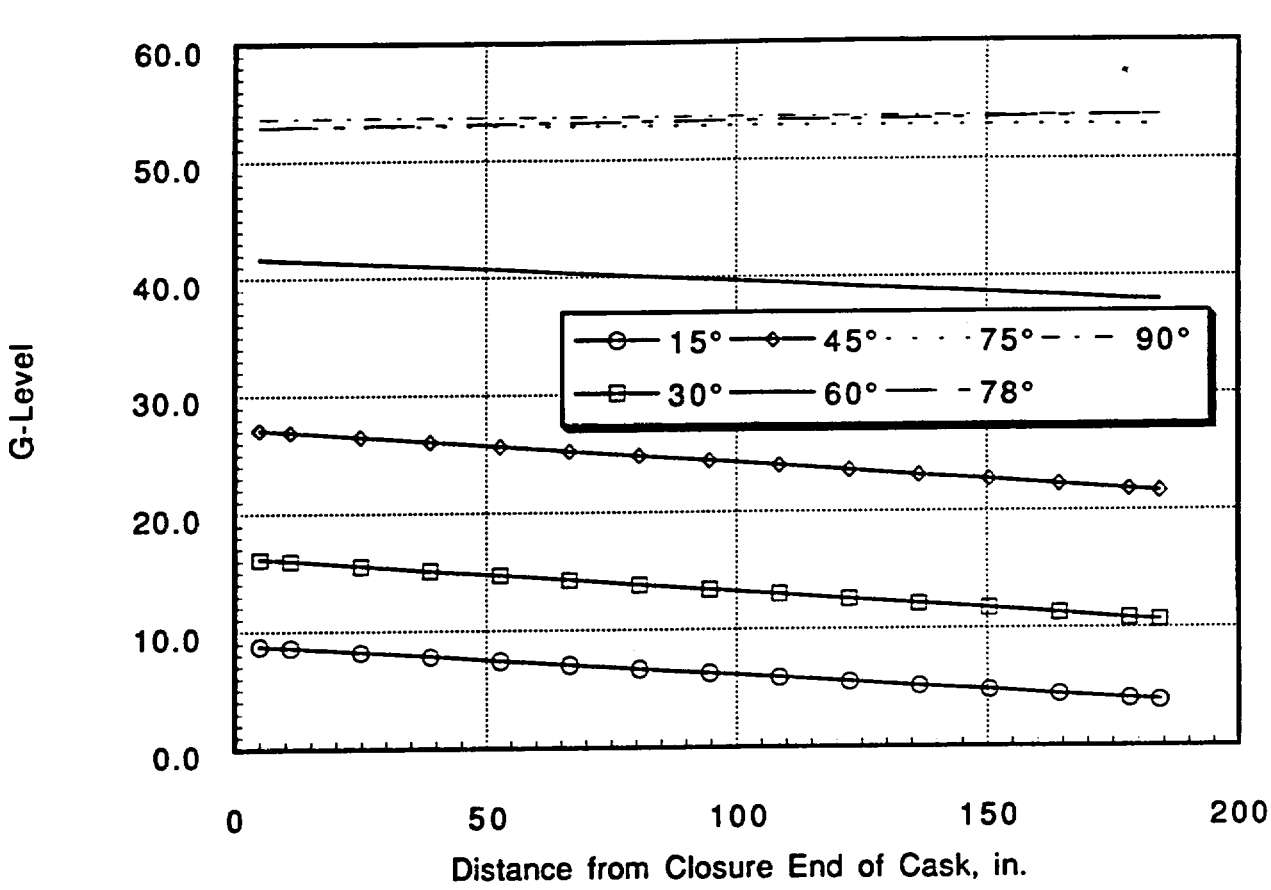

Fig. 2.10.4-19. 30-ft high impact limiter strength and minimum contents weight primary impact, axial g-level

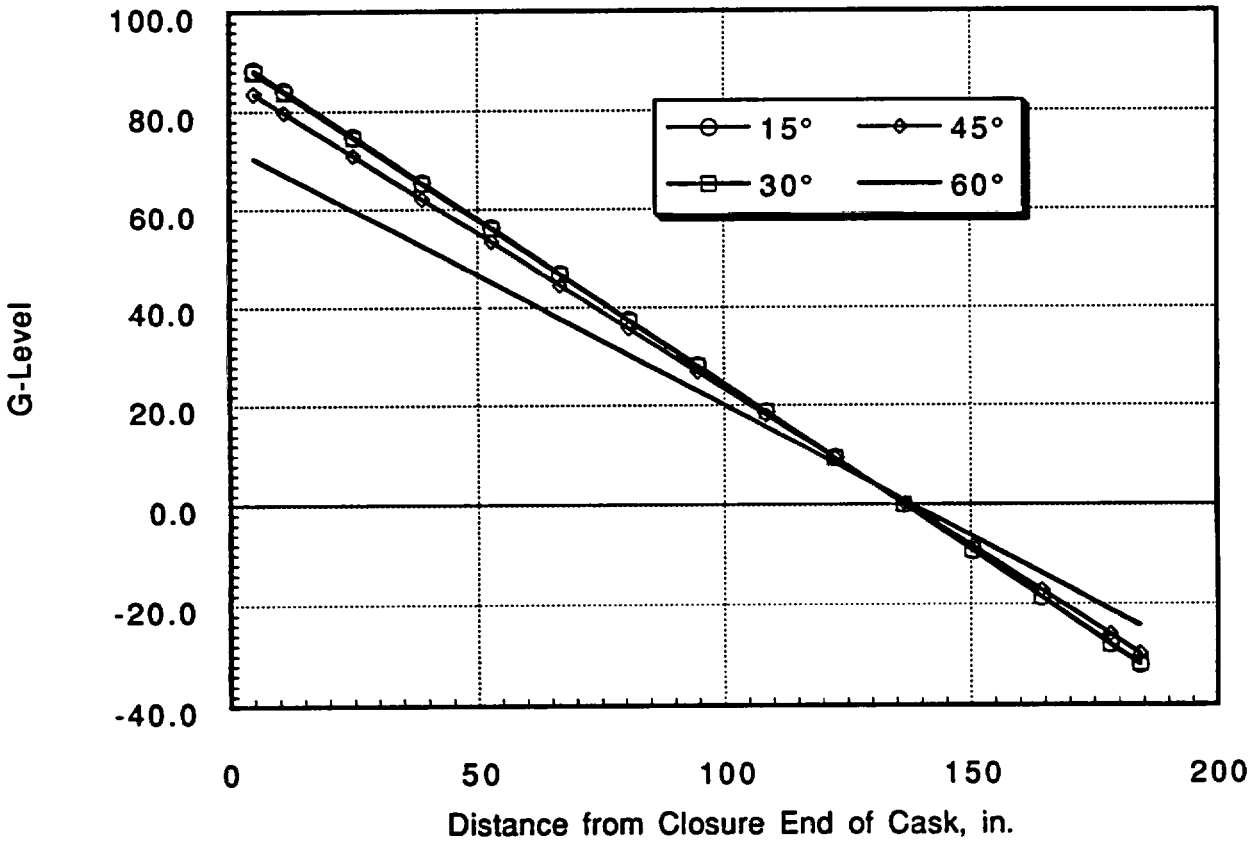

Fig. 2.10.4-20. 30-ft high impact limiter strength and minimum contents weight secondary impact, transverse g-level

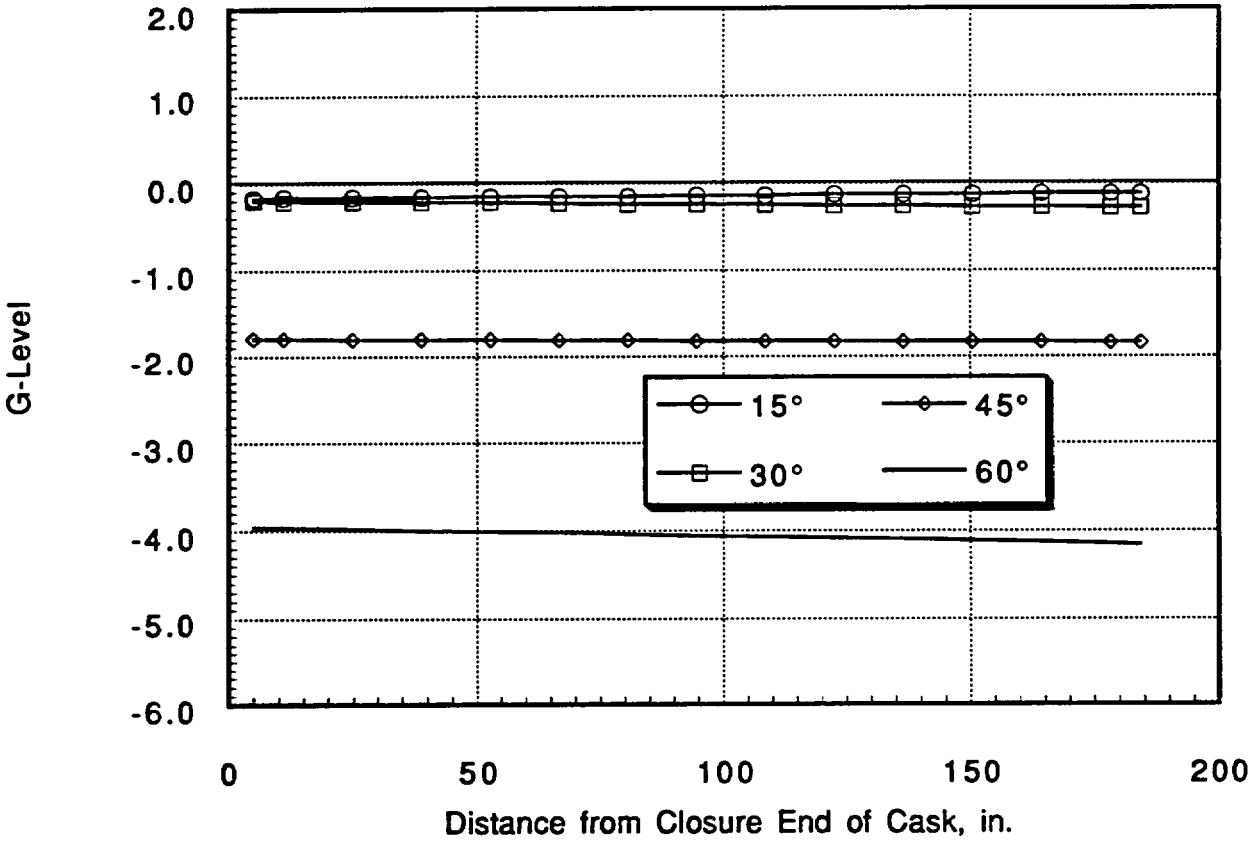

Fig. 2.10.4-21. 30-ft high impact limiter strength and minimum contents weight secondary impact, axial g-level

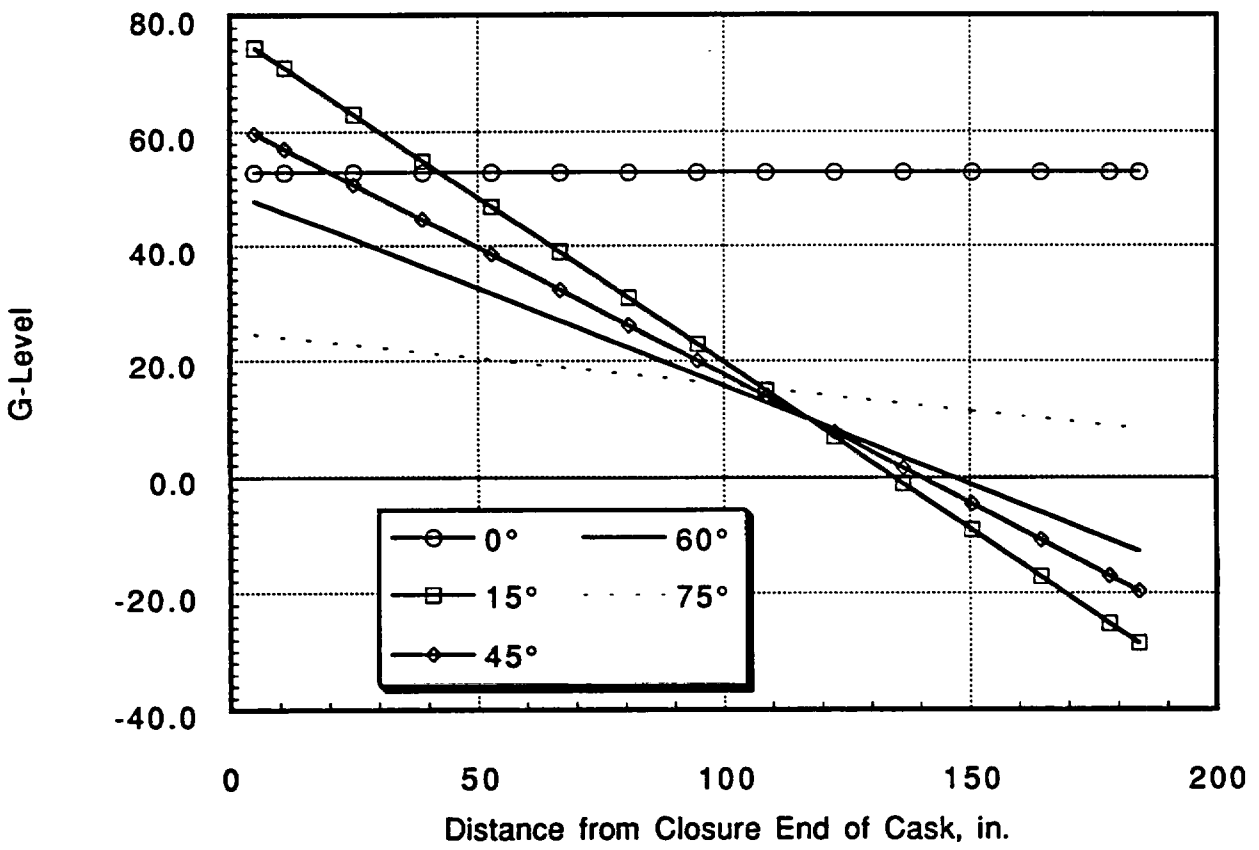

Fig. 2.10.4-22. 30-ft test impact limiter strength, minimum contents weight primary impact, transverse g-level

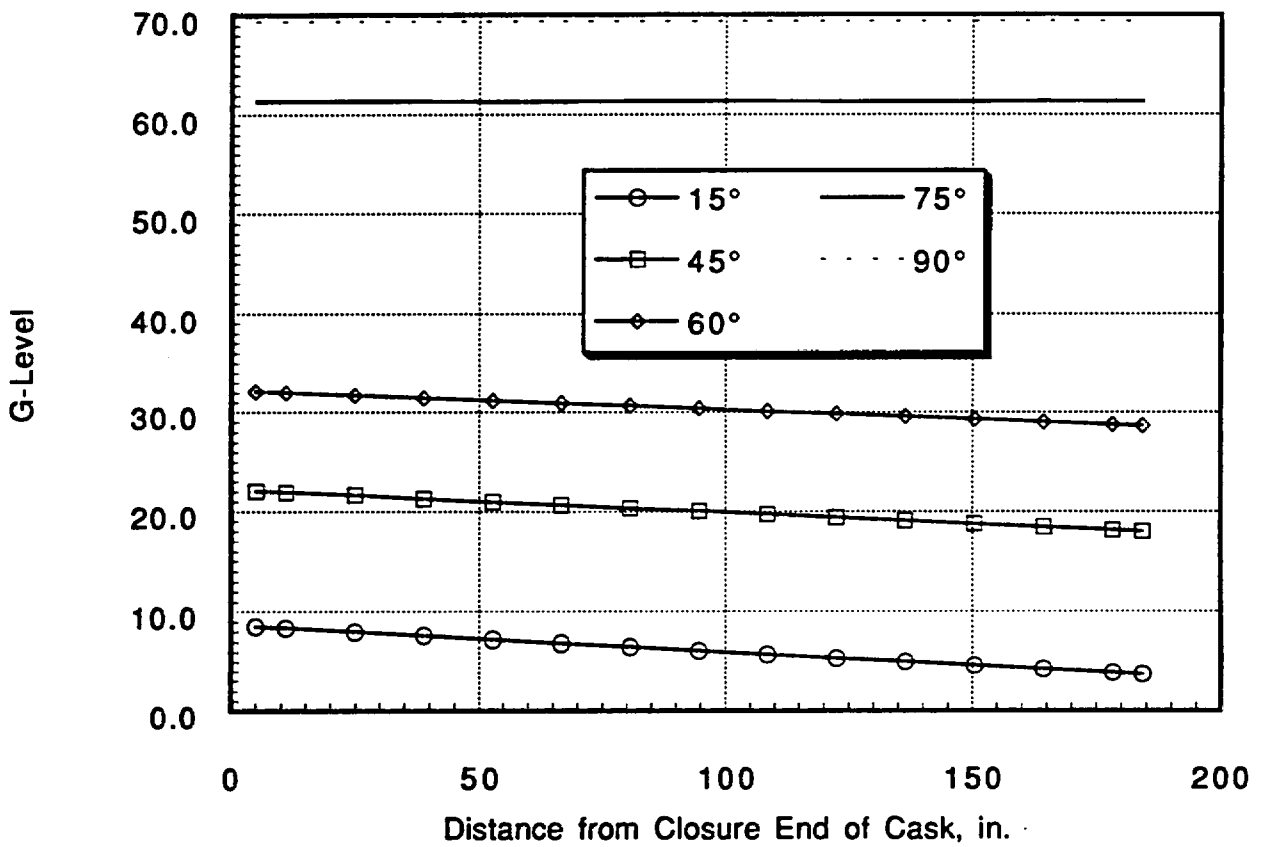

Fig. 2.10.4-23. 30-ft test impact limiter strength, minimum contents weight primary impact, axial g-level

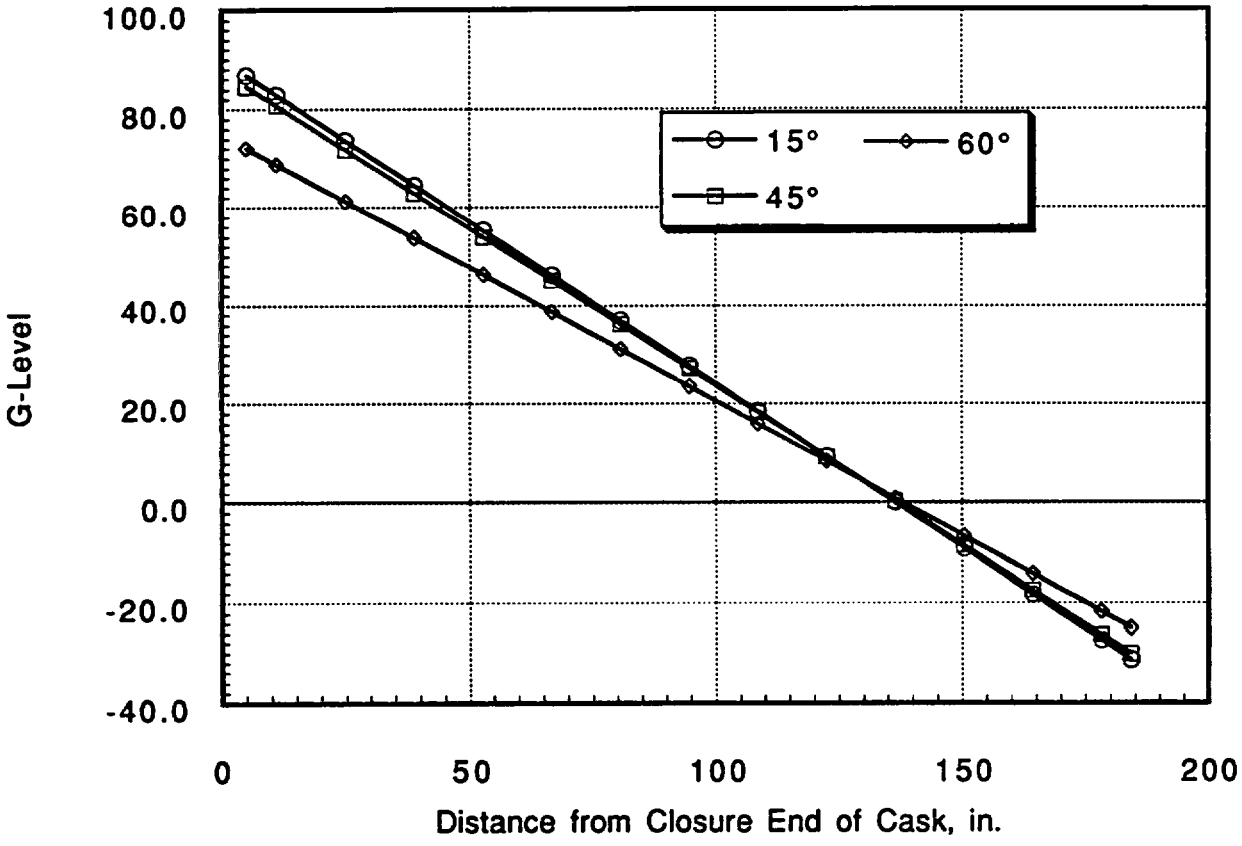

Fig. 2.10.4-24. 30-ft test impact limiter strength, minimum contents weight secondary impact, transverse g-level

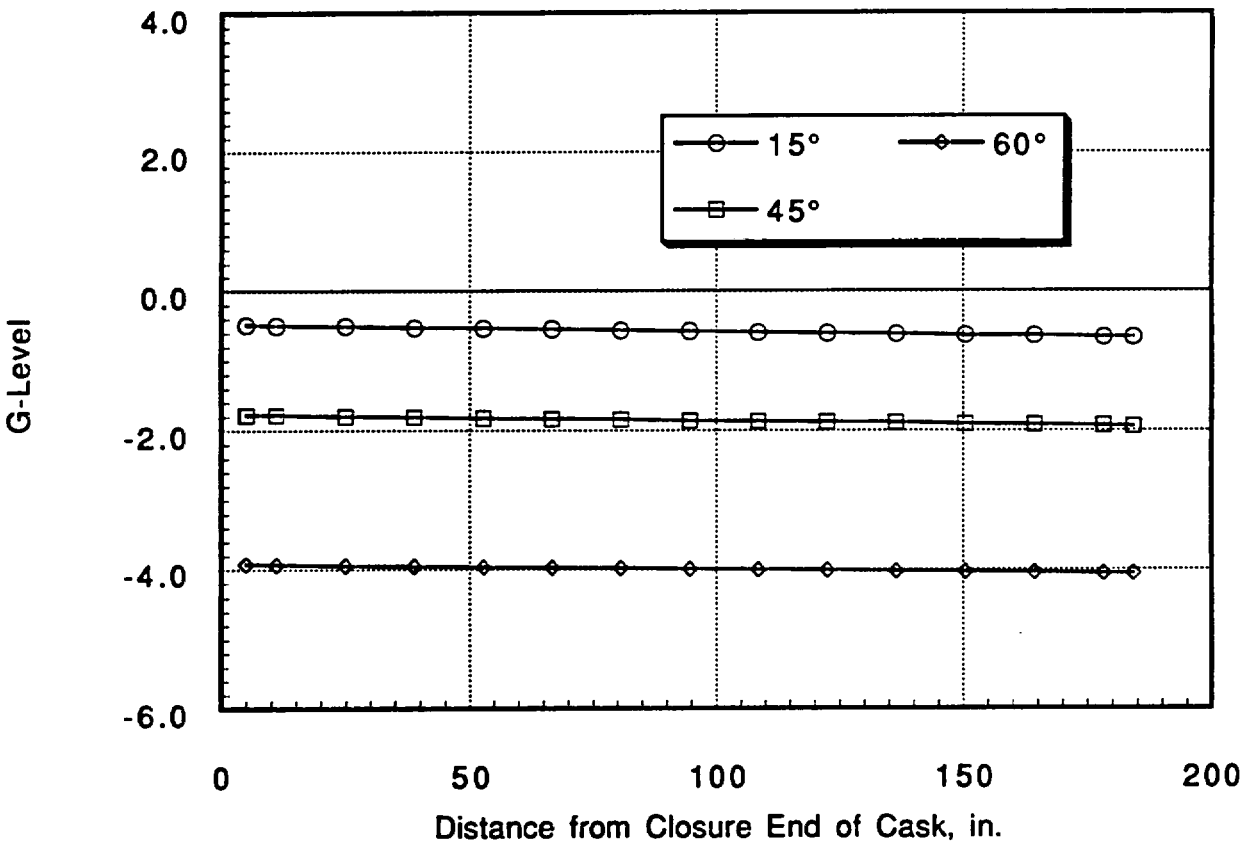

Fig. 2.10.4-25. 30-ft test impact limiter strength, minimum contents weight secondary impact, axial g-level

TABLE 2.10.4-6. CRITICAL G-LEVELS FOR ANALYSIS OF CONTAINMENT BOUNDARY, CLOSURE BOLTS, FSS, CAVITY LINER AND ILSS

Impact Angle (Deg)	1-ft Drop G-Level			30-ft Drop G-Level		
	Transverse G (C.G.)	Axial G (C.G.)	Transverse G-Level along length of cask	Transverse G (C.G.)	Axial G (C.G.)	Transverse G-Level along length of cask
0	15.6 [a]	0	Fig. 2.10.4-26 [a]	47.7 [a]	0 [a]	Fig. 2.10.4-6 [a]
15	7.4 [b]	2.0 [b]	Fig. 2.10.4-28 [b]	21.5 [a]	5.8 [a]	Fig. 2.10.4-6 [a]
30	4.7 [b]	2.7 [b]	Fig. 2.10.4-28 [b]	21.4 [a]	12.3 [a]	Fig. 2.10.4-6 [a]
45	3.7 [b]	3.7 [b]	Fig. 2.10.4-28 [b]	23.1 [a]	23.1 [a]	Fig. 2.10.4-6 [a]
60	6.5 [b]	11.2 [b]	Fig. 2.10.4-28 [b]	21.8 [a]	37.8 [a]	Fig. 2.10.4-6 [a]
75	2.6 [a]	9.9 [a]	Fig. 2.10.4-26 [a]	14.9 [b]	55.4 [b]	Fig. 2.10.4-10 [b]
78				11.9 [d]	56.5 [d]	[d]
90	0	14.9 [a]		0 [b]	61 [b]	
Secondary Impact (0)	N.A.	N.A.	N.A.	26.3 [a,b]	0	Fig. 2.10.4-8 [c]

(a) GACAP results for maximum impact limiter strength and maximum contents weight.
(b) GACAP results for test data impact limiter strength and maximum contents weight.
(c) GACAP secondary impact, maximum impact limiter strength and maximum contents weight 15° drop.
(d) G-levels interpolated between 75° and 90° drops for test impact limiter strength and maximum contents weight.

Table 2.10.4-7 CRITICAL G-LEVELS FOR ANALYSIS OF NEUTRON SHIELD

Drop Angle (Deg)	1-ft Drop G-Level			30-ft Drop G-Level		
	Transverse G (C.G.)	Axial G (C.G.)	Transverse G-Level along length of cask	Transverse G (C.G.)	Axial G (C.G.)	Transverse G-Level along length of cask
0	16.6 [b]	0.0	Fig. 2.10.4-30 [b]	53 [c]	0 [c]	Fig. 2.10.4-22 [c]
15	8.2 [c]	2.2 [c]	Fig. 2.10.4-32 [c]	23.6 [b]	6.3 [b]	Fig. 2.10.4-18 [b]
30	5.4 [c]	3.1 [c]	Fig. 2.10.4-32 [c]	23.2 [b]	13.4 [b]	Fig. 2.10.4-18 [b]
45	4.1 [c]	4.1 [c]	Fig. 2.10.4-32 [c]	24.4 [b]	24.4 [b]	Fig. 2.10.4-18 [b]
60	6.9 [c]	11.9 [c]	Fig. 2.10.4-32 [c]	23 [b]	39.8 [b]	Fig. 2.10.4-18 [b]
75	2.7 [b]	10.1 [b]	Fig. 2.10.4-30 [b]	16.4 [c]	61.3 [c]	Fig. 2.10.4-22 [c]
78	2.2 [a]	11.4 [a]	[a]	13.1 [a]	62.9 [a]	[a]
90	0.0	16.8 [b]		0 [c]	69.4 [c]	
Secondary Impact (0)	N.A.	N.A.	N.A.	28.2 [b]	0	Fig. 2.10.4-20 [b]

(a) G-levels interpolated between 75° and 90° drops.
(b) GACAP results for maximum impact limiter strength and minimum contents weight.
(c) GACAP results for test impact limiter strength and minimum contents weight.

Tables 2.10.4-8 through 2.10.4-10 show the margins against the impact limiters bottoming out for all drop orientations and impact limiter material strengths. The minimum margin is 2.7 in. for the 60° 30-ft drop initial impact. The tables also show that the minimum margin against the trunnions impacting the unyielding surface is 7.1 in.

2.10.4.2 1-ft GACAP Analysis. We evaluated the GA-4 cask for normal condition 1-ft free drops. We ran GACAP cases every 15° from 0° (side drop) to 90° (end drop). To cover all cases, we used the ILMOD-generated maximum impact limiter crush strength data described in Section 2.10.3.3 and the 1/4-scale test results (Section 2.10.3.4) scaled to full size and multiplied by the strain rate effect factor of 1.1. The minimum impact limiter crush strength data are not presented here because this case will not produce higher loadings on the cask than the previously discussed cases. The maximum and minimum content weights were also investigated.

The same method and models discussed in Section 2.10.4.1 for the 30-ft drop analysis were used for the 1-ft drop, except that only the primary impact was investigated for the normal condition 1-ft drops.

Tables 2.10.4-11 through 2.10.4-14 summarize the results for the bounding impact limiter strengths and for maximum and minimum contents weight. The acceleration that would result in the maximum stress for each component of the cask was used for analysis and is summarized in Tables 2.10.4-6 and 2.10.4-7. The rationale for these accelerations is the same as for the 30-ft drop analysis described in Section 2.10.4.1.3.

Figures 2.10.4-26 through 2.10.4-33 show the accelerations along the length of the cask.

TABLE 2.10.4-8 GA-4 30-FT DROP - MARGINS AGAINST BOTTOMING OUT AND HITTING TRUNNION - HIGH IMPACT LIMITER CRUSH STRENGTH

	Primary Impact				Secondary Impact			
Drop Angle (Deg)	Crush (in.)	Bottoming out Crush (in.)[a]	Margin Against Bottoming Out, (in.)	Margin, (in.) Against Hitting Trunnion	Crush (in.)[b]	Bottoming Out Crush (in.)[a][b]	Margin Against Bottoming Out, (in.)	Margin, (in.) Against Hitting Trunnion
0	11.9	20.0	8.1	12.4				
15	11.8	21.0	9.2	N.A.	14.7	20.0	5.3	9.6
30	14.7	22.0	7.3	N.A.	14.5	20.0	5.5	9.8
45	16.5	23.0	6.5	N.A.	13.4	20.0	6.6	10.9
60	18.5	23.0	4.5	N.A.	11.4	20.0	8.6	12.9
75	15.5	21.0	5.5	N.A.				
78	14.2	21.0	6.8	N.A.				
90	9.2	17.0	7.8	N.A.				

(a) Bottoming out crush from Table 2.10.3-2 (1/4 scale crush multiplied by 4 to obtain full-scale).

(b) Secondary impact cask axis angle with impact surface is low.

TABLE 2.10.4-9 GA-4 30-FT DROP - MARGINS AGAINST BOTTOMING OUT AND HITTING TRUNNION - TEST DATA IMPACT LIMITER CRUSH STRENGTH

	Primary Impact				Secondary Impact			
Drop Angle (Deg)	Crush (in.)	Bottoming out Crush (in.)[a]	Margin Against Bottoming Out, (in.)	Margin, (in.) Against Hitting Trunnion	Crush (in.)[b]	Bottoming Out Crush (in.)[a][b]	Margin Against Bottoming Out, (in.)	Margin, (in.) Against Hitting Trunnion
0	12.1	20.0	7.9	12.2				
15	9.2	21.0	11.8	N.A.	14.5	20.0	5.5	9.8
45	14.6	23.0	8.4	N.A.	13.2	23.0	9.8	11.1
60	14.3	23.0	8.7	N.A.	10.1	23.0	12.9	14.2
75	14.1	21.0	6.9	N.A.				
90	7.9	17.0	9.1	N.A.				

(a) Bottoming out crush from Table 2.10.3-2 (1/4 scale crush multiplied by 4 to obtain full-scale).
(b) Secondary impact cask axis angle with impact surface is low.

TABLE 2.10.4-10 GA-4 30-FT DROP - MARGINS AGAINST BOTTOMING OUT AND HITTING TRUNNION - LOW IMPACT LIMITER CRUSH STRENGTH

	Primary Impact				Secondary Impact			
Drop Angle (Deg)	Crush (in.)	Bottoming out Crush (in.)[a]	Margin Against Bottoming Out, (in.)	Margin, (in.) Against Hitting Trunnion	Crush (in.)[b]	Bottoming Out Crush (in.)[a][b]	Margin Against Bottoming Out, (in.)	Margin, (in.) Against Hitting Trunnion
0	14.2	20.0	5.8	10.1				
15	13.3	21.0	7.7	N.A.	17.2	20.0	2.8	7.1
30	16.3	22.0	5.7	N.A.	16.9	20.0	3.1	7.4
45	18.1	23.0	4.9	N.A.	15.7	20.0	4.3	8.6
60	20.3	23.0	2.7	N.A.	12.8	20.0	7.2	11.5
75	17.6	21.0	3.4	N.A.				
78	16.4	21.0	4.6	N.A.				
90	11.5	17.0	5.5	N.A.				

(a) Bottoming out crush from Table 2.10.3-2 (1/4 scale crush multiplied by 4 to obtain full-scale).
(b) Secondary impact cask axis angle with impact surface is low.

TABLE 2.10.4-11 GA-4 1-FT DROP RESULTS FOR HIGH IMPACT LIMITER STRENGTH AND MAXIMUM WEIGHT CONTENTS

Drop Angle (Deg)	Primary Impact Crush (in.)	Primary Impact Force-F (lb)	Primary Impact-G (CG)	Primary Impact-G Axial	Primary Impact-G Transverse	Primary Impact Energy (lb-in.)
0	1.7	8.57E+05	15.6	0.0	15.6	7.20E+05
15	3.7	2.16E+05	3.9	1.0	3.8	2.72E+05
30	4.2	2.02E+05	3.7	1.8	3.2	3.53E+05
45	3.6	2.40E+05	4.4	3.1	3.1	4.72E+05
60	6.3	3.22E+05	5.9	5.1	2.9	7.89E+05
75	5.2	5.61E+05	10.2	9.9	2.6	9.32E+05
90	0.9	8.17E+05	14.9	14.9	0.0	7.07E+05

TABLE 2.10.4-12 GA-4 1-FT DROP RESULTS FOR TEST IMPACT LIMITER STRENGTH AND MAXIMUM WEIGHT CONTENTS

Drop Angle (Deg)	Primary Impact Crush (in.)	Primary Impact Force-F (lb)	Primary Impact-G (CG)	Primary Impact-G Axial	Primary Impact-G Transverse	Primary Impact Energy (lb-in.)
0	1.5	7.74E+05	14.1	0.0	14.1	7.16E+05
15	1.0	4.22E+05	7.7	2.0	7.4	2.22E+05
30	2.2	2.98E+05	5.4	2.7	4.7	3.10E+05
45	3.0	2.90E+05	5.3	3.7	3.7	4.53E+05
60	3.1	7.14E+05	13.0	11.2	6.5	6.51E+05
75	3.8	4.56E+05	8.3	8.0	2.1	8.60E+05

TABLE 2.10.4-13 GA-4 1-FT DROP RESULTS FOR HIGH IMPACT LIMITER STRENGTH AND MINIMUM WEIGHT CONTENTS

Drop Angle (Deg)	Primary Impact Crush (in.)	Primary Impact Force-F (lb)	Primary Impact-G (CG)	Primary Impact-G Axial	Primary Impact-G Transverse	Primary Impact Energy (lb-in.)
0	1.6	8.01E+05	16.6	0.0	16.6	6.29E+05
15	3.5	2.01E+05	4.2	1.1	4.0	2.44E+05
30	3.9	1.89E+05	3.9	2.0	3.4	3.15E+05
45	3.4	2.27E+05	4.7	3.3	3.3	4.16E+05
60	6.0	2.86E+05	5.9	5.1	3.0	6.88E+05
75	4.9	5.06E+05	10.5	10.1	2.7	8.09E+05
90	0.8	8.11E+05	16.8	16.8	0.0	6.12E+05

TABLE 2.10.4-14 GA-4 1-FT DROP RESULTS FOR TEST IMPACT LIMITER STRENGTH AND MINIMUM WEIGHT CONTENTS

Drop Angle (Deg)	Primary Impact Crush (in.)	Primary Impact Force-F (lb)	Primary Impact-G (CG)	Primary Impact-G Axial	Primary Impact-G Transverse	Primary Impact Energy (lb-in.)
0	1.3	7.67E+05	15.9	0.0	15.9	6.27E+05
15	1.0	4.11E+05	8.5	2.2	8.2	2.00E+05
30	2.0	2.99E+05	6.2	3.1	5.4	2.77E+05
45	2.8	2.79E+05	5.8	4.1	4.1	4.01E+05
60	3.0	6.66E+05	13.8	11.9	6.9	5.74E+05
75	3.4	4.56E+05	9.4	9.1	2.4	7.36E+05

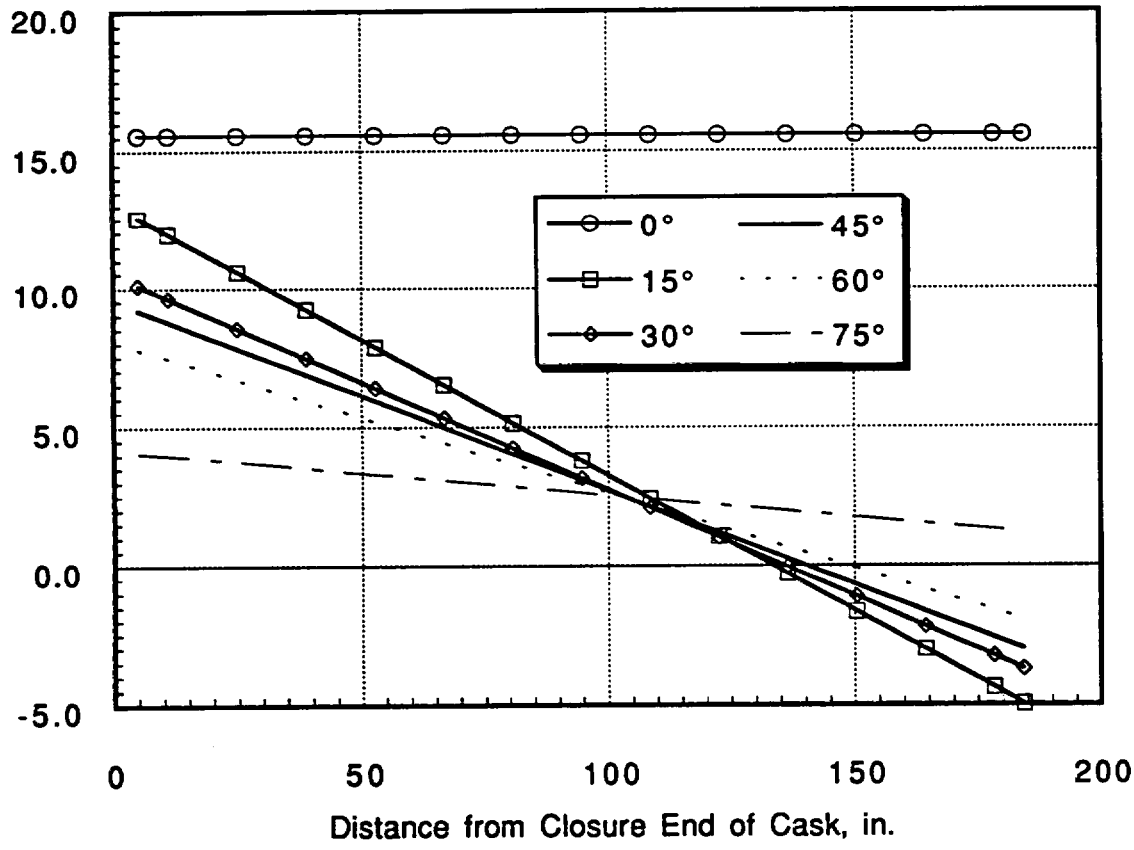

Fig. 2.10.4-26. 1-ft high impact limiter strength, transverse g-level

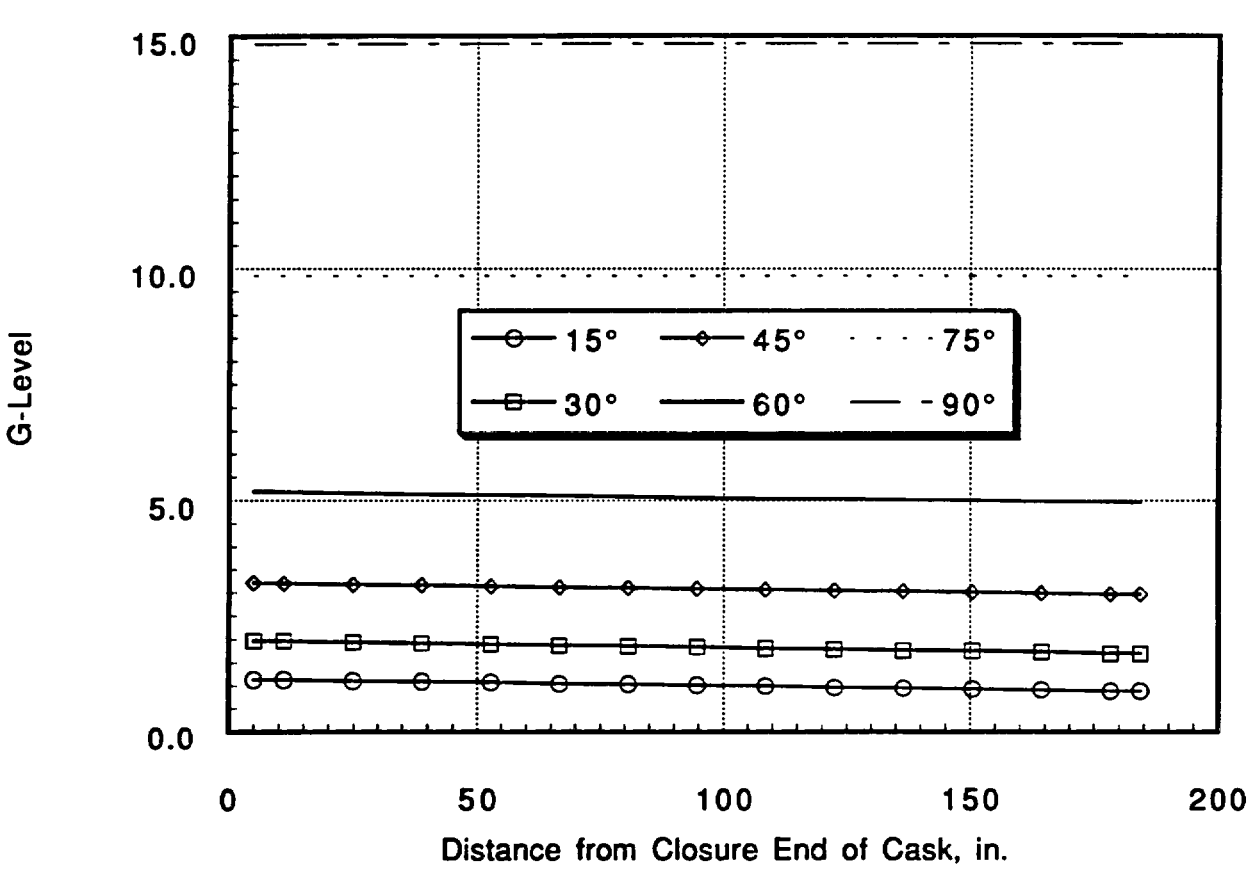

Fig. 2.10.4-27. 1-ft high impact limiter strength, axial g-level

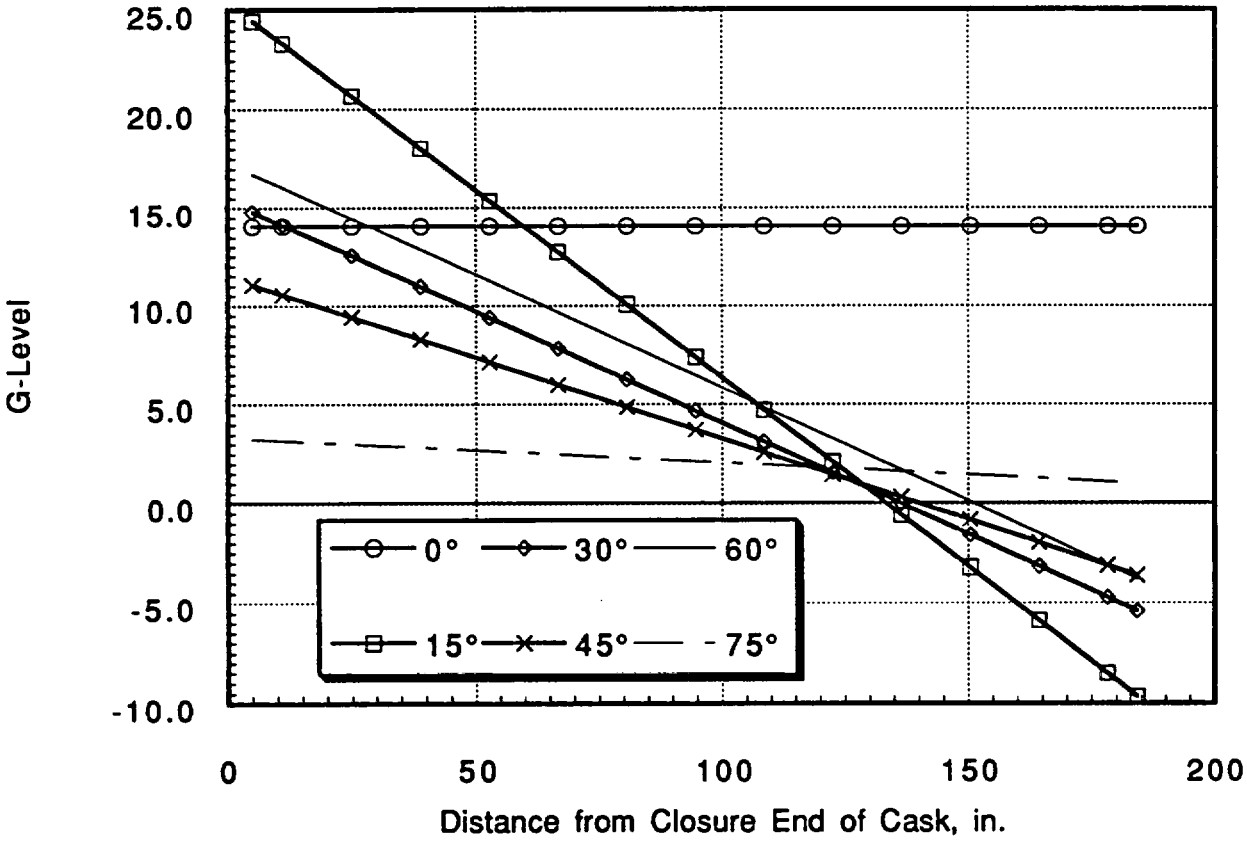

Fig. 2.10.4-28. 1-ft test impact limiter strength, transverse g-level

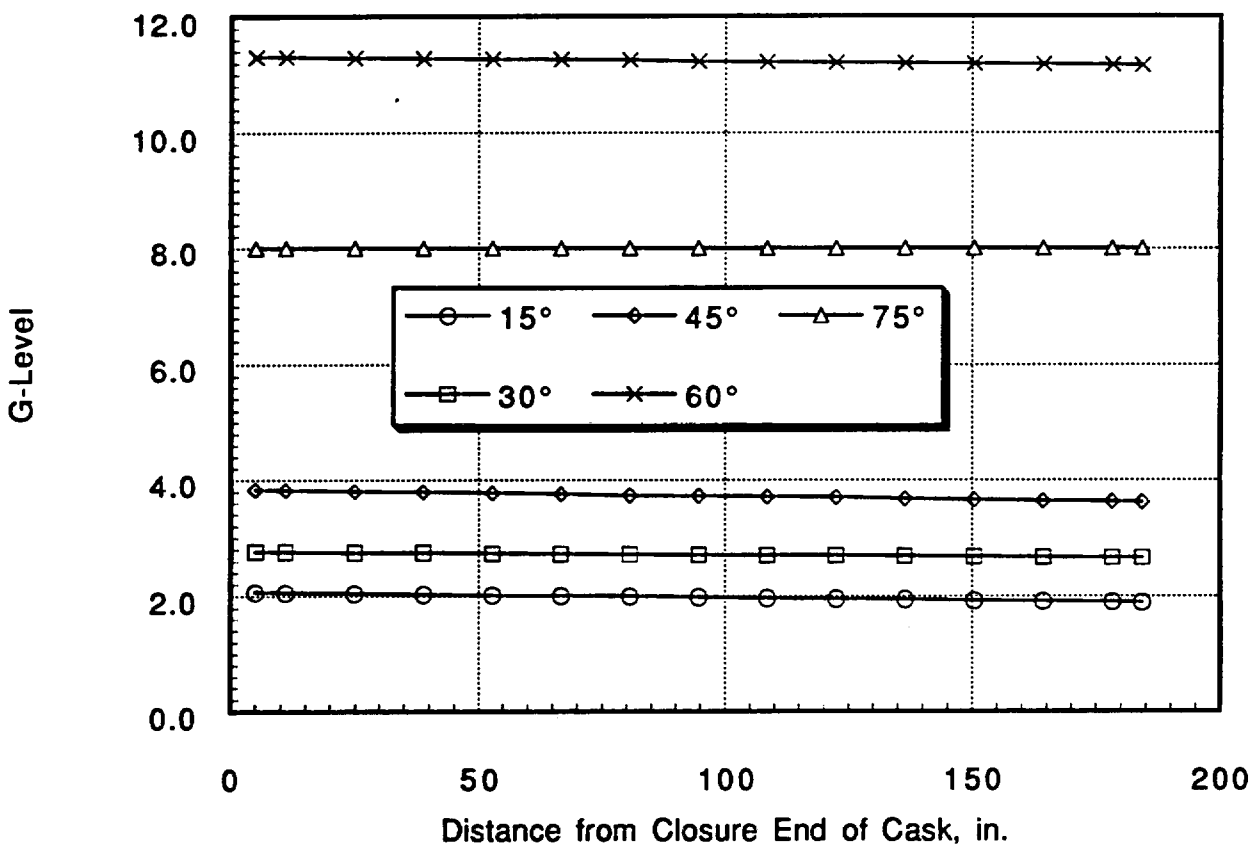

Fig. 2.10.4-29. 1-ft test impact limiter strength, axial g-level

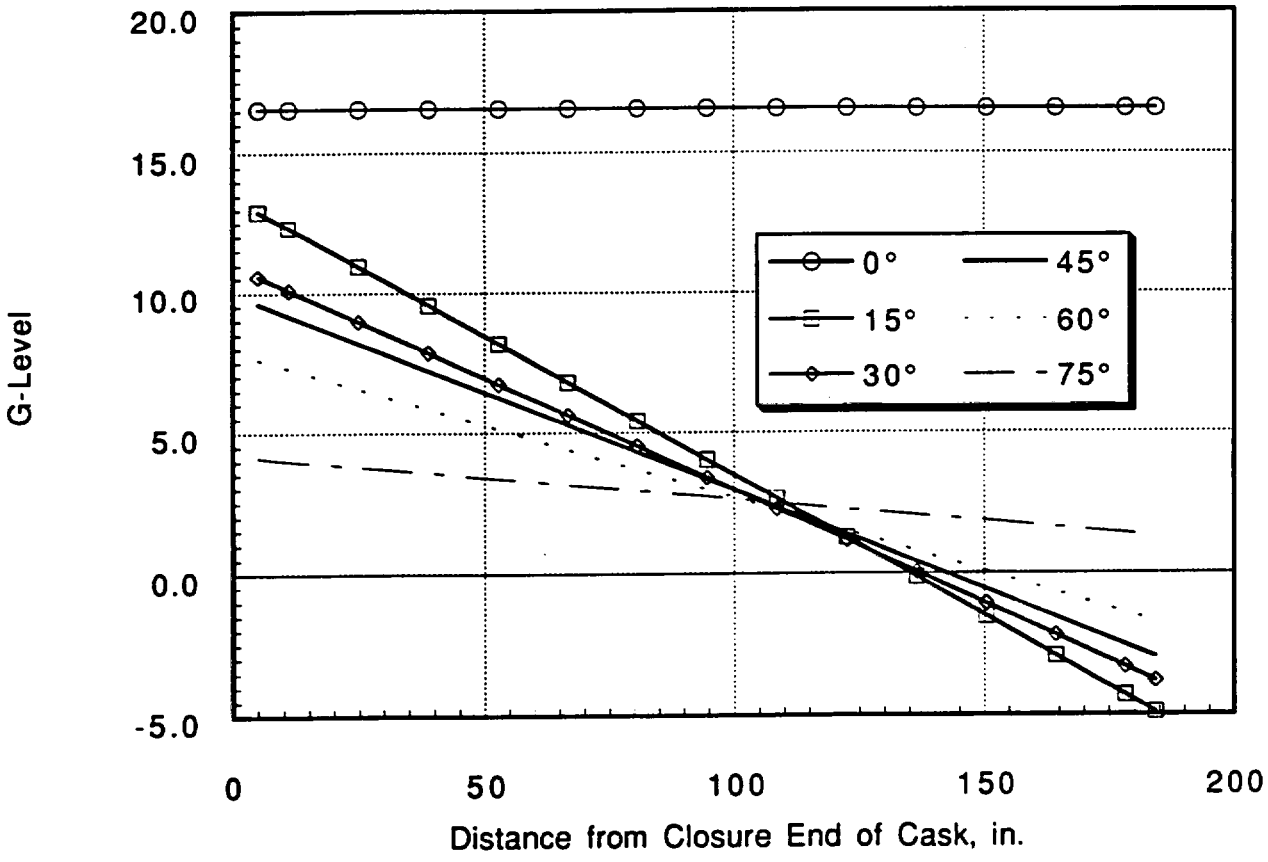

Fig. 2.10.4-30. 1-ft high impact limiter strength and minimum contents weight, transverse g-level

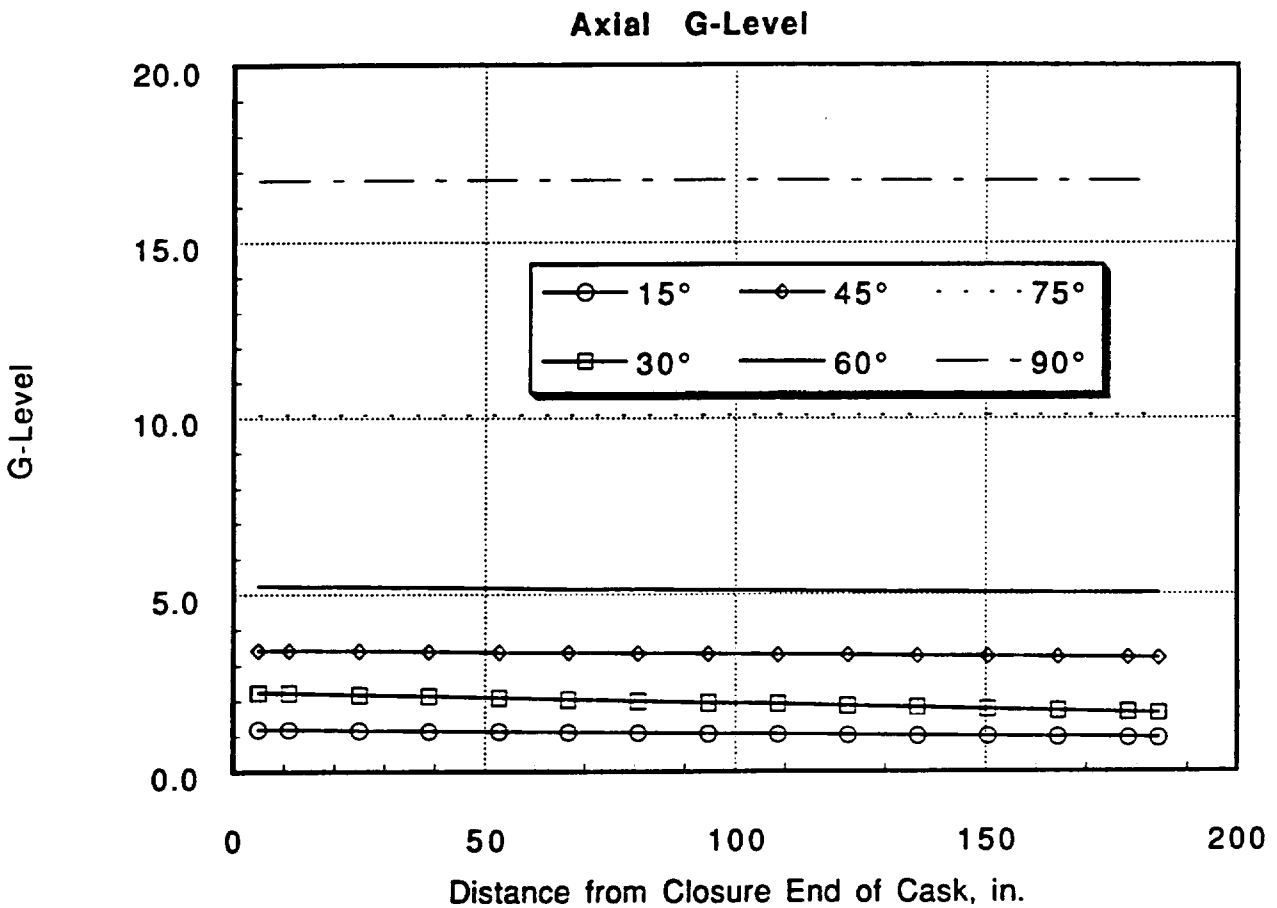

Fig. 2.10.4-31. 1-ft high impact limiter strength and minimum contents weight, axial g-level

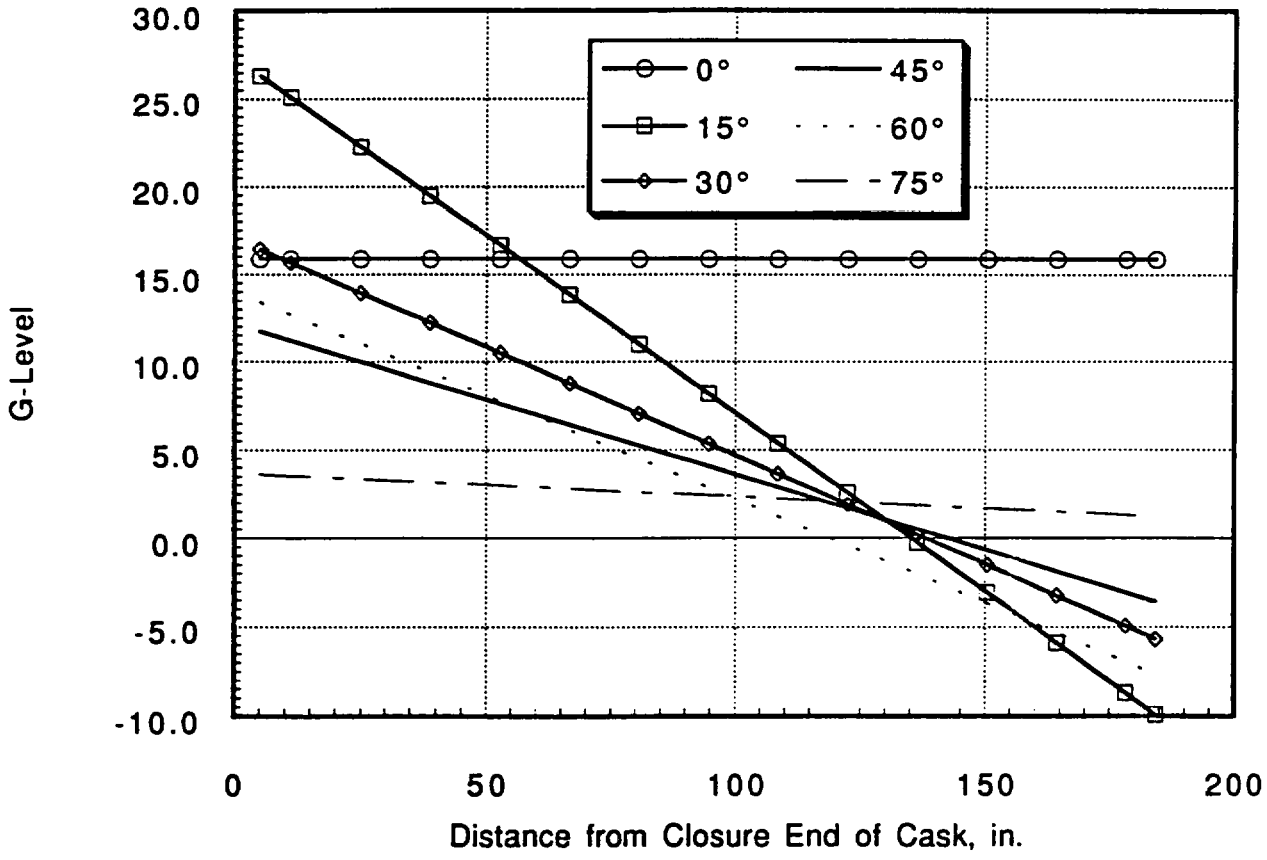

Fig. 2.10.4-32. 1-ft test impact limiter strength and minimum contents weight, transverse g-level

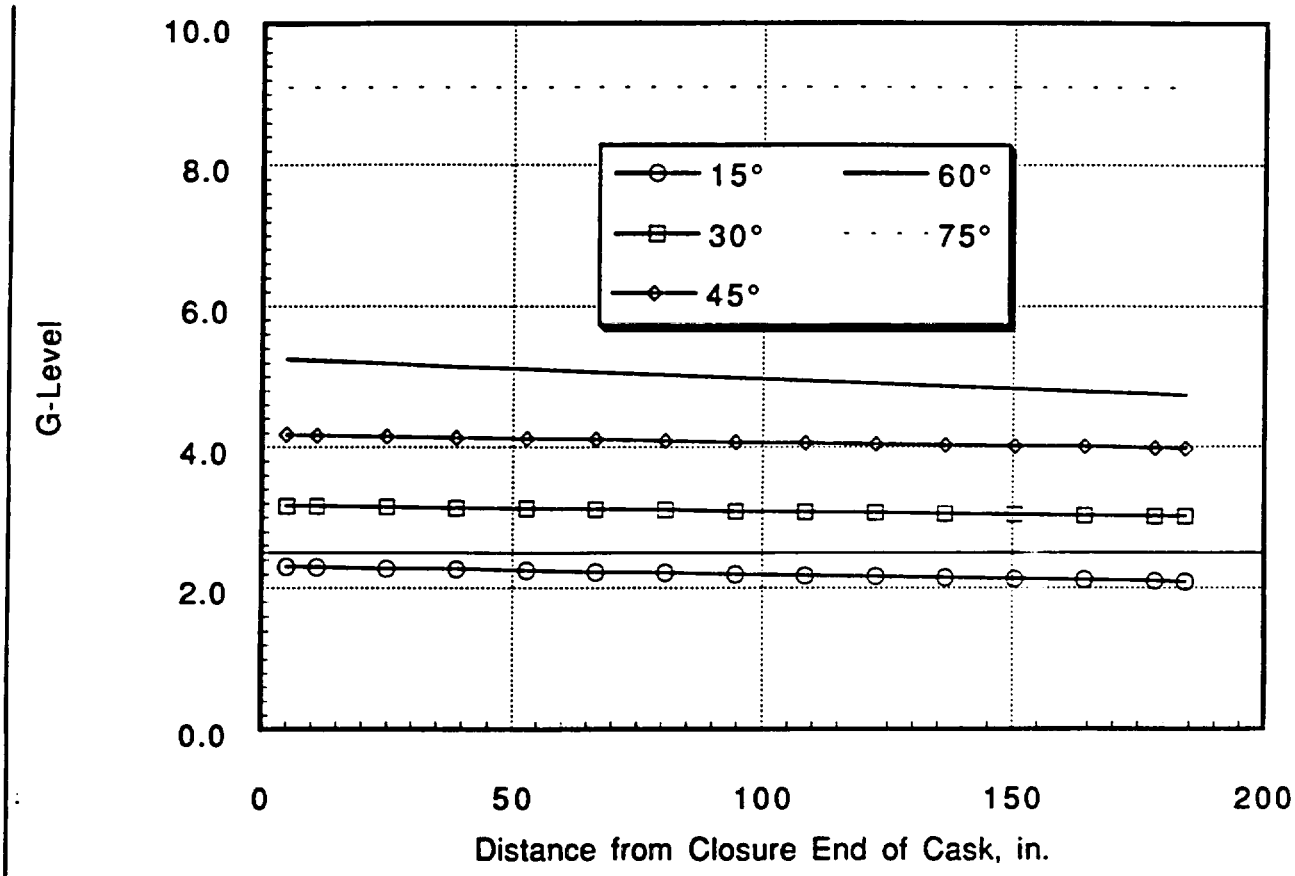

Fig. 2.10.4-33. 1-ft test impact limiter strength and minimum contents weight, axial g-level

THIS PAGE LEFT BLANK INTENTIONALLY